UNIVERSITY OF CAMBRIDGE

Group 11 'Ate Bases: Towards an Understanding of Solid- and Solution-State Structures

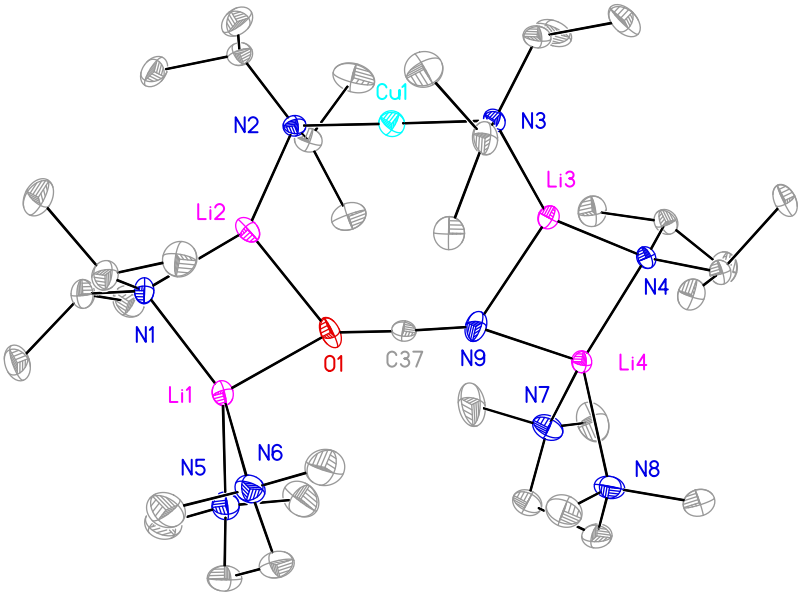

Andrew James Peel

Churchill College, University of Cambridge

August 2017

This dissertation is submitted for the degree of *Doctor of Philosophy*

Group 11 'Ate Bases: Towards an Understanding of Solid- and Solution-State Structures

Andrew James Peel

Lithium bis(amido)cuprates are an important class of bimetallic base, which can chemo- and regioselectively metalate aromatic compounds, *via* directed *ortho* cupration (DoCu). This thesis begins with an introduction to aspects of the chemistry of organolithium compounds, group 11 organometallic compounds and their lithium 'ate complexes. Examples of such synergic bases are presented and the introduction is concluded with a discussion of lithium bis(amido)cuprate bases, which along with their silver congeners, are the subject of this dissertation. In general, syntheses involve the addition of a lithium amide to a group 11 salt, resulting in the formation of a lithium bis(amido)cuprate or argentate.

Structurally focussed work commences with the use of new amide ligands to develop heteroleptic bis(amido)cuprate systems. The reaction of mixtures of lithium amides with CuBr provides a series of novel Lipshutz-type and Gilman cuprates. Interesting structural features are uncovered, which are rationalised in terms of altered steric demands in the newly introduced amide ligands in these systems.

CuSCN and CuOCN are investigated as inexpensive and safer alternatives to CuCN in cuprate formation. In the solid state, a series of Lipshutz-type cuprates $(TMP)_2Cu(SCN)Li_2(L)$ (L = Et_2O, THF, THP) are revealed, whose molecular conformations are influenced by the identity of the Lewis base. However, in benzene solution, *in situ* conversion of Lipshutz-type to Gilman cuprate is found to occur. Moving to the synthetic setting, derivatisation of chloropyridines is attempted and gives functionalised halopyridines in 51-71 % yield. CuOCN is found to behave quite differently when reacted in the same way as CuSCN, whereby X-ray crystallography reveals structures in which Cu-Li substitution is apparent.

The unique reactivity of CuOCN is interpreted with the aid of multinuclear NMR spectroscopy. A new route to Lipshutz-type cuprates is explored by the synthesis of $(TMP)_2Cu(OCN)Li_2(THF)$ from Gilman cuprate and LiOCN. This avoids Cu-Li substitution. Meanwhile, reaction of lithium *N*,*N*-diisopropylamide with CuOCN also avoids metal disorder, to give a novel lithium cuprate-lithium amide adduct.

Further advances in our understanding of group 11 'ate complexes are made by introducing silver as a spectroscopically active nucleus in the lithium argentates $(TMP)_2AgLi$ and $(TMP)_2Ag(CN)Li_2(THF)$. In the solid state, these parallel the structures known for Gilman cuprate $(TMP)_2CuLi$ and Lipshutz cuprate $(TMP)_2Cu(CN)Li_2(THF)$, respectively. In solution, NMR spectroscopy reveals features consistent with retention of these structures. Lastly, the formation of mixed Cu-Li aggregates from combining TMPLi and TMPCu in aromatic solvent are investigated. Surprising reactivity is uncovered, in which the aromatic solvent is metalated and incorporated into mixed-metal aggregates.

This thesis concludes with a summary of the findings and suggestions for future work, including how the findings presented herein may be transformed into practical improvements to cuprate systems. In particular, the possibility that Gilman cuprate may be activated towards the metalation of aromatic substrates by the addition of sub-stoichiometric or catalytic amounts of a lithium salt additive is explored.

Declaration

This dissertation is submitted to the Board of Graduate Studies in partial fulfilment of the requirements for the qualification of Doctor of Philosophy at the University of Cambridge. Research presented herein was carried out by the author at the University Chemical Laboratories between October 2013 and July 2017. Except where specific reference is made to the contrary, it is original work and contains nothing that is the outcome of work done in collaboration. Neither the whole nor any part of the work has been submitted before for a degree in any other institution. This thesis does not exceed 60,000 words including tables, footnotes and the bibliography.

Andrew James Peel
10^{th} August 2017

Acknowledgements

First and foremost, I wish to thank Andrew Wheatley for his support, encouragement and guidance throughout my PhD. In particular, the freedom that I have been given to explore my own ideas and interests has been extremely important to me, and I am very grateful to have had the opportunity to do so.

Thanks are due to members of the Wheatley, Wright and Boss-Barker groups for their friendship and for maintaining such a cordial working atmosphere. I am especially grateful to Peter Matthews, Michael O'Neill, Lily Dixon and Evan Keyzer for many stimulating discussions over recent years. Several Part III students whom I have supervised have made valuable contributions to this project over the years: Jonny Slaughter, György Bensckó, Ryan Ackroyd and James D'Rozario are all thanked for their hard work and perseverance.

I am indebted to many members of the technical and support staff, without whom research could not have proceeded. Thanks are due to John Davies, Andrew Bond and Paul Raithby (University of Bath) for assistance with collecting X-ray data and for valuable discussions on structure refinement. I am grateful to Peter Grice and Duncan Howe for training and assistance with NMR spectroscopy. Lastly, I must thank Alan Dickerson, Patricia Irele and Anya Howe for microanalyisis and for their endless patience with my 'uncooperative' samples.

In Chapter 6, testing of new lithium thiocyanatocuprates in synthesis was conducted in collaboration with Florence Mongin, Madani Hedidi (University of Rennes 1, France) and Ghenia Bentabed-Ababsa (Univeristy of Oran, Oran). I wish express my gratitude for their expertise and valuable contributions to this work.

Lastly, I wish to thank my family and friends for their unwavering support.

Publications

Towards the Synthesis of Amidinate- and Guanidinate-Bridged Dimers of Mn and Ni, F. A. Stokes, L. Kloo, P. J. Harford, A. J. Peel, R. J. Less, A. E. H. Wheatley and D. S. Wright, *Aust. J. Chem.*, 2014, **67**, 1081–1087.

Structural Effects in Lithiocuprate Chemistry: the Elucidation of Reactive Pentametallic Complexes, P. J. Harford, A. J. Peel, J. P. Taylor, S. Komagawa, P. R. Raithby, T. P. Robinson, M. Uchiyama and A. E. H. Wheatley, *Chem. Eur. J*, 2014, **20**, 3908–3912.

New Avenues in the the directed deprotometallation of aromatics: recent advances in directed cupration, P. J. Harford, A. J. Peel, F. Chevallier, R. Takita, F. Mongin, M. Uchiyama and A. E. H. Wheatley, *Dalton Trans.*, 2014, **43**, 14181–14203.

Neutron Diffraction Characterisation of C−H···Li Interactions in a Lithium Aluminate Polymer, J. M. Cole, P. G. Waddell, A. E. H. Wheatley, G. J. McIntyre, A. J. Peel, C. W. Tate and D. J. Linton, *Organometallics*, 2014, **33**, 3919–3923.

Alkali/Coinage metals- organolithium, organocuprate chemistry, P. J. Harford, A. J. Peel and A. E. H. Wheatley, *Organometallic Chemistry*, 2014, **39**, 165–169.

New options in directed cupration: Studies in heteroleptic bis(amido)cuprate formation, A. J. Peel, J. Slaughter and A. E. H. Wheatley, *J. Organomet. Chem*, 2016, **812**, 259–267.

Extending motifs in lithiocuprate chemistry: unexpected structural diversity in thiocyanate complexes, A. J. Peel, M. Hedidi, G. Bentabed-Ababsa, T. Roisnel, F. Mongin and A. E. H. Wheatley, *Dalton Trans.*, 2016, **45**, 6094–6104.

Alkali/Coinage metals- organolithium, organocuprate chemistry, A. J. Peel and A. E. H. Wheatley, *Organometallic Chemistry*, 2016, **40**, 177–198.

Reactions of Trimethylaluminium: Modelling the Chemical Degradation of Synthetic Lubricants, J. Slaughter, A. J. Peel and A. E. H. Wheatley, *Chem. Eur J.*, 2017, **23**, 167–175.

Metal exchange in lithiocuprates: implications for our understanding of structure and reactivity, A. J. Peel, R. Ackroyd and A. E. H. Wheatley, *Chem. Sci.*, 2017, **8**, 4904–4916.

Abbreviations

Bn	benzyl ($PhCH_2$)
*n*Bu	*normal*-butyl
12-c-4	12-crown-4 ($C_8H_{16}O_4$)
CIP	contact ion pair
CIPE	Complex Induced Proximity Effect
CoSHH	Care of Substances Hazardous to Health
CPCH	dispiro[cyclohexane-2,2′-piperidine-6′,2″-cyclohexane]
Cy	cyclohexyl
DG	directing group
DFT	Density Functional Theory
DME	dimethoxyethane ($MeO(CH_2)_2OMe$)
DMP	*cis*-2,6-dimethylpiperidide
DOSY	Diffusion Ordered Spectroscopy
DoAg	directed *ortho* argentation
DoAl	directed *ortho* alumination
DoCu	directed *ortho* cupration
DoLi	directed *ortho* lithiation
DoM	directed *ortho* metalation
DoMg	directed *ortho* magnesiation
DoZn	directed *ortho* zincation
DPPE	1,2-bis(diphenylphosphino)ethane

E	general electrophile
Et	ethyl (CH_3CH_2)
EXAFS	Extended X-ray Absorption Fine Structure
FTIR	Fourier Transform Infrared
HOESY	Heteronuclear Overhauser Effect Spectroscopy
HOMO	Highest Occupied Molecular Orbital
HSQC	Heteronuclear Single-Quantum Coherence
I	nuclear spin quantum number
*i*Bu	*iso*-butyl ($(CH_3)_2CHCH_2$)
*i*Pr	*iso*-propyl ($(CH_3)_2CH$)
m-	*meta*-
Me	Methyl (CH_3)
Mes	mesityl (2,4,6-trimethylphenyl)
MNDO	Modified Neglect of Differential Overlap
MP	2-methylpiperidide
NMR	Nuclear Magnetic Resonance
o-	*ortho*-
p-	*para*-
Ph	phenyl (C_6H_5)
PIP	piperidide
PMDETA	N,N,N',N'',N''-pentamethyldiethylenetriamine
PPE	personal protective equipment
R	general organic group
RI-NMR	rapid-injection NMR
SSIP	solvent-separated ion pair
TAG	1,1,3,3-tetraalklyguanidinate
*t*Bu	*tertiary*-butyl
THF	tetrahydrofuran

THP	tetrahydropyran
THT	tetrahydrothiophene
TMEDA	*N*,*N*,*N*′,*N*′-tetramethylethylenediamine
TMP	2,2,6,6-tetramethylpiperidide
TMS	trimethylsilyl ($(CH_3)_3Si$)

δ	chemical shift (ppm)
γ	gyromagnetic ratio
J	scalar coupling constant
ppm	parts per million
s	singlet
d	doublet
t	triplet
q	quartet
m	multiplet
br	broad
sh	shoulder

M	molecular weight
a, b, c; α, β, γ	unit cell parameters
λ	X-ray wavelength
V	unit cell volume
μ	linear absorption coefficient
Z	number of molecules per unit cell
ρ_{calc}	calculated density
e	electron
$R1$	R-factor (unweighted)
S	Goodness of Fit

$wR2$	R-factor (weighted)
θ	Bragg angle

Definition of Numbered Compounds

1	$[(MP)_2CuLi(THF)_2]_2LiBr$
2	$MP(TMP)Cu(Br)Li_2(THF)_2$
3	$DMP(TMP)Cu(Br)Li_2(THF)_2$
4	PIP(TMP)CuLi
5	$(TMP)_2Cu(CN)Li_2(THP)$
6	$(TMP)_2Cu(SCN)Li_2(OEt_2)$
7	$(TMP)_2Cu(SCN)Li_2(THF)$
8	$(TMP)_2Cu(SCN)Li_2(THP)$
9	$(TMP)_4Cu_{2.7}Li_{1.3}$
9a	TMPLi
9b	$(TMP)_4CuLi_3$
9c	$(TMP)_2CuLi$
***i*-9c**	$[(TMP)_2CuLi]_2$ – *inverse* isomer
9d	$(TMP)_4Cu_3Li$
9e	TMPCu
10	2-chloropyridine
11	2,3-dichloropyridine
12a–d	2-chloropyridine derivatives
13b–d	2,3-dichloropyridine derivatives
14	$(TMP)_2Cu_{0.1}Li_{0.9}(OCN)Li_2(THF)$
14a	$(TMP)_2Cu(OCN)Li_2(THF)$

14b $(TMP)_2Li(OCN)Li_2(THF)$

15 $(TMPH_2)OCN$

16 $(TMP)_2Li(OCN)Li_2(THF)_2$

17 $(DA)_2Cu_{0.09}Li_{0.91}(Br)Li_2(TMEDA)_2$

17a $(DA)_2Cu(Br)Li_2(TMEDA)_2$

17b $(DA)_2Li(Br)Li_2(TMEDA)_2$

18 $(DA)_4Li_4(OCN)(TMEDA)_2$

19 $(TMP)_2AgLi$

20 TMPAg

21 $(TMP)_2Ag(CN)Li_2(THF)$

22a $(\mu\text{-Ph})(TMP)_3CuLi_3$

22b $(\mu\text{-Ph})(TMP)_3Cu_2Li_2$

22c $(\mu\text{-Ph})(TMP)_3Cu_3Li$

23 $(\mu\text{-}Me_2C_6H_3(CH_2))(\mu\text{-TMP})_2Cu_2Li$

Contents

List of Figures

List of Schemes

List of Tables

Chapter 1

Introduction

1.1 Overview

In this introduction, the role of organometallic compounds in the deprotonative functionalisation of aromatic compounds will be discussed. The chemistry of polar organolithium compounds will be presented, with a focus on the use of organolithium reagents in the metalation of aromatic substrates. Organocopper compounds, organosilver compounds and their related lithium 'ate complexes will be explored. For copper in particular, the modulation of reactivity *via* the formation of lithium cuprates will be presented. Examples of the synergistic behaviour of heterobimetallic bases will be introduced, focussing finally on the development of lithium amidocuprate bases for the promotion of directed *ortho* metalation of aromatic substrates.

1.2 Organometallics in synthesis

Organometallics form a vital part of the array of reagents on offer to the synthetic organic chemist and the range of transformations that are achievable by using organometallic chemistry is ever increasing. Organometallic reagents find uses in small-scale laboratory settings and in industrial operations alike, as stoichiometric reagents, catalysts and co-catalysts.[1,2] In the industrial setting, they are vital for the production of chemical feedstocks,[3] polymers[4] and fine chemicals such as

pharmaceuticals[5] and agrochemicals.[6] For pharamaceutical products in particular, aromatic and heterocyclic[7] compounds are very common synthetic building blocks and are present in a broad range of drug classes. These include antibiotics,[8] antimalarial agents,[9] analgesics,[10] antidepressants[11] and many more. Functionalisation of aromatic components is frequently called for during the synthesis of drug target molecules and organometallic chemistry plays a key role in achieving these transformations.[12]

Elaboration of simple aromatic compounds by C−C bond formation is generally considered to have begun in the late 1800's with the discovery of Lewis acid-mediated alkylations, by Friedel and Crafts.[13] Limitations of these reactions include polyalkylation[14] and the formation of isomeric products due to carbocation rearrangement.[15] The next major advance, in the early 20th century, was marked by the discovery that aromatic substrates bearing certain functional groups underwent regioselective metalation when exposed to organolithium bases.[16,17] Though this represented a significant advance in selectivity, issues surrounding functional group tolerance and rearrangement of intermediates persisted.[18] This issue, together with those surrounding atom efficiency, have been addressed with the advent of transition metal-catalysed cross-coupling reactions.[19] The Heck,[20] Suzuki,[21] Sonogashira,[22] Buchwald-Hartwig[23] and Kumada[24] coupling reactions are amongst the most well-known. Despite widespread use, these methods most often call for the use of precious metal catalysts and less costly alternatives have been sought. Modern trends in aromatic functionalisation include the development of 'greener' and catalytic variations of the Friedel-Crafts reactions, using non-toxic Lewis acids and solvents,[25] and the development of heterobimetallic bases for DoM.[26] Heterobimetallic bases have garnered interest over the last two decades for their ability to regioselectively metalate aromatic substrates, whilst maintaining good functional group tolerance. Amongst the various classes of synergic bases, cuprate bases in particular have attracted attention due the high synthetic relevance of organocuprate complexes.

1.3 Organolithium chemistry

1.3.1 Organolithium compounds in organic chemistry

It is now generally accepted that the Li−C bond in organolithium compounds is significantly ionic.[27] Consequently, the rules governing the structures of true organolithiums (having a Li−C bond) are widely applicable to the structures of related complexes, such as lithium amides and imides.[28] These species increase their electrostatic stabilisation by aggregating according to the ring stacking and laddering principles,[29,30] and the oligomeric nature of these aggregates determines their solubilities in organic solvents. As electron donors, Lewis bases can profoundly influence the aggregation state of lithiated organics,[31] often leading to smaller, more reactive aggregates. It is for this reason that many lithiations are conducted in etherate solvents, or with complexing agents deliberately added.[32]

The organometallic chemistry of lithium is rich and extensive; though by no means an exhaustive list, the principal reactivities of organolithums can be classified as addition, lithium-halogen exchange and lithium-hydrogen exchange.[6] The commercial availability of many organolithiums and their chemical simplicity makes them attractive reagents in synthesis, however they are not without their limitations: organolithiums are both highly basic and nucleophilic. This dual reactivity can cause chemoselectivity issues and many functional groups cannot tolerate the assault of an alkyllithium reagent. Nonetheless, there are certain cases where this property can be exploited: the Shapiro reaction, the Brook rearrangement and the Wittig rearrangement are well-known examples where a desirable rearrangement is intiated by lithiation.[33–35]

1.3.2 Directed *ortho* lithiation

Directed *ortho* lithiation belongs to the broader class of directed *ortho* metalation reactions, which involve the regioselective formation of a C−M bond *ortho* to certain functional groups on an aromatic substrate (Scheme 1.1). Synthetically, metalation is often followed by quenching with an electrophile to install new functionality.

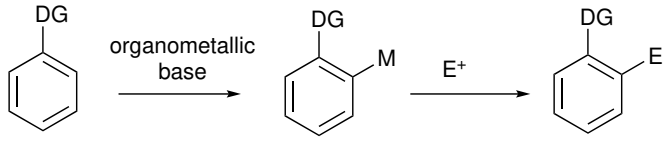

Scheme 1.1: General scheme for directed *ortho* metalation. E = general electrophile.

Organolithiums such as *n*BuLi are thermodynamically capable of metalating unfunctionalised aromatics such as benzene, though this proceeds extremely slowly unless a Lewis base such as TMEDA is added.[36] *Ortho* lithiation was discovered as a side reaction when 4-bromoanisole was treated with lithium metal. Rather than obtaining 4-methoxyphenyllithium (from Li-Br exchange), the major lithiated product was found to be 5-bromo-2-methoxyphenyllithium. This implied that the initially formed 4-methoxyphenyllithium acted as a base towards 4-bromoanisole, regioselectively removing the proton *ortho* to the methoxy group (Scheme 1.2).[37] As such, it demonstrated the ability of the Lewis basic moiety to effect regioselevtivity. Subsequent experiments with *n*BuLi as the base reproduced the regioselective *ortho* metalation,[16] and since then, a great many functional groups have been found which exhibit this directing effect.

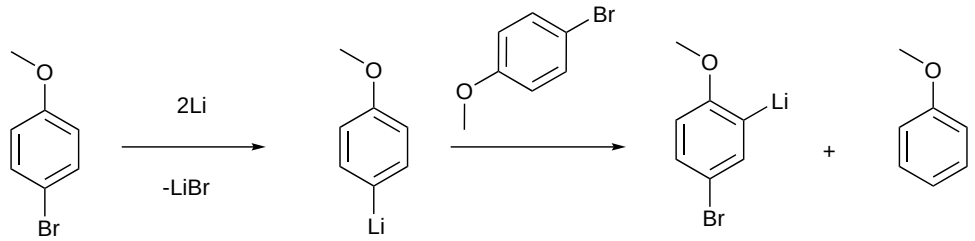

Scheme 1.2: The autometalation reaction of 4-bromoanisole was the first observed instance of DoLi.[37]

Ortholithiation is thought to work by the coordinative action of a heteroatom on the directing group, which enhances the reactivity of the alkylithium reagent in the vicinity of the directing group, leading to a regioselective deprotonation.[38] The exact role of the directing group in the reaction likely varies between weaker and stronger directing groups, though in the latter case (e.g. oxazolines or tertiary amides), it may be supposed that the basic heteroatom of the directing group is involved in deaggregation of the alkyllithium base.[6] Where the heteroatom cannot coordinate to lithium, for steric or electronic reasons, it can be deduced that it is

only the enhanced acidity of the *ortho* protons which directs lithiation. This is the case for fluorobenzene, where *ortho* lithiation proceeds at low temperatures, even though NMR spectroscopy confirms the absence of significant Li-F interactions.[39]

Directing groups can be ranked according to their experimentally observed power to direct lithiation, and with reference to the heteroatom components of the functional groups (Figure 1.1). It should be apparent that directing groups which posses 'amphoteric' properties – that is, having strongly Lewis basic heteroatoms and strong inductively acidifying effects – should be the best directing groups.[6] Accordingly, functional groups such as tertiary amides (in the N+O class) are strong directors of *ortho* lithiation due to the combined effect of the Lewis basic oxygen atom and the electron withdrawing properties of the carbonyl group.[18] Conversely, halogens (of the X class), exhibit only inductive effects and are poor directors of lithiation.

These two examples highlight the pitfalls of *ortho* lithiation. In the case of the amide, the carbonyl group is electrophilic and is therefore vulnerable to addition reactions when combined with an alkyllithium reagent. Similarly, care must be taken when the halogens Br or I are present, as lithium-halogen exchange may compete with deprotonative metalation. A change of directing group – for example to the S+O class – may circumvent these issues, but may be detrimental to the synthesis, as these new functional groups are less commonly desired as components of the target molecule.[40]

1.3.3 Mechanism of DoLi

There is no doubt that *ortho* lithiated aromatics can have significant thermodynamic stabilisation compared to other positional isomers. In the case of lithiated anisole, the *para* lithiate releases 3.6 $kJ\,mol^{-1}$ more than the *ortho* isomer when quenched with *sec*-butylalcohol.[41] However, this data does not necessarily explain the selectivity of the *ortho* lithiation; since most lithiations are conducted at low temperature, it is the kinetic acidity of the *ortho* protons which is of paramount importance.

The CIPE model was proposed on the basis that the interaction of the directing group with an alkyllithium could lead to a pre-reaction complex from which the *or-*

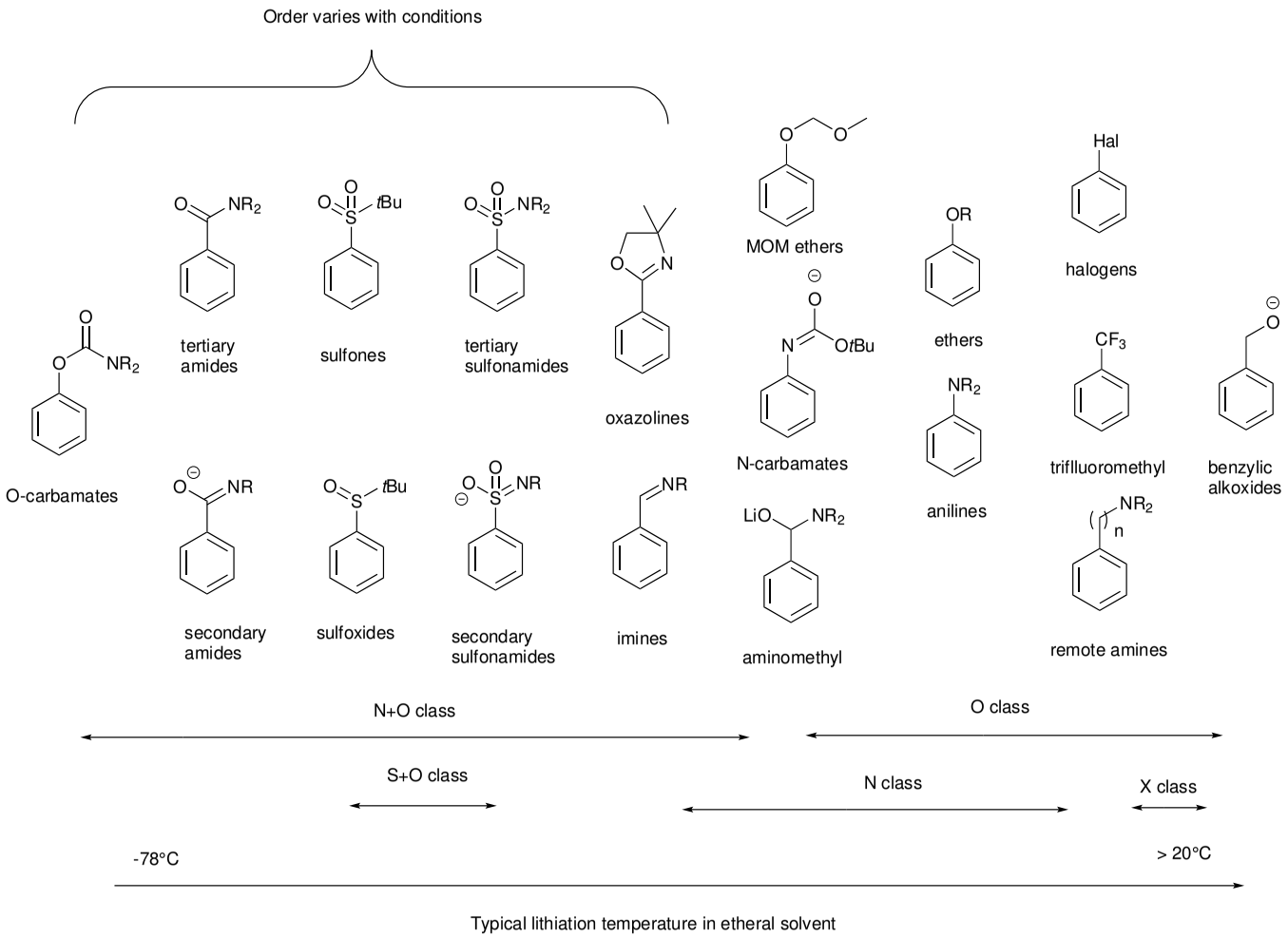

Figure 1.1: A survey of common directing groups, according to their ability to direct metaltion.[6]

tho protons would be removed by virtue of being closest to the base (Scheme 1.3). Experiments with anisole corroborated this possibility when a *n*BuLi-anisole complex was detected by NMR spectroscopy at −64 °C. Furthermore, the spatial proximity of the Li and *ortho* protons was confirmed by ^{6}Li-^{1}H HOESY data, and this was in line with the postulates of CIPE. Crucially, this adduct proved to be unreactive and addition of TMEDA resulted in displacement of ansiole to give a *n*BuLi-TMEDA complex. After this, metalation proceeded readily, bringing into question the relevance of the *n*BuLi-anisole complex in the *ortho* metalation.[39]

An alternative explanation, proposed by Schleyer, relied only on the acidifying effects of the directing groups. The idea of a pre-reaction complex being the rate determining step was not in accordance with the accelerated rates of deprotonation of subsitituted arenes, since an activation energy is to be associated with complexation. Instead, the transition state was proposed to be stabilised by the charge distribution induced by the electronegative substituents, leading to accelerated rates of *ortho* deprotonation.[38,42]

Attemtps to clarify the situation with KIE measurements have only concluded that deprotonation, rather than the formation of a pre-reaction complex, was the *rate limiting* step. The existence of a pre-reaction complex was neither confirmed nor excluded.[43] More recently, investigations with 1,2-dimethoxybenzene indicate that an important function of directing groups can be in the deaggregation of otherwise unreactive hexameric aggregates of *n*BuLi in hydrocarbons to form reactive chelated dimers. These were found to be essential for subsequent *ortho* lithiation.[44] Computational studies have painted similarly conflicting pictures. MNDO methods have emphasised the importance of agostic interactions in lithiation reactions, favouring the notion of CIPE.[45] By contrast, combined kinetic measurements and *ab initio* calculations by Collum and co-workers have suggested that the formation of highly reactive $[n\mathrm{Bu_2Li}]^-$ triple ions and inductive effects are precedent.[46]

Overall, there is a bias towards inductive acidifying effects as the favoured explanation for DoLi, yet most of these studies are conducted with *poor* directing groups (usually, OMe). It would therefore be unreasonable to discount CIPE on this basis, since many of the directing groups for which this mechanism would be expected to operate have not been studied explicitly.

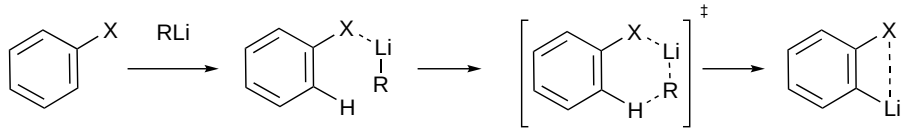

Scheme 1.3: Proposed CIPE mechanism, with a pre-reaction complex formed due to the coordinating effect of X group.

1.4 Organocopper chemistry

The importance of organocopper chemistry in synthesis cannot be understated. Early breakthroughs include the synthesis of phenylcopper by Reich[47] in 1923 and subsequent demonstration of its reactivity towards electrophiles by Gilman in 1936.[48] Not long after, the discovery that catalytic amounts of copper(I) chloride could direct the reaction of isophorone with methylmagnesium bromide to the 1,4-addition product affirmed the synthetic relevance of copper(I) chemistry. Pioneering work by Gilman[49] shed light on the nature of methylcopper and the closely related lithium dimethylcuprate and the synthetic potential of lithium dimethylcuprate was expanded upon by House[50] and Corey,[51] where high yields in conjugate addition and methyl-halogen exchange were noted, respectively.

As a transition metal, copper has available a range of oxidation states, with Cu(I) and Cu(II) being by far the most common. Whilst Cu(II) is most frequently encountered in the inorganic setting, it is not to be found in organocopper compounds, where it is easily reduced to the +1 oxidation state. Similarly, whilst the Cu(III) state is often invoked in reactive intermediates, there are only a handfull of well-characterised examples of Cu(III) compounds containing Cu-C bonds, such as $Cu(CF_3)_2S_2CNEt_2$.[52] Cu(IV) is rarer still, only being found combined with highly electronegative ligands, as in $Cs_2[CuF_6]$.[53]

1.4.1 Aspects of the structures of organocopper compounds

Copper is known to form stable organometallic compounds only in the monovalent state. With one R group per copper atom, the resultant monomer is coordinatively unsaturated and attains stabilisation by aggregation. Many simple organocopper compounds are presumed to be polymeric; they are insoluble in common solvents and are therefore not amenable to the usual methods of characterisation. Conse-

quently, there is a paucity of data about the structures of these compounds. Examples for which solid-state structures are known typically feature ligands specifically chosen to favour smaller aggregates and to increase solubility. These can be grouped into two categories: (1) ligands featuring secondary coordination points and (2) bulky ligands which sterically disfavour aggregation. Another obstacle to characterisation of organocopper species is the low thermal stability of these compounds. β-hydride elimination is understood to play a role in decomposition of alkylcopper compounds and some insight into the structures of organocopper compounds has been gained by deploying carbanions lacking β-hydrogen atoms, or by use of fluorinated derivatives.[54]

Important developments have included the synthesis and characterisation of *o*-, *m*- and *p*-tolylcopper[55] and synthesis of the perfluorinated aryl copper, CuC_6F_5, for which cryoscopy in benzene suggested a tetrameric aggregate.[56,57] By excluding β-hydride elimination pathways, Lappert and co-workers were able to produce $CuCH_2SiMe_3$ as colourless crystals which were stable, in the absence of light, up to 79 °C (Figure 1.2b).[58] In 1970, van Koten demonstrated the stabilising properties of substituted arylcopper compounds by synthesising 2-$(CH_2NMe_2)C_6H_4Cu$ and noted its ability to form stable complexes with metal salts, including the CuBr, from which it was synthesised. Early cryoscopic studies pointed towards organolithium-like aggregates but it was not until 1972 when the crystal structure of 2-$(CH_2NMe_2)C_6H_4Cu$ was solved that their true cyclic nature was revealed (for example, see Figure 1.2a).[59]

Whilst the presence of coordinating groups has been shown to stabilise organocopper complexes, it is noteworthy that several examples demonstrate substantial changes in structure when coordinating solvents are introduced. Mesitylcopper crystallised as a pentamer from hydrocarbon solvent, yet addition of THT resulted in the isolation of a solvated tetramer $Cu_4Mes_4(THT)_2$ (Figure 1.3).[60] This behaviour parallels that of organolithium aggregates, notwithstanding a preference for 'softer' Lewis bases. Additionally, phosphines have been established as excellent ligands for organocopper complexes and their ability to increase the thermal stablility of these complexes has been noted. As an example, upon treatment with Cy_3P, methylcopper forms $CuMe(PCy_3)_3$, the decomposition temperature of which is some 100 °C higher than for MeCu itself.[61] More rarely, a chelating phosphine may induce ionic disproportionation: when CuMes is treated with DPPE, a

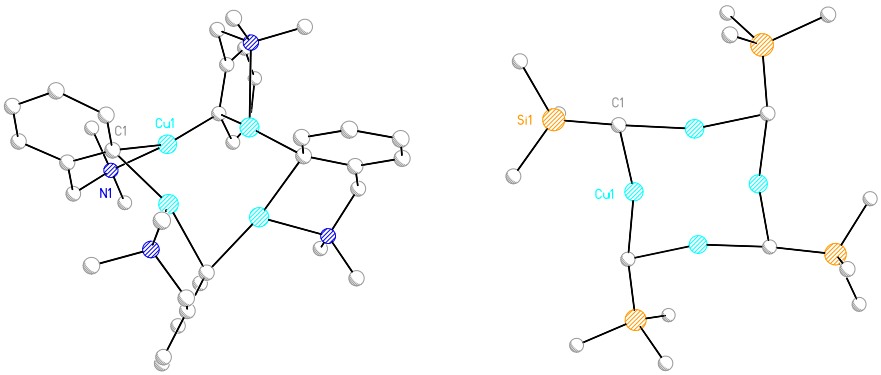

(a) (b)

Figure 1.2: Examples of stable organocopper compounds. (a) 2-$(CH_2NMe_2)C_6H_4Cu$[58] in which Cu is stabilised by interaction with the pendant NMe_2 ligand (b) $CuCH_2SiMe_3$,[59] which is stabilised by the absence of β-H atoms and which prevents decomposition by β-H elimination.

separated ion-pair $[CuMes_2][Cu(DPPE)_2]$ is formed, in which the anion and cation have linear and tetrahedral coordination geometries, respectively.[62]

Ligands of significant steric bulk are also known to favour smaller aggregates of $(RCu)_n$. For example, when 2,4,6-triethylphenyl is deployed, a tetramer is formed (*cf.* a pentamer for CuMes).[63] However, even with the extremely bulky 2,4,6-triphenylphenyl ligand, some degree of association is achieved and unsolvated monomers are unknown (see Figure 1.4).[64]

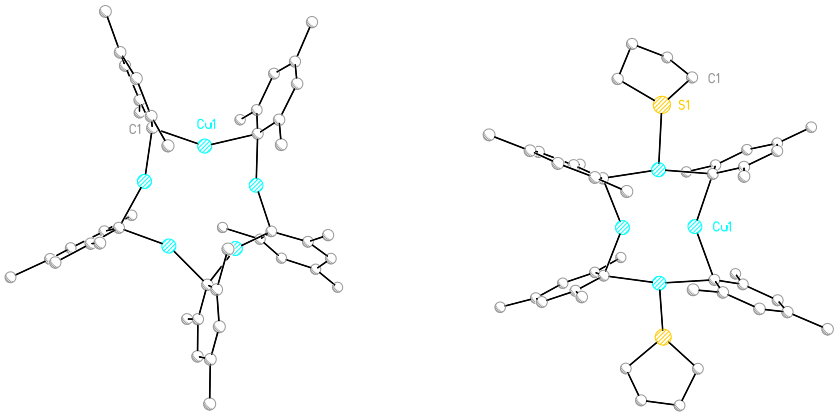

(a) (b)

Figure 1.3: Molecular structures of CuMes aggregates. (a) Cu_5Mes_5 (b) $Cu_4Mes_4(THT)_2$, formed by the addition of THT to CuMes.[60]

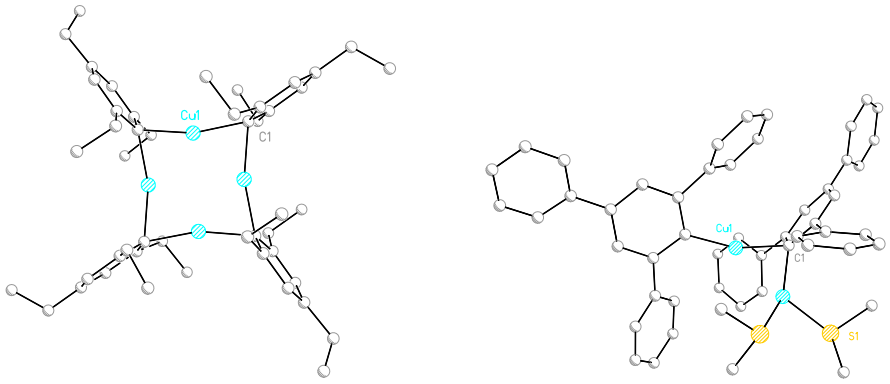

(a) (b)

Figure 1.4: Molecular structures of (a) Cu_4(2,4,6-$Et_3Ph)_4$[63] and (b) Cu_2(2,4,6-$Ph_3Ph)_2(DMS)_2$,[64] illustrating the effect of steric bulk upon aggregation state.

1.4.2 Structurally related copper complexes

Copper amides,[65] alkoxides,[66] imides,[67] guanidinates[68] and phosphinimides[69] are known. These compounds adopt cyclic structures, with varying ring sizes depending upon the nature of the ligand (see Figure 1.5). Though many examples are simply of structural interest, some have been found to have synthetic applications. For example, *t*BuOCu is capable of deprotonating phenylacetylene and cyclopentadiene[70] and very recently, copper amides have been investigated for their ability to participate in modified Ullmann amination reactions.[65]

1.4.3 Organocopper reagents in synthesis

In synthesis, organocopper reagents are almost always to be found in the form of a cuprate, $[R_2Cu^-]$ and most often being paired with Li^+ or (less commonly) Mg^{2+}. The formation of an 'ate complex significantly enhances reactivity towards organic substrates, and of practical importance, increases solubility in hydrocarbon and etherate solvent. This point is illustrated well by Gilman's original synthesis of lithium dimethylcuprate: when one equivalent of MeLi was added to CuI, a yellow precipitate was formed. Upon addition of a second equivalent of MeLi, the yellow precipitate dissolved to give a colourless solution, implying the formation of a new organometallic species (Scheme 1.4).

Cuprates are most often employed in addition and substitution reactions and

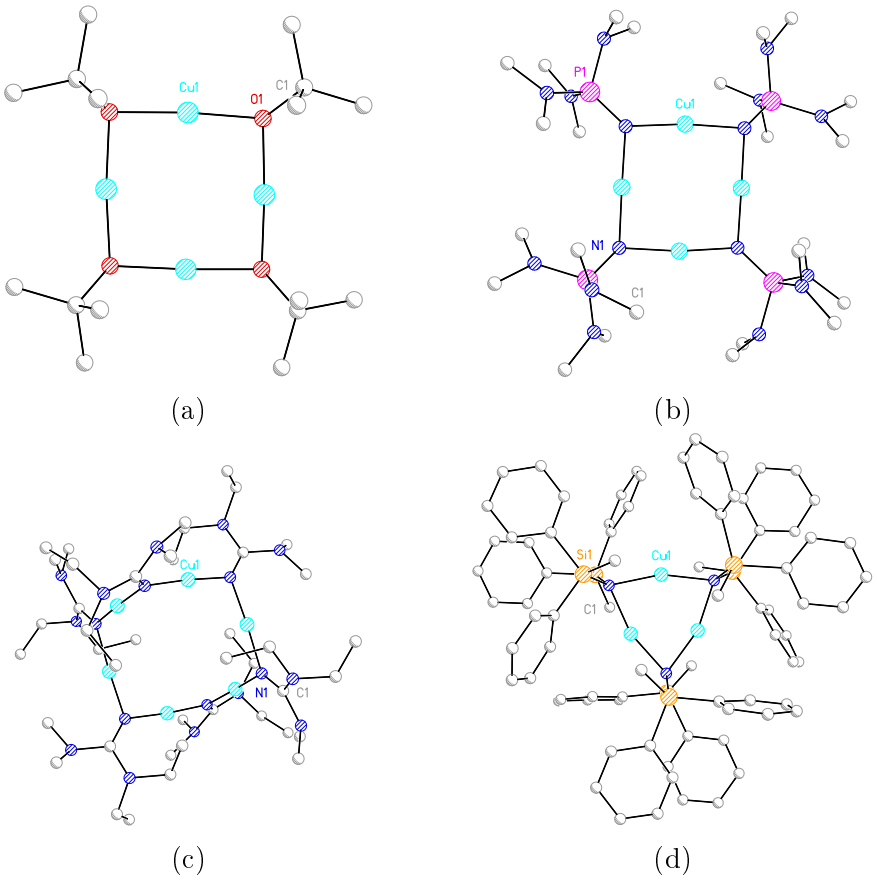

Figure 1.5: Molecular structures of selected copper complexes bearing N- and O-donor ligands, illustrating variations in aggregation number. (a) $Cu_4(t\text{BuO})_4$[66] (b) $Cu_4(NP(NMe_2)_3)_4$[67] (c) $Cu_6(NC(NEt_2)(NMe_2))_6$[68] (d) $Cu_3(N(SiMe(Ph))_2)_3$.[69]

the substrate scope can be rather wide.[2] The synthetic importance of cuprates stems from their modified reactivity: organocuprates provide a 'soft', nucleophilic source of R^- and react selectively with the C=C bond of α,β-unsaturated carbonyl compounds. Similarly, whereas S_N2 substitution cannot be executed cleanly by reaction of an organolithium and alkyl halide, the same reaction proceeds cleanly when a Gilman reagent is deployed. Lastly, an interesting, yet little-explored facet of cuprate chemistry involves the oxidative coupling of the organic moieties which offers, for example, a precious-metal free route to biaryls.[71]

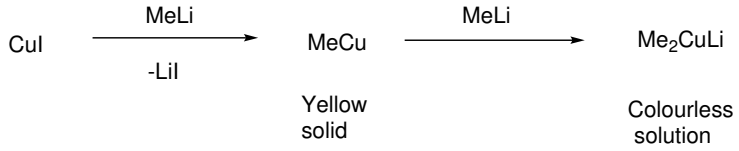

Scheme 1.4: Gilman's original synthesis of Me_2CuLi.[49]

1.4.4 Structural aspects of organocuprate complexes

Historically, the structure of organocuprates has been a controversial topic. The largest body of structural work relates to lithium organocuprates, though a select number of magnesium organocuprates have been crystallographically characterised in recent years.[72] Owing to the highly reactive nature of cuprate complexes, characterisation has proved challenging. Several different types of cuprate can be envisaged: cuprates may be either contact ion pairs or solvent-separated ion pairs, and may be homoleptic or heteroleptic in nature. In addition to this, the cuprate ion itself may be categorised as lower order ($[R_2Cu]^-$) or higher order ($[R_3Cu]^{2-}$).

Early studies focussed on the simplest case, lithium dimethylcuprate. A combination of ^{1}H NMR spectroscopy, vapour pressure depression and solution X-ray scattering established Me_2CuLi as a dimer in Et_2O solution, with a structure based upon alternating C-bridged metals being proposed.[73] Moving from alkyl to aryl carbanions, the synthesis of $(C_6H_4(CH_2NMe_2))_2CuLi$[74] and the Ag[75] and Au[76] homologues proved possible. In the case of the cuprate, ^{1}H and ^{13}C NMR spectroscopy pointed to each aryl anion being bonded to one Cu centre and one Li centre, and indicated that all NMe_2 groups were coordinated to lithium.[74] Further insight was gained from the Ag homologue where, on account of the presence

of $^{107/109}$Ag ($I = 1/2$) nuclei, coupling of the *ipso* carbon to both Li and Ag could be detected ($^{1}J_{^{107}\text{Ag-}^{13}\text{C}} = 118$ Hz; $^{1}J_{^{109}\text{Ag-}^{13}\text{C}} = 136$ Hz; $^{1}J_{^{7}\text{Li-}^{13}\text{C}} = 7.2$ Hz). This pointed towards a cyclic structure involving alternating aryl-bridged metal ions. This was subsequetly vindicated by X-ray crystallography which also confirmed the expected (dimeric) aggregation state inferred from solution-state measurements.[77]

The ability of an asymmetric carbanion to become a stereogenic centre when bridging two different metals has been recognised as a source of complexity, especially with aryl anions bearing benzylic substituents. Notwithstanding that interconversion of stereoisomers could occur by rotation of the aryl anion, different stereoisomers are, in principle, expected to be detectable by NMR spectroscopy. It has been shown that this situation is realised when the energy barrier to rotation is increased by means of an *ortho* substituent, and that this substituent may induce stereoselective assembly.[78] Hence, the organocopper compound $Cu_4(C_6H_4CH(Me)NMe_2)_4$, prepared from the racemic aryl ligand, shows all possible stereoisomers in solution. In contrast, when the related cuprate $Cu_2Li_2(C_6H_4CH(Me)NMe_2)_4$ is prepared from the same racemic ligand, only one isomer is observed, in which each ligand possesses the same configuration at the benzylic and *ipso* carbons.[79]

The influence of Lewis basic solvents upon the structures of organocuprates mimics that of organolithiums. As would be expected, the identity of the Lewis base is deterministic: for example, in the presence of monodentate Et_2O, lithium diphenylcuprate is present as the CIP dimer $[Ph_2CuLi(Et_2O)]_2$,[80] but when 12-crown-4 ether is deployed, a SSIP monomer, $[Ph_2Cu][(12\text{-c-}4)_2Li]$ is created.[81] For the same compound, the structure-type present in solution has been demonstrated to be highly solvent dependent. ^{1}H-^{6}Li HOESY experiments have been used to show that, in Et_2O, equilibrium lies toward the CIP structure, but the position of equilibrium is reversed in more polar THF. These equilibria are also influenced by the presence of Li salts.[82]

1.4.5 Higher order cuprates

Although the vast majority of structurally characterised cuprates contain the linear two coordinate $[R_2Cu]^-$ ion, a few examples displaying three coordinate copper have been isolated. In fact, the complex $[Ph_6Cu_5][Li(THF)_4]$ was the first

organocuprate to be characterised by X-ray diffraction (Figure 1.6).[83] Within the trigonal bipyramidal arrangement of copper atoms, the apical copper atoms are rendered three coordinate by the encapsulating $[Ph_2Cu]^-$ units (this has been termed 'higher-order'). Notably, in the related compounds $[Ph_6Cu_4Li][Li(Et_2O)_4]$[84] and $[Ph_6Cu_3Li_2]_2[Li_4Cl_2(Et_2O)_{10}]$,[85] Li^+ occupies the trigonal sites, perhaps reflecting the relative demand for electrostatic stabilisation of Cu^+ and Li^+, respectively.

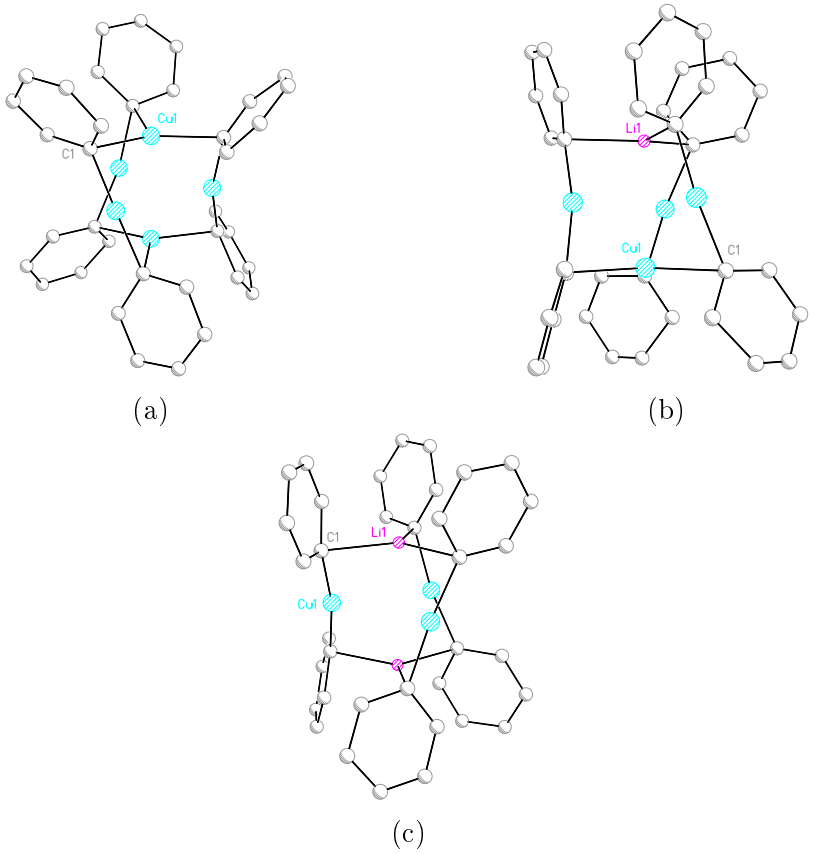

Figure 1.6: Molecular structures of phenylcuprate anions in (a) $[Ph_6Cu_5][Li(THF)_4]$[83] (b) $[Ph_6Cu_4Li][Li(Et_2O)_4]$[84] (c) $[Ph_6Cu_3Li_2]_2[Li_4Cl_2(Et_2O)_{10}]$.[85] Counter-ions omitted for clarity.

Interest in 'higher-order' cuprates (in which Cu is three-coordinate) has its origins in the context of cyanocuprates, a class of cuprates of special interest for their reliably high reactivity. It was noted as early as 1973 that the combination of one equivalent of RLi with CuCN formed a reagent which could be used successfully in 1,4-addition and substitution reactions.[86] In 1981, in an effort to simplify the synthesis of cuprates bearing a non-transferable ligand, and noting the literature

precendent for higher-order cuprates bearing acetylinic groups,[87] Lipshutz and co-workers investigated the replacement of copper acetylide by copper cyanide. By combining two equivalents of RLi with CuCN in THF, reactivity exceeding that shown by Me_2CuLi was achieved.[88] This enhanced reactivity was attributed to the formation of the higher-order cuprate in which cyanide was bound to copper, a notion which proved to be one of contention in the following years.

For the case of the lower-order cuprates, the location of cyanide was determined quite straightforwardly, when NMR spectroscopy revealed a coupling constant $^2J_{\text{C-C}} = 22$ Hz for EtCu(^{13}CN)Li in THF at $-78\,^{\circ}$C. This could only have been the case if both CN^- and Et^- were bonded to the same Cu centre.[89] This view was corroborated by X-ray crystallographic studies of $[t\text{BuCu(CN)Li(OEt}_2)_2]_\infty$, which clearly displayed the expected connectivity (see Figure 1.7).[90]

For the case of the higher-order cyanocuprates, the discourse proved more lively. The assertion of a Cu-CN σ-bond by Lipshutz[91] was challenged by Snyder,[92] who computed a cyclic contacted $[Me_2Cu]^- + [Li_2CN]^+$ structure to be preferred (Figure 1.8). The proposal of a Cu-CN σ-bond was subsequently revised by Lipshutz to incorporate the possibility of a CN$\cdots$Cu π-bond.[93] Once again, this notion was rebuked by Snyder,[94] who calculated this structure to be unstable on the basis of charge repulsion. The fact that 'higher-order' cuprates reagents prepared from CuCN provided higher product yields than those prepared from CuI was in no doubt. However, the use of yield as a metric for reactivity was called into question. In fact, when deployed under the same coniditons, it could be shown that CuCN derived cuprates did *not* exhibit significantly greater reactivity, as measured by logarithmic reactivity profile.[95] Evidence from NMR spectroscopy[96] and EXAFS spectroscopy[97] was presented in favour of the absence of a Cu−CN contact (coincidentally the EXAFS *did* confirm a Cu−CN contact for the lower order cuprate) and the matter was finally resolved with the crystal structure determination of $[(2\text{-}(Me_2NCH_2)C_6H_4)_2CuLi_2CN(THF)_2]_\infty$, which confirmed CN^- to be Li-bound (Figure 1.7).[98,99]

Much more recently, NMR spectroscopic investigations by Gschwind have gone some way to explaining the differences in reactivity of iodo-Gilman and cyano-Gilman reagents. The critical difference in reactivity for the two classes of cuprates bearing solubilising organyl groups was shown to be the fate of the organocopper side product. It could be shown for the case of iodo-Gilman reagents that elon-

gated, soluble, Cu-rich cuprates could be formed. Being less strongly polarised than Gilman cuprates, these Cu-rich cuprates were less reactive and led to lower overall yields in cross coupling reactions. In contrast, the presence of CN^- disfavoured the formation of extended Cu-Li aggregates, hence reactivity was not greatly affected. For small, non-solubilising organic ligands, the insolubility of the organocopper by-product meant that Cu-rich cuprates were not formed for either cyano- or iodo-Gilman reagents.[100]

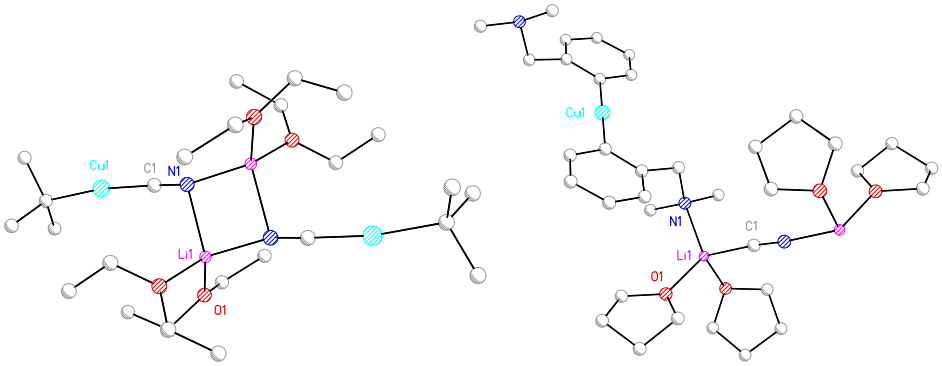

(a) (b)

Figure 1.7: Examples of cyanocuprates (a) $[t\mathrm{BuCu(CN)Li(OEt_2)_2}]$[90] (b)$[(2\text{-}(\mathrm{Me_2NCH_2})\mathrm{C_6H_4})_2\mathrm{Cu(CN)Li_2(THF)_2}]_\infty$. In spite of the potential for (b) to adopt a higher-order structure, lower-order (two-coordinate) copper prevails.

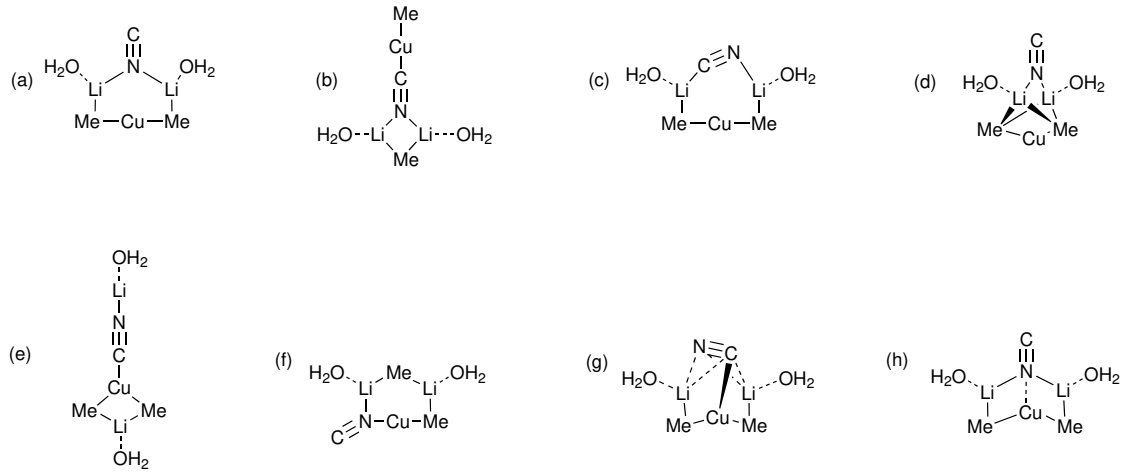

Figure 1.8: Calculated plausible structures of $(\mathrm{Me})_2\mathrm{Cu(CN)Li_2(H_2O)_2}$. In all basis sets (a) which is lower-order, is lowest in energy.[92]

1.4.6 Heterocuprates

Heterocuprates take the form RCu(Het)Li, where Het is a heteroatom or heteroatom-derived ligand. Heterocuprates gained attention because of the ability of the heteroatom derived ligand to function as a non-transferable or 'dummy' ligand. By using a heterocuprate, only one equivalent of the organic group per Cu is consumed. Given that the value of the organic group may frequently exceed that of all other components, it is imperative to avoid unnecessary loss of this group by formation of an unreactive organocopper species.

Posner introduced the phenylthio group (PhS^-) as a non-transferable ligand in 1973, where its stabilising effect upon tertiary alkyl cuprates was noted.[101] Much more recently, *in situ* synthesis at −50 °C provided X-ray quality crystals of monomeric $MeCu(SPh)Li(THF)_3$ (see Figure 1.9), and DOSY experiments confirmed the monomeric CIP structure to be retained in THF solution.[102] Posner cuprates have been largely superseded by alkyl(phosphido)- and alkyl(amido)cuprates; both are known for their thermal stability and reactivity. One solid state structure is known for the former class of cuprate: $MeCu(t Bu_2P)Li(THF)_3$,[103] the structure of which parallels the CIP structure known for $MeCu(SPh)Li(THF)_3$.

In addition to organo(phosphido)cuprates, there is a small body of work devoted to homoleptic lithium bis(phosphido)cuprates. Interest in these compounds stemmed from the desire to incorporate a spectroscopically active nucelus (^{31}P) into the cuprate unit. An unexpected structural motif was obtained when two equivalents of PPh_2H were treated sequentially with *n*BuLi and CuCN in toluene: an adamantane-style SSIP cuprate, $[Cu_4(PPh_2)_6][Li(THF)_4]_2$, crystallised at room temperature.[105] By contrast, when THF was employed as the reaction medium, the lower-order cuprate $[Ph_2PCuCNLi(THF)_2]$ was isolated, associating to give unusual $(CuPPh_2)_3$ rings which function as trigonal nodes in the extended structure. Changing the phospido ligand from Ph_2P^- to Cy_2P^- led to the isolation of a Gilman cuprate, $(Cy_2P)_2CuLi(THF)_2$, which displayed a chain-like polymeric structure. This polymeric motif had also been reported in the context of the structure of $(t Bu_2P)_2CuLi(THF)_3$, which was generated by the addition of $t Bu_2PCu$ to $t Bu_2PLi$.[106]

In comparison to alkyl(phenylthio)- and alkyl(phosphido)cuprates, there is greater interest in organo(amido)cuprates, due to the ready availability of amine precur-

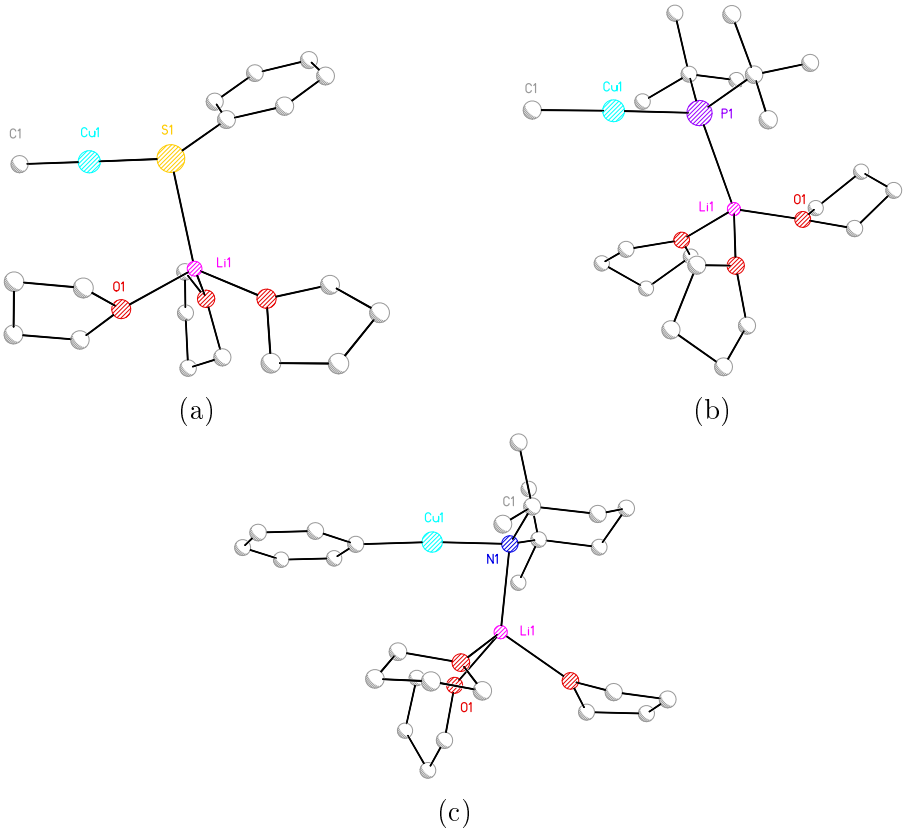

Figure 1.9: Examples of monomeric CIP heterocuprates (a) $MeCu(SPh)Li(THF)_3$,[102] (b) $MeCutBu_2PLi(THF)_3$[103] (c) $PhCuTMPLi(THF)_3$.[104]

sors and their ability to offer a way of introducing chirality through the backbone of the amido ligand. The solvated species MeCu(TMP)Li(TMEDA) and PhCu(TMP)Li$(THF)_3$ exist as CIP monomers,[104] whilst in the absence of coordinating solvent, aryl(amido)cuprates have been isolated as dimers in the solid state. $[MesCu(NBn_2)]_2$,[107] $[MesCuTMP]_2$[108] and $[MesCu(N(CH_2CF_3)(CH(CH_3)Ph))]_2$[109] all feature mono- or bis-η^6-coordinated Li centres, and this also featured prominently in the homocuprate $[Mes_2CuLi]_2$. In $[Mes_2CuLi]_2$, association is fulfilled by both η^6 and η^1 interactions (Figure 1.10). For these species, Schlenk-type equilibria were seen in solution, and individual aggregates could be separated on the basis of their ^{7}Li NMR chemical shifts, aided by inverse-detected ^{1}H-^{7}Li HOESY experiments. In all cases, the isomer determined by crystallography also dominated in solution, but measurable quantities of other isomers were present. In the case of $[MesCu(NBn_2)]_2$, deaggregation of the dimer upon introduction of THF could be monitored by NMR spectroscopy, suggesting a CIP monomer to be dominant in THF; this contrasted with the known propensity of homoleptic organocuprates to form SSIPs in this solvent.[110]

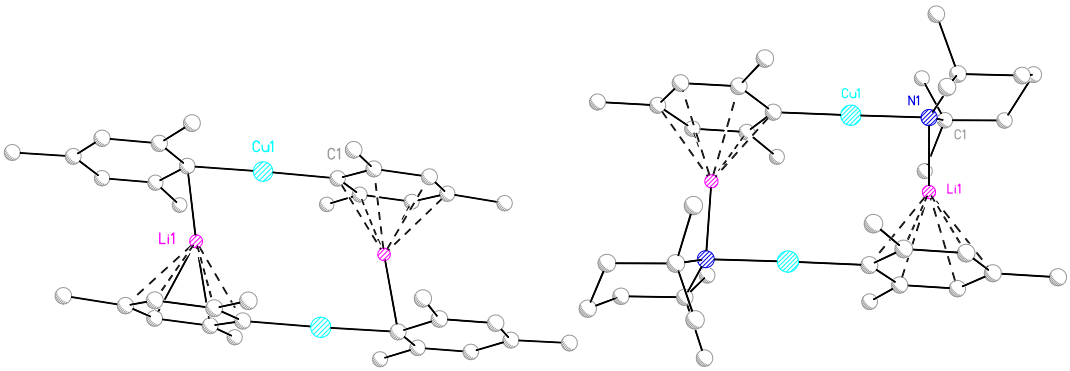

(a) (b)

Figure 1.10: Molecular structures of $[Mes_2CuLi]_2$[108] and $[MesCuTMP]_2$.[109]

Recently, bis(amido)cuprates, especially those bearing the cyclic amide TMP, have been the subject of interest for their ability to effect DoM (see Section 1.7). Prior to the development of TMP-based systems, bis(amido)cuprates have appeared fortuitously in the literature on a number of occasions. The reaction of lithiated secondary aromatic amines with copper salts has been reported to give rise to two cuprates of relevance. Hence, reaction of CuCl with three equivalents of Ph_2NLi in Et_2O allowed for the isolation of $(Ph_2N)_2Cu(Ph_2N)Li_2(OEt_2)$. This complex displays a near linear $(Ph_2N)_2Cu^-$ ion, contacted with two Li^+

ions which are themselves bridged by Ph_2N^- and coordinated by Et_2O (Figure 1.11). The steric bulk of the Li-bridging amide in this case apparently disfavours any further aggregation. Meanwhile, the reaction of a mixture of PhNHLi and MesNHLi in varying proportions with CuSCN led to the isolation of cuprate clusters whose size was influenced by the ratio PhNHLi:MesNHLi. Of greatest relevance, $[(MesNH)Cu(PhNH)Li(DME)]_2$ could be isolated when PhNHLi : MesNHLi = 0.65:1.75. Whilst this complex differs from $(Ph_2N)_2Cu(Ph_2N)Li_2(OEt_2)$ in being dimeric, the near linearity of cuprate unit and the solvation of the Li^+ cations persists (Figure 1.11).[111] Lastly, though the former two examples hint at the dominance of the CIP structures in amidocuprate systems, the use of the highly congested amide $(Ph_2MeSi)_2N^-$ has been reported to give rise to a SSIP structure in the solid state. The 2:1 reaction of $LiN(SiPh_2Me)_2$ and CuBr in Et_2O/THF afforded $[Li(THF)_4][Cu(N(SiMePh_2)_2)_2]$ as a crystalline solid, in which the typical linear geometry around Cu is once again enforced. Ostensibly by virtue of the steric congestion around the amide centres, solvation of Li^+ ions and aggregation are precluded.[112]

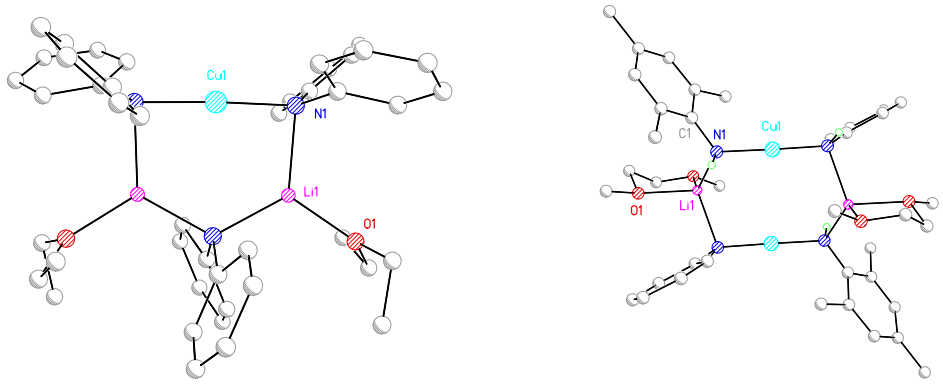

(a) (b)

Figure 1.11: Molecular structures of (a) $(Ph_2N)_2Cu(Ph_2N)Li_2(OEt_2)$ and (b) $[(MesNH)Cu(PhNH)Li(DME)]_2$, revealing CIP structures.[111]

1.5 The structures of organosilver and organoargentate compounds

Organosilver chemistry, which with a few notable exceptions[113] is confined to Ag(I) compounds, has been developed to a much lesser extent than organocopper chem-

istry. This is in no small part due to the low thermal stabilities of organosilver compounds. Hence, for example, simple alkylsilver compounds are highly susceptible to decomposition, generating metallic silver and coupled organic products;[114] consequently, limited data are available regarding their structures. Instead, insight into the structures of organosilver compounds has been gained through the synthesis of arylsilver compounds and their perfluorinated counterparts. Whilst the structure of phenylsilver, which is relatively stable in pure form,[115,116] remains unknown, the use of bulky or perfluorinated ligands has allowed for the isolation of crystalline species. Examples include Mes_4Ag_4[60] and $(C_6F_5)_4Ag_4$,[117] which both display the cyclic tetrameric motif well-known for organocopper compounds (see Figure 1.12). Cyclic aggregates are also known for silver derivatives of N-donor ligands, though these are less common. Amongst these, amides TMP_4Ag_4 and $HMDS_4Ag_4$[118] and the mixed amide-guanidinate aggregates $[Ag_2(\mu\text{-TAG})(\mu\text{-HMDS})]_2$[68] are known.

1.5.1 The structures of lithium argentate complexes

Unlike their copper congeners, well-defined lithium argentate complexes are rarely employed in synthetic chemistry and this reflects the higher costs of Ag(I) precursors and the lower thermal stabilities of argentates when compared to cuprates. Nonetheless, general interest in establishing trends amongst group 11 'ate complexes has resulted in the fabrication of a few examples of argentates[119] (and aurates).[120] For complexes characterised in the solid state, lower-order (two-coordinate) Ag prevails, and some degree of stabilisation is achieved through deployment of sterically congested ligands[121] or by intramolecularity.[119] SSIP and CIP structures are known, with the former type of association being characteristic for sterically congested complexes, as in $[((Me_3Si)_3C)_2Ag][Li(THF)_4]$ (Figure 1.13). Recently, van Koten reported the synthesis of the first homologous series of group 11 bromo- and cyano 'ate complexes $Ar_2M(X)Li_2$ (M = Cu, Ag, Au; X = Br, CN; Ar = $C_6H_4CH_2N(Et)CH_2CH_2NEt_2$-2) from reaction of the aryllithium with MBr and MCN.[119] For M = Cu, Ag and X = Br, these complexes could be characterised by X-ray diffraction, revealing a cyclic motif, in which the coordination sphere of Li^+ was completed by interaction with the pendant amine ligands (Figure 1.13a). Interestingly, some of the features of these six-membered metallacycles (in particular, the predilection for M to remain two-coordinate) are encountered in the

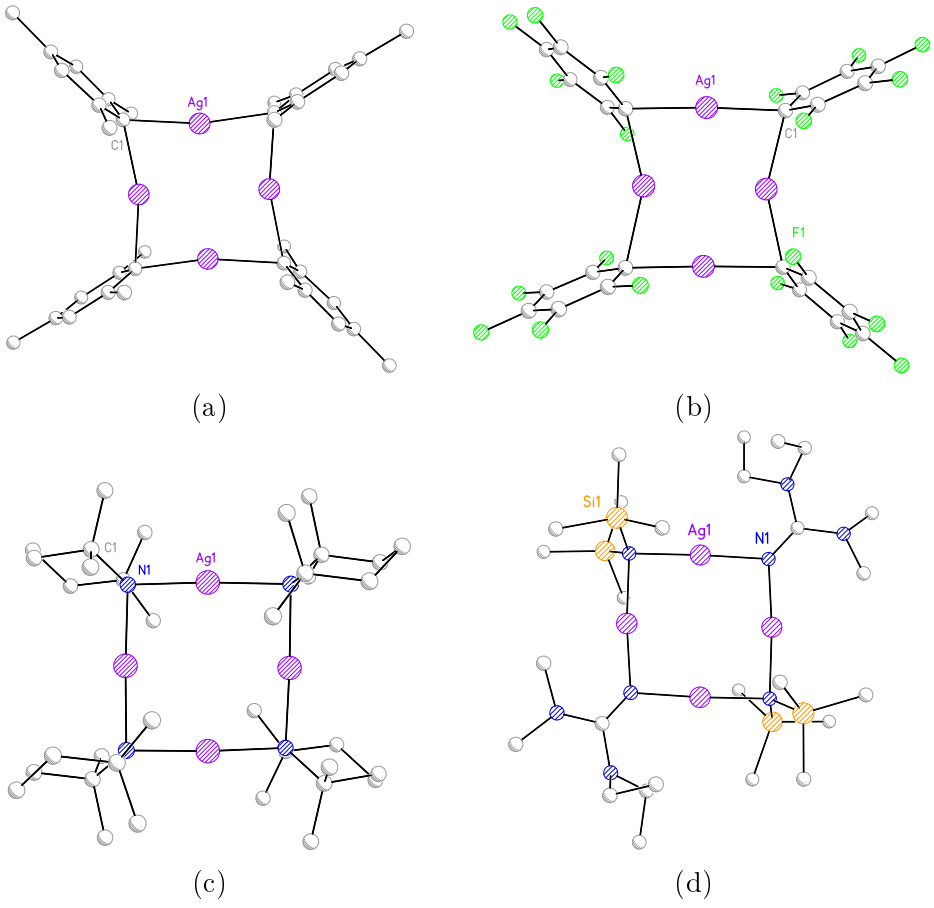

Figure 1.12: The molecular structures of (a) Mes_4Ag_4[60] (b) $(C_6F_5)_4Ag_4$[117] (c)TMP_4Ag_4[118] and (d) $[Ag_2(\mu\text{-TAG})(\mu\text{-HMDS})]_2$.[68]

related field of lithium amidocuprate chemistry (see section 1.7).

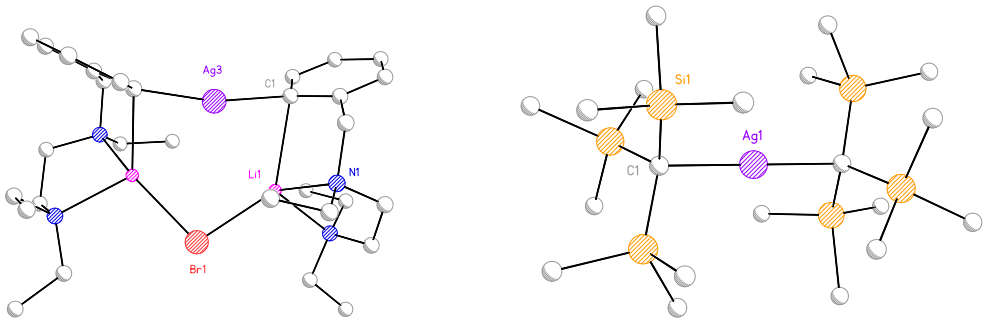

(a) (b)

Figure 1.13: The molecular structures of (a) $Ar_2Ag(Br)Li_2$ (Ar $=C_6H_4CH_2N(Et)CH_2CH_2NEt_2$-2)[119] and (b) $[((Me_3Si)_3C)_2Ag][Li(THF)_4]$,[121] with the cation omitted for clarity.

In spite of argentates being uneconomical reagents for synthesis, the opportunity to gain structural insights from solution measurements remains an excellent motivation for their study. Reports on the structures of lithium organoargentates in *solution* are not common, though spectroscopic data support the retention of cyclic aggregates in hydrocarbon media.[75] In particular, the nuclear properties of ^{107,109}Ag ($I = \frac{1}{2}$) have been exploited through NMR spectroscopic measurements, which have revealed coupling patterns consistent with a structure composed of alternating Ag and Li cations, bridged by organic anions (see also Section 1.4.4). Similarly, for $Me_2Ag(CN)Li_2$ – prepared by the 2:1 reaction of MeLi and AgCN in etherate solvent – the observation of pairs of doublets for the Me resonances by ^{13}C NMR spectroscopy provided direct evidence for the formation of $[Me_2Ag]^-$ ions.

Lastly, very few examples of lithium heteroargentates have been reported in the literature. In synthesis, a few references to lithium amidoargentates can be found; these include the use of 'higher-order' argentate 2DALi-AgCN to effect intramolecular Michael additions,[122] and the silver iodide mediated amination of allylic chlorides. The last of these is thought to proceed *via* the putative lithium bis(amido)-argentate $(HMDS)_2AgLi$.[123] The formation of crystalline heteroargentates has been reported when AgBr is reacted with $[(t\text{BuN})_3SLi_2]_2$ in THF. Only three of the four Li^+ could be replaced by Ag^+ and retention of the lithium halide by-product was found to occur. Most interestingly, the amount of LiBr retained in the product was found to depend upon the reaction time, with longer reac-

tion times leading to greater levels of LiBr sequestration. Hence, monomeric $\{(t\text{BuN})_3\text{S}\}_2\text{Ag}_3(\text{Br})\text{Li}_2(\text{THF})_2$ and dimeric $[\{(t\text{BuN})_3\text{S}\}\text{Ag}_3(\text{Br})\text{Li}_2(\text{THF})]_2$ and $[\{(t\text{BuN})_3\text{S}\}\text{Ag}_3(\text{Br})_2\text{Li}_3(\text{THF})_2]_2$ could be isolated (see Figure 1.14).

For the moment, heavier group 11 'ate complexes remain more of a curiosity rather than utility reagents. Due to the widespread use of lithium cuprates in synthesis, a considerably larger body of evidence has been gathered on the behaviour of organocuprates in solution, and significantly more attention has been devoted to exposing the pathways involved in the most common reactions of organocuprates.

1.5.2 Aspects of the reaction mechanisms of organocuprates

Organocuprates are most often employed in conjugate addition or nucleophilic substitution reactions. Calculations have been used to assess the reasons behind the enhanced reactivities of cuprates, as compared to organocopper compounds. The importance of including electron correlation in the calculation of molecular orbitals for MeCu and Me_2Cu^- has been demonstrated recently, showing that, in the case of Me_2Cu^-, the energy of the $3d_{xz}$ orbital is raised sufficiently to allow π-back donation to the π^* orbital of a olefinic or acetylinic substrate. In contrast, the $3d_{xz}$ orbital energies in MeCu were much lower, precluding significant electron donation to the same substrates. This offers an explanation for the much lower reactivities of RCu comapred to R_2CuLi.[124] Furthermore, cuprate-substrate interactions have been found to be geometry dependent: for dimethylcuprate, calculations at B3LYP/6311A/ /B3LYP/631A level have revealed that the linear $3d_{z^2}$ + 4s HOMO is well-poised to interact with the C−Y σ^* MO of an alkyl halide, yet bending of the Me_2Cu^- ion to $\theta = 113°$ resulted in a change of HOMO to the $3p_z$ + $3d_{xz}$ combination, which interacts favourably with an olefinic C−C π^* orbital (Figure 1.15).[125,126]

In recent years, a number of studies have shed light on the controversial topic of Cu(III) species, which are proposed to be key intermediates in both S_N2 reactions with alkyl halides and conjugate addition reactions. These studies have typically made use of low temperature NMR spectroscopy to detect reactive intermediates. In 2007, by using the technique of rapid-injection NMR spectroscopy at -100 °C, Bertz and Ogle were able to establish the generation of a tetracoordinate, square planar Cu(III) intermediate from the introduction of cyclohexenone

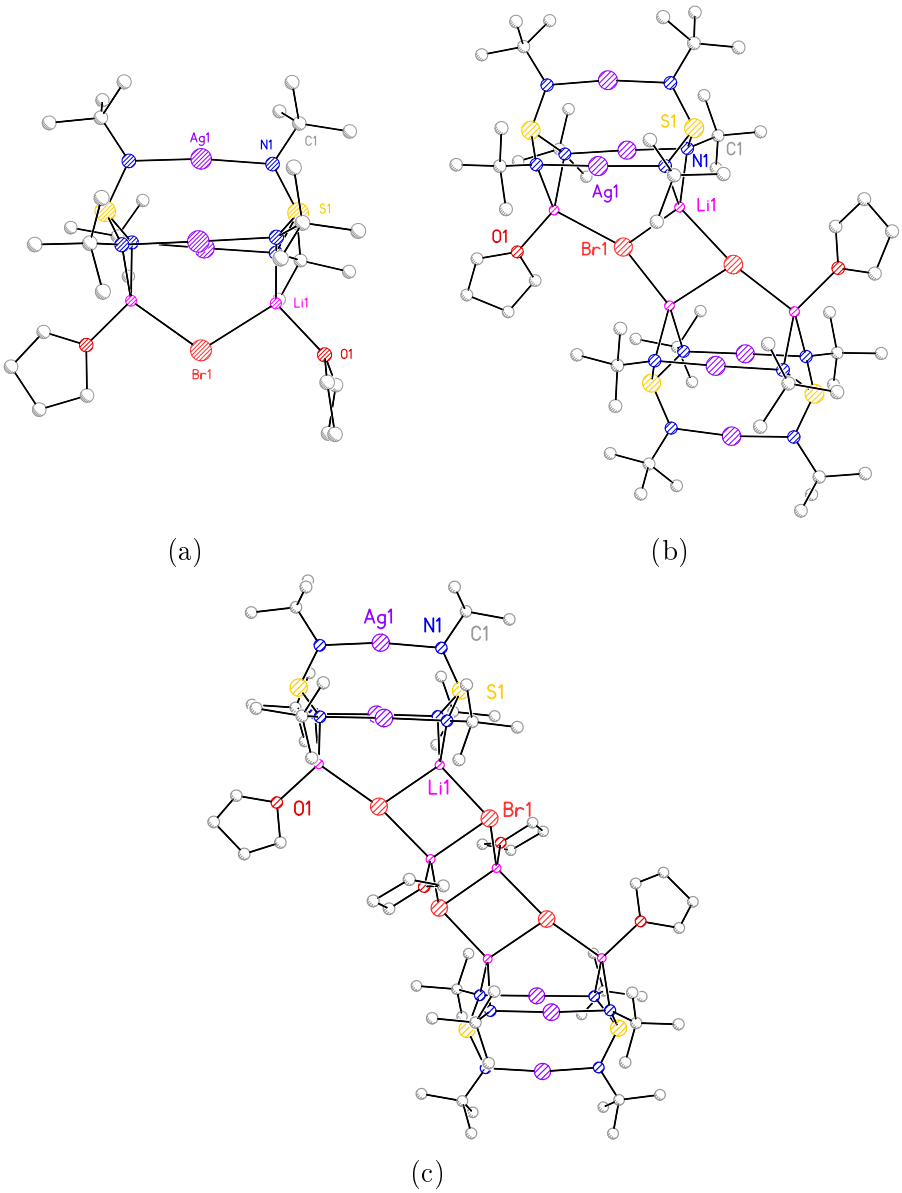

Figure 1.14: Examples of crystallographically characterised heteroargentate complexes (a) $\{(t\text{BuN})_3\text{S}\}_2\text{Ag}_3(\text{Br})\text{Li}_2(\text{THF})_2$ (b) $[\{(t\text{BuN})_3\text{S}\}\text{Ag}_3(\text{Br})\text{Li}_2(\text{THF})]_2$ and (c) $[\{(t\text{BuN})_3\text{S}\}\text{Ag}_3(\text{Br})\text{Li}_3(\text{THF})_2]_2$.

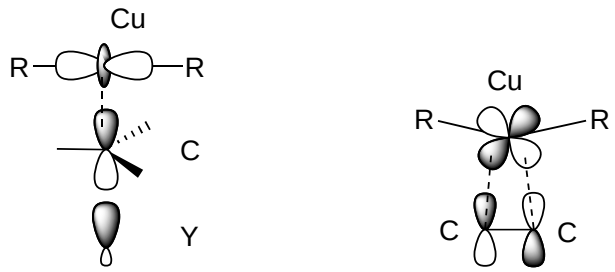

(a) (b)

Figure 1.15: Simplified illustrations of orbital interactions in Me_2Cu^-, showing (a) interaction of Me_2Cu^- with the C−Y σ^*-orbital of an alkyl halide and (b) back bonding interaction between Me_2Cu^- and a C−C π^*-orbital.

to $Me_2CuLi \cdot LiI$ followed by TMSCN or by reaction of $Me_2CuLi \cdot LiCN$ with TMSCl followed by cyclohexenone.[127] The prediction of a square planar intermediate was supported by theoretical studies of Snyder, who showed that the coupling constants for a tetrahedral intermediate were incompatible with those observed by Bertz and Ogle.[128] Not long after Bertz and Ogle's publication, Gschwind was able to demonstrate that similar species could be observed in the reaction of $Me_2CuLi \cdot LiCN$ with MeI.[129] A symmetrical, Me-containing species featured prominent in this work and was suggested (on theoretical predication) to be $[Me_4Cu][Li]$. Accordingly, Bertz and Ogle were able to prepare a series of tetracoordinate square planar intermediates by reaction of $Me_2CuLi \cdot LiX$ (X = I, CN, SCN or SPh) with EtI under low temperature RI-NMR conditions. Upon warming from -100 °C to -10 °C and re-cooling, a tetralkylcopper(III) species $[Me_3EtCu][Li]$ was seen to dominate.[130]

A small number of Cu(III) organometallic species have been characterised crystallographically, including simple homoleptic species, such as $[(CF_3)_4Cu]^-$,[131] and macrocylic species.[132] It must be stressed that the oxidation state of Cu in some of these complexes has been called into question. The bonding in $[(CF_3)_4Cu]^-$ was assessed by computational methods in 1995. Snyder was able to show that, in spite of the formal oxidation number +3, the d-orbital population is much closer to d^{10} than d^8 expected for a true Cu(III) species. The bonding in $[(CF_3)_4Cu]^-$ was calculated to be significantly ionic with small, but non-vanishing contributions from the Cu $d_{x^2-y^2}$ orbital to account for the square planar geometry.[133] These findings have recently been vindicated by spectroscopic measurements, which support the

notion of an inverted ligand field in $[(CF_3)_4Cu]^-$.[134]

The notion that a relatively unreactive, low polarity organometallic compound can be activated by the formation of a polar 'ate complex is of widespread significance: it implies that the formation of a heterobimetallic complex can fundamentally alter the mechanism of a reaction. This phenomenon has been exploited in development synergic bases.

1.6 Heterobimetallic bases

In the preceding section, the synthetic potential of organocopper compounds was presented through the formation of a reactive cuprate complex. The formation of the formally anionic $[R_2Cu]^-$ unit was presented as fundamental to this reactivity, as was the contacted nature of the $[R_2Cu]^-[Li]^+$ ion pair. The reactivity of the lithium cuprate, being so different from the highly reactive organolithium and the virtually unreactive organocopper compounds could be said to be *synergistic* in origin. Organocuprates are principally nucleophiles rather than bases, but the same principle – of modifying reactivity by combining two or more homometallic compounds to form a heterobimetallic system – can be applied equally well to bases. The field of bimetallic base chemistry has flourished over the past few decades, with some members of the family demonstrating truly remarkable deprotonative abilities. Two aspects of bimetallic base chemistry are of particular importance to aromatic chemistry: (1) the ability to metalate unactivated arenes and (2) the ability to *selectively* metalate activated arenes. The latter is tantamount to improving the chemo- and regioselectivity of DoM.

The ability of salts to alter the reactivity of organometallic bases has long been recognised. Lochmann-Schlosser superbase[135] (LiC-KOR) and Knochel's turbo-Grignard[136] reagent, notionally an adduct of Grignard reagent *i*PrMgCl and LiCl (*i*PrMgCl·LiCl), can be thought of as modifications of the two most well-known classes of polar organometallics – organolithiums and Grignard reagents. Whilst these reagents may appear simple in terms of composition, their structures are anything but! It is only very recently that LiC-KOR aggregates have been structurally characterised in the solid state. The use of solubilising neopentyllithium in combination with *t*BuOK afforded an alkane soluble compound which crystallised

as $Li_4K_4(CH_2(CH_3)_3)_{2.75}(OtBu)_{5.25}$. However, structure determination was complicated by both substitutional and positional disorder.[137] Similarly, attempts to isolate the turbo-Grignard iPrMgCl·LiCl by layering a THF solution of the base with Et_2O failed to produce the expected heterobimetallic compound, giving instead the open cubane $[i\text{PrMgCl(THF)}_2 \cdot \text{MgCl}_2\text{(THF)}_2]_2$.[138]

In order to gain insight into the structure-reactivity relationships that are key to the rational design of bimetallic bases, it is necessary to work with well-defined systems and particularly those which are amenable to X-ray analysis. Historically, the sterically hindered ligand TMP has been of special interest due its highly basic nitrogen center and its steric bulk.[139] The former property assists in the bridging of multiple metal centres whilst the latter property retards its reaction as a nucleophile and assists in the crystallisation of molecular species.[140]

1.6.1 Zincate bases

The first class of 'ate complexes to be used in DoM were zincates, beginning with putative zincate (TMP)ZntBu$_2$Li, in 1999. The facile and chemoselective DoZn of a range of aromatic esters, amides and nitriles, as well as a number of heteroaromatic substrates proved possible.[141] The structure of (TMP)ZntBu$_2$Li was not established at the time, but was characterised as the THF-solvate (THF)Li(μ-TMP)(μ-tBu)Zn(tBu) several years later by Mulvey, where the key features of a four membered ZnCLiN metallacycle and 'C−H···Li' agostic interactions were highlighted (Figure 1.16).[142] This structural motif was reproduced even more prominently in the compound EtZn(μ-Et)(μ-TMP)Li, where both intramolecular and intermolecular agostic interactions have been suggested.[143] These agostic interactions, which are not uncommon in main group 'ate chemistry,[144,145] are understood to be of predominantly electrostatic character.[146]

Zincate bases, containing both alkyl and amido groups, could concievably react *via* multiple pathways. Evidence from sodium zincate chemistry appeared to support alkyl basicity, as reaction of (TMEDA)Na(μ-tBu)(μ-TMP)Zn(tBu) with one equivalent of benzene resulted in the elimination of tBuH and formation of (TMEDA)Na(μ-C$_6$H$_5$)(μ-TMP)Zn(tBu). In this case, calculations supported the thermodynamic preference for alkyl basicity, though a two step mechanism, involving deprotonation by TMP, followed by alkyl-amido exchange, could not be ruled

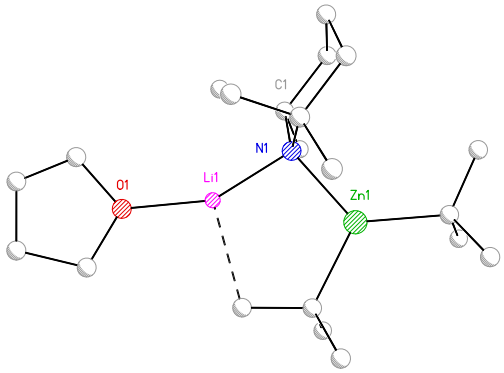

(a)

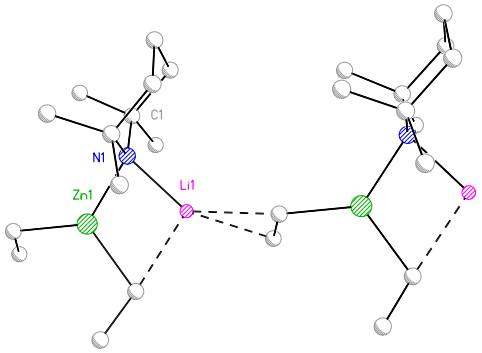

(b)

Figure 1.16: Examples of crystallographically characterised zincates (a) (THF)Li(μ-TMP)(μ-*t*Bu)Zn(*t*Bu)[142] and (b) EtZn(μ-Et)(μ-TMP)Li.[143]

out.[147] When reacted with *N,N*-diisopropylbenzamide, (TMEDA)Na(μ-*t*Bu)(μ-TMP)Zn(*t*Bu) and (TMEDA)Li(μ-*t*Bu)(μ-TMP)Zn(*t*Bu) were found to behave differently, with the latter reagent exhibiting dual alkyl/amido basicity.[142] However, using the related lithium zincate, (THF)Li(μ-TMP)(μ-*t*Bu)Zn(*t*Bu), dibasic behaviour in the DoZn of anisole resulted in the expulsion of only *t*BuH, with TMP retained in the metalated product.[148]

The issue of polybasicity was revisted by Uchiyama and Wheatley, when treatment of *N,N*-diisopropylnaphthamide with EtZn(μ-Et)(μ-TMP)Li in THF resulted in elimination of both TMPH and EtH. Calculations suggested a preference for kinetic amido basicity, where elimination of TMPH was followed by quenching of the pre-coordinated free amine with Et^- (Scheme 1.5). This raised the possibility of threefold reaction with a suitable aromatic substrate. When *N,N*-diisopropylnaphthamide was treated with EtZn(μ-Et)(μ-TMP)Li in THF, EtZn(μ-$C_{10}H_6C(O)N$*i*Pr_2-2)Li$(THF)_2$ was isolated and this was accompanied by the generation of TMPH and EtH (Scheme 1.6). Conversely, when less sterically demanding *N,N*-diisopropylbenzamide was deployed as the subtrate, threefold reaction was realised. Zn(μ-$C_6H_4C(O)N$*i*$Pr_2)_3$Li(THF) was isolated and characterised by X-ray diffractometry. Overall, these experimental data – especially the retention of Et^- in EtZn(μ-$C_{10}H_6C(O)N$*i*Pr_2-2)Li$(THF)_2$ – supported the theoretical prediction of kinetic amido basicity (Scheme 1.5).[143]

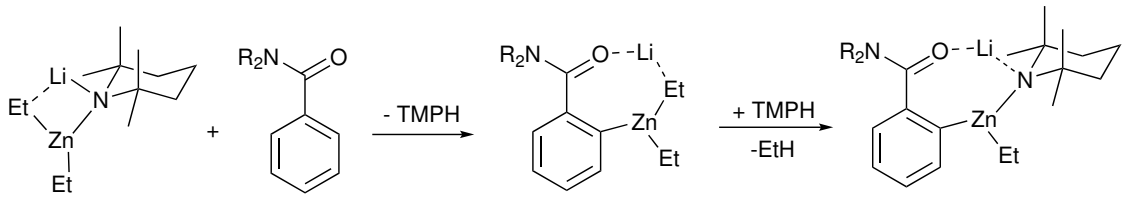

Scheme 1.5: Stepwise deprotonation of *N,N*-diisopropylbenzamide with EtZn(μ-Et)(μ-TMP)Li. Kinetic deprotonation by TMP^- is followed by TMPH/EtH exchange, which is thermodynamically favourable.[143]

Structural studies on a range of zincates and on bimetallic bases in general, have shown that the anionic ligands are σ-bonded to the less polarising metal in these complexes and so the term *alkali-metal-mediated metalation* has been applied to describe their reactions. Substitution of the alkali metal in these complexes can alter the overall polarity of the complex and give rise to more aggressive metalators, despite ostensibly retaining the same complex anion. However, as

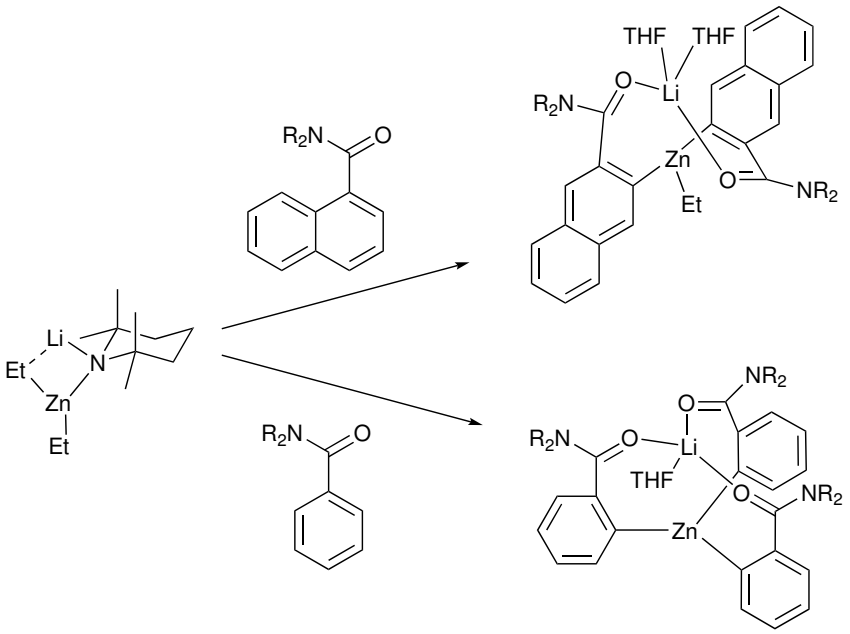

Scheme 1.6: Twofold *vs* threefold reaction of EtZn(μ-Et)(μ-TMP)Li with aromatic amides (R = *i*Pr). For the case of *N*,*N*-diisopropylnaphthamide, steric congestion prevents reaction of a third equivalent.[143]

a practical consideration, this must be balaced against the increased difficulty of handling heavier group 1 organometallics.[149,150] In the present case of zincates, switching from Li to Na permits the deprotonation of benzene by the base (TMEDA)Na(μ-*t*Bu)(μ-TMP)Zn*t*Bu, with overall elimination of *t*BuH.[147] Moreover, the ability of the zincate to stabilise otherwise highly unstable anions was demonstrated with the isolation of the α-deprotonated tetrahydrofuran in (TMEDA)Na(μ-TMP)(μ-C_4H_7O)Zn(CH_2SiMe_3). More remarkably, the use of (PMDETA)K(μ-TMP)(CH_2SiMe_3)Zn(CH_2SiMe_3) allowed for the deprotonation of the ethene, captured as (PMDETA)K(μ-TMP)(μ-CH=CH_2)Zn(CH_2SiMe_3) (Figure 1.17).[151]

1.6.2 Magnesiate bases

Organomagnesiate reagents have received relatively little interest until recently, and only a few examples of DoMg reactions have been reported. This may be due to fact that organomagnesium compounds are well-known to be poorly soluble in common solvents and generally react slowly, often requiring an excess of

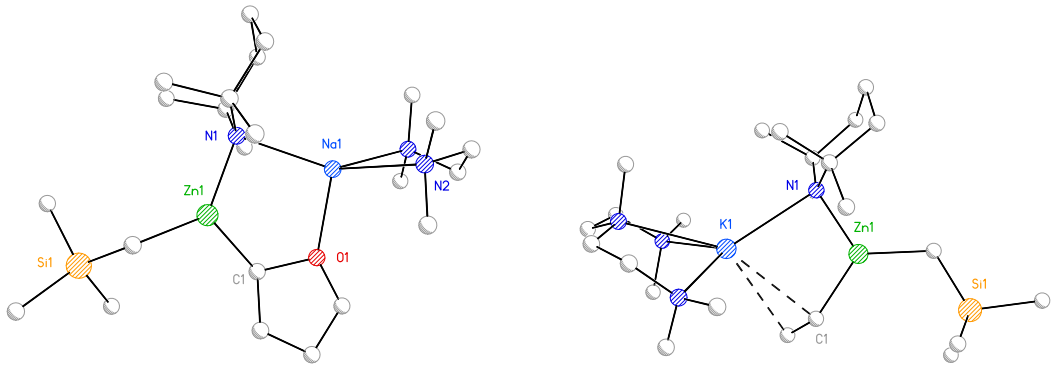

(a) (b)

Figure 1.17: The molecular structures of (a) (TMEDA)Na(μ-TMP)(μ-C_4H_7O)Zn(CH_2SiMe_3) and (b) (PMDETA)K(μ-TMP)(μ-$CH{=}CH_2$)Zn(CH_2SiMe_3).[151]

base.[152,153] That being said, Mongin has demonstrated the base Bu_3MgLi to be active in the DoMg of 3-fluoropyridines when combined in THF at −10 °C: treatment resulted in deprotonation at the 4-position. Modification of the base by the replacement of Bu^- by TMP^- to give $(TMP)_3MgLi$ allowed for the selective deprotonation of 3-fluoroquinolines at the 2-position, which could then furnish homocoupled biheteroaryl products upon treatment with I_2 (Scheme 1.7).[154] The same group were able to apply the mixed Bu/TMP bases to 2-chloro- and 3-chloropyridines, though the isolation of bipyridines when 4-chloropyridine was the substrate demonstrated the migratory aptitude of the arylmagnesiate in the sterically congested intermediate.[155]

Moving to more structurally focussed work, Mulvey has isolated remarkable examples of multiply deprotonated aromatics using sodium- and potassium magnesiate combinations. Hence, when a 1:1:3 molar ratio of *n*BuNa, nBu$_2$Mg and TMPH were combined in toluene or benzene, a 12-membered metallacycle bearing a $N_6Na_4Mg_2$ framework, with bridging TMP anions was formed and found to encapsulate the arenediide (Figure 1.18). The motif consisting of group 1/2 cations encapsualting a templating organic anion has been coined an 'inverse crown' complex, in reference to its similarity with the crown ether ligand, but with the Lewis basic oxygen atoms exchanged for group 1/2 cations.[156] Efforts to elucidate the active base in this reaction by adding TMEDA to the 1:1:3 mixture of *n*BuNa, nBu$_2$Mg and TMPH revealed that only two equivalents of TMPH were incorporated into the base, and it was confirmed that this species could

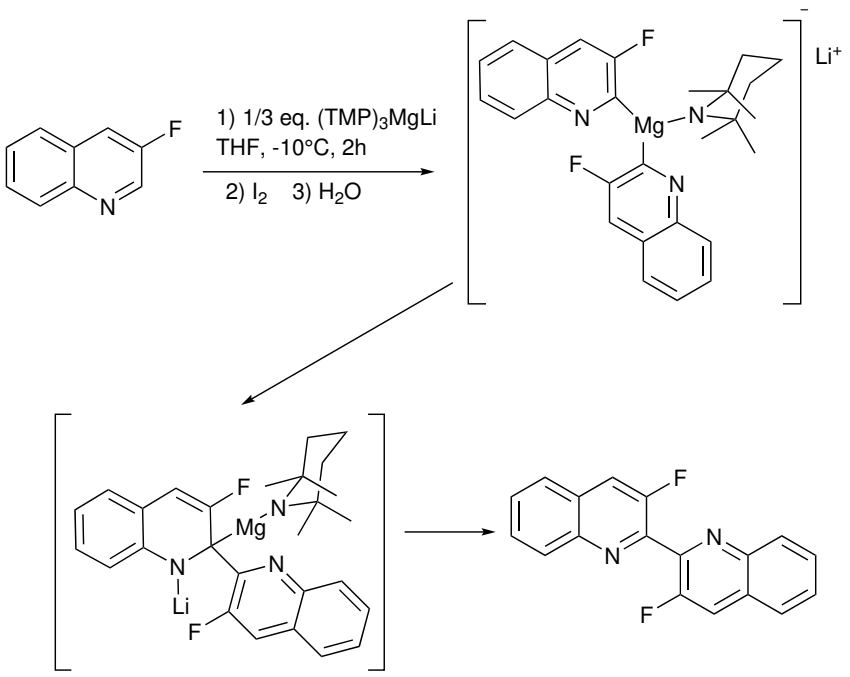

Scheme 1.7: Proposed mechanism for the coupling of quinolines *via* a magnesiate intermediate.[155]

deprotonate benzene, with (TMEDA)Na(μ-Ph)(μ-TMP)Mg(TMP) isolated as a crystalline species.[157] Switching the components of the bimetallic base to a mixture of nBuK, nBu$_2$Mg and TMPH, again in a 1:1:3 ratio, an even larger macrocycle was obtained, based upon a $[\mathrm{KNMgN}]_6^{6+}$ ring coordinating six phenyl anions.[158]

Returning to DoMg reactions, treatment of anisole with (PMDETA)K(μ-TMP)(μ-CH$_2$SiMe$_3$)Mg(TMP) led to the expected *ortho* deprotonated products. In this case, the reaction proceeded slowly enough to be monitored by NMR spectroscopy. This established TMP$^-$ basicity, generating the kinetic product, (PMDETA)K(μ-TMP(o-C$_6$H$_4$OMe)Mg(TMP) as an intermediate. Alkyl/amido exchange then gave (PMDETA)K(μ-TMP)(o-C$_6$H$_4$OMe)Mg(TMP), the thermodynamic product. Both the kinetic and thermodynamic product could be synthesised indepentedly and their NMR spectra were in accord with those obtained for the *in situ*-generated products.[159]

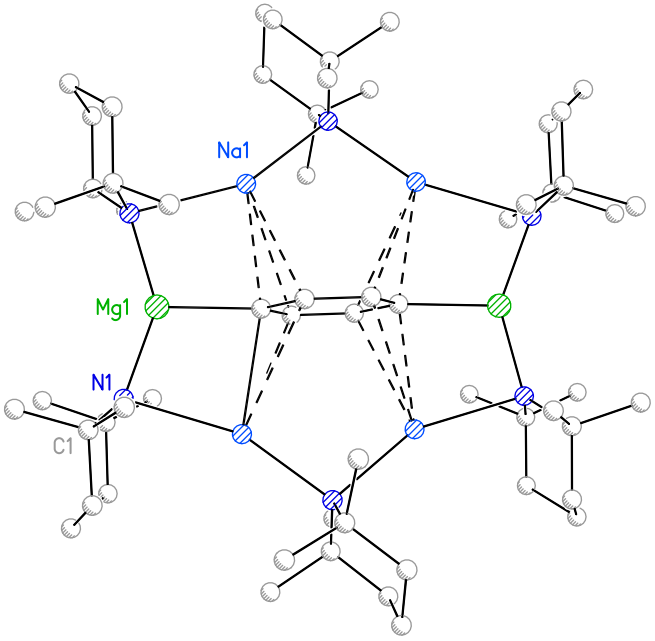

(a)

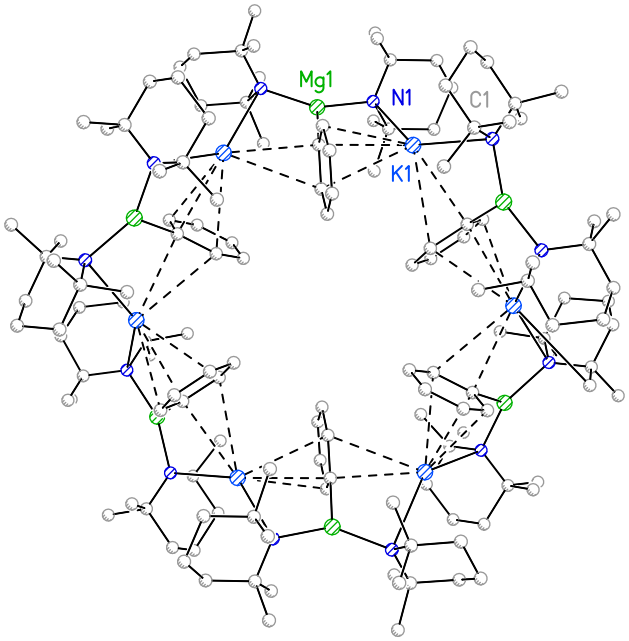

(b)

Figure 1.18: Examples of crystallographially characterised 'inverse crown' complexes (a) $TMP_6Mg_2Na_4(C_6H_4)$[156] and (b) $TMP_{12}Mg_6K_6Ph_6$.[158]

1.6.3 Aluminate bases

Studies into the utility of aluminate complexes for DoAl were initiated in 2004. When aromatic substrates bearing directing groups such as OMe, CN and C(O)NiPr$_2$ were treated with the aluminate base iBu$_3$Al(TMP)Li in THF, and then with D_2O or I_2, excellent yields of *ortho*-functionalised products were obtained. Notably, the bases were resistant to metal-halogen exchange reactions which were known to be problematic for more polar organometallic bases.[160] Characterisation of the aluminate base by X-ray crystallography followed not long after, confirming the CIP nature of the base and revealing that the mono-THF solvated molecules incorporated a four membered AlCLiN ring (Figure 1.19). Computational modelling indicated a preference for amido basicity over deprotonation by iBu group.[161]

Despite the successful deployment of aluminates, doubt has been cast on whether they represent the active bases when prepared in THF solution. When crystalline (THF)Li(μ-TMP)(μ-iBu)Al(iBu)$_2$ was redissolved in THF, it proved incapable of metalating anisole. DOSY experiments allowed for the identification of five species in solution formed when iBu$_3$Al and TMPLi were combined in d_8-THF; of these, only TMPLi appeared capable of metalating anisole, the lithiate being trapped by the Al centre. The sequestering of the *ortho* metalated anisole by Al offered an explanation for the high selectivity observed, since the less polar Al-C bond is not liable to further reaction prior to introduction of an electrophile (Scheme 1.8).[162] This case highlights the tendency of crystallography to elucidate the most thermodynamically stable (resting state) structures of bases, from which the active base may or may not be generated.

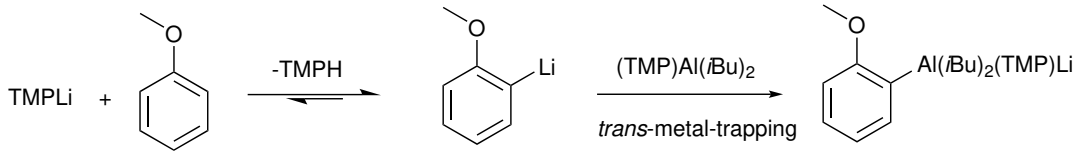

Scheme 1.8: Proposed mechanism for the alumination of anisole. Lithiation is executed by TMPLi, followed by *trans*-trapping by aluminium species. The compound LiTMP $\cdot$ Al(TMP)(iBu)$_2$ has been shown to exist as separate components TMPLi(THF) and Al(TMP)(iBu)$_2$ in solution.[162]

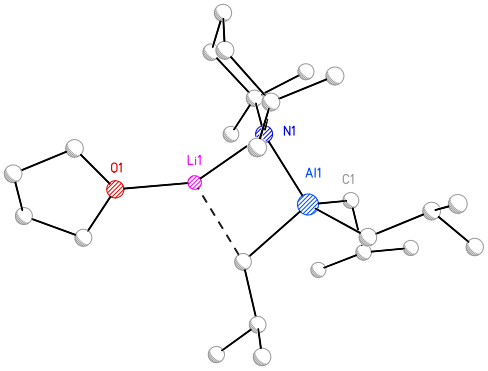

Figure 1.19: The molecular structure of (THF)Li(μ-TMP)(μ-iBu)Al(iBu)$_2$.[160]

1.6.4 Manganate bases

A few examples of lithium and sodium manganates have been synthesised and applied to the metalation of aromatic substrates. In the case of the lithium managnate (TMEDA)Li(μ-TMP)(μ-CH_2SiMe_3)Mn(CH_2SiMe_3), threefold basicity was observed upon treatment with ferrocene in a 2:3 base : ferrocene ratio.[163] Switching to sodium managanates, the di-deprotonation of benzene proved possible, with the generation of an inverse crown complex bearing a $Mn_2N_6Na_4^{2+}$ metallacyclic motif.[164] As is the case with magnesiates, the inverse crown structure is intimately associated with manganate chemistry. Although the potential for bimetallic bases to capture the highly unstable $C_4H_7O^-$ anion had been demonstrated with sodium zincate chemistry, the sodium manganate (TMEDA)Na(μ-TMP)(μ-CH_2SiMe_3)Mn(TMP) proved more aggressive: reaction with THF expelled O^{2-} as the inverse crown $Na_2Mn_2(TMP)_4O$ and encapsulated the butadienediide ion as {(TMEDA)Na(μ-TMP)}$_2${1,4-(Mn(TMP))$_2$-C_4H_4} (Figure 1.20).[165] This type of reaction highlights difficulties in achieving reaction control and possibly as a result of this, heterobimetallic manganate reagents have been developed to a lesser extent than other systems. They are also much more difficult to study by NMR spectroscopy, due to the paramagnetism of Mn(II).

1.7 Cuprates as bases

In Section 1.4.4, cuprates were presented as reagents for substitution and addition reactions. Given the general utility of the organocuprate species, it is a logical

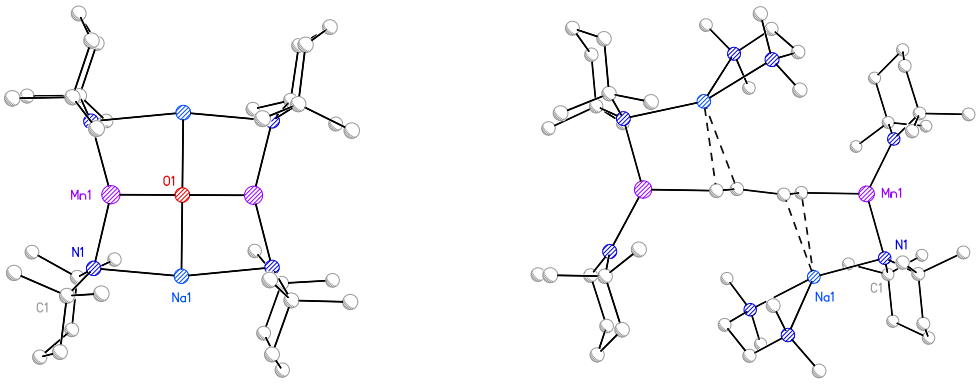

(a) (b)

Figure 1.20: Manganate encapsulated fragments from the break up of THF. (a) $Na_2Mn_2(TMP)_4O$ and (b) $\{(TMEDA)Na(\mu\text{-}TMP)\}_2\{1,4\text{-}(Mn(TMP))_2\text{-}C_4H_4\}$.[165]

extension to ask whether an organocuprate may be synthesised directly from a cuprate base, rather than by transmetalation of an organolithium and a copper(I) salt? In a similar fashion to other 'ate complexes, it might be expected that greater reactivity and chemo/regioselectivity will ensue.

The terms 'Gilman'[166] and 'Lipshutz'[104,167] are used to refer to distinct structure-types within the area of cuprate base chemistry. Those of the form R_2CuLi are known as 'Gilman cuprates'. Cuprate bases incorporating LiCN in addition to the fundamental R_2CuLi unit have been coined 'Lipshutz cuprates', notwithstanding that the CN^- ion is now understood to be bonded in a different manner to that originally suggested by Lipshutz. Additionally, homologous cuprates bearing the key features of Lipshutz structures, but lacking CN^- have been termed 'Lipshutz-type cuprates' (see Figure 1.21).[166,168]

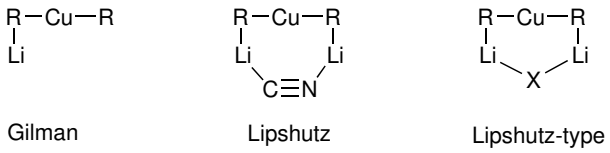

Figure 1.21: Definition of amidocuprate structure-types. R = organyl *or* amido, X = halide.

1.7.1 TMP-cuprate bases for DoCu

Given the success of TMP-zincate bases in DoZn, TMP was deemed a suitable ligand for the fabrication of cuprate bases. These were designed with the functionalisation of aromatic compounds in mind. This idea was first addressed in 2007 with the advent of directed *ortho* cupration.[167] Amido and organo(amido)cuprates synthesised from CuCN or CuI were chosen as suitable reagents for screening with the model substrate benzonitrile. In the case of CuCN, it proved possible to characterise the bis(amido)cuprate $(TMP)_2Cu(CN)Li_2(THF)$ crystallographically, revealing a dimeric Lipshutz structure where CN^- was incorporated into the seven membered metallacycle (Figure 1.22). In this structure, cyanide abstains from interaction with Cu, which remains two-coordinate (lower-order); as such, it provides good evidence for the lower-order nature of cyanocuprates generally, as predicted by Snyder (see also Section 1.4.5).[92]

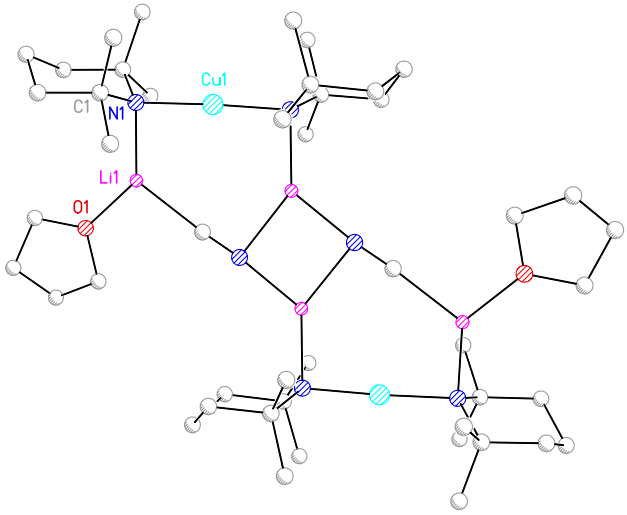

Figure 1.22: The molecular structure of $[(TMP)_2Cu(CN)Li_2(THF)]_2$.[167]

It was noted that at least one TMP ligand was needed for good yield and chemoselectivity, though a range of alkyl groups (or another TMP) as the second ligand were tolerated. Excellent yields in DoCu were observed with PhOMe, PhCN, $PhC(O)NiPr_2$ derivatives and several heterocycles, when cupration was followed by quenching with I_2 (Table 1.1). In addition, a range of electrophiles could be successfully deployed in the cuprate system whilst maintaining consistently high yields (Scheme 1.9). With their being a precedent for R-group coupling in alkylcuprates, it was expected that introduction of an oxidising agent would give

Table 1.1: Screening of lithium cuprates for activity in the *ortho* iodination of benzonitrile. Isolated yields.[167]

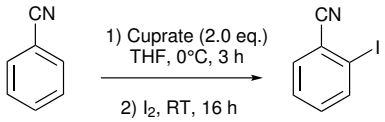

Entry	Cuprate	Yield (%)	Entry	Cuprate	Yield (%)
1	TMPCu(CN)Li	0	6	$(TMP)_2Cu(CN)Li_2$	74
2	$(TMP)_2CuLi \cdot LiI$	0	7	$MeCu(TMP)(CN)Li_2$	91
3	$MeCu(TMP)Li \cdot LiI$	51	8	nBuCu(CN)(TMP)Li_2	83
4	$MeCu(CN)(NMe_2)Li_2$	0	9	tBuCu(CN)(TMP)Li_2	70
5	$MeCu(CN)(NiPr_2)Li_2$	53	10	$PhCu(CN)(TMP)Li_2$	93

coupled products. This was realised, when *N,N*-diisopropylbenzamide was treated by $RCu(TMP)(CN)Li_2$ (R = Me, Ph) or $(TMP)_2Cu(CN)Li_2$ followed by addition of nitrobenzene. For unsymmetrical cuprates, cross-coupled products were obtained, whereas a homocoupled biphenyl was generated in 100 % yield when the symmetrical bis(TMP) base was deployed (Scheme 1.10).

1.7.2 Gilman and Lipshutz-type cuprates – differences in reactivity

Following the establishment of DoCu as a viable route to *ortho* functionalisation of aromatic compounds, a duel crystallographic and computational approach was taken to elucidate the reactive base in these systems.[104] Accordingly, treatment of CuCN with THF solutions of PhLi and TMPLi permitted the isolation of cyanide-free Gilman cuprate, $PhCu(TMP)Li(THF)_3$. Modification of the solvent system to include TMEDA and replacing PhLi with MeLi gave the analogous Gilman cuprate MeCu(TMP)Li(TMEDA), where once again, the failure to incorporate cyanide was noted. Seeking to establish whether or not LiCN played a decisive role in DoCu, solutions prepared from pre-isolated MeCu(TMP)Li(TMEDA) and of MeCu(TMP)Li(TMEDA) in which LiCN was present as a by-product were tested in reaction with *N,N*-diisopropylbenzamide. These metalated intermediates

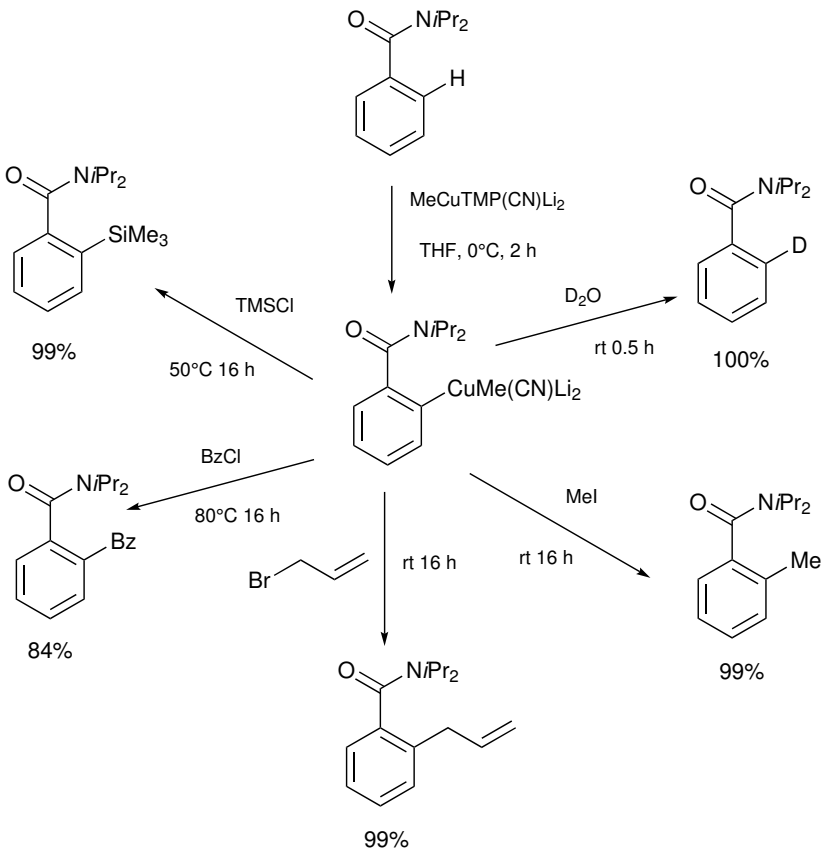

Scheme 1.9: A survey of the transformations achievable through the DoCu of *N,N*-diisopropylbenzamide, followed by quenching with electrophiles.[167]

were quenched with I_2 to give *ortho*-iodinated products. Only the solution known to contain LiCN gave acceptable yields (89 % *vs* 37 % for *in situ* prepared and pre-isolated MeCu(TMP)Li(TMEDA), respectively).

Calculations of the Lipshutz-Gilman equilibrium for a simplified system were undertaken (B3LYP level with SVP basis set for Cu and 6-31+G for other atoms).[104] Results showed a facile equilibrium in the case of the organo(amido)cuprates, but indicated that the equilibrium should be dominated by the Lipshutz-type cuprate for the bis(amido)cuprate. This was in accord with the crystalline material isolated in this (and prior) studies. Intuitively, this can be understood in terms of the greater bridging ability of the amido ligand when compared to carbanionic ligands.

The low reactivity of Gilman cuprate bases was verified in subsequent studies, which showed pre-isolated Gilman cuprate $(TMP)_2CuLi$ to be completely unreac-

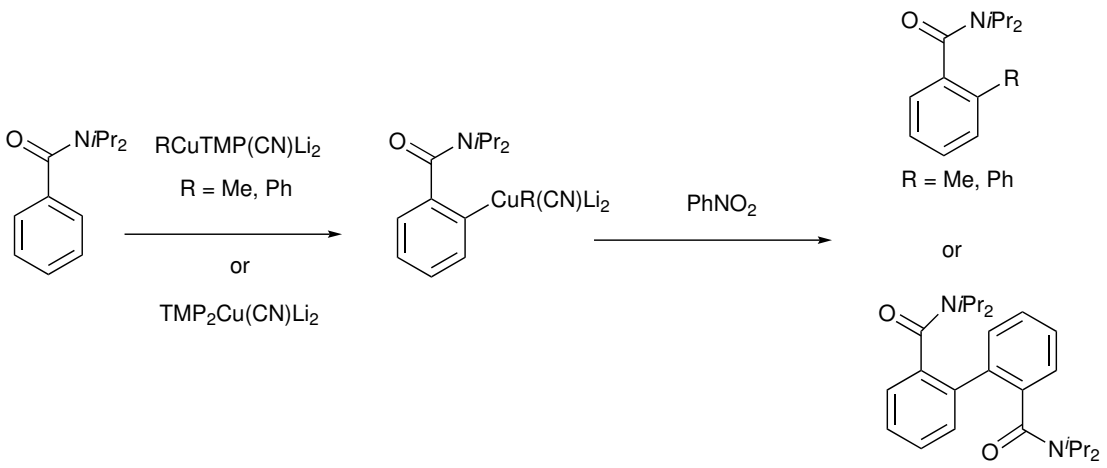

Scheme 1.10: Treatment of *N,N*-diisopropylbenzamide with cuprate base followed by $PhNO_2$ gave cross-coupled and homocoupled products, respectively.[167]

tive towards aromatic substrates, lending weight to the necessity of Lipshutz-type formulations for reactivity. It proved possible to isolate a Lipshutz-type cuprate, $(TMP)_2Cu(I)Li_2(THF)$ (Figure 1.23), from reaction of CuI with TMPLi in the presence of limited quantities of THF. In contrast to the results obtained using $(TMP)_2CuLi$, high reactivity was observed when $(TMP)_2Cu(I)Li_2(THF)$ was introduced to *N,N*-diisopropylbenzamide.[166] Overall, it became clear that the inclusion of lithium salts generally, rather than CN^- was key for reactivity.

Returning to organoamidocuprate systems, DFT calculations examined several plausible reaction pathways. Deprotonation by an amido ligand of a Gilman monomer was found to be favoured; however, calculations suggested that this species was likely to be accessed from a Lipshutz-type starting material. On the other hand, deprotonation by an alkyl ligand was disfavoured, as was quenching of liberated amine by an alkyl moiety. Deprotonation by a Gilman dimer was found to have a high activation energy and did not represent a favourable reaction pathway, supporting the experimental findings.[104]

Shorty thereafter, the utility of Lipshutz-type cuprate bases as applied to azafluorenone synthesis was investigated.[169] When employed in the deprotocupration-aroylation of heterocycles, it proved advantageous to supplement the cuprate mixture with TMEDA, a strategy designed to promote solubilisation of LiCl. This was necessary to promote formation of Lipshutz-type cuprates. A number of pyridines, quinolines and thiophenes could be deprotocuprated and reacted with aroyl chlo-

rides to give funtionalised heterocycles in moderate to good yields. Palladium-catalysed ring closure could then be used to generate azafluorenones, a class of compounds of interest due to their occurrence in natural products and medicinal compounds (Scheme 1.11). Seeking to gain further structural insights into CuCl-derived cuprates, reaction of TMPLi with CuCl in toluene/THF was undertaken. Recrystallisation from toluene afforded $(TMP)_2Cu(Cl)Li_2(THF)$ as a crystalline product which analysed as a dimer in the solid state. Aside from slight differences in the disposition of the solvated Li^+ ions with respect to the metallacyclic core, the structures were congruent with CN^- and I^- containing Lipshutz-(type) cuprates.[104,167]

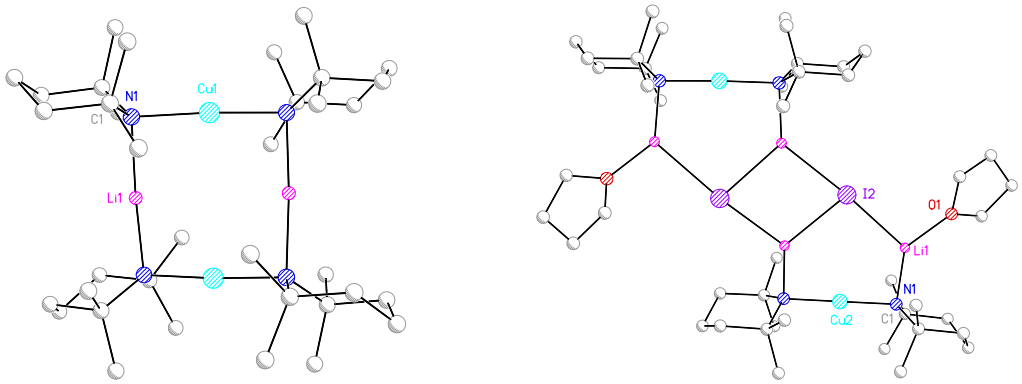

(a) (b)

Figure 1.23: The molecular structures of (a) $[(TMP)_2CuLi]_2$ and (b) $[(TMP)_2Cu(I)Li_2(THF)]_2$.[104]

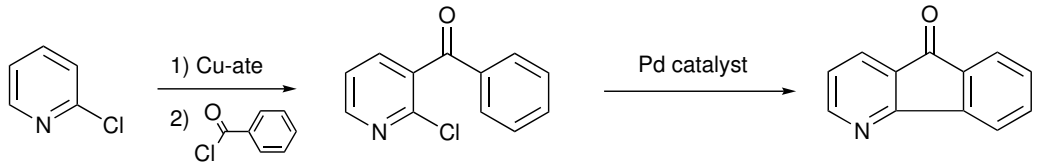

Scheme 1.11: The synthesis of an azafluorenone *via* Pd-catalysed ring closure. The ketones were synthesised by DoCu, followed by quenching with benzoyl chloride. Cu-ate = $(TMP)_2Cu(Cl)Li_2$/TMEDA.[169]

1.7.3 DMP based systems – the advent of adduct cuprates

Once the efficacy of bis(TMP) cuprate systems had been established, the question of whether other sterically demanding amides could take the place of TMP

whilst maintaining high reactivity naturally arose. Given the expense of TMPH, there was an obvious economical imperative to do so. Focus switched to *cis*-2,6-dimethylpiperidine as a precursor. The ability of DMP to assume the structural role of TMP in bimetallic systems had been examined previously in the context of zincates and magnesiates. In these systems it was found that DMP was significantly less sterically hindered than TMP – its behaviour being more akin to that of *N*,*N*-diisopropylamide.[170]

Returning to cuprate systems, when DMPLi was reacted with CuCl in a 2:1 ratio in Et_2O, an unprecedented cuprate structure was obtained.[171] Instead of the expected Gilman or Lipshutz-type structures, the crystalline material was found to consist of a pentametallic complex, $[(DMP)_2CuLi(Et_2O)]_2LiCl$ with two $(DMP)_2CuLi$ units encapsulating one unit of LiCl. This could be viewed as an adduct of Gilman and Lipshutz-type monomers, in which two of the three Li^+ are mono-solvated by Et_2O and the third is unsolvated and bridges two $(DMP)_2CuLi$ units together. This contrasts with the behaviour observed in Lipshutz-type bis(amido)cuprates, in which there are no direct bridges between the cuprate units in the dimer; instead the monomeric units are linked *via* $(LiX)_2$ ($X = Hal^-$, CN^-) only. Adduct cuprates were also obtained when CuBr and CuI were used as starting materials and in the presence of Et_2O, though limited quantities of Et_2O were necessary for the case of X = I. The resulting complexes were isostructural except for changes in the Li−X and N−Li bond lengths, which reflected competing stabilisation of Li^+ by softer and harder halide anions, respectively.

Seeking to establish whether the formation of an adduct structure was imposed by solvent conditions or steric requirements of the amido ligand, TMPLi was combined with CuX ($X = Hal^-$, CN^-) in a 2:1 ratio before Et_2O was introduced. This time, Lipshutz-type cuprates were isolated rather than adduct cuprates, thus ruling out Et_2O as the driving force for adduct formation. Suspecting now that the reduced steric bulk of the DMP was a key factor, DMPLi was combined with CuBr in a 2:1 ratio in the presence of THF. As expected, the crystalline material revealed an adduct motif in the solid state, though the solvated Li^+ ions accommodated two THF per Li, ostensibly facilitated by the reduced steric demand of the cyclic ether when compared to Et_2O.

The influence of steric factors could be understood intuitively in terms of the orientations adopted by the TMP and DMP ligands. As both ligands are derived

from a piperidine ring, a vector drawn from the N1 atom to the C4 atom describes the orientation well. When this vector is co-parallel with Cu→N, the ligand is termed *endo* with respect to the metallacyle and if Cu→N is perpendicular, the ligand is termed *exo*. For the bis(TMP) cuprates, in both Lipshutz-type and Gilman structure-types, the TMP ligands were observed to lie *endo,endo*. This orientation could be rationalised by noting that steric repulsion between TMP-Me_{ax} is minimised, and that the 'core' of the metallacyle is relativelty unhindered, so that the equatorial methyl groups do not repel significantly. Conversely, in DMP-cuprates, DMP lacks axial methyl groups, but the 'core' of the metallacyle is more sterically crowded, so the ligands prefer to orientate themselves *exo,exo* (Figure 1.24).

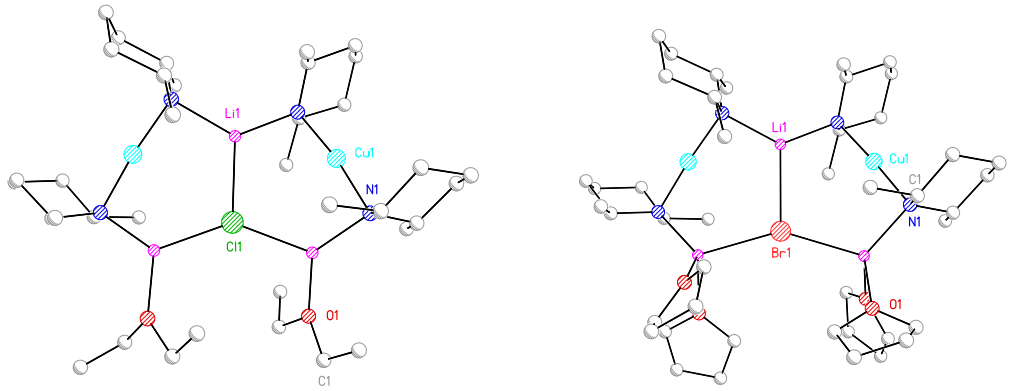

(a) (b)

Figure 1.24: The molecular structures of (a) $[(DMP)_2CuLi(Et_2O)]_2LiCl$ and (b) $[(DMP)_2CuLi(THF)_2]_2LiBr$.[171]

Having established that DMP cuprates could complex lithium halides, the system was screened for activity in DoCu against the model substrate *N,N*-diisopropylbenzamide. Employing conditions expected to favour the formation of adduct cuprate, both *in situ* formed cuprate and pre-isolated $[(DMP)_2CuLi(THF)_2]_2LiBr$ were reacted with the benzamide in THF. Comparable product yields were obtained after quenching with iodine (80 % and 82 %, respectively).

In a similar vein to prior work with Lipshutz-type cuprates, calculations were undertaken to assess the interconversion of Lipshutz-type, adduct and Gilman cuprates using a simplified ligand set of NMe_2^- in place of DMP and Me_2O in the place of Et_2O. The results proved somewhat inconclusive in that the free energy changes associated with the conversion of Liphutz-type cuprate to adduct

cuprate, and then from adduct cuprate to Gilman cuprate were rather small; one could easily appreciate that steric factors, which were not accounted for by the DFT modelling, could tip the balance in favour of any one of the three structure-types. DFT also predicted that adduct cuprates could be an energetically viable source of Gilman monomers, which were exposed as the likely reactive base in alkyl(amido)cuprate systems in prior work (Scheme 1.12).[166]

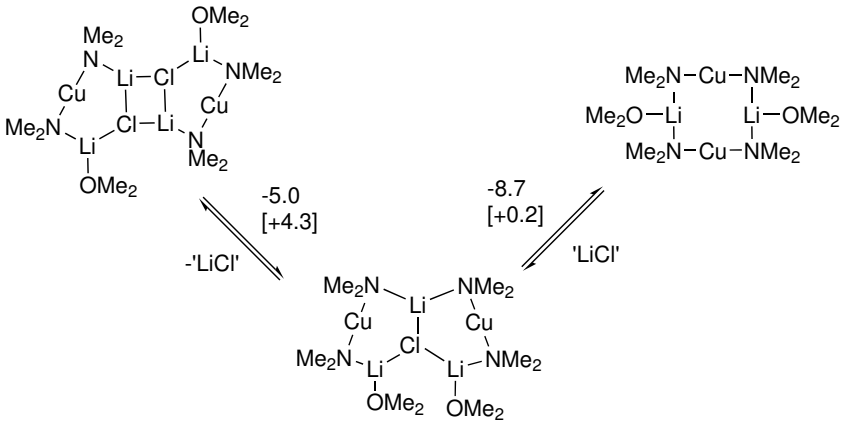

Scheme 1.12: Calculated ΔE and [ΔG] in kcal mol^{-1}. 'LiCl' = $\frac{1}{4}$ [LiCl · OMe_2]$_4$–OMe_2.[171]

1.7.4 New directions in DoCu – towards the catalytic use of cuprates

There is a burgeoning desire to improve the environmental impact and sustainability of chemical processes in general, by increasing atom efficiency, and reducing the emission of toxic waste.[172] Examples of ways in which this can be achieved include adapting transition metal-based systems to the catalyic regime and the use of earth abundant, environmentally-benign main group catalysts.[173–175] Recent advances in the applications of DoCu to the synthesis of *ortho* functionalised phenols and anilines have highlighted some of these issues, where both the chemo- and regioselective properties of DoCu and the redox chemistry of copper have been exploited. Deprotonation of *N,N*-diisopropylbenzamide with $(TMP)_2Cu(CN)Li_2$ in THF, followed by the introduction of ROOH (R = *t*Bu, cumyl) or $RONH_2$ (R = *t*Bu, Bn), gave *ortho* substituted phenols or anilines in high yields (Scheme 1.13).[176] However, performing the deprotonation with $t Bu_2$(TMP)ZnLi followed by treatment

with *t*BuOOH failed to give any phenolic product at all, confirming that a redox process involving copper was operating. Most excitingly, it was possible to employ copper in catalytic quantities in the presence of a zincate base. The advantages of this are manifold: not only is the requirement for toxic CuCN reduced, but the use of the zincate base in place of the cuprate brings with it a cost benefit[i] and has the potential to improve atom economy (TMP-zincates can exhibit polybasicity, see Section 1.6.1).[143]

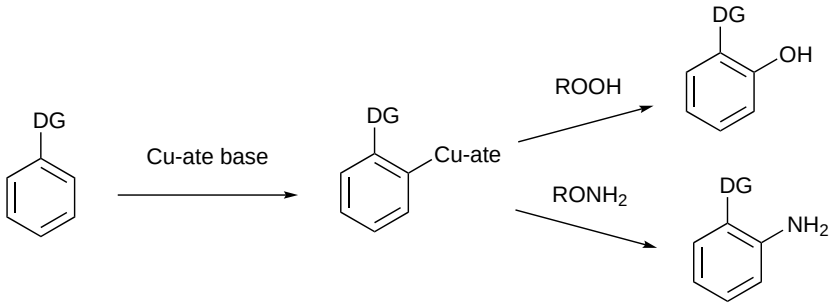

Scheme 1.13: Synthesis of *ortho* functionalised phenols and anilines using DoCu methodology. Cu-ate = $(TMP)_2Cu(CN)Li_2$.[176]

[i]At the time of writing, the price of zinc and copper are *ca.* £2600 and £5600 per ton, respectively.

Chapter 2

Aims

The aims of the work presented in this thesis may now be set out in context. Lithium bis(amido)cuprates will be the main focus of study, while initial attepts at the fabrication of lithium bis(amido)argentates will also be made. Lithium bis(amido)cuprates provide an entry point to aromatic cuprate chemistry, which is of widespread interest to the synthetic community. The work set out in this thesis will follow a dual focussed approach. First, practical improvements to the existing suite of cuprate bases will be attempted through the deployment of different amide ligands and Cu(I) salts. Attention will be devoted to the use of less expensive amines as precursors to amidocuprates and to the deployment of less toxic copper salts. Second, a deeper understanding of the structures of bis(amido)cuprates in the solid state and in solution will be sought, using X-ray diffractometry and NMR spectroscopy as the principal tools of investigation.

Two aspects of lithium cuprate base chemistry in particular are open to improvement: reagent cost and reagent toxicity. These are both practical considerations and addressing these issues will make cuprate bases more attractive to synthetic chemists. One way in which the first of these issues can be tackled is through investigation of amide ligand precursors other than TMPH (which is relatively expensive)[i]. The discovery of reactive adduct cuprates derived from less costly DMPH has gone some way to achieving this.[171] However, there is still considerable scope for exploration. In particular, the related inexpensive amines 2-methylpiperidine and piperidine are worthy of investigation, since close parallels may be drawn

[i]At the time of writing, the cost of TMPH is £2.80 g^{-1} (Sigma Aldrich)

with previously characterised examples.[171] A novel approach to introducing these new ligands would be through the formation of heteroleptic bis(amido)cuprates. Generally, DoCu calls for a cuprate base to be reacted with an aromatic substrate in a 1:1 ratio. The aryl(amido)cuprate that results from this reaction retains one amide ligand. Thus, one of the amide ligands in the bis(amido)cuprate would function as a dummy ligand (see Section 1.4.6) and could, for example, provide a means of introducing chirality to the complex. In addition to the ecomonic benefit that comes with the use of cheaper, less sterically hindered amides, valuable insight into the influence of steric factors upon the structures of the resulting bis(amido)cuprates could be gained.

A second variable in cuprate base chemistry is the choice of Cu(I) precursor. This has an important bearing upon the safety of the resulting cuprate systems and has been shown, on several occasions, to influence the reactivity of cuprates.[177] In particular, copper(I) cyanide produces excellent results in synthesis.[167] However, its use brings with it the risk of generating highly toxic HCN. Copper(I) halides have also been investigated in TMP- and DMP-based systems and have demonstrated efficacy. However, the most synthetically useful copper halide, CuCl,[168] is somewhat air-sensitive. Clearly, this is not an exhaustive list of copper(I) precursors and work presented herein will seek to extend cuprate systems to incorporate triatomic anions such as thiocyanate (SCN^-) and cyanate (OCN^-). These two related anions are of particular interest since cyanate might be regarded as the 'harder' analogue of thiocyanate and so this pair of ions should provide interesting points of contrast in terms of structure and chemistry.

Lastly, work will seek to advance our understanding of amidocuprate systems in solution. TMP-cuprates are amenable to study due to the large body of literature surrounding their solid-state structures. However, an alternative avenue of interest is the development of lithium bis(amido)argentate chemistry; as silver possesses two $I = \frac{1}{2}$ nuclei, it introduces one further NMR 'handle' to TMP-based systems. Thus, initial attempts will be made to prepare lithium bis(amido)argentates, by adapting the synthetic methods which have been developed for lithium bis(amido)cuprates over the past decade.[166–169,171] Returning to lithium cuprates, studies will aim to shed light on the behaviour of TMP-cuprates in solution, making extensive use of NMR spectroscopy. Calculations have suggested the importance of monomeric cuprate species in DoCu,[166] so it would be

particularly valuable to study the *in situ* formation of cuprates in solution. Initial studies will look at a greatly simplified system, where the respective lithium and copper amides will be combined in solution so that the evolution of cuprates can be monitored spectroscopically.

Chapter 3

General Experimental Techniques

3.1 CoSHH considerations

The experiments described herein involved the manipulation of chemicals hazardous to heath. In accordance with this, CoSHH assessments were carried out prior to commencing each experiment and standard PPE (safety glasses, laboratory coat and disposable gloves) were used as appropriate. All chemical manipulations were performed in a ventilated fumehood. Sharps (i.e. syringe needles) were sheathed when not in use and disposed of in dedicated sharps bins.

When copper(I) cyanide and silver(I) cyanide were used, contaminated glassware was treated with sodium hypochlorite solution for 24 hours. A specially trained first aider was notified whenever these chemicals were used. An oxygen cylinder and face mask were accessible for emergencies.

3.2 Inert atmosphere techniques

Many of the materials handled were sensitive to moisture and oxygen. Reagents and products were manipulated in an inert atmosphere of in-house dry nitrogen, using standard Schlenk line techniques. Reaction vessels were oven-dried (80°C) and cycled between high vacuum and dry nitrogen three times prior to use. For light sensitive materials, reaction flasks were wrapped in aluminium foil to exclude

light. Unless otherwise specified, reactions were conducted in Schlenk flasks and filtration was performed using a glass-sinter filter stick (porosity 4) or using a 30 mm diameter 1.2 µm porosity syringe filter. Solid reagents were added to the reaction vessel prior to evacuation and liquid reagents were added under a positive pressure of nitrogen.

Solid products were isolated by removing the supernatant under a positive flow of nitrogen or by use of filter stick apparatus. Residual solvent was removed under vacuum. For analysis, samples were manipulated in a glove box, with an atmosphere of dry nitrogen. The atmosphere was recirculated though molecular sieves (BDH 3Å 16") to remove water and through a copper catalyst (BASF Cu catalyst R11) to remove residual oxygen. Vessels were introduced to the glove box through an antechamber connected to a vacuum pump and nitrogen supply. The antechamber was cycled between high vacuum and dry nitrogen three times before materials were introduced to the glove box.

3.3 Solvents and starting materials

Amines were obtained from Sigma Aldrich, Alfa Aesar or Fisher Scientific and stored over molecular sieves (4 Å). If required, amines were distilled off sodium to remove oxidised impurities and moisture. Inorganic salts were purchased from Sigma Aldrich and used without further purification. Air sensitive salts were stored under nitrogen. *n*-Butyllithium solution in hexanes (1.6 M) was purchased from Acros Organics and stored at +5 °C.

Hexane and toluene were distilled off sodium wire and sodium-potassium amalgam, respectively. Tetrahydrofuran and diethyl ether were distilled off sodium wire/benzophenone. Anhydrous tetrahydropyran and diisopropyl ether were purchased from Sigma Aldrich and used as received.

3.4 Melting point determinations

For air-sensitive compounds, manipulations were performed in a glove box. Glass capillaries (sealed at one end) were filled with a small amount of material, then the

open end was temporarily sealed with a small amount of vacuum grease. Capillaries were then permanently sealed with a flame below the line of the grease. This ensured that no oxygen contaminated the sample. Rough and accurate melting points were determined using a Griffin melting point apparatus.

3.5 Elemental analysis

In a glove box, a few milligrams of analyte was placed into two small, pre-weighed aluminium capsules which were then sealed using a press. The capsules were weighed accurately and analysed for C, H and N with a Perkin Elmer 240 elemental analyser.

3.6 Fourier Transform Infrared Spectroscopy (FTIR)

Samples were analysed neat or (for air-sensitive samples) as an mull (Nujol) on NaCl plates. Data were collected with either a Perkin Elmer Spectrum One or Bruker Alpha FTIR spectrometer.

3.7 Multinuclear Nuclear Magnetic Resonance (NMR) spectroscopy

NMR data were collected on a Bruker Avance III HD 500 MHz Smart Probe FT NMR spectrometer (500.200 MHz for ^{1}H, 125.775 MHz for ^{13}C, 194.397 MHz for ^{7}Li). Spectra were obtained at 298 K using deuterated solvent stored over sodium wire or molecular sieves (3 Å). For ^{1}H and ^{13}C, chemical shifts are referenced through the solvent lock (^{2}H) signal according to IUPAC recommended secondary referencing method and the manufacturer's protocols.[178] For ^{7}Li, an external reference was used (1 M LiCl in D_2O). Chemical shifts are expressed in δ ppm.

3.8 X-Ray diffractometry

Technique varied with the temperature and air stability of the crystals in question. For samples crystallised at low temperature, the sample was transported to a microscope in a bath of anti-freeze, which was pre-chilled to -27°C. Crystals were transferred quickly by means of a spatula to a drop of perfluoropolyether oil on a microscope slide. A stream of cold nitrogen (*ca.* 0°C) was passed over the slide whilst crystals of appropriate quality were selected. The selected crystal was transferred to a pin fitted with a MicroLoop^{TM} and attached quickly to the goniometer head. Data were collected on either a Nonius Kappa CCD diffractometer (Mo K_α λ =0.71073 Å) or a Bruker D8 Quest diffractometer (Cu K_α λ = 1.54184 Å). Structures were solved with the program SHELXT[179] with refinement, based on F^2, by full-matix least squares refinement.[180] Non-hydrogen atoms were refined anisotropically (for disorder, standard restraints and constraints were applied, as appropriate) and a riding model, with idealised geometry was employed for H-atoms.

Chapter 4

Experimental Procedures

4.1 Studies in Heteroleptic Bis(amido)cuprate Formation

4.1.1 Synthesis and characterisation of $[(MP)_2CuLi(THF)_2]_2LiBr$ 1

A stirred solution of MPH (0.47 mL, 4 mmol) and THF (0.32 mL, 4 mmol) in hexane (4 mL) was treated with *n*BuLi (2.5 mL, 1.6 M in hexanes, 4 mmol) at −78 °C. The solution was warmed to room temperature whereupon a yellow suspension formed, which dissolved upon gentle warming. The solution was added dropwise to a stirred suspension of copper(I) bromide (0.286 g, 2 mmol) in hexane (2 mL) at −78 °C. The mixture was warmed to room temperature to give a black suspension. The suspension was filtered to give a bright orange solution that yielded colourless blocks after 7 days at −27 °C. Yield = 342 mg (38 % wrt CuBr). Melting point 73–75°C. Elemental analysis $C_{40}H_{80}BrCu_2Li_3N_4O_4$ requires (%): C, 52.86; H, 8.87; N, 6.16. Found (%): C, 51.09; H, 8.74; N, 6.14. NMR spectroscopy ^{1}H NMR (500 MHz, 298 K, C_6D_6): δ 4.25–3.64 (br, m, 4H, MP-6), 3.57 (m, THF, 16H), 3.37–2.86 (br, m, 4H, MP-6), 2.80–2.29 (br, m, 4H, MP-2), 2.26–2.00 (br, m, 4H, MP-4), 2.00–1.78 (br, m, 10H, MP-3,4,5), 1.78–1.56 (br, m, 10H, MP-3,4,5,Me), 1.56–1.42 (br, m, 12H, MP-3,4,5,Me), 1.36 (m, 16H, THF). ^{13}C NMR (125 MHz, 298 K, C_6D_6): δ 67.8 (THF), 59.3–57.4 (MP-2), 55.1–54.0

(MP-6), 40.6–38.9 (MP-5), 32.4–30.5 (MP-3), 27.3 (MP-4), 27.1 (MP-Me). ^{7}Li NMR (194 MHz, 298 K, C_6D_6): δ 2.03 (br, s, 0.2Li), 1.05 (br, s, 1Li), 0.55 (s, 2Li). X-ray crystallography $C_{40}H_{80}BrCu_2Li_3N_4O_4$, M = 908.89, Triclinc, $P\bar{1}$, a = 12.0150(2), b = 13.1207(3), c = 17.7475(4) Å, α = 83.9875(7), β = 70.3373(7), γ = 67.6336(14)°, V = 2435.59(9) Å^3, Z = 2, ρ_{calc} = 1.239 g cm^{-3}, λ = 0.71073 Å, μ = 1.731 mm^{-1}, 23822 reflections collected, 10967 unique, θ_{max} = 27.470°, R_{int} = 0.0442, $R1$ = 0.0718 ($F_{obs} > 4\sigma(F_{obs})$), $wR2$ = 0.2012, S = 1.033 , 428 parameters, peak/hole 1.051/−0.776 e Å^{-3}.

4.1.2 Synthesis and characterisation of MP(TMP)Cu(Br)Li$_2$(THF)$_2$ 2

nBuLi (2.5 mL, 1.6 M in hexanes, 4 mmol) was introduced to a stirred solution of MPH (0.24 mL, 2 mmol), TMPH (0.34 mL, 2 mmol) and THF (0.32 mL, 4 mmol) in hexane (4 mL) at −78 °C. The solution was warmed to room temperature to give a yellow solution that was then added dropwise to a stirred suspension of copper(I) bromide (0.286 g, 2 mmol) in hexane (2 mL) at −78 °C. The mixture was warmed to room temperature to yield a black suspension that could be filtered to give an orange coloured solution. This yielded crystals after storage −27 °C for 5 days. Yield = 430 mg (40%, wrt CuBr). Melting point dec. > 80 °C. Elemental analysis $C_{46}H_{92}Br_2Cu_2Li_4N_4O_4$ requires (%): C, 51.16; H, 8.59; N, 5.19. Found (%): C, 49.84; H, 8.57; N, 5.39. NMR spectroscopy ^{1}H NMR (500 MHz, 298 K, C_6D_6): δ 3.92–3.63 (br, m, 1H, MP-6), 3.58 (m, 16H, THF), 3.46–2.91 (br, m, 3H, MP-6), 2.91–2.57 (br, m, 2H, MP-2), 2.18–1.88 (m, 4H, TMP-4/MP-4), 1.88–1.59 (m, 18H, TMP-3,4,5/MP-3,4,5), 1.53–1.38 (m, 22H, TMP-3,4,5,Me/MP-3,4,5,Me), 1.38–1.26 (m, 20H, TMP-Me/MP-Me/THF), 1.26–1.14 (m, 4H, TMP-3,5), 1.04 (s, 1.8H, TMPH-Me), 0.94–0.78 (m, 2H, TMP-3,5). ^{13}C NMR (125 MHz, 298 K, C_6D_6): δ 68.1 (THF), 59.0–57.5 (MP-2), 55.2–53.1 (MP-6), 52.0 (TMP-2,6), 49.6 (TMPH-2,6), 43.0–41.2 (TMP-3,5), 40.8–38.6 (MP-5/TMP-Me), 38.5 (TMPH-3,5), 36.2–33.6 (TMP-Me), 31.9 (TMPH-Me), 31.7–29.7 (MP-3), 28.6–25.7 (MP-4,Me), 25.4 (THF), 20.9–19.2 (TMP-4), 18.7 (TMPH-4). ^{7}Li NMR (194 MHz, 298 K, C_6D_6): δ 1.80 (br, s, 0.8Li), 1.54 (s, 0.7Li), 1.21 (s, 0.7Li), 1.05 (s, 1.8Li). X-ray crystallography $C_{46}H_{92}Br_2Cu_2Li_4N_4O_4$, M = 1079.89, Triclinic, $P\bar{1}$, a = 10.9357(3), b = 11.0752(3), c = 12.4262(4) Å, α = 75.6840(10), β =

85.0560(10), γ = 75.4070(10)°, V = 1410.76(7) Å^3 Z = 1, ρ_{calc} = 1.271 g cm^{-3}, λ = 0.71073 Å, μ = 2.209 mm^{-1}, 17855 reflections collected, 5529 unique, θ_{max} = 26.037°, R_{int} = 0.0357, $R1$ = 0.0909 ($F_{obs} > 4\sigma(F_{obs})$), $wR2$ = 0.2740, S = 1.043, 222 parameters, peak/hole 1.591/−0.963 e Å^{-3}.

4.1.3 Synthesis and characterisation of DMP(TMP)Cu(Br)Li$_2$(THF)$_2$ 3

To a stirred solution of DMPH (0.27 mL, 2 mmol), TMPH (0.34 mL, 2 mmol) and THF (0.32 mL, 4 mmol) in hexane (4 mL) was added nBuLi (2.5 mL, 1.6 M in hexanes, 4 mmol) at −78 °C. The mixture was warmed to room temperature to give a yellow solution. This was added dropwise to a stirred suspension of copper(I) bromide (0.286 g, 2 mmol) in hexane (2 mL) at −78 °C. The mixture was warmed to room temperature to give a black suspension. This was filtered to give an orange solution, which yielded the crystalline product after storage −27 °C for 5 days. Yield = 410 mg (38% wrt CuBr). Melting point 78–80 °C. Elemental analysis $C_{48}H_{96}Br_2Cu_2Li_4N_4O_4$ requires (%): C, 52.03; H, 8.73; N, 5.06. Found (%): C, 52.20; H, 8.90; N, 5.38. NMR spectroscopy ^{1}H NMR (500 MHz, 298 K, C_6D_6): δ 3.60 (m, 16H, THF), 2.96–2.68 (br, s, 4H, DMP-2,6), 2.13 (br, m, 2H, DMP-4), 2.00 (br, m, 2H, TMP-4), 1.93–1.68 (br, m, 20H, DMP-3,4,5,Me/TMP-3,5,Me), 1.68–1.37 (br, m, 32H, DMP-Me/TMP-Me), 1.36–1.26 (br, m, 18H, THF, TMP-3,5/DMP-Me), 1.24 (m, 2H, TMP-3,5/DMP-3,5), 1.07 (s, 1.6H, TMPH-Me). ^{13}C NMR (125 MHz, 298 K, C_6D_6): δ 68.0 (THF), 59.0 (DMP-2,6), 53.7 (TMP-2,6), 49.2 (TMPH-2,6), 40.7 (TMP-3,5), 40.6 (DMP-3,5), 38.9 (DMP-3,5), 38.5 (TMP-Me), 38.2 (TMPH-3,5), 34.6 (TMP-Me), 31.6 (TMPH-Me), 27.3 (DMP-4), 26.3 (DMP-Me), 25.0 (THF), 19.4 (TMP-4), 18.3 (TMPH-4). ^{7}Li NMR (194 MHz, 298 K, C_6D_6): δ 1.82 (br, s, 0.2Li), 1.38 (s, 1Li), 1.12 (s, 1Li), 0.92 (s, sh, 0.1Li). X-ray crystallography $C_{48}H_{96}Br_2Cu_2Li_4N_4O_4$, M = 1107.94, Monoclinic, $P2_1/n$, a = 14.4774(5), b = 10.7720(3), c = 18.7374(7)Å, α = 90, β = 99.797(2), γ = 90°, V = 2879.49(17) Å^3, Z = 2, ρ_{calc} = 1.278 g cm^{-3}, λ = 1.54184 Å, μ = 2.837 mm^{-1}, 14155 reflections collected, 4915 unique, θ_{max} = 66.705°, R_{int} = 0.0474, $R1$ = 0.0624 ($F_{obs} > 4\sigma(F_{obs})$), $wR2$ = 0.1883, S = 1.041, 295 parameters, peak/hole 0.795/−0.864 e Å^{-3}.

4.1.4 Synthesis and characterisation of PIP(TMP)CuLi 4

To a stirred solution of TMPH (0.34 mL, 2 mmol) and PIPH (0.20 mL, 2 mmol) in hexane (4 mL), was added *n*BuLi (2.5 mL, 1.6 M in hexanes, 4 mmol) at −78 °C. The solution was allowed to warm to room temperature, whereupon the resulting cream-coloured suspension was added to a suspension of copper(I) bromide (0.286 g, 2 mmol) in hexane (2 mL) at −78 °C. The mixture was left to warm to room temperature, giving a black suspension which was filtered to give a pale straw-coloured solution. Storage at 5 °C for 1 day yielded the crystalline product. Yield = 103 mg (17% wrt CuBr). Melting point 115–117°C. Elemental analysis $C_{28}H_{56}Cu_2Li_2N_4$ requires (%): C, 57.02; H, 9.57; N, 9.50. Found (%): C, 56.52; H, 9.37; N, 9.40. NMR spectroscopy ^{1}H NMR (500 MHz, 298 K, C_6D_6): δ 3.36–2.99 (br, m, 8H, PIP-2,6), 1.84–1.74 (m, 2H, TMP-4), 1.74–1.59 (m, 14H, PIP-3,4,5/TMP-3,5), 1.59–1.51 (m, 4H, PIP-3,5/TMP-4), 1.50 (s, 12H, TMP-Me), 1.42–1.32 (br, m, 1.2H, TMPH), 1.28 (s, 12H, TMP-Me), 1.25–1.14 (m, 0.46H, TMPH), 1.07 (s, 3.16H, TMPH), 1.00–0.19 (m, 4H, TMP-3,5), 0.35 (br, s, 0.2H, TMPH-NH). ^{13}C NMR (125 MHz, 298 K, C_6D_6): δ 53.8 (TMP-2,6), 52.9 (PIP-2,6), 49.2 (TMPH-2,6), 41.3 (TMP-3,5), 38.7 (TMP-Me), 38.1 (TMPH-3,5), 34.3 (TMP-Me), 31.9 (PIP-3,5), 31.6 (TMPH-Me) 26.6 (PIP-4), 19.2 (TMP-4), 18.3 (TMPH-4). ^{7}Li NMR (194 MHz, 298 K, C_6D_6): δ 1.33 (s). X-ray crystallography $C_{28}H_{56}Cu_2Li_2N_4$, M = 589.72, Monoclinic, $C2/c$, a = 20.1573(11), b = 9.0358(5), c = 17.5390(9) Å, α = 90, β = 91.936(2), γ = 90°, V = 3192.7(3) Å^3, Z = 4, ρ_{calc} = 1.227 g cm^{-3}, λ = 1.54184 Å, μ = 1.779 mm^{-1}, 13395 reflections collected, 2797 unique, θ_{max} = 66.704 °, R_{int} = 0.0272, $R1$ = 0.0303 ($F_{obs} > 4\sigma(F_{obs})$), $wR2$ = 0.0927, S = 1.037, 167 parameters, peak/hole 0.511/−0.308 e Å^{-3}.

4.2 Thiocyanatocuprates: Unexpected Structural Diversity in Lithium Cuprates

4.2.1 Synthesis and characterisation of $(TMP)_2Cu(CN)Li_2(THP)$ 5

To a stirred solution of TMPH (0.68 mL, 4 mmol) and THP (0.17 mL, 2 mmol) in hexane (4 mL) was added *n*BuLi (2.5 mL, 1.6 M in hexanes, 4 mmol) at −78 °C. The resulting solution was returned to room temperature to give a yellow solution that was transferred to a suspension of CuCN (0.179 g, 2 mmol) in toluene (6 mL) at −78 °C. The mixture was warmed to room temperature to give a pale cream-coloured suspension. Hexane (4 mL) was added and the mixture was heated to reflux until most of the solid had dissolved. Immediate filtration gave a pale straw-coloured solution. Storage at room temperature for 24 h gave colourless block-like crystals. Yield = 20 mg (27% wrt CuCN). Melting point 185–187 °C. Elemental analysis $C_{48}H_{92}Cu_2Li_4N_6O_2$ requires (%): C, 61.32; H, 9.86; N, 8.94. Found (%): C, 60.69; H, 9.65; N, 8.84. Selected IR spectroscopy (nujol) $\overline{\nu}$ = 2104 (m, CN) cm^{-1}. NMR spectroscopy ^{1}H NMR (500 MHz, 298 K, C_6D_6): δ 3.50 (m, 8H, THP), 2.13–1.80 (br, m, 4H, TMP-4), 1.74 (s, 24H, TMP-Me), 1.71–1.39 (br, m, 34H, TMP-3,5,Me), 1.39–1.23 (m, 14H, THP, TMP-3,5), 1.23–1.15 (br, m, 4H, THP), 1.14 (m, 2H, TMP-3,5), 1.07 (s, 1.6H, TMPH-Me), 0.32 (br, s, 0.13H, TMPH-NH). ^{13}C NMR (125 MHz, 298 K, C_6D_6): δ 69.0 (THP), 54.2 (TMP-2,6, G), 53.7 (TMP-2,6, L), 49.2 (TMPH-2,6), 42.1 (TMP-3,5, G), 40.5 (br, TMP-3,5, L), 40.1 (TMP-Me, G), 38.4 (TMP-Me, L), 38.2 (TMPH-3,5), 34.5 (TMP-Me, G), 34.0 (TMP-Me, L), 31.6 (TMPH-Me), 25.7 (THP), 22.6 (THP), 19.4 (TMP-4, L), 19.2 (TMP-4, G), 18.4 (TMPH-4). ^{7}Li NMR (194 MHz, 298 K, C_6D_6): δ 0.90 (br, s, 0.2Li, G), 0.21 (s, 1Li, L). G = Gilman, L = Lipshutz-type. X-ray crystallography $C_{48}H_{92}Cu_2Li_4N_6O_2$, M = 940.11, Triclinic, $P\overline{1}$, a = 9.0869(4), b = 11.3341(5), c = 13.6040(6) Å, α = 86.210(2), β = 76.776(2), γ = 82.219(2)°, V = 1350.49(10) $Å^3$, Z = 1, ρ_{calc} = 1.156 g cm^{-3}, λ = 1.54184 Å, μ = 1.258 mm^{-1}, 13834 reflections collected, 4736 unique, θ_{max} = 66.54°, R_{int} = 0.0324, $R1$ = 0.0624 ($F_{obs} > 4\sigma(F_{obs})$), $wR2$ = 0.1896, S = 1.072, 393 parameters, peak/hole 0.925/−0.446 $e\,Å^{-3}$.

4.2.2 Synthesis and characterisation of $(TMP)_2Cu(SCN)Li_2(OEt_2)$ 6

To a stirred solution of TMPH (0.68 mL, 4 mmol) and Et_2O (0.21 mL, 2 mmol) in toluene (2 mL) at −78 °C was added *n*BuLi (2.5 mL, 1.6 M in hexanes, 4 mmol). The solution was returned to room temperature whereupon it was transferred to a suspension of CuSCN (0.243 g, 2 mmol), in toluene (2 mL), at −78 °C. The mixture was warmed to room temperature to give a pale cream-coloured suspension which was then heated to reflux until it turned grey-black. The mixture was filtered immediately, giving a yellow solution. Storage at room temperature gave needle-like crystals after 1 day, which dissolved with further standing, to be replaced after several days with crystals of *pseudo*-rhombic habit. Yield = 97 mg (10% wrt CuSCN). Melting point 173–175 °C. Elemental analysis $C_{48}H_{92}Cu_2Li_4N_6O_2$ requires (%): C, 56.63; H, 9.46; N, 8.57. Found (%): C, 55.58; H, 9.34; N, 8.46. Selected IR spectroscopy (nujol) $\overline{\nu}$ 2065 (s, CN), 1997 (m, CN) cm^{-1}. NMR spectroscopy ^{1}H NMR (500 MHz, 298 K, C_6D_6): δ 3.28 (q, $^3J_{HH}$ = 7 Hz, 8H, Et_2O), 1.89–1.76 (m, 4H, TMP-4), 1.66–1.61 (m, 8H, TMP-3,5), 1.60 (s, 24H, TMP-Me), 1.59–1.57 (m, 4H,TMP-4), 1.56 (s, 24H, TMP-Me) 1.14–1.06 (m, 20H, Et_2O + TMP-3,5), 1.06 (s, 7H, TMPH-Me), 0.32 (br, s, 0.44H, TMPH-NH). ^{13}C NMR (125 MHz, 298 K, C_6D_6): δ 65.4 (Et_2O), 54.2 (TMP-2,6, G), 53.6 (TMP-2,6, L), 49.2 (TMPH-2,6), 42.2 (TMP-3,5, G), 40.6 (TMP-3,5, L), 40.1 (TMP-Me, G), 38.4 (TMP-Me, L), 38.2 (TMPH-3,5), 34.5 (TMP-Me, G), 34.4 (TMP-Me, L), 31.6 (TMPH-Me), 19.2 (TMP-4, G + L), 18.4(TMPH-4), 15.0 (Et_2O). ^{7}Li NMR (194 MHz, 298 K, C_6D_6): δ 0.90 (s, 1Li, G), 0.65 (s, 0.4 Li, L). G = Gilman, L = Lipshutz-type. X-ray crystallography $C_{46}H_{92}Cu_2Li_4N_6O_2S_2$, M = 980.21, Monoclinic, $P2_1/c$, a = 16.1549(5), b = 11.4981(3), c = 15.2650(5) Å, α = 90, β = 98.687(2), γ = 90°, V = 2802.96(15) Å^3, Z = 2, ρ_{calc} = 1.161 g cm^{-3}, λ = 1.54184 Å, μ = 1.908 mm^{-1}, 29571 reflections collected, 4914 unique, θ_{max} = 66.7193 °, R_{int} = 0.0513, $R1$ = 0.0409 ($F_{obs} > 4\sigma(F_{obs})$), $wR2$ = 0.1043, S = 1.016, 326 parameters, peak/hole 0.538 /−0.251 e Å^{-3}.

4.2.3 Synthesis and characterisation of $(TMP)_2Cu(SCN)Li_2(THF)$ 7

*n*BuLi (2.5 mL, 1.6 M in hexanes, 4 mmol) was added to a stirred solution of TMPH (0.68 mL, 4 mmol) and THF (0.16 mL, 2 mmol) in hexane (4 mL) at −78 °C. The resulting solution was returned to room temperature and transferred to a suspension of CuSCN (0.243 g, 2 mmol), in hexane (2 mL), at −78 °C. The mixture was warmed to room temperature to a give a pale cream-coloured suspension which was heated to reflux until it turned grey-black. Immediate filtration gave a pale yellow solution. Storage at −27 °C for 24 h gave colourless prismatic crystals. Yield = 516 mg (53%). Melting point 143–145 °C. Elemental analysis $C_{46}H_{88}Cu_2Li_4N_6O_2S_2$ requires (%): C, 56.60; H, 9.09; N, 8.61. Found (%): C, 57.63; H, 9.35; N, 8.61. Selected IR spectroscopy (nujol) $\overline{\nu}$ 2050 (s, CN), 1998 (m, CN) cm^{-1}. NMR spectroscopy ^{1}H NMR (500 MHz, 298 K, C_6D_6): δ 3.66 (m, 8H, THF), 1.99–1.75 (m, 4H, TMP-4), 1.66 (m, 24H, TMP-3,5, Me), 1.63–1.52 (br, m, 18H, TMP-4, Me), 1.50 (s, 18H, TMP-Me), 1.42 (m, 8H, THF), 1.21–1.06 (m, 8H, TMP-3,5), 1.07 (s, 5.4H, TMPH-Me), 0.33 (br, s, 0.3H, TMPH-NH). ^{13}C NMR (125 MHz, 298 K, C_6D_6): δ 141.5 (SCN), 68.4 (THF), 54.2 (TMP-2,6, G), 53.5 (TMP-2,6, L), 49.2 (TMPH-2,6), 42.1 (TMP-3,5, G), 40.6 (TMP-3,5, L), 40.1 (TMP-Me, G), 38.3 (TMP-Me, L), 38.2 (TMPH-3,5), 34.5 (TMP-Me, G), 34.4 (TMP-Me, L), 31.6 (TMPH-Me), 25.0 (THF), 19.2 (TMP-4, G + L), 18.4 (TMPH-4). ^{7}Li NMR (194 MHz, 298 K, C_6D_6): δ. 0.89 (s, 0.2Li, G), 0.71 (s, 1Li, L). G = Gilman, L = Lipshutz-type. X-ray crystallography $C_{46}H_{88}Cu_2Li_4N_6O_2S_2$, M = 976.18, Monoclinic, $P2_1/c$, a = 15.1170(7), b = 14.7117(7), c = 25.3458(11) Å, α = 90, β = 104.763(2), γ = 90 °, V = 5450.7(4) Å^3, Z = 4, ρ_{calc} = 1.190 g cm^{-3}, λ = 1.54184 Å, μ = 1.962 mm^{-1}, 73948 reflections collected, 9650 unique, θ_{max} = 66.831 °, R_{int} = 0.0610, $R1$ = 0.0474 ($F_{obs} > 4\sigma(F_{obs})$), $wR2$ = 0.1294, S = 1.030, 575 parameters, peak/hole 0.717/−0.556 e Å^{-3}.

4.2.4 Synthesis and characterisation of $(TMP)_2Cu(SCN)Li_2(THP)$ 8

A stirred solution of TMPH (0.68 mL, 4 mmol) and THP (0.17 mL, 2 mmol) in hexane/toluene (4 mL/2 mL) at −78 °C was treated with *n*BuLi (2.5 mL, 1.6

M in hexanes, 4 mmol). The resulting solution was returned to room temperature whereupon it was transferred to a suspension of CuSCN (0.243 g, 2 mmol) in hexane/toluene (2 mL/1 mL) at −78 °C. The mixture was warmed to room temperature to a give a pale cream-coloured suspension which was then heated to reflux until it became grey-black. The mixture was filtered immediately. This gave a yellow solution, the storage of which at room temperature for 24 h gave colourless blocks. Yield = 250 mg (27%). Melting point 176–178 °C. Elemental analysis $C_{48}H_{92}Cu_2Li_4N_6O_2S_2$ requires (%): C, 57.41; H, 9.23; N, 8.37. Found (%): C, 57.17; H, 9.23; N, 8.45. Selected IR spectroscopy (nujol) $\overline{\nu}$ 2063 (s, CN), 2007 (w, CN) cm^{-1}. NMR spectroscopy ^{1}H NMR (500 MHz, 298 K, C_6D_6): δ 3.62 (t, $^3J_{HH}$ = 5 Hz, 8H, THP), 1.98–1.75 (m, 4H, TMP-4), 1.73–1.52 (m, 46H, TMP-Me,3,5,4), 1.49 (s, 12H, TMP–Me), 1.32 (m, 8H, THP), 1.27–1.15 (m, 10H, THP + TMP-3,5), 1.15–1.04 (m, 4H, TMP-3,5), 1.07 (s, 5H, TMPH-Me), 0.32 (br, s, 0.4H, TMPH-NH). ^{13}C NMR (125 MHz, 298 K, C_6D_6): δ 68.8 (THP), 54.2 (TMP-2,6, G), 53.5 (TMP-2,6, L), 49.2 (TMPH-2,6), 42.1 (TMP-3,5, G), 40.6 (TMP-3,5, L), 40.1(TMP-Me, G), 38.3 (TMP-Me, L), 34.5 (TMP-Me, G), 34.4 (TMP-Me, L), 31.6 (TMPH-Me), 25.9 (THP), 22.7 (THP), 19.2 (TMP-4, G + L), 18.4 (TMPH-4). ^{7}Li NMR (194 MHz, 298 K, C_6D_6): δ 0.90 (s, 0.3Li, G), 0.60 (s, 1Li, L). G = Gilman cuprate, L = Lisphutz-type cuprate. X-ray crystallography $C_{48}H_{92}Cu_2Li_4N_6O_2S_2$, M = 1004.23, Monoclinic, $P2_1/c$, a = 15.8974(7), b = 8.1755(3), c = 22.0201(9) Å, α = 90, β = 100.199(2), γ = 90°, V = 2816.7(2)Å^3, Z = 2, ρ_{calc} = 1.184 g cm^{-3}, λ = 1.54184 Å, μ = 1.912 mm^{-1}, 41304 reflections collected, 4945 unique, θ_{max} = 66.556 °, R_{int} = 0.0495, $R1$ = 0.0360 ($F_{obs} > 4\sigma(F_{obs})$), $wR2$ = 0.0929, S = 1.037, 297 parameters, peak/hole 0.545/−0.394 e Å^{-3}.

4.2.5 Synthesis and recharacterisation of $(TMP)_2CuLi$ 9c

*n*BuLi (2.5 mL, 1.6 M in hexanes, 4 mmol) was added to a stirred solution of TMPH (0.68 mL, 4 mmol) in hexane/toluene (2 mL/2 mL) at −78 °C. The resulting solution was returned to room temperature and transferred to a suspension of CuSCN (0.243 g, 2 mmol), in hexane/toluene (2 mL/2 mL), at −78 °C. The mixture was warmed to room temperature to a give a pale cream-coloured suspension which was heated to reflux until it turned grey-black. Immediate filtration gave a pale yellow solution that was concentrated until precipitation occurred, after which the solid was redissolved by gentle warning. Storage of the resulting

bright yellow solution at room temperature for 24 h gave very large blade-shaped crystals. Yield 201 mg (40% wrt CuSCN). Melting point 198–200 °C. Elemental analysis, $C_{36}H_{72}Cu_2Li_2N_4$ requires (%) C, 61.60; H, 10.34; N 7.98. Found (%) C, 60.83; H, 10.30; N 7.89. NMR spectroscopy ^{1}H NMR (500 MHz, 298 K, C_6D_6): δ 1.89–1.77 (m, 4H, TMP-4), 1.67–1.61 (m, 8H, TMP-3,5), 1.60 (s, 24H, TMP-Me), 1.59–1.57 (m, 4H, TMP-4), 1.56 (s, 24H, TMP-Me), 1.14–1.06 (m, 8H, TMP-3,5). ^{13}C NMR (125 MHz, 298 K, C_6D_6): δ 54.2 (TMP-2,6), 42.1 (TMP-3,5), 40.1 (TMP-Me), 34.5 (TMP-Me), 19.2 (TMP-4). ^{7}Li NMR (194 MHz, 298 K, C_6D_6): δ 0.90 (s). The identity of this compound was verified by X-ray crystallography.

4.2.6 Derivatisation of chloropyridines 10 and 11 to give 12a–d and 13b–d

The derivitisation of chloropyridines **10** and **11** to give **12a–d** and **13b–d** was conducted by collaborators. Experimental details for the synthesis of these compounds are published.[181]

4.3 Studies into the Chemistry of Cyanatocuprates: Cu-Li Exchange in Lithium Cuprates

4.3.1 Synthesis and characterisation of CuOCN

[182] $Cu(NO_3)_2(H_2O)_3$ (2.4 g, 0.01 mol) was added to a solution of $LiOAc(H_2O)_2$ (3 g, 0.03 mol) in water (8 mL) to give a dark blue solution. To this was added a solution of filtered $Li_2SO_4(H_2O)$ (1.28 g, 0.01 mol) and $Ba(OCN)_2$[182] (2.2 g, 0.01 mol) in water (30 mL). Aqueous SO_2 (15 mL, 0.7 M) was added to the mixture until it became green. The resultant green solution was left for 30 mins, the precipitate collected by filtration, washed with deaerated water (2 mL) and dried *in vacuo*. Yield 0.54 g (51 % wrt Cu). Melting point dec. >140 °C. Elemental Analysis, CuCNO requires (%) C, 11.38; N, 13.27. Found (%) C, 11.38; N 13.27. Selected IR spectroscopy 2116 (s) cm^{-1}. NMR spectroscopy ^{13}C NMR (125 MHz, 298 K, CD_3CN): δ NMR 126.3 (t, J = 23 Hz).

4.3.2 Synthesis and characterisation of $(TMP)_2Cu_{0.1}Li_{0.9}(OCN)Li_2(THF)$ 14

To a stirred solution of TMPH (0.34 mL, 2 mmol) and THF (0.08 mL, 1 mmol) in hexane (4 mL) was added *n*BuLi (1.25 mL, 1.6 M in hexanes, 2 mmol) at −78 °C. The resulting solution was returned to room temperature to give a yellow solution. This was transferred to a suspension of CuOCN (0.11g, 1 mmol) in hexane (1 mL) at −78 °C. The resulting mixture was returned to room temperature to give a pale yellow suspension, the filtration of which gave a yellow solution. Storage at −27 °C gave crystalline products. Yield = 54 mg. A well-faceted block-like crystal was selected for X-ray diffraction. Selected IR spectroscopy (nujol) $\overline{\nu}$ 2208 (s, CN), 1340 (m, CO), 1229 (m, CO) cm^{-1}. NMR spectroscopy ^{1}H NMR (500 MHz, 298 K, C_6D_6): δ 3.56 (m, 8H, THF), 2.17–1.77 (br, 8H, TMP-4), 1.75 (s, 6H, TMP-Me), 1.74–1.60 (br, m, 12H, TMP-3,5,Me), 1.57 (s, 12H, TMP-Me), 1.56–1.41 (br, m, 12H, TMP-3,5,4,Me), 1.39 (s, 6H, TMP-Me), 1.36 (m, 8H, THF), 1.34–1.13 (br, 12H, TMP-3,5), 1.12–1.07 (m, 4H, TMP-3,5), 1.06 (s, 2H, TMPH-Me). ^{13}C NMR (125 MHz, 298 K, C_6D_6): δ 64.8 (THF), 56.9 (TMP-2,6 *i*-**9c**), 54.2 (TMP-2,6 *i*-**9c**/TMP-2,6 **9c**), 53.4 (TMP-2,6 **14b**), 52.0 (TMP-2,6 *i*-**9c**), 51.6 (TMP-2,6 **16**), 49.2 (TMPH-2,6), 42.6 (TMP-3,5 *i*-**9c**), 42.5 (TMP-3,5 *i*-**9c**), 42.4 (TMP-3,5 **14**), 42.1 (TMP-3,5 *i*-**9c**/TMP-3,5 **9c**), 41.9 (TMP-3,5 **16**), 40.5 (TMP-Me **14b**), 40.2 (TMP-Me **9c**), 39.7 (TMP-Me *i*-**9c**), 38.1 (TMPH-3,5), 37.5 (br, TMP-Me **16**), 37.0 (TMP-Me *i*-**9c**), 36.8 (TMP-Me *i*-**9c**), 35.7 (TMP-Me **14b**), 34.5 (TMP-Me **9c**), 34.2 (TMP-Me *i*-**9c**), 33.5 (br, TMP-Me **16**), 31.6 (TMPH-Me), 25.1 (THF), 20.1 (TMP-4 **16**), 19.6 (TMPH-4 *i*-**9c**), 19.2 (TMP-4 *i*-**9c**/TMP-4 **9c**), 19.1 (TMP-4 **14b**), 19.1 (TMP-4 *i*-**9c**), 18.4 (TMPH-4). ^{7}Li NMR (194 MHz, 298 K, C_6D_6): δ 2.17 (br, s, 1Li, TMPLi), 1.64 (s, 1.5Li, *i*-**9c**), 1.39 (br, s, 2Li, **16**), 0.9 (s, 0.5Li, **9c**), 0.48 (s, 0.5Li, **14**). X-ray crystallography $C_{46}H_{88}Cu_{0.21}Li_{5.79}N_6O_4$, M = 842.74, Triclinic, $P\overline{1}$, a = 7.9156(3), b = 13.4775(5), c = 13.8111(6) Å, α = 110.986(2), β = 94.546(2), γ = 104.331(2)°, V = 1309.70(9) Å^3, Z = 1, ρ_{calc} = 1.068 g cm^{-3}, λ = 1.54184 Å, μ = 0.583 mm^{-1}, 17570 reflections collected, 4631 unique, θ_{max} = 66.840°, R_{int} = 0.0395, $R1$ = 0.0515 ($F_{obs} > 4\sigma(F_{obs})$), $wR2$ = 0.1388, S = 1.026, 4631 parameters, peak/hole 0.431/-0.450 e Å^{-3}.

4.3.3 Synthesis and characterisation of $(TMP)_2Cu(OCN)Li_2(THF)$ 14a

To a stirred solution of TMPH (0.68 mL, 4 mmol) in hexane (2 mL) and toluene (2 mL) was added *n*BuLi (2.5 mL, 1.6 M in hexanes, 4 mmol) at −78 °C. The solution was warmed to room temperature and transferred to a suspension of CuSCN (0.243 g, 2 mmol) in hexane (2 mL) and toluene (2 mL). The suspension was warmed to room temperature and heated to reflux whereupon a grey discolouration was observed. This mixture was filtered whilst hot onto LiOCN (0.10 g, 2 mmol) and the solvent was removed *in vacuo*. THF (6 mL) was added and the suspension was stirred at room temperature for 30 minutes, during which time partial dissolution of the LiOCN occurred. The THF was removed *in vacuo* to give a sticky solid, which dissolved when hexane (6 mL) was added. The solution was filtered and the filtrate stored at −27 °C for 1 week during which time **14a** deposited as radiating fans of crystals. Yield = 310 mg (32 % wrt CuSCN). Melting point 192–194°C. Elemental analysis $C_{24}H_{48}CuLi_2N_3O_2$ requires (%) C, 58.52; H, 9.40; N, 8.90. Found (%) C, 58.06; H, 9.38; N, 9.01. Selected IR spectroscopy $\overline{\nu}$ 2241 (s, CN), 2208 (s, CN), 1340 (m, CO), 1228 (m, CO) cm^{-1}. NMR spectroscopy ^{1}H NMR (500 MHz, 298 K, C_6D_6): δ 3.57 (br, m, 4H, THF), 1.89–1.76 (br, m, 2H, TMP-4), 1.67–1.61 (m, 4H, TMP-3,5), 1.60 (s, 12H, TMP-Me), 1.59–157 (m, 2H, TMP-4), 1.56 (s, 12H, TMP-Me), 1.41 (br, m, 4H, THF), 1.09 (m, 4H, TMP-3,5), 1.06 (s, 1.3H, TMPH-Me). ^{13}C NMR (125 MHz, 298 K, C_6D_6): δ 67.4 (br, THF), 54.2 (TMP-2,6), 49.2 (TMPH-2,6), 42.1 (TMP-3,5), 40.1 (TMP-Me), 38.2 (TMPH-3,5), 34.5 (TMP-Me), 31.6 (TMPH-Me), 25.3 (br, THF), 19.2 (TMP-4), 18.4 (TMPH-4). ^{7}Li NMR (194 MHz, 298 K, C_6D_6): δ 0.90. X-ray crystallography $C_{46}H_{88}Cu_2Li_4N_6O_4$, M = 944.06, Triclinic, $P\overline{1}$, a = 8.4118(4), b = 11.5807(5) , c = 13.5645(6) Å, α = 98.376(2), β = 95.058(2), γ = 94.955(2)°, V = 1295.58(10) $Å^3$, Z = 1, ρ_{calc} = 1.210 g cm^{-3}, λ = 1.54184 Å, μ = 1.344 mm^{-1}, 4430 reflections collected, θ_{max} = 66.793°, R_{int} = 0.0361[i] $R1$ = 0.0351 ($F_{obs} > 4\sigma(F_{obs})$), $wR2$ = 0.1026, S = 1.082, 289 parameters, peak/hole 0.261/-0.452 $e\,Å^{-3}$. **14a** crystallized as a two-component non-merohedral twin. Orientation matrices for the two components were found using the program Cell Now and the two components were integrated with SAINT.[183] The exact twin law determined by the integra-

[i]Based on agreement between observed single and composite intensities and those calculated from refined unique intensities and twin fractions.

tion program was (–0.99994, 0.00004, 0.00042), (–0.00003, –1.00011, –0.00063), (0.32832, 0.36100, 1.00005). The data were corrected for absorption using Twinabs.[183] 6927 reflections (2275 unique) involved domain 1 only (mean $I/\sigma = 46.9$), 6872 reflections (2247 unique) involved domain 2 only (mean $I/\sigma = 15.6$) and 5721 reflections (2638 unique) involved two domains (mean $I/\sigma = 42.9$). The structure was solved with SHELXT[179] using data from domain 1 only (HKLF 4) and for refinement, overlaps were also included (HKLF 5).

4.3.4 Synthesis and characterisation of $(TMP)_4Cu_{2.7}Li_{1.3}$ 9

To a stirred solution of TMPH (0.34 mL, 2 mmol) and THF (2 mL) was added *n*BuLi (1.25 mL, 1.6 M in hexanes, 2 mmol) at −78 °C. The solution was allowed to reach room temperature to give a yellow solution. This was transferred to a suspension of CuOCN (0.11g, 1 mmol) in THF (1 mL) at −78 °C. The mixture was returned to room temperature to give a pale yellow suspension. The solvent was removed and the resulting yellow solid dissolved in hexane (4 mL). Filtration gave a yellow solution that was stored at −27 °C to give crystalline needles. Yield = 65 mg. NMR spectroscopy ^{1}H NMR (500 MHz, 298 K, C_6D_6): δ 1.89–1.80 (m, 4H, TMP-4), 1.79 (s, 6H, TMP-Me), 1.76 (s, 8H, TMP-Me), 1.73 (s, br, 6H, TMP-Me), 1.72–1.69 (br, m, 4H, TMP-4), 1.68–1.61 (m, 4H, TMP-3,5), 1.59 (s, 12H, TMP-Me; TMP-Me **9c**), 1.57 (s, 10H, TMP-Me; TMP-3,5; TMP-4), 1.56 (s, 12H, TMP-Me **9c**), 1.10 (m, 6H, TMP-3,5), 1.06 (s, 1H, TMPH-Me). ^{13}C NMR (125 MHz, 298 K, C_6D_6): δ 56.9 (TMP-2,6), 54.2 (TMP-2,6), 54.2 (TMP-2,6 **9c**), 49.2 (TMPH-2,6), 42.6 (TMP-3,5), 42.5 (TMP-3,5), 42.1 (TMP-3,5 **9c**), 42.1 (TMP-3,5), 40.1 (TMP-Me **9c**), 39.7 (TMP-Me), 38.2 (TMPH-3,5), 37.6 (br, TMP-Me), 37.2 (br, TMP-Me), 36.6 (br, TMP-Me), 34.8 (TMP-Me), 34.5 (TMP-Me **9c**), 31.6 (TMPH-Me), 19.3 (TMP-4), 19.2 (TMP-4 **9c**), 19.2 (TMP-4), 18.4 (TMPH-4). ^{7}Li NMR (194 MHz, 298 K, C_6D_6): δ 1.65 (s, 0.16Li, *i*-**9c**), 0.94 (sh, 0.8Li), 0.91 (s, 1.0Li, **9c**). X-ray crystallography $C_{36}H_{72}Cu_{2.70}Li_{1.30}N_4$, M = 741.41, Monoclinic, $P2_1/c$, a = 11.6661(3), b = 22.7624(5), c =15.2664(4) Å, α = 90, β = 108.6770(10), γ = 90°, V = 3840.48(17) Å^3, Z = 4, ρ_{calc} = 1.282 g cm^{-3}, λ = 1.54184 Å, μ = 1.952 mm^{-1}, 19840 reflections collected, 5479 unique, θ_{max} = 59.106°, R_{int} = 0.0469, $R1$ = 0.0501 ($F_{obs} > 4\sigma(F_{obs})$), $wR2$ = 0.1167, S = 1.055, 417 parameters, peak/hole 0.782/-0.382 e Å^{-3}.

4.3.5 Synthesis and characterisation of $(TMPH_2)OCN$ 15

A solution of $(TMPH_2)_2SO_4$ (0.76 g, 2 mmol) in water (10 mL) was added to $Ba(OCN)_2$ (0.44 g, 2 mmol) in water (10 mL), whereupon a white precipitate formed immediately. The suspension was stirred for 10 minutes and filtered twice. The solvent was removed *in vacuo* and the product extracted in ethanol (absolute, 20 mL). The solution was concentrated and Et_2O slowly added until crystallization initiated. The crystalline product was collected by filtration and washed with Et_2O (3×5 mL) to give $(TMPH_2)OCN$. Yield 0.34 g (46 % wrt OCN). Melting point $>$ 300 °C. Elemental analysis, $C_{10}H_{20}N_2O$ requires (%) C, 65.18; H, 10.94; N, 15.20. Found (%) C, 64.26; H, 10.99; N, 14.54. Selected IR spectroscopy $\overline{\nu}$ 3020–2350 (w, br, NH), 2134 (s, CN), 1601 (m, CO) cm^{-1}. NMR spectroscopy ^1H NMR (500 MHz, 298 K, CD_3OD): δ 1.80 (m, 2H, TMP-4), 1.66 (m, 4H, TMP-3,5), 1.43 (s, 12H, TMP-Me). ^{13}C NMR (125 MHz, 298 K, CD_3OD): δ 130.3 (OCN), 57.8 (TMP-2,6), 36.2 (TMP-3,5), 27.8 (TMP-Me), 17.3 (TMP-4).

4.3.6 Synthesis and characterisation of $(TMP)_2Li(OCN)Li_2(THF)_2$ 16

Method (a): A suspension of $(TMPH_2)OCN$ (0.09 g, 0.5 mmol) in THF (2 mL) was treated with TMPH (0.08 mL, 0.5 mmol) and *n*BuLi (0.95 mL, 1.5 mmol) at −78 °C. The resulting suspension was left to warm to room temperature, whereupon it dissolved to give a pale yellow solution. The solvent was removed *in vacuo* and replaced with hexane (3 mL). The colourless solution was filtered, with storage of the filtrate at −27 °C for 1 day giving colourless crystals. Yield 65 mg (27 % wrt NCO). Method (b): TMPH (0.34 mL, 2 mmol) in THF (2 mL) was treated with *n*BuLi (1.25 mL, 1.6 M in hexanes, 2 mmol) at −78 °C. The pale yellow solution was returned to room temperature whereupon it was transferred to a suspension of LiOCN (0.05 g, 1 mmol) in THF at −78 °C. The mixture warmed to room temperature and was stirred for *ca.* 15 minutes, during which time the LiOCN was observed to dissolve. The solvent was removed *in vacuo*, leaving a sticky white solid which dissolved upon the addition of hexane (6mL) with gentle warming. The solution was filtered and the filtrate stored at −27 °C for 24 hours to give colourless crystals. Yield = 75 mg (15 % wrt LiOCN). Melting point 90–92

°C. Elemental Analysis, $C_{27}H_{52}Li_3N_3O_3$ requires (%) C, 66.52; H, 10.75; N, 8.62. Found (%) C, 66.08; H, 10.76; N, 8.83. Selected IR spectroscopy (nujol) $\overline{\nu}$ 2207 (s, CN), 1352 (s, CO), 1226 (s, CO) cm^{-1}. NMR spectroscopy ^{1}H NMR (500 MHz, 298 K, C_6D_6): δ 3.56 (m, 8H, THF), 2.31–1.38 (br, 30H, TMP), 1.35 (m, 8H, THF), 1.32–1.12 (br, 6H, TMP), 1.06 (s, 1H, TMPH). ^{13}C NMR (125 MHz, 298 K, C_6D_6): δ 67.9 (THF), 51.6 (TMP-2,6), 49.2 (TMPH-2,6), 41.9 (TMP-3,5), 38.2 (TMPH-3,5), 37.1 (br, TMP-Me), 33.5 (br, TMP-Me), 31.6 (TMPH-Me), 25.0 (THF), 20.1 (TMP-4), 18.4 (TMPH-4). ^{7}Li NMR (194 MHz, 298 K, C_6D_6): δ 1.38 (s, br). X-ray crystallography: $C_{54}H_{104}Li_6N_6O_6$, M = 975.07, Triclinic, $P\overline{1}$, a = 11.8638(3), b = 12.0430(3), c = 12.2033(3) Å, α = 82.4990(10), β = 66.9060(10), γ = 72.4890(10)°, V = 1529.35(7) Å^3, Z = 1, ρ_{calc} = 1.059 g cm^{-3}, λ = 1.54184 Å, μ = 0.511 mm^{-1}, 16485 reflections collected, 5374 unique, θ_{max} = 66.691 °, R_{int} = 0.0303, $R1$ = 0.0502 ($F_{obs} > 4\sigma(F_{obs})$), $wR2$ = 0.1400, S = 1.035, 343 parameters, peak/hole 0.535/-0.313 e Å^{-3}.

4.3.7 Synthesis and characterisation of $(DA)_2Cu_{0.09}Li_{0.91}(Br)Li_2(TMEDA)_2$ 17

*n*BuLi (2.5 mL, 1.6 M in hexanes, 4 mmol) was added to a stirred solution of DAH (0.56 mL, 4 mmol) and TMEDA (0.6 mL, 4 mmol) in hexane (4 mL) at −78 °C. The resulting solution was returned to room temperature to give a yellow solution that was transferred to a −78 °C suspension of CuBr (0.28 g, 2 mmol) in hexane (2 mL). The mixture was returned to room temperature to give a brown suspension. Filtration gave a pale yellow solution. Storage of this filtrate at −27 °C for 24 hours gave colourless blocks. Yield = 350 mg. NMR spectroscopy for two independent representative examples is reported. *Representative sample* (1) ^{1}H NMR (500 MHz, 298 K, C_6D_6): δ 3.76 (sh, br, 0.36H, DA-CH, **17a**), 3.67 (s, br, 3.15H, DA-CH, **17b**), 3.25 (septet, $^3J_{HH}$ = 6 Hz, 0.02H, DA-CH, **17a**), 3.16 (septet, $^3J_{HH}$ = 6 Hz, 0.08H, DA-CH, **17a**), 3.10 (septet, $^3J_{HH}$ = 6 Hz, 0.28H, DA-CH, **17a**), 2.78 (octet, $^3J_{HH}$ = 6 Hz, 0.4H, DAH-CH), 2.13 (s, 24H, TMEDA-Me), 1.99 (s, 8H, TMEDA-CH_2), 1.63–1.20 (br, m, 24H, **17a** + **17b**), 0.95 (d, $^3J_{HH}$ = 6 Hz, 2H, DAH-Me). ^{13}C NMR (125 MHz, 298 K, C_6D_6): δ 57.0 (TMEDA-CH_2), 50.1 (DA-CH, **17a**), 48.8 (DA-CH, **17b**), 46.5 (TMEDA-Me), 44.9 (DAH-CH), 28.2 (DA-Me, **17a**), 27.0 (DA-Me, **17a**), 26.2 (br, DA-Me, **17b**),

23.2 (DAH-Me). ^{7}Li NMR (194 MHz, 298 K, C_6D_6): δ 2.34 (s, 1Li, (DA)2Li, **17b**), 1.58 (s, 0.4Li, Li(TMEDA), **17a**), 1.18 (s, 2Li, Li(TMEDA), **17b**) *Representative sample* (2) ^{1}H NMR (500 MHz, 298 K, C_6D_6): δ 3.76 (sh, br, 0.11H, DA-CH, **17a**), 3.67 (s, br, 1.90H, DA-CH, **17b**), 3.25 (septet, $^{3}J_{HH}$ = 6 Hz, 0.02H, DA-CH, **17a**), 3.16 (septet, $^{3}J_{HH}$ = 6 Hz, 0.64H, DA-CH, **17a**), 3.11 (septet, $^{3}J_{HH}$ = 6 Hz, 1.00H, DA-CH, **17a**), 2.78 (octet, $^{3}J_{HH}$ = 6 Hz, 0.16H, DAH-CH), 2.14 (s, 24H, TMEDA-Me), 2.02 (s, 8H, TMEDA-CH_2), 1.60–1.31(br, m, 20H, DA-Me , **17a** + **17b**), 1.25 (d, $^{3}J_{HH}$ = 6 Hz, 2H, **17a**), 1.22 (d, $^{3}J_{HH}$ = 6 Hz, 2H, **17a**), 0.94 (d, $^{3}J_{HH}$ = 6 Hz, 1H, DAH-Me). ^{13}C NMR (125 MHz, 298 K, C_6D_6): δ 57.0 (TMEDA-CH_2), 50.9 (DA-CH, **17a**), 50.4 (DA-CH, **17a**), 50.1 (DA-CH, **17a**), 48.8 (DA-CH, **17b**), 46.3 (TMEDA-Me), 44.8 (DAH-CH), 28.4 (DA-Me, **17a**), 28.2 (DA-Me, **17a**), 27.6 (DA-Me, **17a**), 27.5 (DA-Me, **17a**), 27.0 (DA-Me, **17a**), 26.9 (DA-Me, **17a**), 26.1 (br, DA-Me, **17b**), 23.4 (DAH-Me). ^{7}Li NMR (194 MHz, 298 K, C_6D_6): δ 2.37 (s, 1.0Li, **17b**), 1.63 (s, 1.2Li, **17a**), 1.59 (s, 1.0Li, **17a**), 1.17 (s, 2Li, **17b**). X-ray crystallography $C_{24}H_{60}BrCu_{0.09}Li_{2.91}N_6$, M = 538.60, Monoclinic, $P2_1/c$, a = 17.7591(8), b = 12.2389(6), c = 17.2889(8) Å, α = 90, β = 118.227(2), γ = 90°, V = 3310.9(3) Å^3, Z = 4, ρ_{calc} = 1.081 g cm^{-3}, λ = 1.54184 Å, μ = 1.878 mm^{-1}, 25251 reflections collected, 5837 unique, θ_{max} = 66.842°, R_{int} = 0.0843, $R1$ = 0.0825 ($F_{obs} > 4\sigma(F_{obs})$), $wR2$ = 0.1524, S = 1.117, 317 parameters, peak/hole 0.510/-0.632 e Å^{-3}.

4.3.8 Synthesis and characterisation of $(DA)_2Li(Br)Li_2(TMEDA)_2$ 17b

To a suspension of (DAH_2)Br (0.18 g, 1 mmol) in hexane (6 mL) was added DAH (0.14 mL, 1 mmol) and TMEDA (0.30 mL, 2 mmol). The mixture was cooled to −78 °C, treated with *n*BuLi (1.9 mL, 1.6 M in hexanes, 3 mmol) and returned to room temperature to give a pale yellow solution. The solution was filtered, concentrated (*ca.* 4 mL) and stored at −27 °C for 1 day, after which time colourless block-like crystals were deposited. Yield 320 mg (60 % wrt Br). Melting point 76–78°C. Elemental Analysis, $C_{24}H_{60}BrLi_3N_6$ requires (%) C, 54.03; H, 11.34; N, 15.75. Found (%) C, 54.09; H, 11.66; N, 15.58. NMR spectroscopy ^{1}H NMR (500 MHz, 298 K, C_6D_6): δ 3.66 (s, br, 2H, DA-CH), 2.79 (octet, $^{3}J_{HH}$= 6 Hz, 0.06H, DAH-CH), 2.13 (s, 24H, TMEDA-Me), 1.96 (s, 8H, TMEDA-CH_2), 1.41 (s, br,

24H, DA-Me), 0.95 (d, $^3J_{HH}$ = 6 Hz, 1.35H, DAH-Me). ^{13}C NMR (125 MHz, 298 K, C_6D_6): δ 56.9 (TMEDA-CH_2), 48.8 (DA-CH), 46.5 (TMEDA-Me), 44.9 (DAH-CH), 26.2 (DA-Me), 23.2 (DAH-Me). ^{7}Li NMR (194 MHz, 298 K, C_6D_6): δ 2.28 (s, br, 1Li, $(DA)_2Li$), 1.26 (s, 2Li, Li(TMEDA)). X-ray crystallography $C_{24}H_{60}BrLi_3N_6$, M = 533.51, Monoclinic, $P2_1/c$, a = 17.7718(4), b = 12.1985(3), c = 17.2945(5) Å, α = 90, β = 118.2370(10), γ = 90°, V = 3303.09(15) Å^3, Z = 4, ρ_{calc} = 1.073 g cm^{-3}, λ = 1.54184 Å, μ = 1.823 mm^{-1}, 26193 reflections collected, 5811 unique, θ_{max} = 66.687°, R_{int} = 0.0562, $R1$ = 0.0414 ($F_{obs} > 4\sigma(F_{obs})$), $wR2$ = 0.0901, S = 1.023, 307 parameters, peak/hole 0.277/-0.345 e Å^{-3}.

4.3.9 Synthesis and characterisation of $(DA)_4Cu(OCN)Li_4(TMEDA)_2$ 18

*n*BuLi (1.25 mL, 1.6 M in hexanes, 2 mmol) was added to a stirred solution of DAH (0.28 mL, 2 mmol) and TMEDA (0.3 mL, 2 mmol) in hexane (4 mL) at −78 °C. The resulting solution was returned to room temperature to give a yellow solution that was transferred to a suspension of CuOCN (0.11 g, 1 mmol) in hexane (1 mL) at −78 °C. The mixture was returned to room temperature to give a grey suspension, which was filtered to give a pale yellow solution. Storage at 5 °C for 24 hours gave white block-like crystals. Yield 0.11 g (14 % wrt. CuOCN). Melting point dec. >95 °C. Elemental Analysis, $C_{37}H_{88}CuLi_4N_9O$ requires (%) C, 57.98; H, 11.57; N, 16.45. Found (%) C, 57.77; H, 11.68; N, 16.76. Selected IR spectroscopy (nujol) $\overline{\nu}$ 2207 (s, CN), 1353 (m, CO), 1293 (m, CO) cm^{-1}. NMR spectroscopy ^{1}H NMR (500 MHz, 298 K, C_6D_6): δ 3.88–3.40 (br, m, 6.2H, DA-CH), 3.3 (br, m, 0.53H, DA-CH), 3.14 (m, 0.15H, DA-CH), 3.11 (septet, $^3J_{HH}$ = 6 Hz, 1.12H, DA-CH), 2.78 (octet, $^3J_{HH}$ = 6 Hz, 0.14H, DAH-CH), 2.01 (s, 24H, TMEDA-Me), 1.94 (s, 8H, TMEDA-CH_2), 1.71–1.38 (br, m, 22H, DA-Me), 1.37 (d, $^3J_{HH}$ = 6 Hz, 3H, DA-Me), 1.35–1.25 (br, m, 16H, DA-Me), 1.23 (d, $^3J_{HH}$ = 6 Hz, 3H, DA-Me), 1.22–1.14 (br, m, 4H, DA-Me), 0.94 (d, $^3J_{HH}$ = 6 Hz, 0.8H, DAH-Me). ^{13}C NMR (125 MHz, 298 K, C_6D_6): δ 57.3 (TMEDA-CH_2), 50.1 (DA-CH), 49.8 (DA-CH), 49.6 (DA-CH), 49.2 (DA-CH), 48.6 (DA-CH), 48.3 (DA-CH), 45.9 (TMEDA-Me), 44.9 (DAH-CH), 44.8 (DAH-CH), 28.2 (DA-Me), 27.8 (DA-Me), 27.7 (DA-Me), 27.0 (DA-Me), 26.0 (DA-Me), 25.8 (DA-Me), 25.2 (DA-Me), 25.1 (DA-Me), 25.2 (DAH-Me), 25.1 (DAH-Me). ^{7}Li NMR (194 MHz,

298 K, C_6D_6): δ 2.34 (br, s, 0.78Li), 2.14 (sh, 0.22Li), 1.58 (s, 0.94Li), 0.84 (s, 0.40Li), 0.37 (s, 1.66Li). X-ray crystallography $C_{37}H_{88}CuLi_4N_9O$, M = 766.46, Triclinic, $P\bar{1}$, a = 11.9447(8), b = 13.7635(9), c = 16.4214(11) Å, α = 80.989(3), β = 78.164(3), γ = 67.824(3)°, V = 2437.5(3) Å^3, Z = 2, ρ_{calc} = 1.044 g cm^{-3}, λ = 1.54184 Å, μ = 0.881 mm^{-1}, 35010 reflections collected, 8630 unique, θ_{max} = 66.920°, R_{int} = 0.0420, $R1$ = 0.0572 ($F_{obs} > 4\sigma(F_{obs})$), $wR2$ = 0.1881, S = 513 parameters, peak/hole 0.547/-0.874 e Å^{-3}.

4.3.10 Synthesis and characterisation of TMPLi 9a

To a solution of TMPH (0.68 mL, 4 mmol) in hexane (4 mL) was added *n*BuLi (2.5 mL, 1.6 M in hexanes, 4 mmol) at −78 °C. The solution was warmed to room temperature and stirred for *ca.* 5 minutes. Storage of the pale yellow solution at −27 °C for 24 h gave a crop of colourless block-like crystals. Yield 247 mg (42 %). Melting point 196 °C. Elemental Analysis, $C_9H_{18}Li$ requires (%) C, 73.44; H, 12.33; N, 9.52. Found (%) C, 72.82; H, 12.41; N, 9.85. NMR spectroscopy ^{1}H NMR (500 MHz, 298 K, C_6D_6): δ 1.77 (m, 2H, TMP-4-tet), 1.72 (m, 0.66H, TMP-4-tri), 1.53 (m, 0.25H, TMPH-4), 1.37 (m, 4H, TMP-3,5-tet), 1.36 (br, 1.35 (s, 12H, TMP-Me-tet), 1.30 (s, 4H, TMP-Me-tri), 1.29 (m, 1.33H, TMP-3,5-tri), 1.24 (m, 0.5H, TMPH-3,5), 1.06 (s, 1.5H, TMPH-Me). ^{7}Li NMR (194 MHz, 298 K, C_6D_6): δ 2.24 (s). ^{13}C NMR (125 MHz, 298 K, C_6D_6): δ 52.0 (TMP-2,6-tet), 51.9 (TMP-2,6-tri), 49.2 (TMPH-2,6), 42.7 (TMP-3,5-tri), 42.4 (TMP-3,5-tet), 38.2 (TMPH-3,5), 36.6 (TMP-Me-tri), 36.5 (TMP-Me-tet), 31.6 (TMPH-Me), 19.7 (TMP-4-tet), 19.4 (TMP-4-tri), 18.4 (TMPH-4).

4.3.11 Synthesis and characterisation of TMPCu 9e

To a solution of TMPH (0.68 mL, 4 mmol) in hexane/THF (3mL/3mL) was added *n*BuLi (2.5 mL, 1.6 M in hexanes, 4 mmol) at −78 °C. The solution was warmed to room temperature, then transferred to a suspension of CuCl (0.4 g, 4 mmol) in hexane/THF (3mL/3mL) at −78 °C. The suspension was warmed to room temperature and stirred for *ca.* 15 mins after which time a black discolouration occurred. The solution was heated to reflux and filtered whilst hot. The solution was stored and room temperature for 1 h and then at 5 °C for 24 h to give colourless

crystals. Yield = 147 mg (18 % wrt Cu). Melting point 236 °C. Elemental Analysis, $C_9H_{18}Cu$ requires C, 53.04; H, 8.90; N, 6.76. Found (%) C, 52.78; H, 8.78; N, 6.87. NMR spectroscopy ^{1}H NMR (500 MHz, 298 K, C_6D_6): δ 1.71 (s, 12H, TMP-Me), 1.60 (br, m, 2H, TMP-4), 1.40 (m, 4H, TMP-3,5). ^{13}C NMR (125 MHz, 298 K, C_6D_6): δ 56.5 (TMP-2,6), 41.8 (TMP-3,5), 37.9 (br, TMP-Me), 18.6 (TMP-4).

4.4 Towards the Synthesis of Lithium Bis(amido)-argentates

4.4.1 Synthesis and characterisation of $(TMP)_2AgLi$ 19

Method (a) To a solution of TMPH (0.34 mL, 2 mmol) and THF (0.08 mL, 1 mmol) in hexane (3 mL) was added *n*BuLi (1.25 mL, 1.6 M in hexanes, 2 mmol) at −78 °C. The solution was returned to room temperature, whereupon it was transferred to a slurry of AgSCN (0.165 g, 1 mmol) in hexane (1 mL) at −78 °C. The mixture darkened upon warming to room temperature to give a black suspension, which was filtered to give a yellow solution. Storage of the filtrate at −27 °C for 24h gave a few needle-like crystals. *Method* (b) To a solution of TMPH (0.34 mL, 2 mmol) in toluene/diisopropyl ether (3 mL/1 mL) was added *n*BuLi (1.25 mL, 1.6 M in hexanes, 2 mmol) at −78 °C. The solution was warmed to room temperature and transferred to a slurry of AgSCN (0.165 g, 1 mmol) in toluene/diisopropyl ether (1 mL/1 mL). The mixture was warmed to room temperature to give a dark (but translucent) solution and filtered to give a straw-coloured solution. Storage of the filtrate at −27 °C for 24h gave a crop of needle-like crystals. Yield 75 mg (18 % wrt AgSCN). Melting point 173 °C (decomp.). NMR spectroscopy ^{1}H NMR (500 MHz, 298 K, C_6D_6): δ 1.91–1.79 (m, 2H, TMP-4), 1.74–1.67 (m, 8H, TMP-3,5), 1.67–1.58 (m, 4H, TMP-4), 1.54 (s, 12H, TMP-Me), 1.46 (s, 12H, TMP-Me), 1.19–1.09 (s, 8H, TMP-3,5), 1.06 (s, 1H, TMPH-Me). ^{13}C NMR (125 MHz, 298 K, C_6D_6): δ 54.8 (d, $^2J_{Ag-C} = 3$ Hz, TMP-2,6), 49.2 (TMPH-2,6), 41.1 (d, $^3J_{Ag-C} = 6$ Hz, TMP-3,5), 40.1 (s, TMP-Me), 38.2 (TMPH-3,5), 35.5 (s, TMP-Me), 31.6 (TMPH-Me), 19.5 (s, TMP-4), 18.4 (TMPH-4). ^{7}Li NMR (194 MHz, 298 K, C_6D_6): δ 1.06 (s). Elemental Analysis, $C_{36}H_{72}Ag_2Li_2N_4$ requires (%) C, 54.69;

H, 9.18; N, 7.09. Found (%) C, 51.84; H, 8.91; N, 7.31. X-ray crystallography: $C_{36}H_{72}Ag_2Li_2N_4$, M = 790.59, Monoclinic, $C2/c$, a = 22.1326(5), b = 8.3936(2), c = 22.8868(6) Å, α = 90, β = 109.5610(10), γ = 90°, V = 4006.34(17) Å^3, Z = 4, ρ_{calc} = 1.311 g cm^{-3}, λ = 1.54184 Å, μ = 8.026 mm^{-1}, 18817 reflections collected, 3517 unique, θ_{max} = 66.621°, R_{int} = 0.0489 , $R1$ = 0.0257 ($F_{obs} > 4\sigma(F_{obs})$), $wR2$ = 0.0537, S = 1.128, parameters, peak/hole 0.295 /-0.496 e Å^{-3}.

4.4.2 Synthesis and characterisation of TMPAg 20

To a solution of TMPH (0.34 mL, 2 mmol) in toluene/diisopropyl ether (6 mL/2 mL) was added nBuLi (1.25 mL, 1.6 M in hexanes, 2 mmol) at −78 °C. The solution was warmed to room temperature whereupon it was transferred to a slurry of AgSCN (0.33 g, 2 mmol) in toluene/diisopropyl ether (2 mL/2 mL) at −78 °C. The mixture was warmed to room temperature to give a grey-blue suspension, which was subsequently filtered to give a colourless solution and concentrated. Storage at −27 °C gave a crop of needle-like crystals. Yield 135 mg (27 % wrt AgSCN). Melting point 245 °C (decomp.). Elemental analysis, $C_9H_{18}Ag$ requires (%) C, 43.57; H, 7.31; N, 5.65. Found (%) C, 46.48; H, 7.23; N, 5.87. ^{1}H NMR (500 MHz, 298 K, C_6D_6): δ 7.13–6.99 (m, 0.5H, toluene), 3.44 (septet, $^3J_{HH}$ = 6 Hz, 0.04H, DIPE), 2.11 (s, 0.3H, toluene), 1.76 (m, 2H, TMP-4), 1.63 (s, 12H, TMP-Me), 1.55 (m, 4H, TMP-3,5), 1.06 (d, $^3J_{HH}$ = 6 Hz, DIPE). ^{13}C NMR (125 MHz, 298 K, C_6D_6): δ 128.5, 128.1, 127.9, 125.2 (toluene), 67.6 (DIPE), 56.7 (t, $^2J_{Ag-C}$ = 2 Hz, TMP-2,6), 42.2 (t, $^3J_{Ag-C}$ = 3 Hz, TMP-3,5), 38.4 (br, TMP-Me), 31.6 (TMPH-Me), 22.6 (toluene), 20.9 (DIPE), 19.6 (TMP-4).

4.4.3 Synthesis and characterisation of $(TMP)_2Ag(CN)Li_2(THF)$ 21

To a solution of TMPH (0.34 mL, 2 mmol) in toluene (4 mL) at −78 °C was added nBuLi (1.25 mL, 2 mmol). The solution was warmed to room temperature whereupon it was transferred to a slurry of AgCN (0.13 g, 1 mmol) in toluene (2 mL) at −78 °C. The suspension was warmed to 0 °C and stirred for 10 minutes, and then stirred at room temperature for a further 10 minutes. During this time, the solution darkened. After no further darkening occurred, the solvent was re-

moved *in vacuo* and THF (3 mL) was added. This was subsequently removed *in vacuo* and the residue digested in hexane (6 mL) and then toluene (6 mL). Filtration gave an orange-yellow solution, which was concentrated until precipitation occurred. The precipitate was dissolved with gentle warming and the solution was stored at 5 °C for 24h, after which time a crop of block-like crystals formed. Yield 65 mg (13 % wrt AgCN). Melting point 115 °C (decomp.). Elemental Analysis, $C_{46}H_{88}Ag_2Li_4N_6O_2$ requires (%) C, 55.21; H, 8.86; N, 8.40. Found (%) C, 54.49; H, 8.57; N, 8.43. Selected IR spectroscopy (nujol) $\overline{\nu}$ 2150 (br, w), 2102 (s) cm^{-1}. NMR spectroscopy ^{1}H NMR (500 MHz, 298 K, C_6D_6): δ 3.54 (br, m, 4H, THF), 2.01 (br, m, 2H, TMP-4), 1.81 (br, m, 4H, TMP-3,5), 1.67 (s, 12H, TMP-Me), 1.64–1.61 (br, 2H, TMP-4), 1.46 (br, s, 16H, TMP-Me + TMP-3,5), 1.31 (br, m, 4H, THF), 1.06 (s, 1.5H, TMPH-Me). ^{13}C NMR (125 MHz, 298 K, C_6D_6): δ 168.2 (CN), 68.2 (THF), 54.1 (d, $^2J_{Ag-C}$ = 3 Hz, TMP-2,6), 49.1 (TMPH-2,6), 38.8 (br, TMP-3,5), 38.4 (TMP-Me), 38.2 (TMPH-3,5), 35.2 (TMP-Me), 31.6 (TMPH-Me), 24.9 (THF), 19.7 (TMP-4), 18.4 (TMPH-4). ^{7}Li NMR (194 MHz, 298 K, C_6D_6): δ 1.09 (s, 0.07Li, G), 0.29 (s, 1Li, L). G = Gilman, L = Lipshutz-type. X-ray crystallography $C_{46}H_{88}Ag_2Li_4N_6O_2$, M = 1000.72, Triclinic, $P\overline{1}$, a = 8.3861(3), b = 11.5994(4), c = 14.0500(5) Å, α = 86.881(2), β = 79.282(2), γ = 83.876(2)°, V = 1334.35(8) Å^3, Z = 1, ρ_{calc} = 1.245 g cm^{-3}, λ = 1.54184 Å, μ = 6.165 mm^{-1}, 14620 reflections collected, 4655 unique, θ_{max} = 66.637 °, R_{int} = 0.0325, $R1$ = 0.0272 ($F_{obs} > 4\sigma(F_{obs})$), $wR2$ = 0.0673, S = 1.077, 307 parameters, peak/hole 0.486/−0.377 e Å^{-3}.

4.5 Studies of TMPLi-TMPCu Aggregates in Solution: Unexpected Reactivity with Aromatic Solvents

4.5.1 Reactions of TMPLi and TMPCu with C_6D_6

Reaction of TMPLi and TMPCu (3:1) in C_6D_6

An NMR tube was charged with TMPLi (33 mg, 0.22 mmol) and TMPCu (15 mg, 0.07 mmol). C_6D_6 (0.7 mL) was added and the sample was heated to 50 °C

for *ca.* 24h. ^{7}Li NMR (194 MHz, 298 K, C_6D_6): δ 2.20 (s, 2Li, **9a**), 2.09 (s, 2Li, d_5-**22a**), 1.64 (s, 1Li, **9b**), 1.40 (s, 0.1Li, d_5-**22b**), −2.94 (s, 0.1Li, **22b**), −4.34 (s, 1Li, d_5-**22a**).

Reaction of TMPLi and TMPCu (2:1) in C_6D_6

An NMR tube was charged with TMPLi (29 mg, 0.20 mmol) and TMPCu (20 mg, 0.10 mmol). C_6D_6 (0.7 mL) was added and the sample was heated to 50 °C for *ca.* 24h. ^{7}Li NMR (194 MHz, 298 K, C_6D_6): δ 2.20 (s, 1Li, **9a**), 2.09 (s, 2Li, d_5-**22a**), 1.64 (s, 0.7Li, **9b**), 1.40 (s, 0.5Li, d_5-**22b**), 0.90 (s, 0.3Li, **9c**), −2.94 (s, 0.5Li, **22b**), −3.78, (s, 0.1Li, unidentified), −4.34 (s, 1Li, d_5-**22a**).

Reaction of TMPLi and TMPCu (1:1) in C_6D_6

An NMR tube was charged with TMPLi (23 mg, 0.16 mmol) and TMPCu (30 mg, 0.15 mmol). C_6D_6 (0.7 mL) was added and the sample was heated to 50 °C for *ca.* 24h. ^{7}Li NMR (194 MHz, 298 K, C_6D_6): δ 2.20 (s, 1.4Li, **9a**), 2.09 (s, 2Li, d_5-**22a**), 1.64 (s, 3Li, *i*-**9c**), 1.40 (s, 0.7Li, d_5-**22b**), 0.90 (s, 1.7Li, **9c**), −1.53 (s, 0.7Li, d_5-**22c**), −2.94 (s, 0.7Li, **22b**), −3.78, (s, 0.3Li, unidentified), −4.34 (s, 1Li, d_5-**22a**).

Reaction of TMPLi and TMPCu (1:2) in C_6D_6

An NMR tube was charged with TMPLi (15 mg, 0.10 mmol) and TMPCu (40 mg, 0.20 mmol). C_6D_6 (0.7 mL) was added and the sample was heated to 50 °C for *ca.* 24h. ^{7}Li NMR (194 MHz, 298 K, C_6D_6): δ 2.20 (s, 0.1Li, **9a**), 1.64 (s, 0.7Li, *i*-**9c**), 1.40 (s, 0.2Li, d_5-**22b**), 0.90 (s, 1.2Li, **9c**), −1.53 (s, 1Li, d_5-**22c**), −2.94 (s, 0.2Li, **22b**), −3.78, (s, 0.1Li, unidentified).

Reactions of TMPLi and TMPCu (1:3) in C_6D_6

An NMR tube was charged with TMPLi (15 mg, 0.10 mmol) and TMPCu (60 mg, 0.30 mmol). C_6D_6 (0.7 mL) was added and the sample was heated to 50 °C for *ca.* 24h. ^{7}Li NMR (194 MHz, 298 K, C_6D_6): δ 1.64 (s, 1.7Li, *i*-**9c**), 1.30 (s,

0.2Li, unidentified), 0.90 (s, 1Li, **9c**), 0.66 (s, 0.2Li, unidentified), −1.53 (s, 1Li, d_5-**22c**).

4.5.2 Reactions of TMPLi and TMPCu with C_6H_6

Reaction of TMPLi and TMPCu (3:1) in C_6H_6

An NMR tube was charged with TMPLi (33 mg, 0.22 mmol) and TMPCu (15 mg, 0.07 mmol). C_6H_6 (0.7 mL) was added and the sample was heated to 50 °C for *ca.* 24h. The solvent was removed *in vacuo* and replaced with C_6D_6 for NMR spectroscopy. ^{7}Li NMR (194 MHz, 298 K, C_6D_6): δ 2.20 (s, 1.6Li, **9a**), 2.09 (s, 2Li, **22a**), 1.65 (s, 0.3Li, **9b**), 1.40 (s, 0.1Li, **22b**), −2.86 (s, 0.1Li, **22b**), −4.26 (s, 1Li, **22a**).

Reaction of TMPLi and TMPCu (2:1) in C_6H_6

An NMR tube was charged with TMPLi (29 mg, 0.20 mmol) and TMPCu (20 mg, 0.10 mmol). C_6H_6 (0.7 mL) was added and the sample was heated to 50 °C for *ca.* 24h. The solvent was removed *in vacuo* and replaced with C_6D_6 for NMR spectroscopy. ^{7}Li NMR (194 MHz, 298 K, C_6D_6): δ 2.20 (s, 0.7Li, **9a**), 2.09 (s, 2Li, **22a**), 1.65 (s, 0.4Li, **9b**), 1.40 (s, 0.5Li, **22b**), 0.90 (s, 0.1Li, **9c**), −2.42 (0.05Li, unidentified), −2.86 (s, 0.5Li, **22b**), −3.70 (s, 0.1Li, unidentified), −4.26 (s, 1Li, **22a**).

Reaction of TMPLi and TMPCu (1:1) in C_6H_6

An NMR tube was charged with TMPLi (23 mg, 0.16 mmol) and TMPCu (30 mg, 0.15 mmol). C_6H_6 (0.7 mL) was added and the sample was heated to 50 °C for *ca.* 24h. The solvent was removed *in vacuo* and replaced with C_6D_6 for NMR spectroscopy. ^{7}Li NMR (194 MHz, 298 K, C_6D_6): δ 2.09 (s, 0.2Li, **22a**), 1.65 (s, 0.2Li, *i*-**9c**), 1.40 (s, 1Li, **22b**), 0.90 (s, 0.2Li, **9c**), −0.63 (s, 0.05Li, unidentified), −1.46 (s, 0.3Li, **22c**), −2.42 (0.1Li, unidentified), −2.86 (s, 1Li, **22b**), −3.70 (s, 0.2Li, unidentified), −4.03 (s, 0.05Li, unidentified), −4.26 (s, 0.1Li, **22a**).

Reaction of TMPLi and TMPCu (1:2) in C_6H_6

An NMR tube was charged with TMPLi (15 mg, 0.10 mmol) and TMPCu (40 mg, 0.20 mmol). C_6H_6 (0.7 mL) was added and the sample was heated to 50 °C for *ca.* 24h. The solvent was removed *in vacuo* and replaced with C_6D_6 for NMR spectroscopy. ^{7}Li NMR (194 MHz, 298 K, C_6D_6): δ 1.65 (s, 0.5Li, *i*-**9c**), 1.40 (s, 1Li, **22b**), 0.90 (s, 0.6Li, **9c**), −0.63 (s, 0.1Li, unidentified), −0.90 (s, 0.lLi, unidentified), −1.46 (s, 0.8Li, **22c**), −2.54 (0.05Li, unidentified), −2.86 (s, 1Li, **22b**), −3.08 (s, 0.15Li, unidentified).

Reaction of TMPLi and TMPCu (1:3) in C_6H_6

An NMR tube was charged with TMPLi (15 mg, 0.10 mmol) and TMPCu (60 mg, 0.30 mmol). C_6H_6 (0.7 mL) was added and the sample was heated to 50 °C for *ca.* 24h. The solvent was removed *in vacuo* and replaced with C_6D_6 for NMR spectroscopy. ^{7}Li NMR (194 MHz, 298 K, C_6D_6): δ 1.65 (s, 0.6Li, *i*-**9c**), 1.40 (s, 0.6Li, **22b**), 0.90 (s, 0.8Li, **9c**), −1.46 (s, 1Li, **22c**), −2.86 (s, 0.6Li, **22b**).

4.5.3 Reactions of TMPLi and TMPCu in mesitylene

Reaction of TMPLi and TMPCu (3:1) in mesitylene

An NMR tube was charged with TMPLi (33 mg, 0.22 mmol) and TMPCu (15 mg, 0.07 mmol). Mesitylene (0.7 mL) was added and the sample was heated to 50 °C for *ca.* 24h. The solvent was removed *in vacuo* and replaced with C_6D_6 for NMR spectroscopy. ^{7}Li NMR (194 MHz, 298 K, C_6D_6): δ 2.21 (s, 1Li, **9a**), 1.65 (s, 1Li, **9b**), 0.90 (s, 0.25Li, **9c**), −3.57 (s, 0.05Li, uidentified).

Reaction of TMPLi and TMPCu (2:1) in mesitylene

An NMR tube was charged with TMPLi (29 mg, 0.20 mmol) and TMPCu (20 mg, 0.10 mmol). Mesitylene (0.7 mL) was added and the sample was heated to 50 °C for *ca.* 24h. The solvent was removed *in vacuo* and replaced with C_6D_6 for NMR spectroscopy. ^{7}Li NMR (194 MHz, 298 K, C_6D_6): δ 2.21 (s, 0.6Li, **9a**), 1.65

(s, 1Li, **9b** + *i*-**9c**), 0.90 (s, 0.5Li, **9c**), −3.57 (s, 0.05Li, unidentified), −4.53 (s, 0.1Li, **23**).

Reaction of TMPLi and TMPCu (1:1) in mesitylene

(a) An NMR tube was charged with TMPLi (23 mg, 0.16 mmol) and TMPCu (30 mg, 0.15 mmol). Mesitylene (0.7 mL) was added and the sample was heated to 50 °C for *ca.* 24h. The solvent was removed *in vacuo* and replaced with C_6D_6 for NMR spectroscopy. ^{7}Li NMR (194 MHz, 298 K, C_6D_6): δ 2.21 (s, 0.5Li, **9a**), 1.65 (s, 1Li, **9b** + *i*-**9c**), 0.90 (s, 1Li, **9c**), −0.43 (s, 0.05Li, unidentified), −3.57 (s, 0.05Li, unidentified), −4.53 (s, 0.2Li, **23**). (b) An NMR tube was charged with TMPLi (23 mg, 0.16 mmol) and TMPCu (30 mg, 0.15 mmol). Mesitylene (0.7 mL) was added and the sample was heated to 50 °C for *ca.* 72h. The solvent was removed *in vacuo* and replaced with C_6D_6 for NMR spectroscopy. ^{7}Li NMR (194 MHz, 298 K, C_6D_6): δ 1.65 (s, 0.16Li, *i*-**24c**), 0.90 (s, 1Li, **9c**), −0.43 (s, 0.11Li, unidentified), −4.53 (s, 0.85Li, **23**).

Reaction of TMPLi and TMPCu (1:2) in mesitylene

An NMR tube was charged with TMPLi (15 mg, 0.10 mmol) and TMPCu (40 mg, 0.20 mmol). Mesitylene (0.7 mL) was added and the sample was heated to 50 °C for *ca.* 24h. The solvent was removed *in vacuo* and replaced with C_6D_6 for NMR spectroscopy. ^{7}Li NMR (194 MHz, 298 K, C_6D_6): δ 2.21 (s, 0.2Li, **9a**), 1.65 (s, 0.6Li, **9b** + *i*-**9c**), 0.90 (s, 1Li, **9c**), −0.43 (s, 0.2Li, unidentified), −4.53 (s, 0.3Li, **23**).

Reaction of TMPLi and TMPCu (1:3) in mesitylene

An NMR tube was charged with TMPLi (15 mg, 0.10 mmol) and TMPCu (60 mg, 0.30 mmol). Mesitylene (0.7 mL) was added and the sample was heated to 50 °C for *ca.* 24h. The solvent was removed *in vacuo* and replaced with C_6D_6 for NMR spectroscopy. ^{7}Li NMR (194 MHz, 298 K, C_6D_6): δ 2.21 (s, 0.2Li, **9a**), 1.65 (s, 0.3Li, *i*-**9c**), 0.90 (s, 1Li, **9c**), −0.43 (s, 0.1Li, unidentified), −4.53 (s, 0.2Li, **23**).

The following compounds were identified by their occurrence in ^{1}H, ^{7}Li and ^{13}C NMR spectra obtained from multiple reaction mixtures.

4.5.4 $(TMP)_4CuLi_3$ 9b

^{1}H NMR (500 MHz, 298 K, C_6D_6): δ 1.72 (br, m, 4H, TMP-4), 1.64 (br, m, 4H, TMP-3,5), 1.59 (s, 12H, TMP-Me), 1.56 (s, 12H, TMP-Me), 1.54 (br, m, 2H, TMP-4), 1.47 (br, m, 4H, TMP-3,5), 1.36 (s, 24H, TMP-Me), 1.23 (br, m, 4H, TMP-3,5), 1.08 (br, m, 4H, TMP-3,5). ^{13}C NMR (125 MHz, 298 K, C_6D_6): δ 54.16, 51.98 (TMP-2,6); 42.44, 42.11 (TMP-3,5); 39.73, 37.76, 35.74, 34.03 (TMP-Me); 19.60, 19.13 (TMP-4). ^{7}Li NMR (194 MHz, 298 K, C_6D_6): δ 2.22 (s, 1Li), 1.65 (s, 2Li).

4.5.5 $(TMP)_4Cu_3Li$ 9d

^{1}H NMR (500 MHz, 298 K, C_6D_6): δ 1.84 (m, 2H, TMP-4), 1.79 (s, 12H, TMP-Me), 1.72 (s, 12H, TMP-Me), 1.72 (br, m, 4H, TMP-4), 1.65 (m, 4H, TMP-3,5), 1.60 (s, 12H, TMP-Me), 1.57 (s, 12H, TMP-Me), 1.57 (br, m, 2H, TMP-4), 1.56 (br, m, 8H, TMP-3,5), 1.13 (m, 4H, TMP-3,5). ^{13}C NMR (125 MHz, 298 K, C_6D_6): δ 56.93, 54.24 (TMP-2,6); 42.60, 42.09 (TMP-3,5); 39.73, 37.65 (br), 36.60 (br) , 34.81 (TMP-Me); 19.26, 19.15 (TMP-4). ^{7}Li NMR (194 MHz, 298 K, C_6D_6): δ 0.96 (s).

4.5.6 d_5-(μ-Ph)$(TMP)_3CuLi_3$ d_5-22a

^{1}H NMR (500 MHz, 298 K, C_6D_6): δ 1.73 (m, 4H, TMP-4), 1.69 (s, 6H, TMP-Me), 1.60 (m, 4H, TMP-3,5), 1.58 (m, 2H, TMP-4), 1.55 (s, 6H, TMP-Me), 1.44 (m, 4H, TMP-3,5), 1.41 (s, 6H, TMP-Me), 1.39 (s, 6H, TMP-Me), 1.16 (s, 6H, TMP-Me), 0.90 (s, 6H, TMP-Me), 0.80 (m, 4H, TMP-3,5). ^{13}C NMR (125 MHz, 298 K, C_6D_6): δ 53.86, 51.94, 50.87 (TMP-2,6), 42.15, 42.01, 41.42 (TMP-3,5), 37.26, 36.96, 36.69, 36.67, 36.07, 35.09 (TMP-Me), 19.74, 19.51 (TMP-4). ^{7}Li NMR (194 MHz, 298 K, C_6D_6): δ 2.09 (s, 2Li), -4.33 (s, 1Li).

4.5.7 d_5-(μ-Ph)(TMP)$_3$Cu$_2$Li$_2$ d_5-22b

^{1}H NMR (500 MHz, 298 K, C_6D_6): δ 1.78 (br, m, 2H, TMP-4), 1.73 (s, 6H, TMP-Me), 1.68 (br, m, 2H, TMP-3,5) 1.62 (s, 6H, TMP-Me), 1.58 (br, m, 2H, TMP-4), 1.57 (br, m, 2H, TMP-4), 1.55 (s, 6H, TMP-Me), 1.52 (br, m, 2H, TMP-3,5), 1.51 (s, 6H, TMP-Me), 1.45 (br, m, 2H, TMP-3,5), 1.44 (br, m, 2H, TMP-3,5), 1.41 (s, 6H, TMP-Me), 1.37 (br, m, 2H, TMP-4), 1.15 (s, 6H, TMP-Me), 1.14 (br, m, 2H, TMP-3,5), 0.45 (m, 2H, TMP-3,5). ^{13}C NMR (125 MHz, 298 K, C_6D_6): δ 54.05, 53.96, 53.01 (TMP-2,6); 42.51, 41.85, 41.05 (TMP-3,5); 39.46, 39.26, 38.20, 35.87, 34.10, 33.29 (TMP-Me); 19.60, 19.20, 18.80 (TMP-4). ^{7}Li NMR (194 MHz, 298 K, C_6D_6): δ 1.40 (s, 1Li), -2.94 (s, 1Li).

4.5.8 d_5-(μ-Ph)(TMP)$_3$Cu$_3$Li d_5-22c

^{1}H NMR (500 MHz, 298 K, C_6D_6): δ 1.99 (s, 6H, TMP-Me), 1.83 (br, m, 2H, TMP-4), 1.82 (s, 6H, TMP-Me), 1.77 (s, 6H, TMP-Me), 1.65 (br, m, 2H, TMP-3,5) , 1.64 (br, m, 2H, TMP-4), 1.60 (br, m, 2H, TMP-3,5), 1.59 (s, 6H, TMP-Me), 1.46 (br, m, 2H, TMP-3,5), 1.45 (br, m, 2H, TMP-3,5), 1.40 (s, 6H, TMP-Me), 1.37 (m, 2H, TMP-3,5), 1.35 (br, m, 2H, TMP-4), 1.20 (s, 6H, TMP-Me), 0.45 (m, 2H, TMP-3,5). ^{13}C NMR (125 MHz, 298 K, C_6D_6): δ 56.44, 53.17 (TMP-2,6); 43.18, 42.51, 41.27 (TMP-3,5); 40.45, 39.10, 36.84*, 33.30, 32.48 (TMP-Me) ;19.32, 19.15, 18.72. ^{7}Li NMR (194 MHz, 298 K, C_6D_6): δ -1.53 (s). * HSCQ spectroscopy shows two TMP-Me cross-peaks to this carbon resonance (i.e. two coincident Me signals)

4.5.9 (μ-Ph)(TMP)$_3$CuLi$_3$ 22a

^{1}H NMR (500 MHz, 298 K, C_6D_6): δ 7.83 (d, $^3J_{HH}$ = 7 Hz, 2H, Ar-o), 6.98 (t, 2H, $^3J_{HH}$ = 7 Hz, Ar-m), 6.80 (t, $^3J_{HH}$ = 7 Hz, 1H, Ar-p), 1.73 (m, 4H, TMP-4), 1.69 (s, 6H, TMP-Me), 1.60 (m, 4H, TMP-3,5), 1.58 (m, 2H, TMP-4), 1.55 (s, 6H, TMP-Me), 1.44 (m, 4H, TMP-3,5), 1.41 (s, 6H, TMP-Me), 1.39 (s, 6H, TMP-Me), 1.16 (s, 6H, TMP-Me), 0.90 (s, 6H, TMP-Me), 0.80 (m, 4H, TMP-3,5). ^{13}C NMR (125 MHz, 298 K, C_6D_6): δ 167.7 (Ar-i), 141.3 (Ar-o), 128.1 (Ar-m), 124.1 (Ar-p), 53.86, 51.94, 50.87 (TMP-2,6), 42.15, 42.01, 41.42 (TMP-3,5), 37.26, 36.96,

36.69, 36.07, 35.09 (TMP-Me), 19.74, 19.51 (TMP-4). ^{7}Li NMR (194 MHz, 298 K, C_6D_6): δ 2.09 (s, 2Li), −4.26 (s, 1Li).

4.5.10 (μ-Ph)(TMP)$_3$Cu$_2$Li$_2$ 22b

^{1}H NMR (500 MHz, 298 K, C_6D_6): δ 7.85 (d, $^{3}J_{HH}$ = 7 Hz, 2H, Ar-*o*), 7.09 (t, $^{3}J_{HH}$ = 7 Hz, 2H, Ar-*m*), 6.93 (t, $^{3}J_{HH}$ = 7 Hz, 1H, Ar-*p*), 1.78 (br, m, 2H, TMP-4), 1.73 (s, 6H, TMP-Me), 1.68 (br, m, 2H, TMP-3,5) 1.62 (s, 6H, TMP-Me), 1.58 (br, m, 2H, TMP-4), 1.57 (br, m, 2H, TMP-4), 1.55 (s, 6H, TMP-Me), 1.52 (br, m, 2H, TMP-3,5), 1.51 (s, 6H, TMP-Me), 1.45 (br, m, 2H, TMP-3,5), 1.44 (br, m, 2H, TMP-3,5), 1.41 (s, 6H, TMP-Me), 1.37 (br, m, 2H, TMP-4), 1.15 (s, 6H, TMP-Me), 1.14 (br, m, 2H, TMP-3,5), 0.45 (m, 2H, TMP-3,5). ^{13}C NMR (125 MHz, 298 K, C_6D_6): δ 164.3 (Ar-*i*), 140.8 (Ar-*o*), 128.9 (Ar-*m*), 125.5 (Ar-*p*), 54.05, 53.96, 53.02 (TMP-2,6); 42.51, 41.85, 41.05 (TMP-3,5); 39.46, 39.27, 38.21, 35.86, 34.10, 33.29 (TMP-Me); 19.60, 19.20, 18.80 (TMP-4). ^{7}Li NMR (194 MHz, 298 K, C_6D_6): δ 1.40 (s, 1Li), −2.86 (s, 1Li).

4.5.11 (μ-Ph)(TMP)$_3$Cu$_3$Li 22c

^{1}H NMR (500 MHz, 298 K, C_6D_6): δ 7.88 (d, $^{3}J_{HH}$ = 7 Hz, 2H, Ar-*o*), 7.15 (t, $^{3}J_{HH}$ = 7 Hz, 2H, Ar-*m*), 7.01 (t, 1H, $^{3}J_{HH}$ = 7 Hz, 1H, Ar-*p*) 1.99 (s, 6H, TMP-Me), 1.83 (br, m, 2H, TMP-4), 1.82 (s, 6H, TMP-Me), 1.77 (s, 6H, TMP-Me), 1.65 (br, m, 2H, TMP-3,5) , 1.64 (br, m, 2H, TMP-4), 1.60 (br, m, 2H, TMP-3,5), 1.59 (s, 6H, TMP-Me), 1.46 (br, m, 2H, TMP-3,5), 1.45 (br, m, 2H, TMP-3,5), 1.40 (s, 6H, TMP-Me), 1.37 (m, 2H, TMP-3,5), 1.35 (br, m, 2H, TMP-4), 1.20 (s, 6H, TMP-Me), 0.45 (m, 2H, TMP-3,5). ^{13}C NMR (125 MHz, 298 K, C_6D_6): δ 165.2 (Ar-*i*), 140.8 (Ar-*o*), 129.1 (Ar-*m*), 126.1 (Ar-*p*), 56.44, 53.17 (TMP-2,6); 43.18, 42.51, 41.27 (TMP-3,5); 40.45, 39.10, 36.84 (br) *, 33.30, 32.48 (TMP-Me) ;19.32, 19.15, 18.72. ^{7}Li NMR (194 MHz, 298 K, C_6D_6): δ −1.46 (s). * HSCQ shows two TMP-Me cross-peaks to this carbon resonance (i.e. two coincident Me signals)

4.5.12 (μ-$Me_2C_6H_3(CH_2)$)(μ-TMP)$_2$$Cu_2$Li 23

^{1}H NMR (500 MHz, 298 K, C_6D_6): δ 6.66 (s, 2H, Ar-*ortho*-CH), 5.88 (s, 1H, Ar-*para*-CH), 2.38 (s, 2H, Ar-CH_2), 1.89 (s, 6H, TMP-Me), 1.86 (s, 6H, Ar-Me), 1.81 (m, 2H, TMP-4), 1.56 (s, 6H, TMP-Me), 1.46 (m, 6H, TMP-4 + TMP-3,5), 1.45 (s, 6H, TMP-Me), 1.15 (s, 6H, TMP-Me), 0.63 (m, 4H, TMP-3,5). ^{13}C NMR (125 MHz, 298 K, C_6D_6): δ 160.7 (Ar-*ipso*), 138.8 (Ar-*meta*), 121.9 (Ar-*ortho*), 116.1 (Ar-*para*), 56.15, 53.16 (TMP-2,6); 42.47, 41.91 (TMP-3,5); 39.69, 38.36, 34.13, 33.91 (TMP-Me); 22.42 (Ar-CH2), 20.84 (Ar-Me), 19.26, 19.00 (TMP-4). ^{7}Li NMR (194 MHz, 298 K, C_6D_6): δ -4.53 (s).

Chapter 5

Studies in Heteroleptic Bis(amido)cuprate Formation

5.1 Introduction

Heterocuprates were introduced in Section 1.4.6, which addressed the case when copper is directly bonded to two different classes of ligand, for example an alkyl ligand and a thiolate ligand. Little subsequent work has been devoted to the understanding of heteroleptic cuprates bearing different ligands of the same class, though they are implicated in the generation of cross-coupled products in conjugate addition and oxidative coupling reactions.[110,130]

Steric effects have been proposed as a determining factor in the isolation of Lipshutz-type cuprates (TMP-based) and adduct cuprates (DMP-based), but there have been no attempts to form heteroleptic cuprates bearing these two different amido ligands. Two primary questions would arise in such a situation. First, is a heteroleptic cuprate favoured over the respective homoleptic cuprates? Second, what type of cuprate structure would be observed?

Synthetically, the approach taken was to prepare a mixture of two amidolithium compounds and combine these with a suitable copper(I) precursor in hydrocarbon solvent, with stoichiometric quantities of donor solvent included in the mixture.

5.2 Results and discussion

Investigations initially focussed upon amine 2-methylpiperidine as a source of the amido ligand MP. Three features of this ligand were of potential interest: its steric similarity to DMP, its inexpensivity and its chirality. Commercial MPH is available as a racemic mixture of enatiomers and hence serves as a suitable point for the introduction of chirality into amidocuprate systems. Since MP had not previously been utilised in cuprate chemistry, attention was first directed toward synthesising the homoleptic cuprate. This was achieved by combining a hexane solution of preformed MPLi also containing THF (1 eq. wrt MPLi) with a suspension of CuBr (0.5 eq. wrt Li) in hexane (Scheme 5.1). Prolonged chilling of the orange filtrate at −27 °C gave a crystalline material which was shown by ^{1}H NMR spectroscopy to contain MP and THF in a 1:1 ratio, consistent with a structure-type seen for $[(DMP)_2CuLi(THF)_2]_2LiBr$. This view was reinforced by ^{7}Li NMR spectroscopy which revealed two Li environments in a 1:2 ratio (see Figure 5.1), a feature which has been previously interpreted in terms of retention of the solid-state structure of adduct cuprates in solution.[171] This structure-type consists of a pentametallic complex which can be viewed as an adduct of monomeric units of Gilman and Lipshutz-type cuprates; alternatively, this structure could be interpreted as two fused Lipshutz-type monomers. ^{13}C NMR spectroscopy gave the expected number of resonances; however, all MP resonances were best described as clusters of peaks, rather than well-resolved singlets. From this, it could be inferred that a number of chemically similar species were likely present in solution. X-ray crystallography confirmed the structure as $[(MP)_2CuLi(THF)_2]_2LiBr$ **1** with the structural features characteristic of adduct cuprates being evident (Figure 5.2).

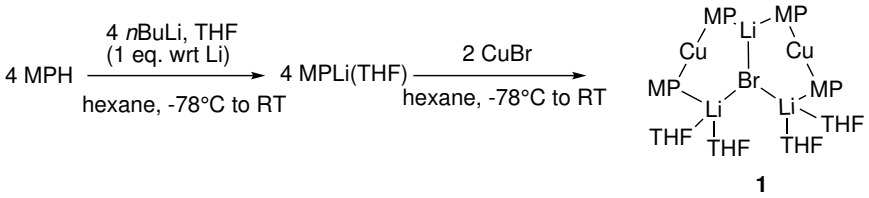

Scheme 5.1: The synthesis of **1**.

Detailed analysis of the crystal structure is complicated by extensive positional disorder of the MP ligands, whereby both enantiomers of the chiral MP ligand are found to occupy similar positions. The space group $P\bar{1}$ (which possesses inversion

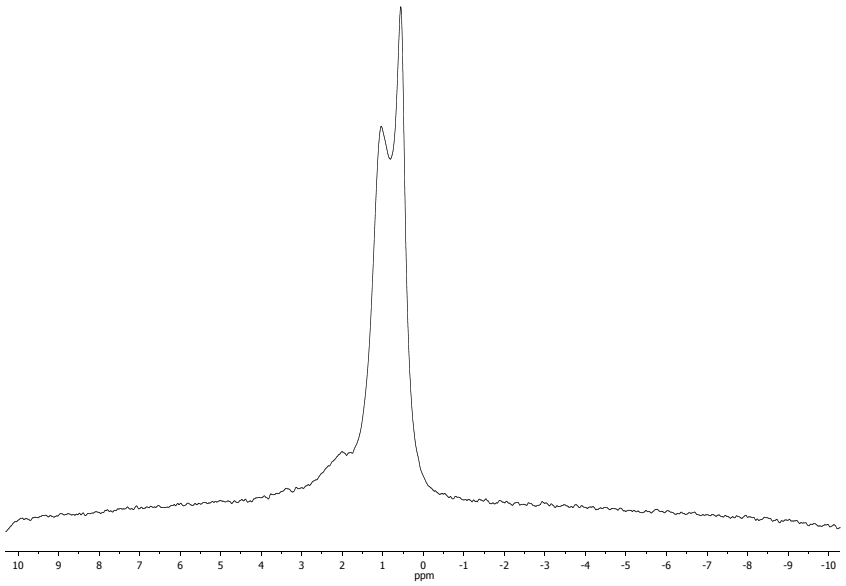

Figure 5.1: ^{7}Li NMR spectrum of **1** in C_6D_6 revealing a 1:2 ratio of low-field and high-field Li environments, respectively. This is consistent with the solid-state data. The resonance at 2.03 ppm is attributable to low-level MPLi formation *in situ*.

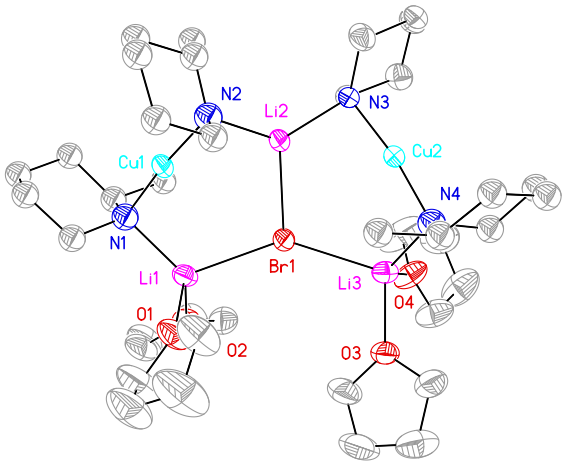

Figure 5.2: Thermal ellipsoid plot of **1** (30 % probability) H-atoms and disorder omitted. One unique stereoisomer is pictured. Selected bond lengths (Å) and angles (°): N1–Cu1 1.885(5), N2–Cu1 1.876(5), N3–Cu2 1.886(4), N4–Cu2 1.880(5), N1–Li1 2.050(10), N2–Li2 1.991(9), N3–Li2 2.018(9), N4–Li3 2.005(10), Br1–Li1 2.568(9), Br1–Li2 2.555(8), Br1–Li3 2.601(10), Cu1–N1–Li1 93.5(3), Cu1–N2–Li2 94.7(3), Cu2–N3–Li2 89.3(3), Cu2–N4–Li3 93.9(3).

symmetry) suggests that equal proportions of *R*- and *S*-MP ligands are present, and this is in accordance with the racemic nature of the starting material. Though individual cuprate aggregates must possess a definite stereochemistry, the average of all possible combinations is seen in the structure, which manifests as severe disorder. Nonetheless, the structure is clearly analogous to previously reported DMP cuprates,[171] with *exo* orientated MP ligands and the equatorial methyl group facing inwards, towards Cu. Assuming that the solid-state structure is retained in solution, as indicated by ^{7}Li NMR spectroscopy, each adduct possesses a unique stereochemistry and distinct resonances are to be expected for each.[i] This may account for the observation of clusters of peaks observed by ^{13}C NMR spectroscopy.

Having established the potential for incorporation of the MP ligand into cuprate systems, attention turned to its deployment with TMP in a heteroleptic system. A 1:1 mixture of TMPH and MPH was treated with *n*BuLi and THF (1 eq. wrt Li) in hexane before being introduced to CuBr (0.5 eq. wrt Li) in hexane (Scheme 5.2). After filtration, this gave an orange solution which deposited crystalline material after 5 days storage at −27 °C.

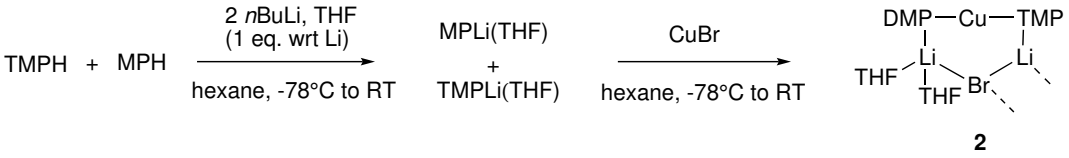

Scheme 5.2: Synthesis of **2**.

^{1}H NMR spectroscopy indicated the presence of MP, TMP and THF in a 1:1:2 ratio – pointing towards the successful fabrication of a heteroleptic species. This could potentially take the form of a Lipshutz-type dimer or an adduct cuprate, both of which would be consistent with the presence of THF. Some decomposition was evidenced through the detection of small amounts of TMPH which is likely due to the extreme moisture sensitivity of these compounds.

X-ray crystallography confirmed the production of a genuine heteroleptic species of Lipshutz-type structure, MP(TMP)Cu(Br)Li$_2$(THF)$_2$ **2** (Figure 5.3). Given the racemic nature of the MPH precursor, it was expected that a centrosymmetric dimer incorporating both enatiomers of the MP ligand would be formed, with the

[i] 10 isomers in total, 4 pairs of enantiomers and two unique isomers which possess mirror-fold symmetry.

enatiomers related by the centre of symmetry. In the event, the projection of the MP methyl groups imparted little steric influence upon the structure and so discrimination between enatiomers of MP adjacent to THF did not occur – this manifests as positional disorder of TMP and MP ligands[ii]. That being said, the two different ligands adopt very different orientations with respect to the metallacyclic core. The TMP ligand lies *endo* with respect to the core, in a manner analogous to behaviour displayed in previously reported Lipshutz-type cuprates.[167,169] In contrast, the MP ligand takes an *exo* stance with respect to the core, as seen in DMP-based adduct cuprates.[171] This leaves sufficient space for two THF molecules to coordinate to the adjacent Li^+ centre, which then becomes four-coordinate (*cf.* TMP-based Lipshutz-type cuprates, which contain mono THF-solvated Li centres[169]).

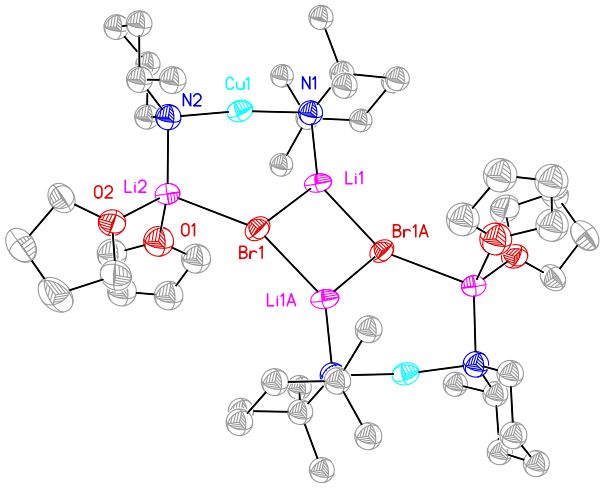

Figure 5.3: Thermal ellipsoid plot of $\mathbf{2}_2$ (30 % probability). H atoms and disorder omitted. One stereoisomer is pictured. Selected bond lengths (Å) and angles (°): N1–Cu1 1.900(7), N2–Cu1 1.878(7), N1–Li1 1.969(13), N2–Li2 2.013(13), Br1–Li1 2.498(13), Br1A–Li1 2.478(12), Br1–Li2 2.625(13), Cu1–N1–Li1 90.9(5), Cu1–N2–Li2 98.0(5).

In an effort to improve the quality of structural information available about het-

[ii]Considering only the chirality of the MP ligands, two unique stereoisomers could possibly be involved – the centrosymmetric {R,S} isomer and the enantiomeric pair of {R,R} and {S,S}. The latter pair of enatiomers must be equally populated and disordered about the centre of symmetry.

eroleptic cuprates, the MP ligand was substituted for DMP, which is not significantly more expensive than MPH. DMP is achiral and therefore was not expected to cause the disorder problems associated with racemic MP. Synthetically, a 1:1 mixture of DMPH and TMPH was lithiated in the presence of THF (1 eq. wrt Li) and subsequently combined with CuBr in hexane (Scheme 5.3). Storage of the orange filtrate at −27 °C gave a crystalline material which ^{1}H NMR spectroscopy indicated contained TMP, DMP and THF in a 1:1:2 ratio, notwithstanding small quantities of free TMPH from decomposition. A structure similar to Lipshutz-type **2**, or else an adduct cuprate was expected and X-ray crystallography verified the compound to be DMP(TMP)Cu(Br)Li_2(THF)$_2$ **3**, with linearly coordinated Cu participating in a centrosymmetric dimer (Figure 5.4).

As for $\mathbf{2}_2$, the monomeric units of $\mathbf{3}_2$ are based upon a six-membered N_2CuLi_2Br rings (Cu–N^{TMP}–Li 91.3(3)°, Cu–N^{DMP}–Li 94.1(3)°) with the occurrence of *endo*-TMP and *exo*-DMP permitting bis(THF) coordination of Li2 (see Figure 5.4). The dimer possesses a chair-like structure in which Li2 and Li2A project above and below the plane of the $(LiBr)_2$ core to accommodate the THF in *pseudo*-axial and *pseudo*-equatorial positions with respect to the six-membered N_2CuLi_2Br monomeric ring to which they belong. This contrasts with the much more planar arrangement seen for the recently reported Lipshutz-type $(TMP)_2Cu(Br)Li_2(THF)$ (see Figure 5.5). Lastly, it is notable that the increased solvation of Li2 is reflected in the coordination sphere of Li2, whereby longer bonds to both N and Br are found compared to those in $(TMP)_2Cu(Br)Li_2(THF)$ (N1–Li1 1.987(11), Br1–Li1 2.461(10), N2–Li2 2.075(12) and Br1–Li2 2.660(11) in **3** *vs.* N2–Li2 1.963(4), Br1–Li2 2.485(4), N1–Li1 2.002(5) and Br1–Li1 2.545(4) in $(TMP)_2Cu(Br)Li_2(THF)$).[168]

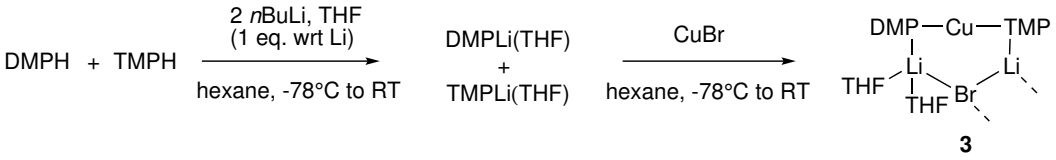

Scheme 5.3: Synthesis of **3**.

With the solid state-structures at hand, the convoluted spectroscopic data of **2** and **3** can be explained. Some decomposition of these compounds in solution was evident, most easily identified through the presence of free TMPH. This notwithstanding, NMR spectroscopy revealed multiple species to be present in C_6D_6 solution. In light of the documented ability of Lipshutz-type cuprates to produce

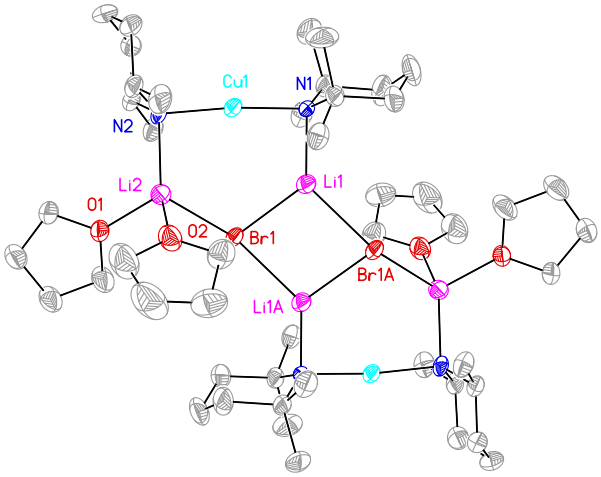

Figure 5.4: Thermal ellipsoid plot of $\mathbf{3}_2$ (30 % probability). H atoms omitted. Selected bond lengths (Å) and angles (°): N1–Cu1 1.921(4), N2–Cu1 1.920(4), N1–Li1 1.987(11), N2–Li2 2.075(12), Br1–Li1 2.461(10), Br1–Li2 2.660(11), Br1–Li1A 2.493(10), Cu1–N1–Li1 91.3(3), Cu1–N2–Li2 94.1(3).

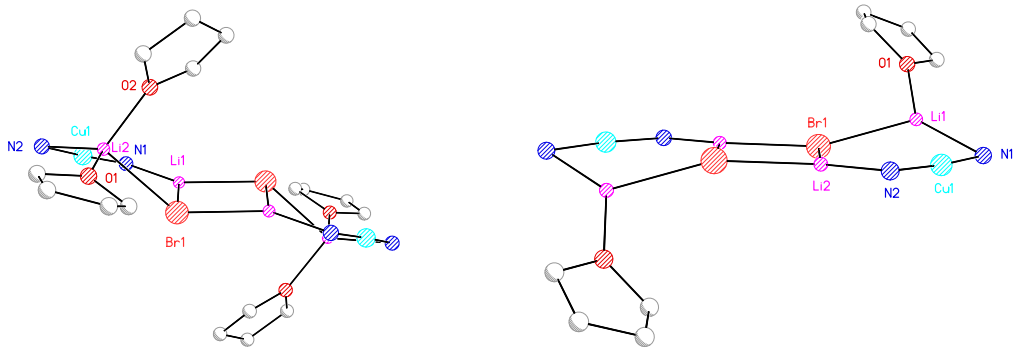

(a) (b)

Figure 5.5: Side view of (a) $\mathbf{3}_2$ and (b) $[(TMP)_2Cu(Br)Li_2(THF)]_2$,[168] with TMP-carbons omitted, highlighting the chair-like conformation of the former complex and equatorial/axial THF positions.

Gilman cuprate *in situ*,[168] the presence of both cuprate-types in solution is suggested. Divergent behaviour was identified for **2** and **3**, with substantially greater conversion of the former compound to Gilman cuprate in solution. For **2**, ^{13}C NMR spectroscopy gave a convoluted spectrum, which could be attributed to the presence of the chiral MP ligand and the presence of Gilman and Lipshutz-type cuprates. ^{7}Li NMR spectroscopy painted a similarly complex picture, revealing four resonances, at δ 1.80, 1.54, 1.21 and 1.05 ppm, which are suggested to belong to Lipshutz-type and Gilman cuprates, the latter being formed *in situ*. In contrast, for **3**, ^{7}Li NMR spectrosocopy revealed a simpler spectrum, dominated by two resonances, at δ 1.38 and 1.12 ppm in 1:1 ratio, there being also a minor shoulder at δ 0.92 ppm. This is consistent with two distinct Li environments which arise from the presence of different amido ligands in **3**. This view is reinforced by comparison with an authentic sample of Lipshutz-type (TMP)$_2$Cu(Br)Li$_2$(THF), whose chemical shift tallies with the highfield signal at δ 1.12 ppm in **3** (see Figure 5.6). The observation of a single Li-resonance for (TMP)$_2$Cu(Br)Li$_2$(THF) suggests that the inequivalence of the Li-centres (due to THF-solvation) in the solid-state structure is not necessarily maintained in C_6D_6 solution. Nonetheless, it can be inferred by comparison of **3** with (TMP)$_2$Cu(Br)Li$_2$(THF) that the low-field signal in **3** at δ 1.38 ppm likely belongs to the DMP-coordinated Li environment.

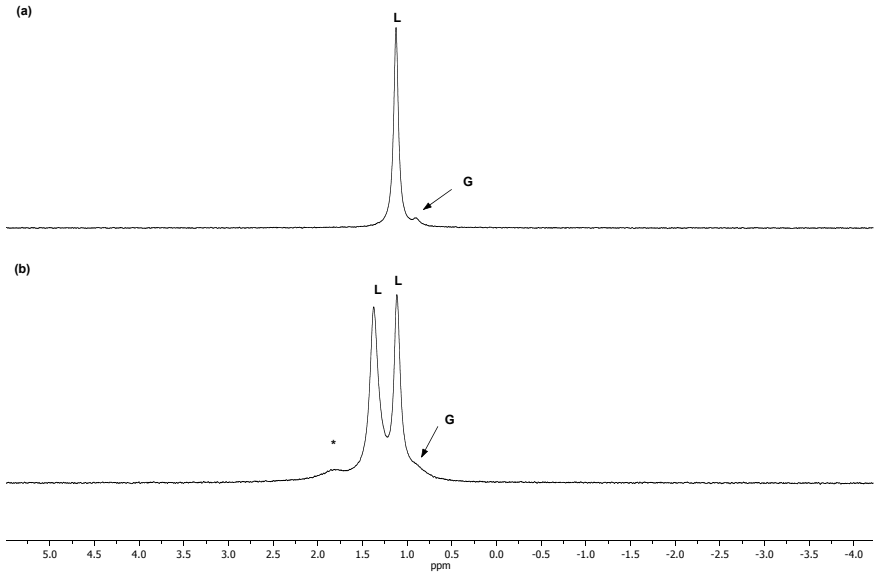

Figure 5.6: ^{7}Li NMR spectra in C_6D_6 of (a) (TMP)$_2$Cu(Br)Li$_2$(THF) and (b) **3**. G = Gilman, L = Lipshutz-type, * = lithium amide.

Though the number of Lipshutz-type and adduct cuprates has steadily grown over the past decade, hitherto only one example of a Gilman bis(amido)cuprate which is relevant to DoCu chemistry has been reported, namely $(TMP)_2CuLi$ **9c**.[166] In this compound, which is dimeric in the solid state, all TMP ligands adopt the *endo* conformation – a motif which is also expressed in bis(TMP) Lipshutz-type cuprates. Seeking to explore the possibility that heteroleptic systems could participate in Gilman cuprate formation, a preformed equimolar mixture of PIPLi and TMPLi in hexane was combined with CuBr (0.5 eq. wrt Li). Following the removal of LiBr by filtration and storage of the straw-coloured filtrate at 5 °C, crystalline material was obtained (Scheme 5.4). ^{1}H and ^{13}C NMR spectroscopy indicated the presence of PIP and TMP in a 1:1 ratio, which pointed to the formation of a heteroleptic cuprate PIP(TMP)CuLi **4**. X-ray crystallography confirmed this to be the case, revealing a head-to-tail[109] aggregated dimer (Figure 5.7).

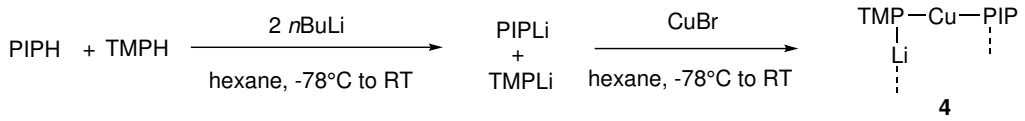

Scheme 5.4: Synthesis of **4**

As for $[(TMP)_2CuLi]_2$ $\mathbf{9c}_2$, the metal sites are well-defined, so that ligand orientations may be understood both in terms of sterics and in terms of proximity to a particular metal site. Though there is superficial similarity between $\mathbf{9c}_2$ and $\mathbf{4}_2$, the TMP ligands lie flat with respect to Cu in the former, whilst a paddlewheel motif is adopted by the latter – with TMP *endo* and PIP *exo* (see Figure 5.8). The paddlewheel motif is easily understood in terms of steric interactions. These are prominent in examples such as TMP_4Cu_4 and TMP_nLi_n (n = 3,4).[65,184,185] In the present case, it is interesting to note that the *endo* disposition of the TMP ligand with respect to copper permits the close approach of two of the four TMP-Me groups to the adjacent Li centre (Figure 5.9). The observed Li$\cdots$C distances (C7$\cdots$Li1A 2.866(4), C9$\cdots$Li1A 2.844(4) Å) lie within the range that has previously been taken as evidence of a stabilising interaction in organolithium and lithium 'ate complexes, and for which neutron diffraction has confirmed the coordinative behaviour of the methyl H-atoms.[186–188]

This view was reinforced by NMR spectroscopy. ^{1}H NMR spectroscopy revealed two chemically distinct TMP-Me environments, at δ 1.50 and 1.28 ppm, indicative

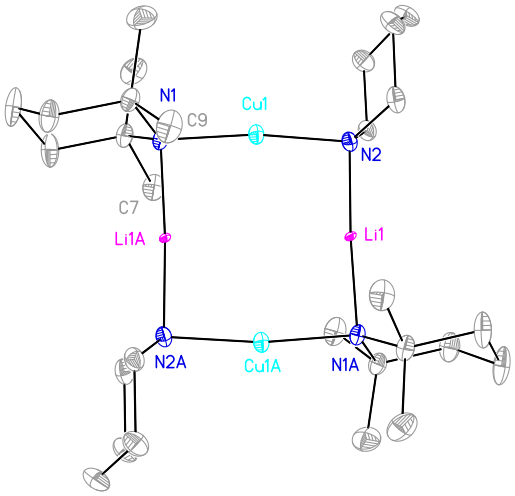

Figure 5.7: Thermal ellipsoid plot of $\mathbf{4}_2$ (30 % probability). H atoms omitted. Selected bond lengths (Å) and angles (°): N1–Cu1 1.8909(16), N2–Cu1 1.8757(16), N1–Li1A 1.952(3), N2–Li1 1.910(3), Cu1–N1–Li1A 92.16(10), Cu1–N2–Li1 92.16(11).

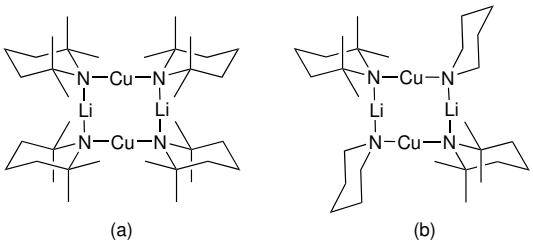

Figure 5.8: Illustration of the contrasting ligand orientations in (a) $\mathbf{9c}_2$ and (b) $\mathbf{4}_2$. In (a) both TMP-ligands lie *endo*, whereas in (b) TMP remains *endo* but PIP lies *exo* with respect to the N→Cu vector.

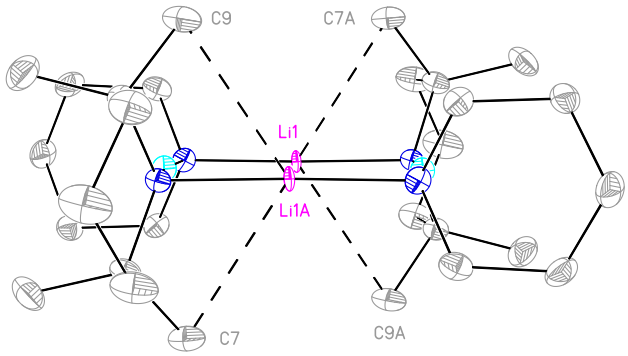

Figure 5.9: Side view of $\mathbf{4}_2$ (% 30 probability), showing the proximity of one set of TMP-Me groups (C7 and C9) to the Li centres (Li1A).

of a fixed TMP-conformation. ^{7}Li NMR spectroscopy revealed a single resonance at δ 1.33 ppm and 2D ^{1}H-^{7}Li HOESY experiments showed a cross-peak between this ^{7}Li resonance and the ^{1}H NMR signal at δ 1.28 ppm, but not to that at δ 1.50 ppm (Figure 5.10). This pattern is consistent with retention of the *endo* position of TMP ligands displayed in the solid state.

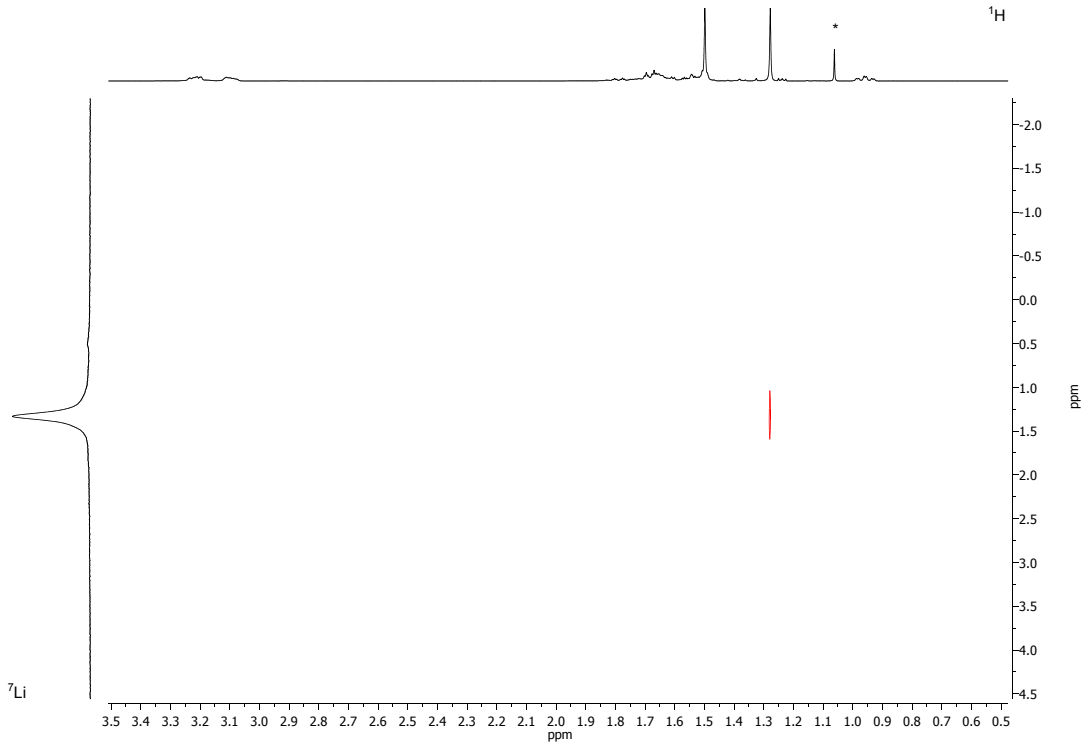

Figure 5.10: ^{1}H-^{7}Li HOESY spectrum of **4** in C_6D_6. * = TMPH.

5.3 Summary

The chiral amine MPH has been used to fabricate adduct cuprate **1**. The deployment of racemic MPH led to stereochemical complexity in the solid state and NMR spectroscopy was consistent with the retention of these features in solution. Subsequently, MP was incorporated into Lipshutz-type cuprate **2**, which dimerises by means of a $(LiBr)_2$ core. In contrast to previously reported cuprates of this type, each monomer incorporates individually heteroleptic cuprate units. Differences in ligand orientation in homoleptic TMP- and DMP-cuprates have been attributed

speculatively to steric effects.[171] However, weight is lent to this explanation by the observation in heteroleptic $\mathbf{2}_2$ and $\mathbf{3}_2$ that TMP retains its *endo* orientation and that the less sterically congested amide (DMP or MP) adopts an *exo* configuration. Similar geometrical effects in $\mathbf{4}_2$, which incorporates the sterically undemanding PIP ligand, led to a paddlewheel motif, in which the TMP are orientationally stabilised by C−H$\cdots$Li interactions. In solution, NMR spectroscopy suggested retention of the solid-state structure of **1**, whereas for **2** and **3** the presence of multiple species (most logically Lipshutz-type and Gilman cuprates) is suggested, and this behaviour is expressed most strongly by **2**.

Chapter 6

Thiocyanatocuprates: Unexpected Structural Diversity in Lithium Cuprates

6.1 Introduction

The development of Lipshutz amidocuprates (i.e. containing CN^-) was followed by the fashioning of Lipshutz-type cuprates from CuX (X = Cl, Br, I), having the general formula $(TMP)_2Cu(X)Li_2(THF)$. Both Lipshutz and Lipshutz-type cuprates have been shown by a series of studies over the past decade to form dimers in the solid state.[166–169,171] Lipshutz-type structures were evidenced by X-ray crystallographic methods and high reactivity of the LiTMP/CuCl system was demonstrated with heterocyclic substrates in the synthesis of substituted azafluorenones.[169] Later, replacement of THF by Et_2O was investigated in order to probe the relationship between Lewis base identity and structure-type. Concordance of the Et_2O-containing structures with their THF-containing counterparts was apparent, with $(TMP)_2Cu(X)Li_2(Et_2O)$ (X = CN, Cl, Br, I) taking the form of nearly planar, centrosymmetric dimers.[171]

It was recognised as early as 1952 that CuSCN represented a viable precursor to organocuprates,[49] yet it was not until the development of cyanocuprate reagents that signifcant attention was paid to it.[189] Lipshutz and co-workers noted that

RLi/CuSCN systems demonstrated superior thermal stability to RLi/CuI-based reagents. The synthetic relevance of the CuSCN-derived systems was demonstrated in the same study and in later work,[190] though CuCN remained the copper salt of choice for many reactions, with CuSCN receiving little attention thereafter. The reason for this is not that CuSCN-derived cuprates are unreactive, but rather that CuCN gives generally more consistent results when used in the synthetic setting.[177] This restriction need not necessarily apply to bis(amido)cuprate systems.

As a precursor, CuSCN presents a number of advantages over other frequently encountered copper(I) salts: it is not oxygen sensitive (unlike CuCl and CuBr), nor light sensitive (unlike CuI). Moreover, CuSCN has the benefit of being significantly less toxic than CuCN. These reasons alone are sufficient to justify extension of lithium bis(amido) cuprate systems to include CuSCN derivatives. For some time, TMP has been the go-to ligand for developing bimetallic bases, owing to its high basicity and low nucleophilicity.[191] In light of the prior body of work devoted to TMP-cuprates,[166–169,171] this ligand was selected for the development of TMP-based thiocyanatocuprates. In addition to the utility Lewis bases THF and Et_2O, which have been shown previously to promote the retention of LiX (X = CN, Cl, Br, I) in cuprate structures,[166–169,171] THP was investigated for its ability to assume this role.

6.2 Results and discussion

6.2.1 Synthesis and X-ray crystallography – cyanocuprates revisited

The use of CuCN as a precursor to TMP-cuprates has been shown to favour the formation of Lipshutz cuprates in the presence of the Lewis bases THF and Et_2O.[167,171] It was therefore logical to assess the ability of THP to participate in Lipshutz cuprate formation by attempting to fabricate $(TMP)_2Cu(CN)Li_2(THP)$ **5**. To do this, a hexane solution of TMPLi containing THP (0.5 eq. wrt Li) was added to CuCN in toluene (Scheme 6.1). Following the addition of further toluene and heating to reflux, filtration gave a straw-coloured solution from which crystals were deposited at room temperature. ^{1}H NMR spectroscopy using C_6D_6

indicated the presence of TMP and THP in a 2:1 ratio, consistent with the formation of $(TMP)_2Cu(CN)Li_2(THP)$ **5**. X-ray crystallography confirmed this to be the case, with a relatively flat structure being observed, analogous to that of $(TMP)_2Cu(CN)Li_2(L)$ (L = Et_2O or THF) (Figure 6.1). IR spectroscopy showed a dominant stretching mode at $\overline{\nu}$ = 2104 cm^{-1}, with exposure to air resulting in the development of a signal at 2138 cm^{-1}. These spectroscopic data were consistent with that previously reported for $(TMP)_2Cu(CN)Li_2(THF)$.[167]

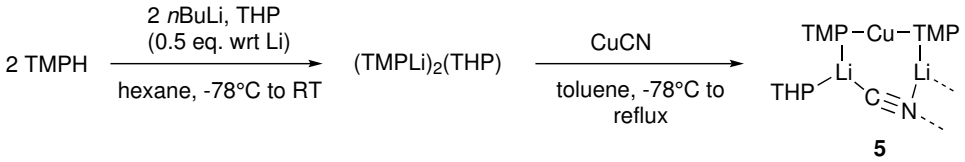

Scheme 6.1: Synthesis of **5**

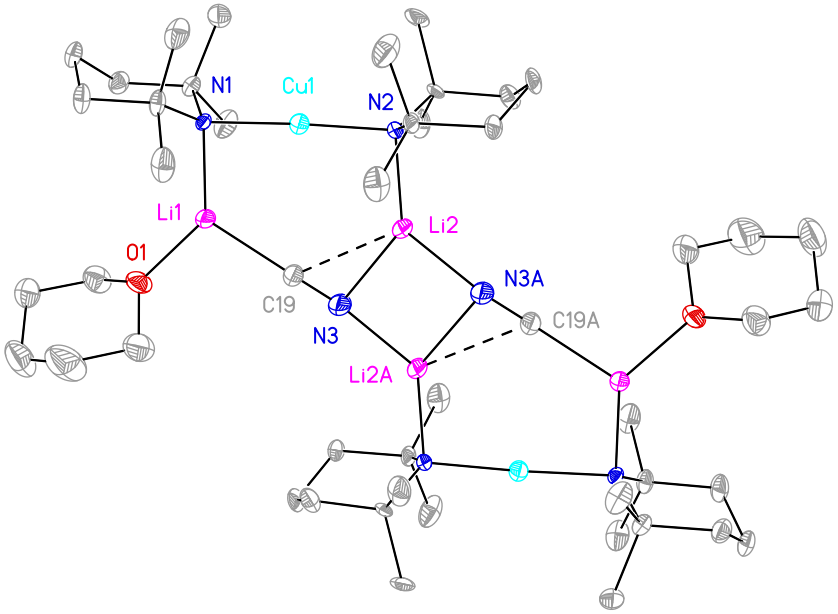

Figure 6.1: Thermal ellipsoid plot of $\mathbf{5}_2$ (30 % probability). H-atoms and ligand disorder omitted. Selected bond lengths (Å) and angles (°): N1–Cu1 1.950(3), N2–Cu1 1.926(3), N1–Li1 1.981(7), N2–Li2 1.951(7), C19–Li1 2.111(13), N3–Li2 2.171(13), N3–Li2A 2.047(14), Cu1–N1–Li1 90.9(2), Cu1–N2–Li2 97.2(2), N1–Li1–C19 122.3(5), N2–Li2–N3 135.2(5), N2–Li2–N3A 130.5(5).

6.2.2 Synthesis and X-ray crystallography – thiocyanatocuprates

Moving to non-toxic CuSCN as a cuprate precursor, the synthesis of Lipshutz-type cuprates was attempted. The use of different Lewis bases (Et_2O, THF and THP) was investigated in order to probe their suitability to participate in the formation of Lipshutz-type structures. This focussed first on the weakest Lewis base, Et_2O. Accordingly, a solution of TMPLi in toluene which also contained Et_2O was added to CuSCN in the same solvent (Scheme 6.2). Heating to reflux resulted in a grey discolouration and hot filtration gave a yellow solution. Storage of this solution at room temperature gave needle-like crystals (a distictive habit, associated with $(TMP)_2CuLi$ **9c**) which were replaced by crystals of a *pseudo*-rhombic habit with further standing. ^{1}H NMR spectroscopy showed that these crystals contained TMP and Et_2O in a 2:1 ratio, though no signal corresponding to SCN^- could be identified by ^{13}C NMR spectroscopy. IR spectroscopy, however, confirmed that the crystals contained SCN^-, with peaks at 2065 (s) and 1997 (m) cm^{-1} observed.[192]

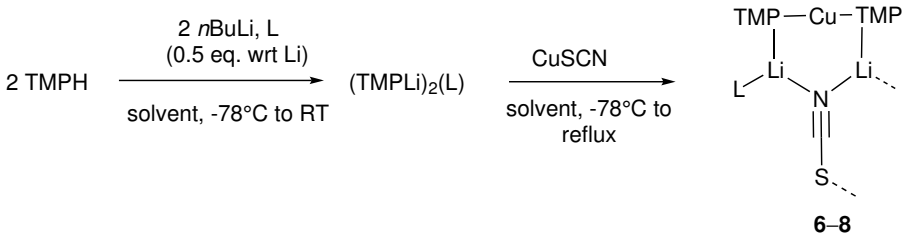

Scheme 6.2: Synthesis of **6**–**8**. **6**, L = Et_2O (solvent = toluene); **7**, L = THF (solvent = hexane); **8**, L = THP (solvent = hexane/toluene).

The Lipshutz-type structure suggested by spectroscopic data was confirmed by X-ray crystallography, which revealed $(TMP)_2Cu(SCN)Li_2(Et_2O)$ **6** to comprise a nearly planar, centrosymmetric dimer (Figure 6.2). The flatness of the metallacyclic $Li_2(SCN)_2$ core was established, with the maximum deviation of these atoms from the mean plane being only 0.12 Å. The suggestion from spectroscopy that the thiocyanate ions are formally N≡C−S$^-$ is most convincingly evidenced by the shortness of N3–C19 (1.149(3) Å), though the S1–C19 distance (1.631(3) Å) does suggest some level of delocalisation in the anionic ligand.[192] This view is reinforced by the inequality of the N2–Li2 and N2–Li1 bond lengths (2.250(5) and 1.998(5) Å, respectively), which are consistent with a single N-based lone pair

dividing Li1–N3–Li2, but having the strongest interaction with Li2, on grounds of electrostatic directionality.[193]

Having established the structure of $\mathbf{6}_2$ to be comparable to previously isolated examples of Et_2O-containing Lipshutz-type cuprates,[171] attention was diverted to the THF-solvate. Accordingly, TMPLi and THF (0.5 eq. wrt TMPLi) were combined with CuSCN in hexane. Hot filtration, followed by storage at −27 °C gave a crop of prismatic crystals. ^{1}H NMR spectroscopy showed this material to incorporate TMP and THF in a 2:1 ratio and ^{13}C NMR spectroscopy indicated the presence of SCN^- at δ 141.5 ppm. IR spectroscopy corroborated the last point, with strong bands seen at 2065 and 1996 cm^{-1}.

With spectroscopic evidence pointing towards the successful synthesis of a Lipshutz-type cuprate, X-ray diffractometery was undertaken. This revealed $\mathbf{7}_2$ in a novel boat-shaped conformation, formed by the association of two crystallographically independent monomers (parameters relating to one representative monomer will be discussed here), with sulfur acting as a hinge about which $\mathbf{7}_2$ is folded (Figure 6.3). In spite of the substantially altered geometry at sulfur with respect to $\mathbf{6}_2$, diffraction fails to disclose any significant differences in the bond lengths associated with sulfur (*cf.* S1–C19 1.631(3), S1–Li2A 2.518(4) Å in $\mathbf{6}_2$ and S2–C24 1.625(3), S2–Li1 2.500(6) Å in $\mathbf{7}_2$). This suggests equivalence of thiocyanate anions in these two structures despite the constriction of the Li–S–C bond angle caused by the folding of $\mathbf{7}_2$ along the S$\cdots$S vector (Li2–S1A–C19A 103.92(13)° in $\mathbf{6}_2$ compares with Li1–S2–C24 91.72(17)° in $\mathbf{7}_2$). Despite the overall non-planar shape in $\mathbf{7}_2$, the $CuLi_2N_3$ rings within each of the two monomeric units barely deviate from planarity, with angles at Li1 and N3 summing to 359.9° and 359.6°, respectively.

Having established markedly different structures when THF or Et_2O were deployed, attention was diverted to the use of THP as a Lewis base. A solution of TMPLi also containing THP (0.5 eq. wrt Li) in hexane/toluene was combined with CuSCN in the same solvent. Heating the mixture to reflux was followed by hot filtration and storage of the filtrate at room temperature gave block-like crystals. IR spectroscopy revealed bands at 2063 (s) and 2007 (w) cm^{-1} which were attributed to the presence of SCN^-. Meanwhile, ^{1}H NMR spectroscopy indicated TMP and THP to be present in a 2:1 ratio – consistent with the THP analogue of **6** and **7**. X-ray crystallography confirmed this to be the case, revealing the

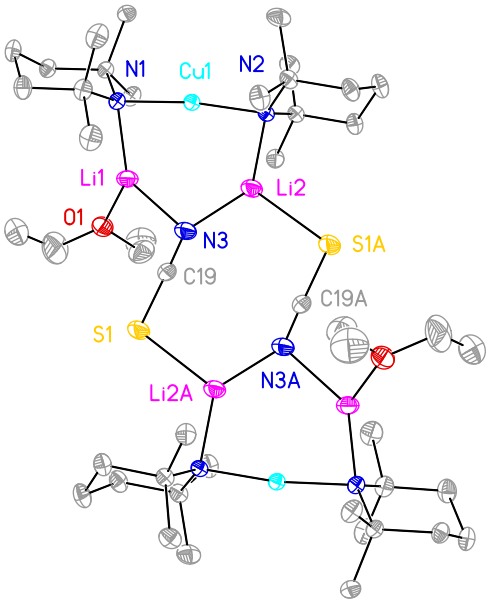

(a)

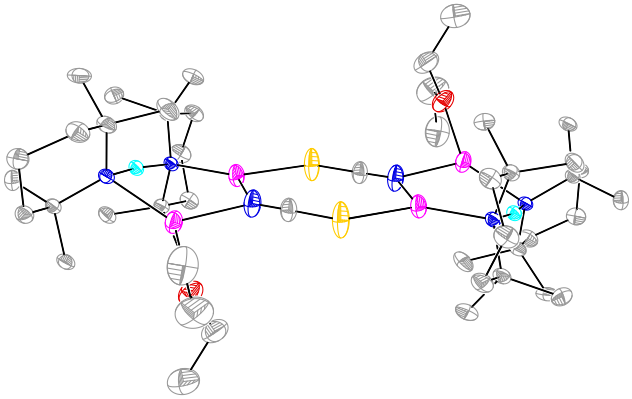

(b)

Figure 6.2: (a) Thermal ellipsoid plot of $\mathbf{6}_2$ (30 % probability). H-atoms omitted for clarity. Selected bond lengths (Å) and angles (°): N1–Cu1 1.9175(18), N2–Cu1 1.9074(18), N1–Li1 2.015(4), N2–Li2 1.970(4), S1A–Li2 2.518(4), N3–Li1 2.250(5), N3–Li2 1.998(5), N3–C19 1.149(3), S1–C19 1.631(3), Cu1–N1–Li1 83.82(15), Cu1–N2–Li2 89.46(15), N1–Li1–N3 123.7(2), N2–Li2–N3 128.7(2), Li1–N3–C19 110.7(2), Li2–N3–C19 140.0(2), S1A–Li2–N3 113.17(19), Li2–S1A–C19A 103.92(13); (b) Side view of $\mathbf{6}_2$.

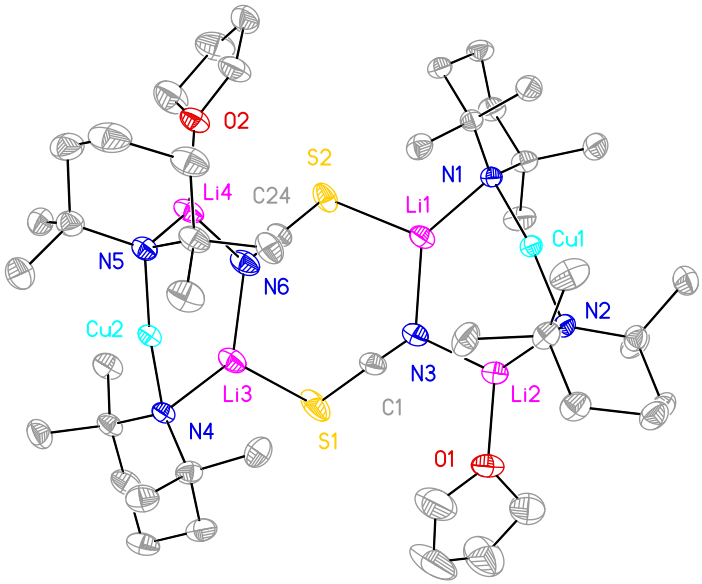

(a)

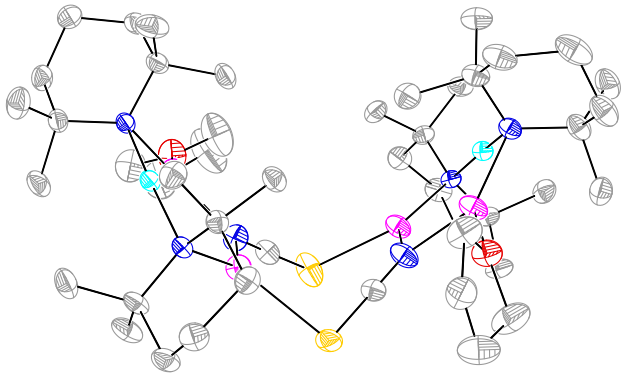

(b)

Figure 6.3: (a) Thermal ellipsoid plot of $\mathbf{7}_2$ (30 % probability). H-atoms omitted for clarity. Selected bond lengths (Å) and angles (°): N1–Cu1 1.908(2), N2–Cu1 1.906(2), N1–Li1 1.977(5), N2–Li2 1.995(6), S2–Li1 2.500(6), N3–Li1 2.071(6), N3–Li2 2.105(6), N3–C1 1.159(4), S1–C1 1.627(3), Cu1–N1–Li1 87.45(18), Cu1–N2–Li2 87.66(18), N1–Li1–N3 130.7(3), N2–Li2–N3 128.9(3), Li1–N3–C1 125.0(3), Li2–N3–C1 124.8(3), S2–Li1–N3 108.8(2), Li1–S2–C2491.72(17); (b) Side view of $\mathbf{7}_2$.

dimeric aggregate of $(TMP)_2Cu(SCN)Li_2(THP)$ **8**, which in contrast to $\mathbf{6}_2$ and $\mathbf{7}_2$ adopts a distinctly chair-like structure in the solid state (Figure 6.4). The chair-like motif is facilitated, ostensibly, by the deviation of Li2 and its symmetry equivalent from the mean plane describing the $(SCN)_2Li_2$ core of the structure by $\pm$ 0.43 Å. The displacement of S1 from the mean plane necessarily ensures that N3 also deviates from this plane, the angles around N3 now summing to 351.6°. The small displacement of N3 from planarity (which is presumably permissible since it does not affect the electrostatic directionality of N3) means that the Li–S–C angle (96.09(12)°) is intermediate compared to the two previous structures (103.92(13)° in $\mathbf{6}_2$, 91.72(17)° in $\mathbf{7}_2$). Lastly, the S1–C19 and S1–Li2A bond lengths in $\mathbf{8}_2$ (1.632(3) and 2.464(4) Å, respectively), being essentially the same as in $\mathbf{6}_2$ and $\mathbf{7}_2$ indicate a common electronic structure for SCN^- in all cases.

Having demonstrated the suitability of CuSCN as precursor to Lipshutz-type cuprates, its reactivity in the absence of Lewis basic solvents was investigated. TMPLi was combined with CuSCN in a 2:1 ratio in hexane/toluene, heated to reflux and filtered whilst hot. Upon concentration of the yellow solution and standing at room temperature, large needles formed, which crystallography revealed to be previously reported $(TMP)_2CuLi$ **9c** – which forms a dimer in the solid state. ^{7}Li NMR spectroscopy on the dissolved crystals showed a single resonance at δ 0.90 ppm and IR spectroscopy confirmed the absence of SCN^-, suggesting a new, clean and efficient route to **9c**. This allowed detailed re-characterisation to take place, resulting in a simple ^{13}C NMR spectrum. This served as a reference point for interpretation of the complex solution behaviour of **6**–**8** described in the next section.

6.2.3 NMR spectroscopy

The improved purity of **9c** synthesised from CuSCN provided a clean set of reference spectra which could be used to interpret the convoluted solution behaviour of **6**–**8** (see Figure 6.5, Figure 6.6 and Figure 6.7). In C_6D_6, ^{13}C NMR spectroscopy revealed five resonances for the TMP ring carbon 2,6-, 3,5-, Me- and 4-positions at δ 54.2, 42.1, 40.1, 34.5 and 19.2 ppm (see Figure 6.7d). Comparison with a sample of **6** in C_6D_6 (*ca.* 30 mg mL^{-1}) revealed identical signals to those presented by pure **9c** in addition to traces of **6**, Et_2O and TMPH (the last due to decomposition).

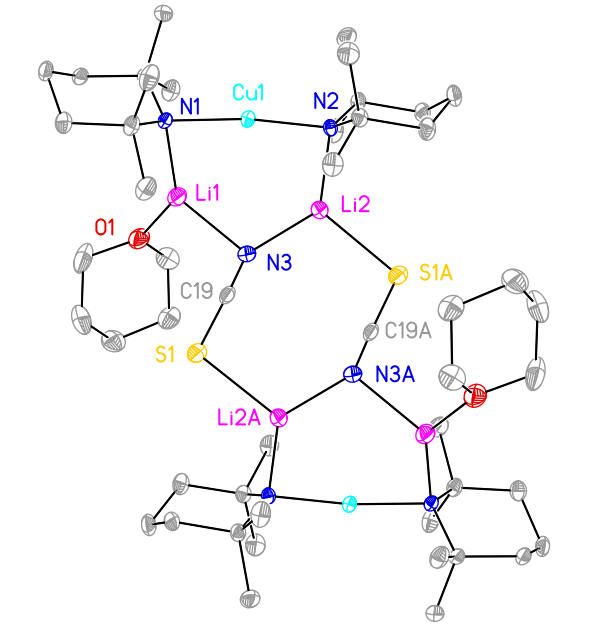

(a)

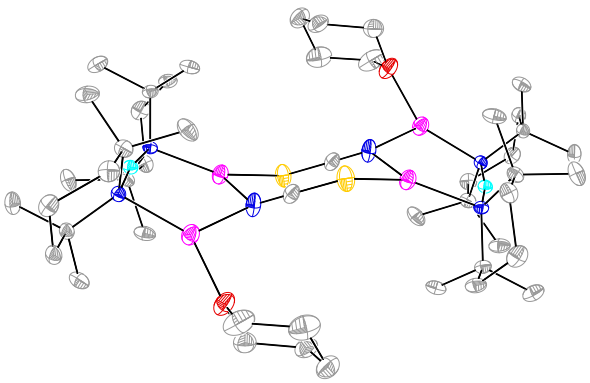

(b)

Figure 6.4: (a) Thermal ellipsoid plot of $\mathbf{8}_2$ (30 % probability). H-atoms omitted for clarity. Selected bond lengths (Å) and angles (°): N1–Cu1 1.9204(17), N2–Cu1 1.9148(17), N1–Li1 1.990(4), N2–Li2 1.968(4), S1A—Li2 2.464(4), N3–Li1 2.164(5), N3–Li2 2.005(4), N3–C19 1.162(3), S1–C19 1.632(3), Cu1–N1–Li1 110.75(19), Cu1–N2–Li2 88.84(13), N1–Li1–N3 123.4(2), N2–Li2–N3 128.5(2), Li1–N3–C19 106.7(2), Li2–N3—C19 134.5(2), S1A–Li2–N3 107.90(18), Li2A–S1–C19 96.09(12); (b) Side view of $\mathbf{8}_2$.

Notably, a fine white solid was observed to precipitate from this solution and this could be reproduced on a larger scale using benzene as the solvent. This control experiment permitted the isolation of the white powder, which IR spectroscopy suggested to be LiSCN through the observation of bands at 2150 (w) and 2086 (w, br) cm^{-1}. The precipitation of LiSCN from benzene solutions of **6** can therefore account for the inability to detect a ^{7}Li NMR signal attributable to this salt in the supernatant. Overall these data strongly suggest the near complete *in situ* conversion of Lipshutz-type **6** to Gilman cuprate **9c** in C_6D_6.

In contrast, when dissolved in C_6D_6 (*ca.* 30 mg mL^{-1}), **7** and **8** displayed more complex spectra. In both cases ^{13}C NMR spectroscopy indicated **9c** to be present (see Figure 6.7c–d), though these signals were added to by those of the corresponding Lipshutz-type cuprates **7** and **8**. For **7**, the Lipshutz-type species dominates, with four signals for TMP^- (δ 53.5, 40.6, 38.3 and 34.4 ppm) being well-separated from those of Gilman cuprate (δ 54.2, 42.1, 40.1 and 34.5 ppm) and one being coincident (δ 19.2 ppm). Furthermore, through the preparation of a more concentrated sample in C_6D_6 (*ca.* 70 mg mL^{-1}), the thiocyanate carbon could be detected at δ 141.5 ppm. For **8**, similar behaviour was evident, though the ratio of Gilman to Lipshutz-type cuprate now approached equivalence. As for **7**, a more concentrated sample (*ca.* 70 mg mL^{-1}) located SCN^- at δ 141.7 ppm by ^{13}C NMR spectroscopy.

^{7}Li NMR spectroscopy corroborated the presence of two lithium-containing species in samples of **6**–**8** suggested by ^{13}C NMR spectroscopy (see Figure 6.5). Hence for **6** in C_6D_6, the spectrum was dominated by a resonance at δ 0.90 ppm, which coincided precisely with the signal observed for reference compound **9c**, though development of a minor high-field signal at δ 0.65 ppm was noted, attributed to the retention of small quantities of Lipshutz-type **6** in solution (Figure 6.5a). A lithium ratio of 1:0.4 was determined by integration of the dominant and minor species, which corresponds to a Gilman : Lipshutz-type ratio of *ca.* 1:0.2, when the stoichiometry is accounted for. Similar analysis of the ^{7}Li NMR spectra of **7** and **8** (Figure 6.5b–c) indicated binary systems – the Lipshutz-type components being identified at δ 0.71 and 0.61 ppm for **7** and **8**, respectively. Integration of these resonances and those of **9c** indicated approximate Gilman:Lipshutz-type ratios of 0.2:1 and 0.6:1 (corrected for stoichiometry). These data were in broad agreement with ^{1}H and ^{13}C NMR spectroscopic data (see Figure 6.6 and Figure 6.7).

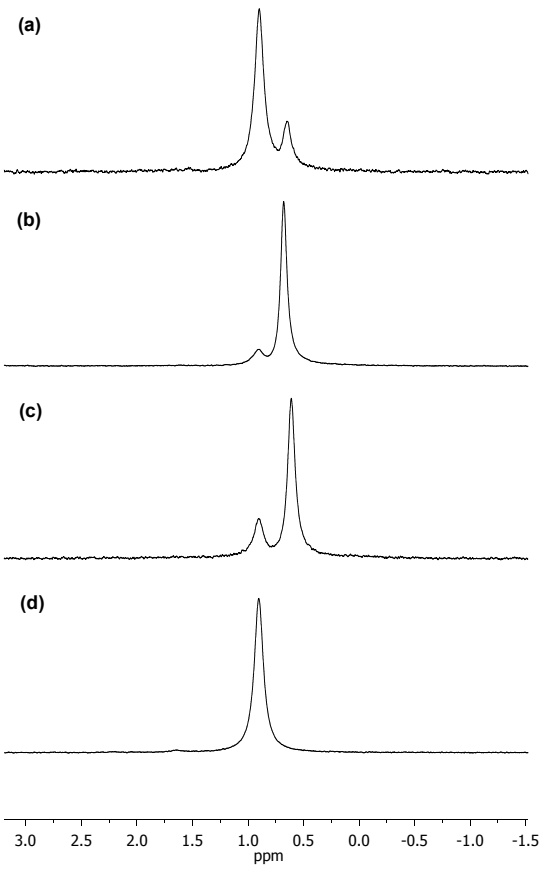

Figure 6.5: ^{7}Li NMR spectra in C_6D_6 at *ca.* 30 mg mL^{-1}. (a) **6** (b) **7** (c) **8** (d) **9c**.

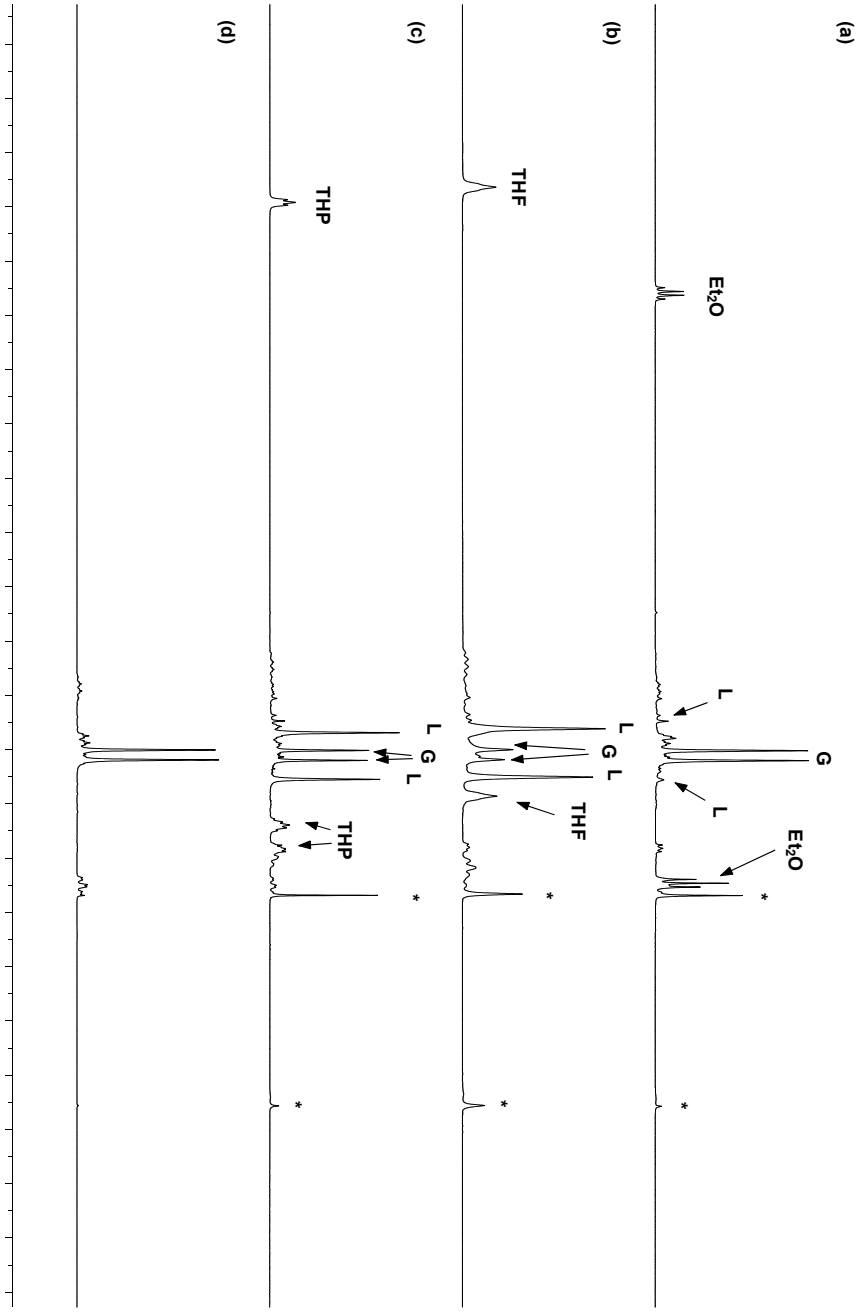

Figure 6.6: ^{1}H NMR spectra in C_6D_6 (*ca.* 30 mg mL^{-1}) of (a) **6** (b) **7** (c) **8** and (d) **9c**. TMP-Me resonances are highlighted. L = Lipshutz-type, G = Gilman, * = TMPH.

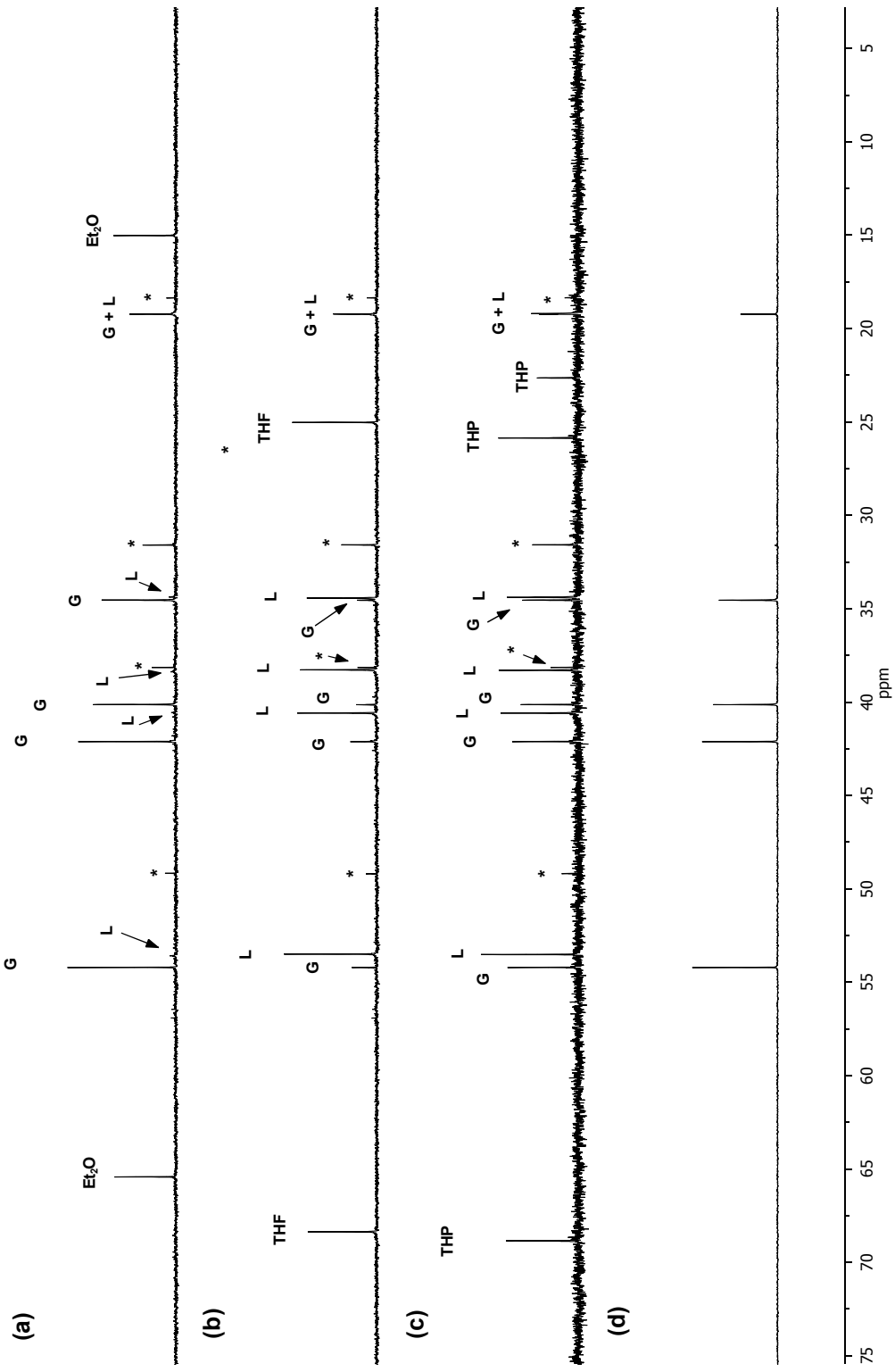

Figure 6.7: ^{13}C NMR in C_6D_6 of (a) **6** (b) **7** (c) **8** (d) **9c**. G = Gilman, L = Lipshutz-type, * = TMPH). Sample concentrations *ca.* 30 mg mL^{-1}.

6.2.4 Derivatisation of chloropyridines

The work described in this section was conducted by collaborators.[181]

In light of the recent demonstration that halide-bearing Lipshutz-type amidocuprates can be used in the synthesis of azafluorenones, it was decided to test the new thiocyanate-containing Lipshutz-type cuprates in the functionalisation of halopyridines. To facilitate comparison with previously explored systems, reagent **7** was prepared *in situ* in THF and reacted with 2-chloropyridine **10** or 2,3-dichloropyridine **11**. It was expected that the reaction would be promoted at the aromatic 3-position for **10** and that the combined acidifying effect of the two adjacent halogens in **11** would favour reaction at the 4-position (see Scheme 6.3).

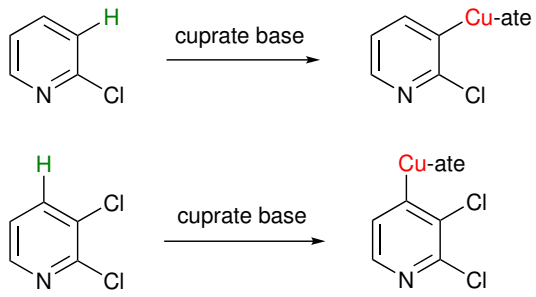

Scheme 6.3: The expected outcome of the metalation of chloropyridines **10** and **11** by cuprate base (Cu-ate) **7**. Most acidic protons highlighted in green.

The results of the *in situ* reaction of **7** with **10** followed by reaction with electrophiles (4-methoxybenzoyl chloride, methyl iodide and diphenyl disulfide) to give **12a-c** are presented in Table 6.1. **12a-c** were obtained in 46–71 % yield. **12a** is obtained in a modest yield of 55 % using chlorocuprate $(TMP)_2Cu(Cl)Li_2(THF)$, in light of which the thiocyanatocuprate base compares satisfactorily (achieving 46 % yield). There is a literature precedent for the ability of TMP-cuprates to promote the oxidative coupling of *N,N*-diisopropylbenzamide in the presence of $PhNO_2$.[167] It was therefore decided to test the efficacy of **7** in the oxidative homocoupling of **10** in the presence of $PhNO_2$ as an oxidising agent. This proceeded to give homocoupled **12d** in a modest 69 % yield.

Turning to **11** as a substrate, deprotonation was expected at the 4-position; this being the result observed when **11** is reacted with DALi or *n*BuLi in THF at −78 °C.[194] This was realised in reaction of **7** with **11**, to give funtionalised

Table 6.1: *In situ* reaction of **7** with **10** followed by quench with electrophiles or oxidation with $PhNO_2$ to give **12a–d**

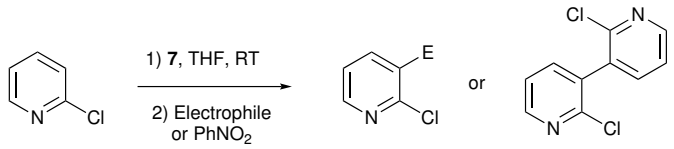

Entry	Electrophile or $PhNO_2$	E	Product, Yield (%)
1	4-$MeOC_6H_4COCl$	COC_6H_4-4-OMe	**12a**, 46[a,b]
2	MeI	Me	**12b**, 65[c]
3	PhSSPh	SPh	**12c**, 71[a]
4	$PhNO_2$	—	**12d**, 69[a]

[a]Isolated yield. [b]55 % using CuCl instead of CuSCN. [c]Yield estimated from ^{1}H NMR spectroscopy due to product volatility.

chloropyridines **13b** and **13c** in yields of 58 and 62 %, respectively. Oxidative homocoupling could also be achieved to give **13d** in a yield of 51 % (Table 6.2).

Table 6.2: *In situ* reaction of **7** with **11** followed by quench with electrophiles or oxidation with $PhNO_2$ to give **13b–d**.

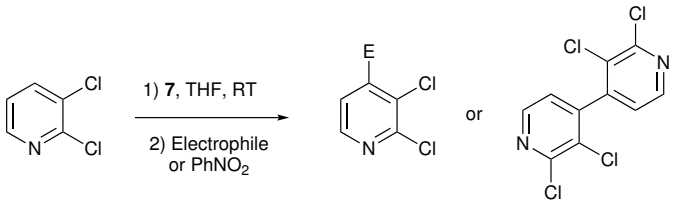

Entry	Electrophile or $PhNO_2$	E	Product, Yield (%)
1	MeI	Me	**13b**, 58[a]
2	PhSSPh	SPh	**13c**, 62[b]
3	$PhNO_2$	—	**13d**, 51[b]

[a]Yield estimated from ^{1}H NMR spectroscopy due to product volatility. [b]Isolated yield.

6.3 Summary

The family of TMP-cuprates $(TMP)_2Cu(CN)Li_2(L)$ (L = Et_2O and THF) has been extended to include $(TMP)_2Cu(CN)Li_2(THP)$ **5**. In the solid state, the prevalence of approximately flat dimers has been noted.[171] Seeking to improve the safety profile of bis(amido)cuprates without redirecting reactivity in ways recently described for halide-containing cuprates,[195] CuSCN was investigated as a cheap and non-toxic precursor to replace CuCN. The resulting Lipshutz-type complexes exhibited structural variability that arose from the ability of the central $Li_2(SCN)_2$ core to adopt different conformations. The use of Et_2O gave an essentially flat arrangement in $\mathbf{6}_2$, whereas boat- and chair-like conformations resulted from the inclusion of THF and THP in $\mathbf{7}_2$ and $\mathbf{8}_2$, respectively. NMR spectroscopy was harnessed to probe the dynamic behaviour of **6**–**8** in hydrocarbon solution. This made use of an authentic sample of **9c**, which was made in high purity from CuSCN, *via* a Lewis base-free synthesis. In benzene solution, Lipshutz-type structures were not necessarily maintained, with variable levels of *in situ* conversion to Gilman cuprate **9c** found to occur in each case. The extent of this conversion was found to be dependent upon the donor ability of the Lewis base, with Et_2O-solvate **6** undergoing near quantitative conversion to **9c**, and **7** being mostly retained in C_6D_6 solution. Meanwhile, **8** displayed intermediate levels of *in situ* conversion to **9c**. Moving to the synthetic setting, **7** was successfully deployed in the metalation of halopyridines **10** and **11** to give functionalised products **12a**–**d** and **13b**–**d** in moderate yields of 46–71 % and 51–62 %, respectively. Though modest, these results were comparable to those achievable using a TMP-chlorocuprate base; further optimisation of reaction conditions is certainly warranted. In particular, it is important to compare yields using pre-isolated cuprate bases for which the purity is known. This is particularly true for cuprates incorporating 'soft' anions (e.g. SCN^-), where a limited amount of Lewis base is necessary for the isolation of Lipshutz-type **6**–**7**. However, this is often not reflected in the protocol used in synthetic procedures, where the use of bulk etherate solvent is more typical. Lastly, it is worth pointing out that the halopyridine substrates used in this work would not be considered to possess strong directing effects (see Section 1.3.2) and that considerable variability in isolated yields have been noted with these types of substrates previously.[196]

Chapter 7

Studies into the Chemistry of Cyanatocuprates: Cu-Li Exchange in Lithium Cuprates

7.1 Introduction

The synthesis of Lipshutz and Lipshutz-type cuprates has now been achieved for a variety of inorganic anions. The generality of the Lipshutz-type structure has been verified for cuprates incorporating CN^-,[167] Cl^-,[166] Br^-,[169] I^-[168] and most recently, SCN^-.[181] The last of these was investigated as a non-toxic alternative to CN^-. Whilst the synthesis of thiocyanatocuprates proved sucessful, their performance in deprotometalation reactions was not outstanding. Previous work has highlighted the need to consider the influence of the inorganic anion upon the reactivity of cuprates and has exposed a preference for 'harder' inorganic anions in order to maintain consistent reactivity.[168] In this context, cyanate (OCN^-) may be considered the 'harder' analogue of SCN^- and also possesses the desirable property of low toxicity. In light of the sucessful fabrication of Lipshutz-type cuprates from CuSCN, it was decided to attempt to fashion lithium cuprates from CuOCN. Compared to CuSCN, CuOCN presents with some challenges: CuOCN is not commercially available and (to the authors best knowledge) its synthesis has been reported only twice in the literature.[182,197] In spite of its scarcity in the literature, CuOCN proved straightforward to synthesise and cuprates could be accessed from

this salt, albeit with complications arising from Cu-Li substitution. Data gathered from cyanate systems has progressed our understanding of Cu-Li substitution in lithium cuprates and significantly advanced our knowledge of the solution-state behaviour of amidocuprates.

7.2 Results and discussion

7.2.1 Synthesis and X-ray crystallography

CuOCN was prepared by modification of the literature method,[182] and was obtained in modest yield as a high-purity crystalline material. TMPLi was prepared as a hexane solution, also containing THF (0.5 eq. wrt Li) before being introduced to a hexane suspension of CuOCN (0.5 eq. wrt Li) at low temperatures. Warming to room temperature produced a cream-coloured suspension from which a yellow filtrate was obtained and storage at −27 °C gave crystalline material (Scheme 7.1). IR spectroscopy indicated the presence of cyanate ($\overline{\nu} = 2208\,\mathrm{cm}^{-1}$) and NMR spectroscopy indicated the presence of both TMP and THF. A well-faceted crystal was selected for X-ray diffraction which superficially confirmed the expected Lipshutz-type structure-type $(TMP)_2M(OCN)Li_2(THF)$ **14**, but revealed substitutional disorder at the TMP-bridging metal site. Crystallographic refinement indicated the optimal formulation M = $Cu_{0.1}Li_{0.9}$, and the absence of metal disorder at the other sites suggests that the structure is best regarded as a co-crystal of $(TMP)_2Cu(OCN)Li_2(THF)$ **14a** and $(TMP)_2Li(OCN)Li_2(THF)$ **14b** (see Figure 7.1).

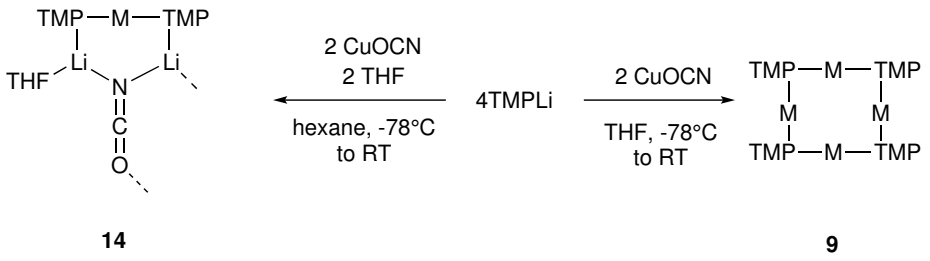

Scheme 7.1: Solvent-dependent synthesis of **14** and **9**. M = Cu, Li; see text for further details.

The crystal structure of **14** reveals a dimer, whose formation is supported by an

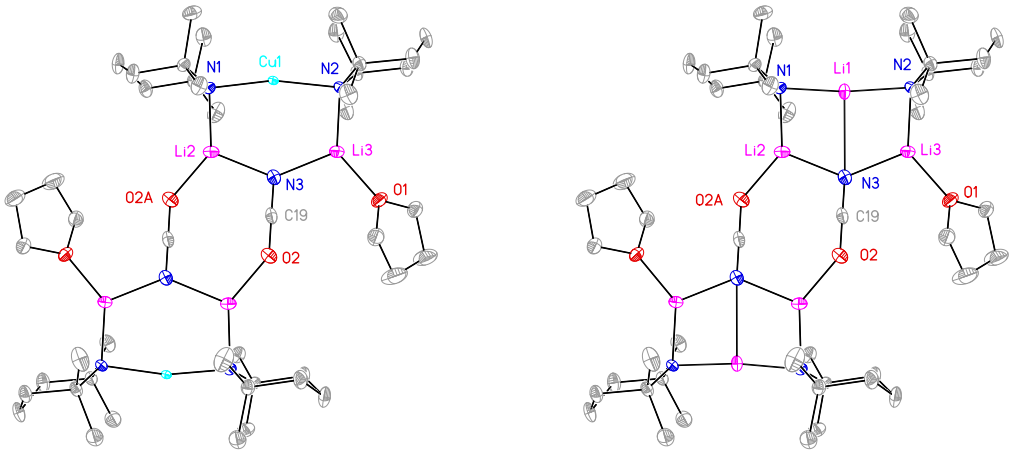

(a) (b)

Figure 7.1: Thermal ellipsoid plots (30 % probability) for $\mathbf{14}_2$, showing components (a) $\mathbf{14a}_2$ and (b) $\mathbf{14b}_2$ separately. H-atoms omitted for clarity. Selected bond lengths (Å) and angles (°): N1–Cu1 1.968(11), N2–Cu1 2.029(11), N3–Cu1 1 2.93(1), N1–Li1 1.970(16), N2–Li1 2.009(16), N3–Li1 2.597(11), N1–Li2 1.969(3), N2–Li3 1.935(3), N3–Li2 2.056(4), N3–Li3 2.040(4), O2–Li2A 1.904(3), O2–C19 1.211(3), N3–C19 1.168(3), N1–Cu1–N2 167.3(4), N1–Li1–N2 173.4(6), N1–Li1–N3 94.5(5), N2–Li1–N3 92.1(5).

8-membered $Li_2(OCN)_2$ core, which is nearly planar (mean deviation from plane of 0.0468 Å). The core supports two peripheral 6-membered MLi_2N_3 (M = $Cu_{0.1}Li_{0.9}$) rings and the structure is completed by the THF-solvation of Li3. The structure retains overall flatness (excluding TMP and THF carbons) and in so doing contrasts with thiocyanate-bridged $\mathbf{7}_2$ and cyanide-bridged $[(TMP)_2Cu(CN)Li_2(THF)]_2$.[167] Of particular interest, the geometries of the 6-membered MLi_2N_3 rings in **14** are dependant upon the identity of M. In **14a** (M = Cu), the N1–Cu1–N2 angle is obtuse (167.3(4)°), and this results in a non-bonding N3–Cu1 distance of 2.93(1) Å, ensuring that **14a** is formally lower-order. Contrastingly, for **14b** (M = Li), interaction between Li1 and N3 is evidenced by the Li1–N3 distance of 2.597(11) Å with a corresponding N1–Li1–N2 reflex angle of 186.6(5)°. Though the interaction is clearly weak,[198] the motif is reminiscent of intercepted ladder-type structures which have been reported for amidolithium compounds in the past.[199]

Reasoning that the depletion of copper in **14** might originate from the sequestration of *in situ*-generated LiOCN by TMPLi during the reaction, an alternative route was sought which ensured that these two components could not be present simultaneously. Accordingly, Gilman cuprate **9c** was prepared as a donor solvent-

free solution which was then treated with LiOCN. THF was introduced and later replaced by hexane for crystallisation. After storage of the yellow solution at −27 °C for 5 days, radiating fans of crystals were obtained, which were found to be simple non-merohedral twins by X-ray diffraction (Scheme 7.2).

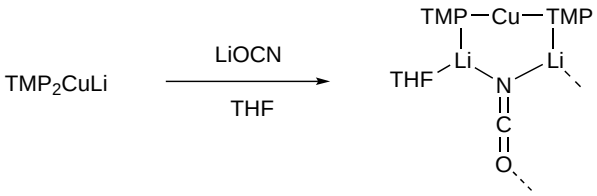

Scheme 7.2: The synthesis of pure **14a**.

Crystallography confirmed these crystals to be $(TMP)_2Cu(OCN)Li_2(THF)$, **14a** (Figure 7.2). Though pure $\mathbf{14a}_2$ is not isomorphous with its counterpart in $\mathbf{14}_2$, the differences are small. In particular, $\mathbf{14a}_2$ exhibits marginally reduced planarity when compared to its partner component in $\mathbf{14}_2$, with a mean deviation from the plane of 0.205 Å (excluding THF and TMP-carbons, *cf.* 0.085 Å for $\mathbf{14a}_2$ in $\mathbf{14}_2$). These observations imply that, whilst weak, the the N3···Li1 transannular interaction in the major component $\mathbf{14b}_2$ of $\mathbf{14}_2$ exerts an influence (*via* crystal packing) over the minor component $\mathbf{14a}_2$ in the same structure.

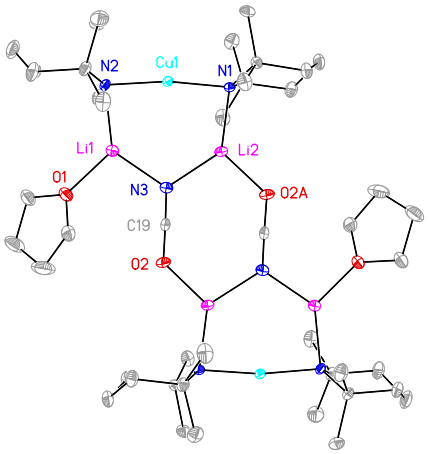

Figure 7.2: Thermal ellipsoid plot of $\mathbf{14a}_2$ (30 % probability). H-atoms omitted for clarity. Selected bond lengths (Å) and angles (°): Cu1–N1 1.9120(17), Cu1–N2 1.9173(17), N2–Li1 2.006(4), N1–Li2 2.013(4), N3–Li1 2.020(5), N3–Li2 2.037(5), O2–Li2A 1.931(4), N1–Cu1–N2 171.47(7), Cu1–N1–Li2 86.61(14), Cu1–N2–Li1 87.43(14), N2–Li1–N3 130.5(2), Li1–N3–Li2 110.28(18), N1–Li2–N3 128.5(2).

To target pure **14b**, two different synthetic routes were pursued. Noting the liter-

ature precedent for the use of a secondary ammonium salt to generate a lithium amide-lithum halide aggregate,[200] cyanate salt $(TMPH_2)OCN$ **15** was synthesised. Reaction of this salt with TMPH and *n*BuLi (1:1:3) in THF, followed by recrystallisation from hexane gave a crystalline material. Alternatively, it was found that direct reaction of TMPLi with LiOCN (2:1) in THF gave the same product after recrystallisation from hexane. The presence of cyanate was confirmed by IR spectroscopy ($\overline{\nu} = 2207\,cm^{-1}$). However, NMR spectroscopy indicated TMP and THF to be present in equal proportions rather than the expected 2:1 ratio and in due course crystallography revealed $(TMP)_2Li(OCN)Li_2(THF)_2$ **16** (Figure 7.3).

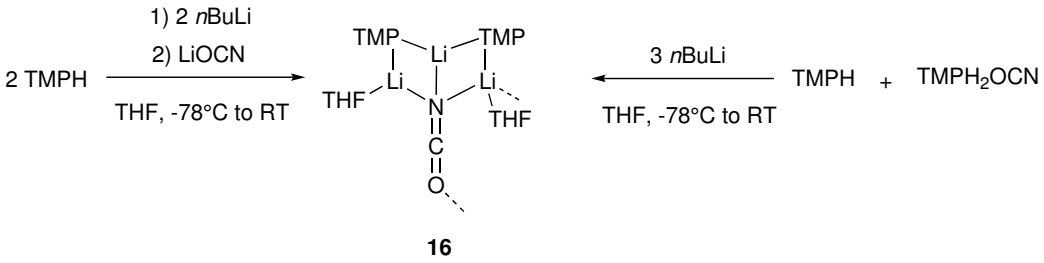

16

Scheme 7.3: Synthesis of **16** in bulk THF *via* two different routes.

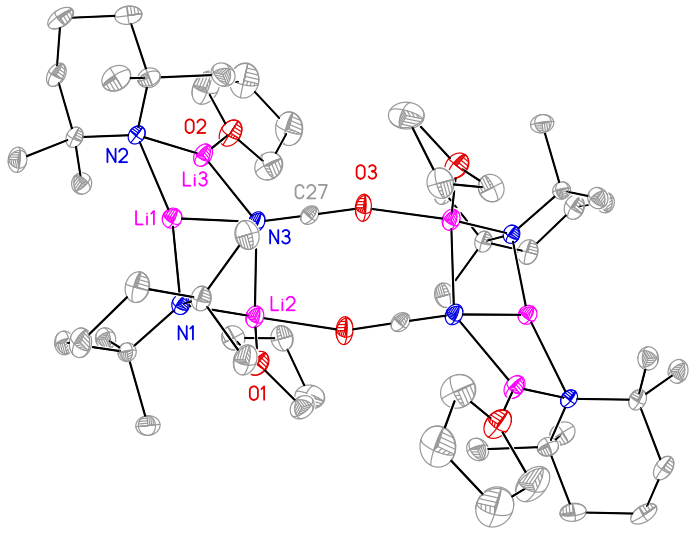

Figure 7.3: Thermal ellipsoid plot of $\mathbf{16}_2$ (30 % probability). H-atoms omitted for clarity. Selected bond lengths (Å) and angles (°): N1–Li1 2.029(3), N2–Li1 2.088(3), N3–Li1 2.198(3), N1–Li2 2.030(3), N2–Li3 1.930(3), N3–Li2 2.228(3), N3–Li3 2.036(3), O3–Li2A 1.968(3), O3–C27 1.208(2), N3–C27 1.172(2), N1–Li1–N2 163.39(16), N1–Li1–N3 100.56(12), N2–Li1–N3 95.39(12).

In $\mathbf{16}_2$, dimerisation occurs in the same manner as in $\mathbf{14b}_2$. However, in $\mathbf{16}_2$, the coordination of additional THF to Li2, which subsequently becomes 4-coordinate (see Figure 7.3), results in weakening of the Li−O interaction (O3A–Li2 1.968(3) Å). As a consequence of Li2 now becoming *pseudo*-tetrahedral, $\mathbf{16}_2$ adopts a chair conformation, with only the central $Li_2(OCN)_2$ ring maintaining planarity. The peripheral Li_3N_3 metallacycles adopt a geometry similar to that in **14**, though the expanded N1–Li1–N2 reflex angle of 196.61(16)° facilitates a transannular interaction (N3–Li1 2.189(3) Å), which is shorter than in **14** but comparable to other Li−N bonds in the structure. A further point of contrast between $\mathbf{16}_2$ and $\mathbf{14}_2$ lies in the orientation of the TMP ligands with respect to the core of the dimer. In **14b**, the TMP ligands adopt an *endo*,*endo* orientation, which is known for TMP-cuprates.[166,167,169,171] However, in **16** the same ligands adopt an *endo*,*exo* disposition and in so doing, this mimics the arrangement noted in $(TMP)_4Li_4$ $\mathbf{9a}_4$ in the solid state.[184]

Moving to more polar reaction media, the synthesis of **14** was attempted in bulk THF. After recrystallisation from hexane, diffractometry revealed $(TMP)_4Cu_{2.70}Li_{1.30}$ **9**, an 8-membered, Cu-rich metallacycle in which substitutional disorder at each metal site was apparent. Crystallography alone could not determine the individual contributions from $TMP_{m+n}Cu_mLi_n$, though solution studies hint at a possible model (see later). The Cu-rich nature of this material can be accounted for by the ability of polar THF to abstract and solubilise LiOCN;[201,202] this view could also account for the Cu-deficiency in **14**.

Next, it was decided to introduce the utility amide *N*,*N*-diisopropylamide to cyanate-based systems. Cu(I) reagents were combined in 1:2 ratio with a hexane solution of DALi, also containing TMEDA. Having not previously explored the cuprate chemistry of this ligand, its suitability for this purpose was screened by reaction with CuBr, a precursor which has been used successfully to fabricate amidocuprate systems in the past (see Chapter 5). Treatment of DAH with TMEDA and *n*BuLi, then CuBr (2:2:2:1) in hexane gave an isolable product, which NMR spectroscopy indicated contained DA and TMEDA in a 1:1 ratio (Scheme 7.4). Data pointed towards the formation of Lipshutz-type $(DA)_2Cu(Br)Li_2(TMEDA)_2$ **17a**, and X-ray diffraction confirmed the expected structure-type, but once again indicated metal disorder at the amide-bridging site. Refinement suggested the composition of this metal site to be $Cu_{0.1}Li_{0.9}$, making **17** most logically interpreted

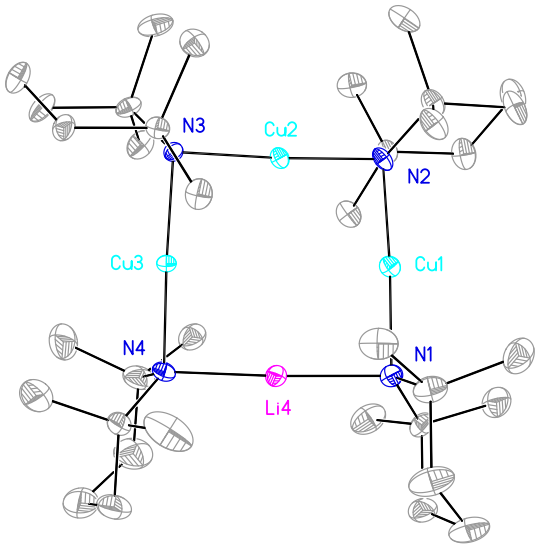

Figure 7.4: Thermal ellipsoid plot of **9** (30 % probability). H-atoms and minor metal disorder omitted for clarity. Where more than one atom type is constrained to occupy the same position, the major element type is reported. Selected bond lengths (Å): N1–M1 1.953(3), N2–M1 1.973(3), N2–M2 1.931(3), N3–M2 1.922(3), N3–M3 1.961(3), N4–M3 1.955(3), N4–M4 2.001(4), N1–M4 2.018(4).

as a co-crystal of $(DA)_2Cu(Br)Li_2(TMEDA)_2$ **17a** and $(DA)_2Li(Br)Li_2(TMEDA)_2$ **17b** (see Figure 7.5).

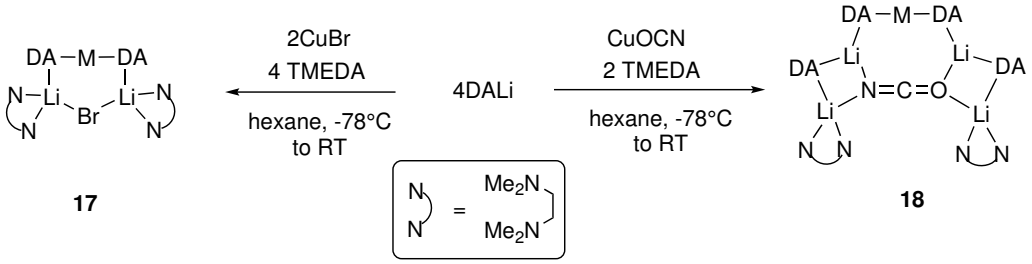

Scheme 7.4: Synthesis of **17** and **18**. M = Cu, Li; see text for details.

Focussing on monomeric **17a** (M = Cu), the 6-membered $N_2Cu(Br)Li_2$ motif is well-known in amidocuprate chemistry, though the use of monodentate Lewis bases has usually led to dimers,[168,169,171] $(Ph_2N)_2Cu(Ph_2N)Li_2(Et_2O)_2$ being the only reported CIP monomer to date.[111] In common with previously reported amidocuprates, **17a** presents with near linear Cu (N1–Cu1–N2 176.0(7)°) with no discernible bonding interaction with Br1 (Br1–Cu1 3.073(10) Å). Contrast this with **17b**, in which the larger N1–Li1–N2 reflex angle of 208.4(8)° places Br1 significantly closer to Li1 (Br1–Li1 2.624(14) Å).[i] This transannular interaction, being somewhat more obvious than that in **14b**, highlights the tendency for Cu to abstain from this type of bonding, preferring to remain two-coordinate (lower order).

Comparisons can be drawn between **17b** and the unusual lithium amide-lithium halide adduct, $(DA)_2Li(Cl)Li_2(TMEDA)$, which can be accessed from secondary ammonium salt $(DAH_2)Cl$.[200] It proved straightforward to adapt this synthesis to the present system by preparing $(DAH_2)Br$. Treatment of a 1:1:2 mixture of $(DAH_2)Br$, DAH and TMEDA with 3 equivalents of *n*BuLi in hexane afforded pure **17b** and X-ray diffraction established congruence with the Li-only containing portion of co-crystalline **17**.

Seeking to expand the range of structures accessible from CuOCN, its reaction with DALi and TMEDA (1:2:2) was attempted in hexane solution. Crystalline material could be obtained from this reaction and IR spectroscopy confirmed the presence of cyanate with a peak at 2208 cm^{-1}. However, ^1H NMR spectroscopy indicated DA and TMEDA to be present in a 2:1 ratio, suggesting a different

[i] A search of the CSD for the fragment 'LiBr' indicated a mean bond distance of 2.549 Å.[203]

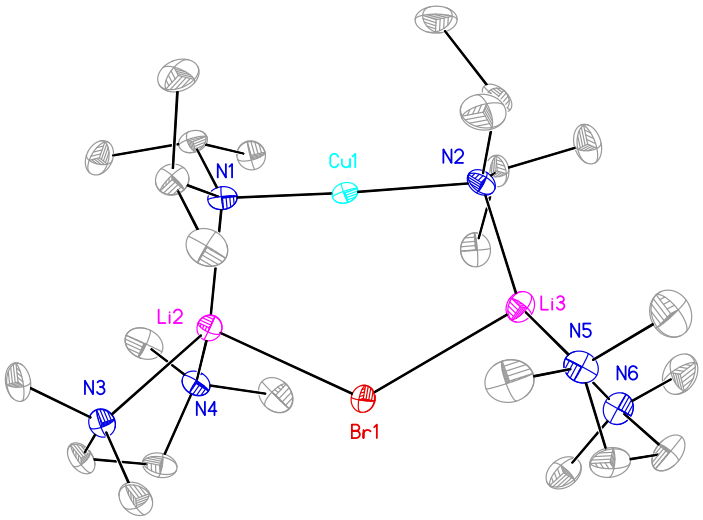

(a)

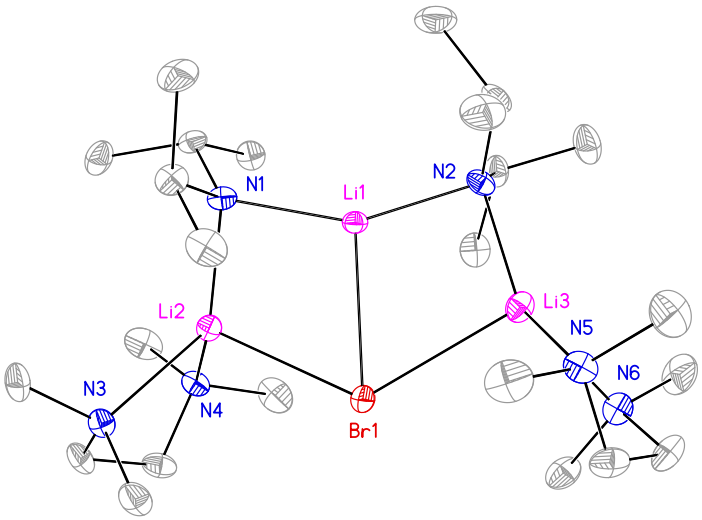

(b)

Figure 7.5: Thermal ellipsoid plot (30 % probability) of **17** showing components (a) **17a** and (b) **17b** separately. Cu1 and Li1 are disordered. Selected bond lengths (Å) and angles (°): N1–Cu1 1.823(13), N2–Cu1 2.064(13), Br1–Cu1 3.073(10), N1–Li1 2.009(16), N2–Li1 1.997(16), Br1–Li1 2.624(14), N1–Li2 2.047(9), N2–Li3 2.022(10), Br1–Li2 2.640(8), Br1–Li3 2.688(9), N1–Cu1–N2 176.0(7), N1–Li2–Br1 101.1(4), N2–Li3–Br1 102.5(4), Li2–Br1–Li3 125.5(3).

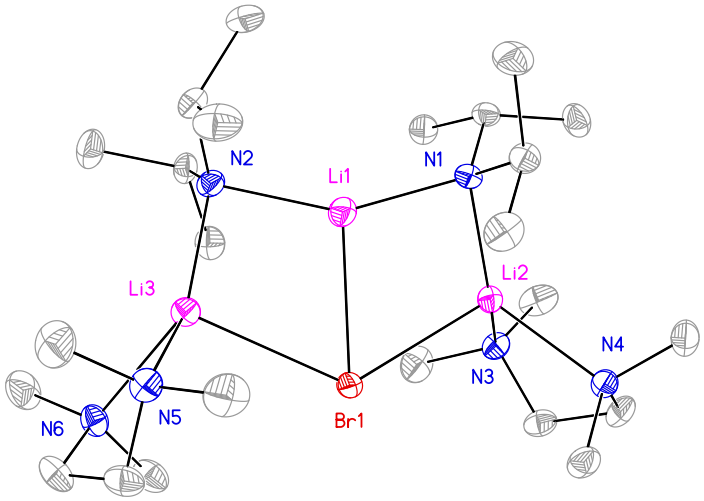

Figure 7.6: Thermal ellipsoid plot of pure **17b** (30 %) probability. H-atoms omitted for clarity. Selected bond lengths (Å) and angles (°): N1–Li1 1.977(5), N1–Li2 2.038(5), N2–Li1 2.024(5), N2–Li3 2.019(5), N3–Li2 2.255(5), Br1–Li1 2.601(5), Br1–Li2 2.650(4), Br1–Li3 2.708(5), N1–Li1–N2 151.8(3), Li1–N1–Li2 86.9(2), Li3–N2–Li1 87.5(2), N2–Li3–Br1 101.05(18), Li2–Br1–Li3 126.46(14).

structure-type to that displayed by **17**. X-ray diffraction revealed the novel cuprate $(DA)_4Cu(OCN)Li_4(TMEDA)_2$ **18**, which can be formally represented as the adduct of a Lipshutz-type monomer $(DA)_2Cu(OCN)Li_2(TMEDA)_2$ and two units of DALi. Perhaps surprisingly, **18** presents without metal disorder at the DA-bridging position. Moreover, the bridging mode of cyanate clearly differs from that of **14**. In **14a**, cyanate engages in the formation of 6-membered $CuLi_2N_3$ rings, leaving the oxygen centre free to participate in dimer formation. In **18**, cyanate participates in the formation an 8-membered N_2CuLi_2OCN ring. This bonding mode facilitates the capture of two units of DALi to give 4-membered Li_2N_2 and Li_2NO rings (though cyanate is disordered in the solid state) and the coordination sphere of the peripheral Li^+ is completed by TMEDA. In contrast to **14a**, the 8-membered $(DA)_2Cu(OCN)Li_2$ ring incorporates a substantial twist, evidently to accommodate OCN^- in a 'side-on' fashion, leaving the DA ligands projecting above and below the plane incorporating the N–Cu–N unit and the C of cyanate (Figure 7.7).

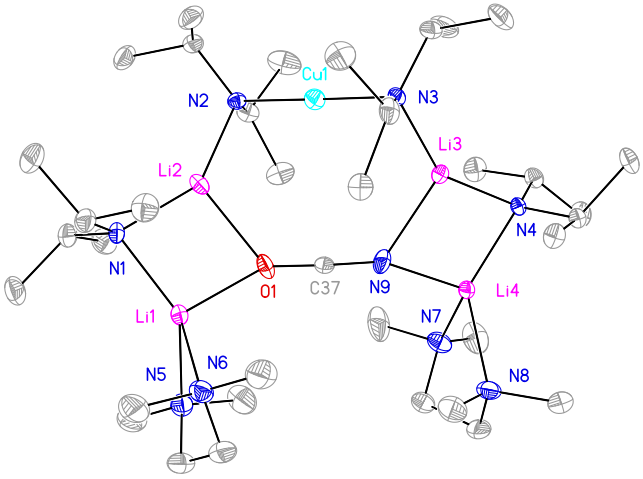

(a)

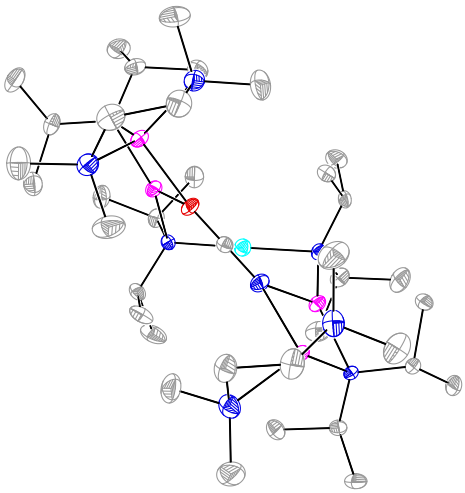

(b)

Figure 7.7: (a) Thermal ellipsoid plot of **18** (30 % probability). H-atoms and minor disorder omitted for clarity. Selected bond lengths (Å) and angles (°): N2–Cu1 1.910(2), N3–Cu1 1.909(2), N2–Li2 2.058(5), N1–Li2 1.991(5), N1–Li1 2.044(5), N3–Li3 2.053(5), N4–Li3 1.985(5), N4–Li4 2.048(5), N9–Li3 2.159(6), N9–Li4 2.026(5), O1–Li2 2.137(6), O1–Li1 2.009(5), N9–C37 1.202(4), O1–C37 1.205(4), N2–Cu1–N3 179.09(11), N2–Li2–O1 117.7(2), N3–Li3–N9 117.4(2), Li2–O1–C37 126.3(2), Li2–O1–Li1 81.6(2), Li2–N1–Li1 84.4(2), N1–Li1–O1 98.0(2), Li3–N9–C37 121.9(2), Li3–N9–Li4 81.3(2), Li3–N4–Li4 85.1(2), N4–Li4–N9 97.9(2); (b) side view of **18**, projected down the Cu1→C37 vector, N2–Cu1–N3 horizontal.

7.2.2 NMR spectroscopy

With the solid state structures of **14**–**18** to hand, interpretation of the convoluted solution-state behaviour of these systems was attempted. It was anticipated that co-crystalline **14** would give rise to two species in solution: **14a** and **14b**. In the event, spectroscopic data for bulk **14** could not be reconciled with a simple model of metal disorder. This was evidenced most clearly through ^{7}Li NMR spectroscopy, where multiple solution species were observed in proportions suggestive of a *mixture* of products (Figure 7.8). Comparison with authentic samples of Gilman cuprate **9c** and TMPLi **9a** established their presence as minor components of the mixture (δ 0.90 and 2.18 ppm, respectively). To aid assignment of the other species, **16** was investigated. In common with all TMP-based systems, limited amounts of TMPH were identified (by ^{1}H and ^{13}C NMR spectroscopy), presumed to arise from reaction with trace moisture in the deuterated solvent. TMPH notwithstanding, **16** was identified as a single species in solution by ^{13}C NMR spectroscopy (Figure 7.9).

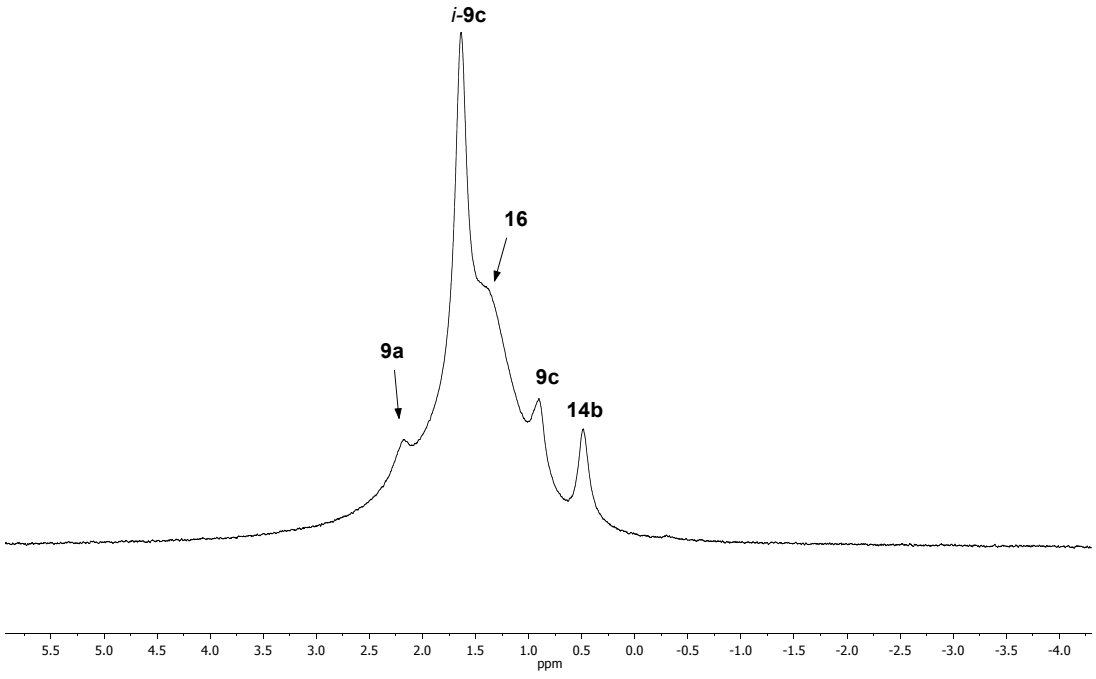

Figure 7.8: ^{7}Li NMR spectrum of bulk product **14** in C_6D_6.

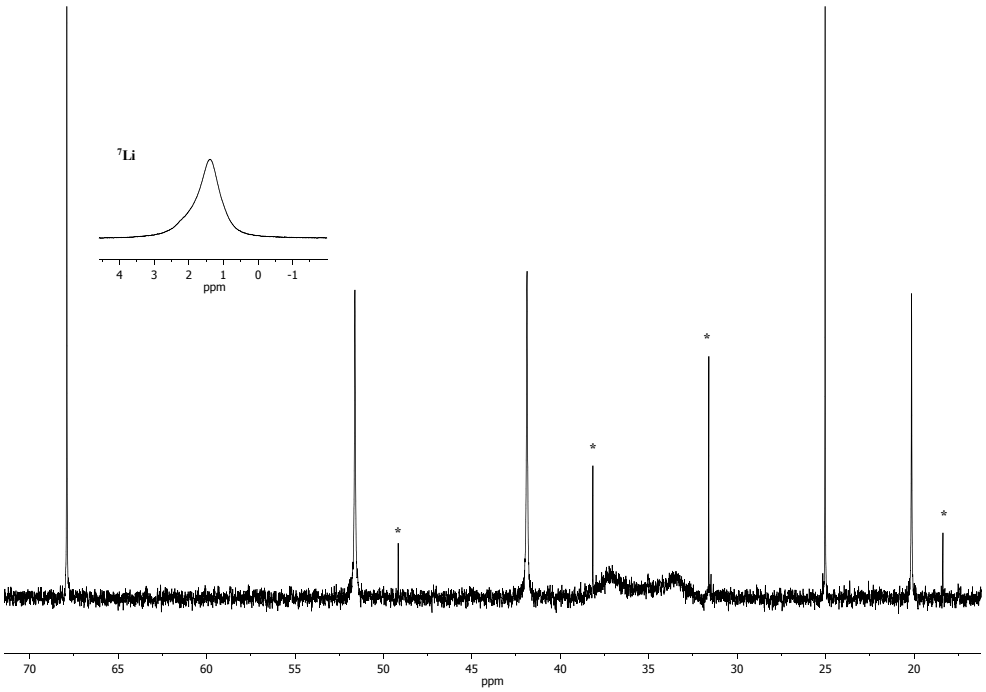

Figure 7.9: ^{13}C NMR spectrum of **16** in C_6D_6, with ^{7}Li NMR spectrum inset. * = TMPH.

Returning to bulk reaction mixture from which **14** was isolated, the major broad feature at δ 1.41 ppm was now accounted for by **16**, leaving two resonances, at δ 1.65 and 0.48 ppm, to be accounted for. To assign the first of these, ^{1}H NMR spectroscopy was deployed. THF notwithstanding, the spectrum was dominated by three singlets, at δ 1.76, 1.57 and 1.39 ppm, in a 1:2:1 integral ratio. 2D-HSQC spectroscopy established these signals to belong to TMP-Me groups and comparison with authentic samples of TMPCu **9e**, $(TMP)_2CuLi$ **9c** and TMPLi **9a** revealed that the aforementioned signals fall within the chemical shift ranges typical for these compounds. These data pointed towards a 1:1 aggregate of a dimer of TMPLi and TMPCu, giving an 8-membered metallacyle in which metals of the same type occur adjacent to one another (Figure 7.10). In *i*-**9c**, this yields three distinct TMP-environments. It was hypothesised that *i*-**9c** might be a kinetic product from this reaction since it could form by catenation of dimeric units of TMPCu **9e** and TMPLi **9a**, without requiring the formation of Gilman cuprate **9c**. This hypothesis requires that, given suitable conditions, rearrangement of *i*-**9c** to the thermodynamic product **9c** should occur. This was found to be the case: when a typical sample prepared from the reaction of TMPLi with CuOCN

was heated to reflux and allowed to crystallise at room temperature, fine needles were formed which were confirmed (by NMR spectroscopy) to be **9c**.

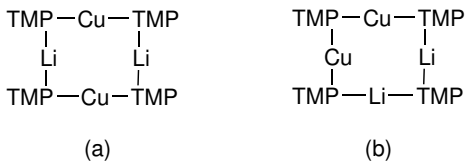

Figure 7.10: Molecular diagram of the aggregated structures of (a) $\mathbf{9c}_2$ and (b) *i*-**9c**. The molecular symmetry in (a) gives rise to only one distinct TMP environment, whereas in (b) three arise in a 1:2:1 ratio.

Only the ^{7}Li resonance at δ 0.48 ppm remained to be assigned. Logically, this belonged to either **14a**, **14b** or LiOCN. Pure **14a** was therefore analysed by NMR spectroscopy. This revealed a system which closely resembled thiocyanate **6**, with a fine white precipitate (presumed LiOCN) deposited upon dissolution in benzene. No signal attributable to solvated LiOCN could be detected. Apart from THF, the signals matched **9c** precisely (^{7}Li NMR δ 0.90 ppm), suggesting that the signal at δ 0.48 ppm in Figure 7.8 belonged to **14b**.

Both metal disorder in single crystal **14** and the multiple species identified in the bulk reaction mixture are unusual features of amidocuprate systems. Nonetheless, the results can be explained by three major competing reactions (Scheme 7.5). In reaction **(1)** TMPCu is generated by reaction of CuOCN with TMPLi, expelling LiOCN as a by-product. *In situ*-generated LiOCN is sequestered by TMPLi in **(2)** at a rate competitive with **(3)**. The remaining TMPLi can simultaneously react with remaining TMPCu to generate any compound in the series $TMP_{m+n}Cu_mLi_n$ (such as **9c** and *i*-**9c**). The failure to isolate *i*-**9c** in previous work is best explained by its kinetic properties, and the fact that **9c** can be accessed from Lipshutz-type cuprates (which have typically been the focus of work in the past) whereas *i*-**9c** cannot.

Moving to more polar media, 1:2 combination of CuOCN with TMPLi in bulk THF, followed by recrystallisation from hexane gave $(TMP)_4Cu_{2.70}Li_{1.30}$ **9**. Whilst this empircal formula hints at the presence of a TMPLi-TMPCu aggregate such as $(TMP)_4Cu_3Li$, crystallography could not establish the individual contributions from $TMP_{m+n}Cu_mLi_n$. However, ^{7}Li NMR spectroscopy identified three Li-containing species in solution: minor amounts of *i*-**9c** were identified at δ 1.65

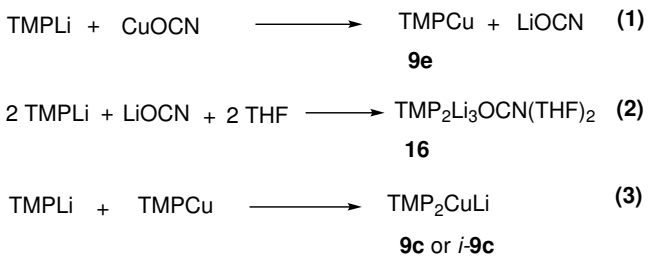

Scheme 7.5: Reactions producing the products found in the bulk reaction mixture from which **14** was isolated.

ppm, whilst the spectrum was dominated by **9c** at δ 0.91 ppm. The final resonance was identified as a shoulder at δ 0.94 ppm. *i*-**9c** and **9c** contribute equal amounts of Cu and Li, so the remaining species should be Cu-rich in order for the bulk composition to agree with the solid-state formula. One of these species, an aggregate of **9e**, was identified by ^{1}H NMR (δ 1.76 ppm) and strong contenders for the remaining Li-containing species would be $(TMP)_4Cu_3Li$ or $(TMP)_3Cu_2Li$ (there being tetrameric and trimeric variants for end-member phases **9a**[185] and **9e**[204,205]).

Lastly, the solution behaviour of **17** was probed in conjunction with that of pure **17b**. Spectroscopic data for **17b** proved straightforward to interpret, with a single species in solution being suggested (alongside minor reformation of DAH[206]). In particular, ^{7}Li NMR spectroscopy revealed two resonances – δ 2.28 and 1.26 ppm – in the expected 1:2 integral ratio. Turning to co-crystalline **17**, signals for component **17b** are added to by those of **17a**. Interestingly, analysis of different samples of **17** clearly indicates variable proportions of **17a** and **17b**. These data point towards the possibility of incorporating higher levels of Cu in **17** than predicted from crystallographic data (Figure 7.11).

7.3 Summary

The ability of CuOCN to participate in the formation of Lipshutz-type cuprates has been evaluated. Results have shown that Lipshutz-type structures can be supported by OCN^-, but that cuprate formation does not proceed in a straightforward manner. Copper-lithium substitution in these systems has been uncovered through the isolation of co-crystalline $(TMP)_2M(OCN)Li_2(THF)$ (M =

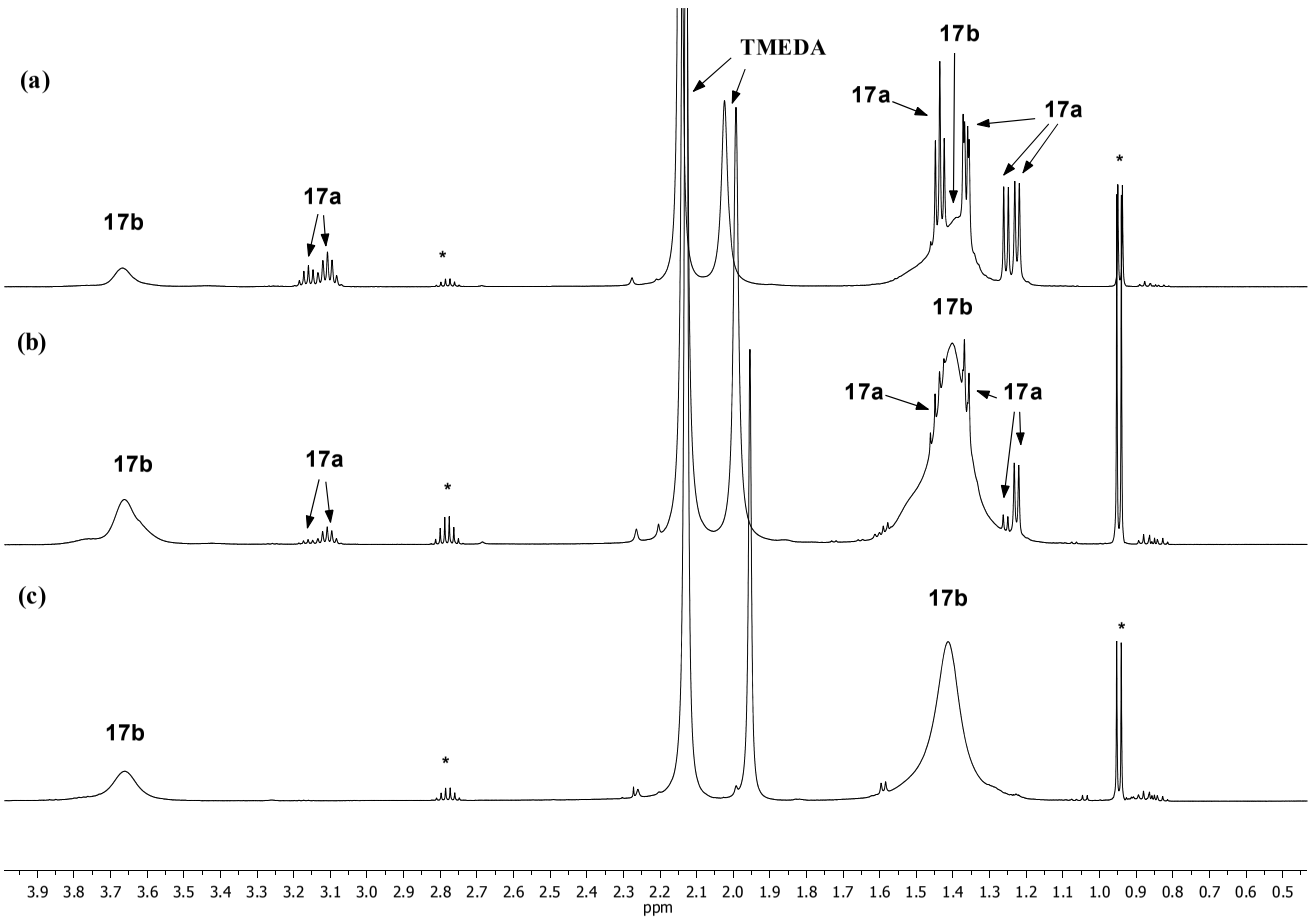

Figure 7.11: ^{1}H NMR spectrum in C_6D_6 of (a) **17** (b) a different sample of **17** and (c) **17b.** Differences in samples (a) and (b) can be accounted for by variable proportions of **17a** and **17b** in co-crystalline **17.**

$Cu_{0.1}Li_{0.9}$) **14**. The preference for Cu to remain lower-order (two-coordinate) in **14** and pure **14a** is highlighted by comparison with the behaviour of Li in the same amide-bridging position, where for **14b**, transannulation emerges, and in $(TMP)_2Li(OCN)Li_2(THF)_2$ **16** the interaction renders Li^+ fully three-coordinate. When CuOCN is introduced to the less sterically demanding ligand DA, no Cu-Li substitution occurs. However, the Lipshutz-type monomer sequesters DALi to form a lithium amide-lithium cuprate adduct $(DA)_4Cu(OCN)Li_4(TMEDA)_2$ **18**. In this complex, cyanate bridges in a different manner to that in **14** and **16**, allowing for the coordination of four Li^+. Taken together, these results highlight the tendency for OCN^- to maximise its interactions with lithium, which is in accord with the rules of HSAB theory (i.e. 'hard-hard' interactions).[207] That Cu-Li substitution is not merely a feature unique to cyanate chemistry has been evidenced through attempts to fabricate monomeric Lipshutz-type cuprates, with resulting co-crystalline $(DA)_2M(Br)Li_2(TMEDA)_2$ **17** ($M = Cu_{0.09}Li_{0.91}$) exhibiting metal disorder at the amide-bridging site. In this complex, the predilection for linear Cu in **17a** and trigonal Li in **17b** at the amide-bridging site is exhibited very clearly. Finally, insight into the fate of the residual copper in these reaction systems has been gleaned by the isolation of TMPCu-TMPLi aggregate $(TMP)_4Cu_{2.70}Li_{1.30}$ **9**, the generation of which is assisted by an excess of Li-solubilising donor solvent.

NMR spectroscopy has been used to elucidate the complex solution state chemistry offered by these systems. In particular, the use of multinuclear NMR spectroscopy has made it possible establish that **14** is amongst a mixture of products that include **16**, **9c** and *i*-**9c**, a newly identified isomeric variant of aggregated $\mathbf{9c}_2$. *i*-**9c** is proposed to be a kinetic form of $\mathbf{9c}_2$ that can be generated by direct reaction of TMPLi and *in situ*-generated TMPCu. Meanwhile, for **17**, crystallographic analysis could be combined with NMR spectroscopic data to distinguish between solution forms of Cu-containing and Li-only species, and pointed to variability in the levels of Cu-Li substitution in **17**.

Perhaps most significantly, a new route to Lipshutz-type cuprates has been established through the reaction of LiOCN with Gilman cuprate in THF, to give pure **14a**. The reaction of *in situ*-generated lithium salts with Gilman cuprate has previously been observed implicitly through the formation of $(TMP)_2Cu(X)Li_2(Et_2O)$ (X = CN, Cl, Br and I).[171] However, this has not been reported during the synthesis of $(TMP)_2Cu(X)Li_2(THF)$ (X = Cl, Br and I), when strictly limited quantities

of THF were called for.[168,169] This is of significance because THF is the most commonly used solvent for deprotocupration[196] and the formation of Lipshutz-type cuprates under these conditions has been exposed as necessary for good reactivity.[166] By introducing LiOCN independent of the synthesis of Gilman cuprate, the possibility of deploying this salt in sub-stoichiometric or catalytic amounts arises (Scheme 7.6). Provided that the aryl(amido)cuprate has a lower affinity for LiOCN than Gilman cuprate (as suggested by theoretical work),[104] the reaction should turn over.

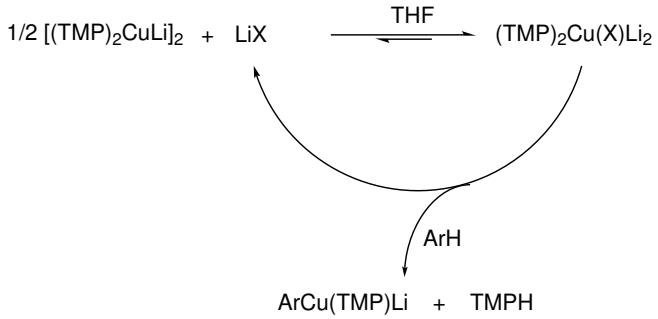

Scheme 7.6: Proposed pathway for DoCu that employs catalytic amounts of LiX (X = OCN). THF-solvation omitted for simplicity.

Chapter 8

Towards the Synthesis of Lithium Bis(amido)argentates

8.1 Introduction

Organosilver compounds have been studied extensively in the solid state; in addition to numerous examples of N-heterocyclic carbene complexes[208] and silver ethynide clusters,[209] examples of conventional σ-bonded organosilver compounds are known (see Section 1.5). The synthesis of organosilver compounds is normally by transmetalation, although the tendency of organolithium and Grignard reagents to reduce silver(I) sometimes calls for the use of less reducing organozinc,[115] organotin or organolead[116] metathesis agents. Related to organosilver compounds, amidosilver compounds are much more scarse, with only a few homoleptic examples (e.g. $(TMP)_4Ag_4$ and $(HMDS)_4Ag_4$[118]) characterised in the solid state. A small number of heteroleptic examples are also known (e.g. $[Ag_2(\mu\text{-TAG})(\mu\text{-HMDS})]_2$[68]) and these have also been characterised crystallographically. Though rare, these compounds are not without applications – for example, $(HMDS)_4Ag_4$ has recently received attention for its role as a catalyst component in the [3+2] cycloaddition of α-aminophosphonate[210] or α-aminoester[211] Schiff bases to olefins.

Though lithium organocuprates have been studied extensively, it is apparent that lithium argentates remain relatively unexplored. The expense of silver in comparison to copper, combined with generally poorer stabilities of organosilver and

organoargentate complexes likely serve to discourage their investigation for synthetic applications. That said, one study concerning cyanoargentates has highlighted interesting selectivities in the ring opening of epoxides.[212] Furthermore, investigation of these compounds in the field of organometallic chemistry has not been entirely neglected and structural comparisons with organocuprates have been sought. Unlike Cu and Au, the common isotopes of Ag (^{107}Ag and ^{109}Ag in 51.8 % and 48.2 % abundance, respectively) possess $I = 1/2$ nuclei,[212] making organoargentate compounds enticing candidates for solution-state structure determination. In fact, the structure of (2-(Me_2NCH_2)C_6H_4)$_2$AgLi was determined entirely by solution-state techniques.[75] A combination of cryoscopic measurements and detailed analysis of coupling patterns revealed by ^{1}H NMR and ^{13}C NMR spectroscopy indicated a dimer with alternating Li and Ag cations – consistent with the structure of the copper homologue.[74]

In light of the progress made with lithium amidocuprates in recent years, it was a natural extension of work to ask whether this chemistry could be adapted to silver derivatives. The motivations for pursuing lithium amidoargentates are twofold: first, to establish trends in structure and bonding, and second, to probe the unique spectroscopic features of silver in these compounds. In this chapter, initial attempts at the synthesis of lithium bis(amido)argentates and their characterisation in the solid state will be presented.

8.2 Results and discussion

8.2.1 Synthesis and X-ray crystallography

Initially, a synthetic strategy was adopted which paralleled the synthesis of amidocuprate reagents. Previously, this involved the addition of a hydrocarbon solution of TMPLi (also containing THF) to a Cu(I) salt at low temperatures. In the present case, addition of TMPLi solution to AgX (X = Cl, Br and I) in the presence of THF at low temperature resulted in almost instantaneous decomposition to give a black suspension (presumed to be metallic silver). When reacted with AgSCN instead, significant decomposition occurred, but qualitatively to a lesser degree than with the silver halides (Scheme 8.1). Prolonged chilling of the filtrate

allowed for the isolation of needle-like crystals in a very low yield, which X-ray diffraction confirmed to be $(TMP)_2AgLi$ **19** (Figure 8.1).

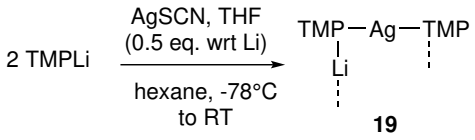

Scheme 8.1: Synthesis of **19**.

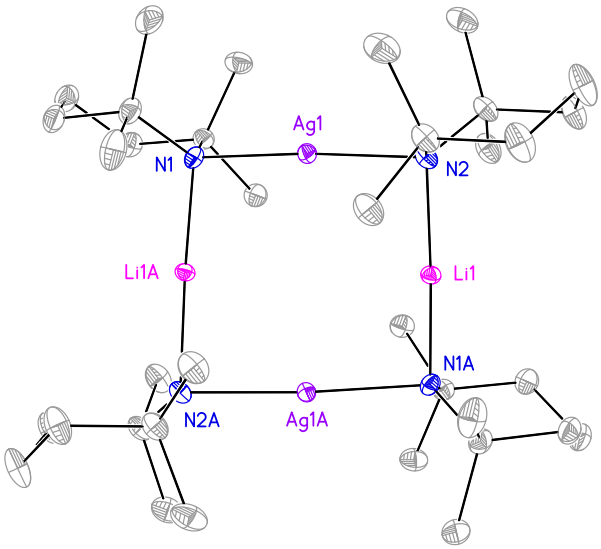

Figure 8.1: Thermal ellipsoid plot of $\mathbf{19}_2$ (30 % probability). H-atoms omitted for clarity. Selected bond lengths (Å) and angles (°): N1–Ag1 2.129(2), N2–Ag1 2.127(2), N1–Li1A 2.014(3), N2–Li1 2.051(3), N1–Ag1–N2 176.37(8), Ag1–N2–Li1 87.35(9), Ag1–N1–Li1A 88.76(9), N2–Li1–N1A 177.72(14).

This structure closely approximated that of previously reported Gilman cuprate TMP_2CuLi **9c**, which is a dimer in the solid state. Though the overall structure is centrosymmetric, each dimer $\mathbf{19}_2$ (which lies on a diad) is itself non-centrosymmetric and exhibits significant twisting, ostensibly to reduce repulsion of the bulky TMP ligands. Crystallographic refinement indicated approximately 6 % Ag-Li disorder, which complicates comparisons of the bonding parameters with those previously reported for $\mathbf{9c}_2$. Nonetheless, it is evident that the N–Ag bond lengths (2.127(2) Å and 2.129(2) Å in $\mathbf{19}_2$) are significantly longer than the corresponding N–Cu bond lengths in $\mathbf{9c}_2$ (1.922(2) Å and 1.926(2) Å) and that the average N–Li bond lengths are slightly shorter (2.014(3) Å and 2.051(3) Å in

$\mathbf{19}_2$; 2.047(4) Å and 2.075(3) Å in $\mathbf{9c}_2$). Significant differences in the associated bond angles are also evident and when projected along the Li→Li vectors, torsion angles of 32.92(6)° and 28.59(7)° are found for $\mathbf{19}_2$ and $\mathbf{9c}_2$, respectively. Tentatively, this increased distortion may compensate for the marginally reduced N–Li bond lengths in $\mathbf{19}_2$.

The reaction conditions described above were expected to lead to the isolation of $(TMP)_2Ag(SCN)Li_2(THF)$, though this could not be realised, despite repeated attempts. Additionally, the yields of **19** were very low, hence an alternative preparative method was sought. Avoidance of Lewis base altogether once again led to decomposition. However, it was found that a 2:1 mixture of toluene/diisopropyl ether led to a much slower reaction and (qualitatively) significantly reduced decomposition (Scheme 8.2). NMR spectroscopic analysis of **19** prepared *via* this route indicated that small quantities of the impurity TMPAg **20** was present (confirmed by comparison with an authentic sample), a result which was consistent with elemental analysis. This could not be removed by recrystallisation since (unlike their copper congeners) **19** and **20** are isomorphous and readily co-crystallise.

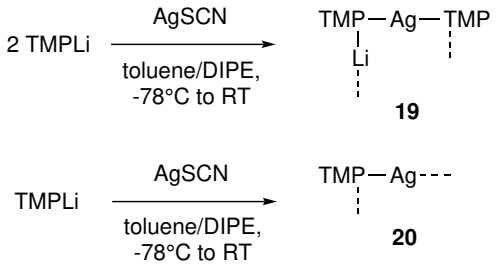

Scheme 8.2: Alternative synthesis of **19** and **20**.

In view of the fact that **19** does not present any inherent thermal instability, it is thought to be unlikely that a Lipshutz-type argentate would behave much differently. More likely is that an intermediate compound or by-product, in which thiocyanate is coordinated to silver – for example (TMP)Ag(SCN)Li – undergoes decomposition to Ag and other products.[i] These data suggest that it is the ability of the Lewis basic solvent to effectively solvate the LiSCN by-product and discourage coordination of SCN to Ag (for example, by steric hindrance) which is necessary for good product yields. It is possible that this solvent system favours

[i]Occasionally, during the synthesis of **19** and **20**, an intense but transitory blue colour was observed. Blue colouration in thiocyanate-based systems have been attributed previously to radical anions, such as $(SCN)_2^{-\bullet}$.[213,214]

a stepwise reaction mechanism, whereby **20** is formed first, and that this then combines with another equivalent of TMPLi to give **19**. This view would also explain the small amount of TMPAg present in samples of **19** prepared *via* this method.

Reasoning that a π-acceptor ligand might stabilise the increase in negative charge at Ag during argentate formation, attention was diverted to AgCN as a precursor. TMPLi could be reacted with AgCN (2:1) in THF without decomposition at low temperature, but rapid darkening of the reaction mixture occurred at room temperature and no product could be isolated. However, an alternative method proved more fruitful: TMPLi and AgCN were reacted (2:1) in toluene and warmed to room temperature. A small amount of black decomposition product was formed. However, removal of the toluene and addition of THF did not result in any obvious further decomposition. Replacement of the solvent with hexane/toluene, filtration and finally, concentration gave a yellow solution from which crystals deposited after storage at 5 °C for 24h (Scheme 8.3). IR spectroscopy on these crystals confirmed the presence of CN^- by revealing a sharp peak at 2102 cm^{-1} and a weak, broad signal at 2150 cm^{-1}. The latter of these two signals grew upon exposure to air and this behaviour was consistent with that previously reported for cyanocuprate $(TMP)_2Cu(CN)Li_2(THF)$.[104] ^1H NMR spectroscopy revealed TMP and THF to be present in a 2:1 ratio, consistent with the formula $(TMP)_2Ag(CN)Li_2(THF)$ **21**. X-ray diffraction confirmed this formula, revealing a dimer composed of individually 7-membered $AgN_2Li_2(CN)$ metallacycles which associate by the formation of Li_2N_2 rings (Figure 8.2).

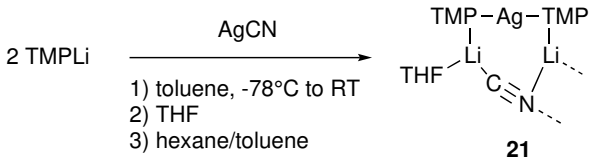

Scheme 8.3: The synthesis of **21**.

The structure of $\mathbf{21}_2$ is plainly very similar to that of the previously reported cuprate $(TMP)_2Cu(CN)Li_2(THF)$.[167] In particular, the TMP ligands adopt an *endo,endo* orientation with respect to the core of the dimer. The only significant differences in bond length are found for the Ag−N bonds. These are extended by 0.218(4) Å, on average, relative to their counterparts in $(TMP)_2Cu(CN)Li_2(THF)$. Whilst significant, this difference is readily accounted for by the larger ionic radius

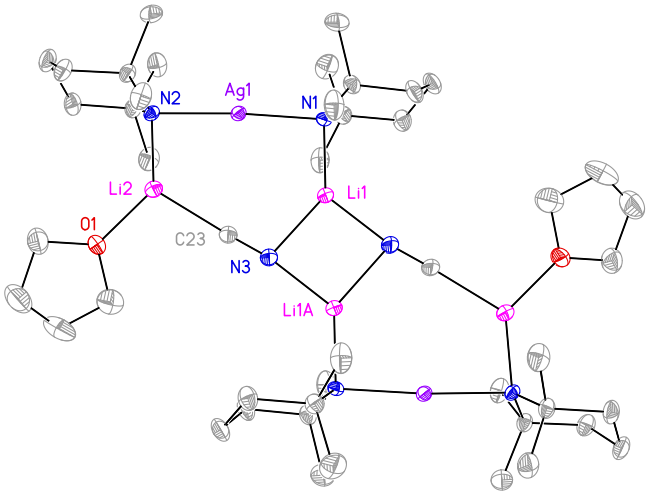

Figure 8.2: Thermal ellipsoid plot of **21**$_2$ (30 % probability). H-atoms and minor THF-disorder omitted for clarity. Selected bond lengths (Å) and angles (°): Ag1–N1 2.134(2), Ag1–N2 2.147(2), N1–Li1 1.957(5), N3–Li1 2.125(6), N3–Li1A 2.014(6), N2–Li2 1.976(5), Li2–C23 2.139(6), N3–C23 1.140(4), N1–Ag1–N2 176.01(8), Ag1–N1–Li1 93.96(17), Ag1–N2–Li2 88.29(17), N1–Li1–N3 138.0(3), N2–Li2-C23 123.9(3), N3–C23–Li2 177.8(3), C23–N3–Li1 102.0(3), Li1–N3–Li1A 87.3(2).

of Ag as compared to Cu (0.21 Å).[215] Despite the larger ionic radius of Ag – and hence the possibility of a larger coordination number[216] – the Ag1$\cdots$C23 distance, at 3.128(3) Å, is plainly non-bonding and hence the argentate remains lower-order. To accommodate the larger group 11 metal centre, most bond angles within the 7-membered metallacycle of **21** differ significantly from those in the cuprate congener. This difference is most exaggerated for C23–N3–Li1, where this angle (102.0(3)°) is significantly expanded compared to the cuprate (95.5(2)°). The most noticeable consequence of this is that the 7-membered $AgN_2(CN)Li_2$ rings in **21** are less twisted than in $(TMP)_2Cu(CN)Li_2(THF)$ (angle between the vectors joining N1→N2 and Li1→Li2 of 1.52(1)° and 6.81(9)° in **21** and $(TMP)_2Cu(CN)Li_2(THF)$, respectively).

8.2.2 NMR spectroscopy

Moving to solution-state work, ^{7}Li NMR spectroscopy on **19** in C_6D_6 indicated a single lithium environment at δ 1.06 ppm. In addition to minor reformed TMPH, ^{13}C NMR spectroscopy revealed a simple spectrum with resonances attributable

to five distinct TMP^- carbon environments: δ 54.8, 41.4, 40.1, 35.5 and 19.5 ppm (Figure 8.3). These compare closely with the signals seen for Gilman cuprate **9c**. Interestingly, expansion of the signals at δ 54.8 and 41.4 ppm reveals them to be doublets, with coupling constants of $^2J_{\text{Ag-C}} = 3\,\text{Hz}$ and $^3J_{\text{Ag-C}} = 6\,\text{Hz}$, respectively. Evidently, the resolution is too low to reveal the expected pair of doublets for coupling to both ^{107}Ag and ^{109}Ag, though with the ratio $\gamma_{^{107}\text{Ag}}/\gamma_{^{109}\text{Ag}} = 0.87$,[212] this is not surprising. Significantly then, the multiplicity of the TMP-2,6 and TMP-3,5 carbons provides direct evidence that the TMP ligands remain bonded to Ag^+ in solution. Taken together with the observation of a single set of resonances attributable to TMP, this suggests that the solid-state structure is retained in solution. Furthermore, ^{1}H NMR spectroscopy provides evidence for the retention of discreet TMP orientations in solution, with two distinct TMP-Me resonances being revealed, at δ 1.54 and 1.46 ppm. Accordingly, inverse detected ^{1}H-^{7}Li HOESY data showed a single cross-peak between the TMP-Me resonance at δ 1.46 ppm and the ^{7}Li resonance at δ 1.06 ppm (Figure 8.4).

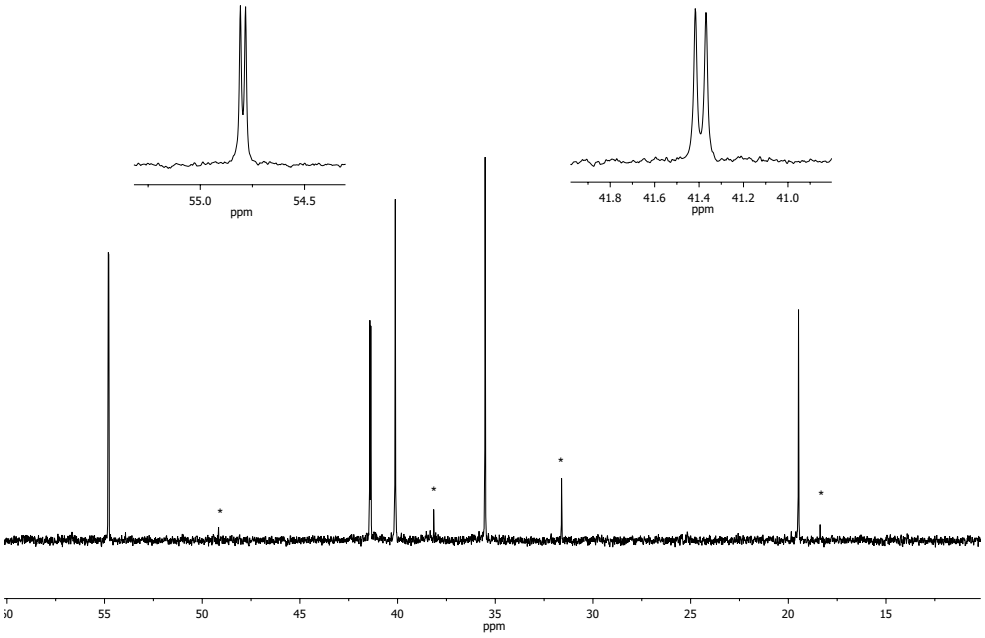

Figure 8.3: ^{13}C NMR spectrum of **19** in C_6D_6, with expansions (inset) of doublets due to coupling to Ag. * = TMPH.

Turning to **21**, ^{7}Li NMR spectroscopy in C_6D_6 revealed a dominant resonance at δ 0.29 ppm, with a very minor resonance attributable to **19** at δ 1.09 ppm. This

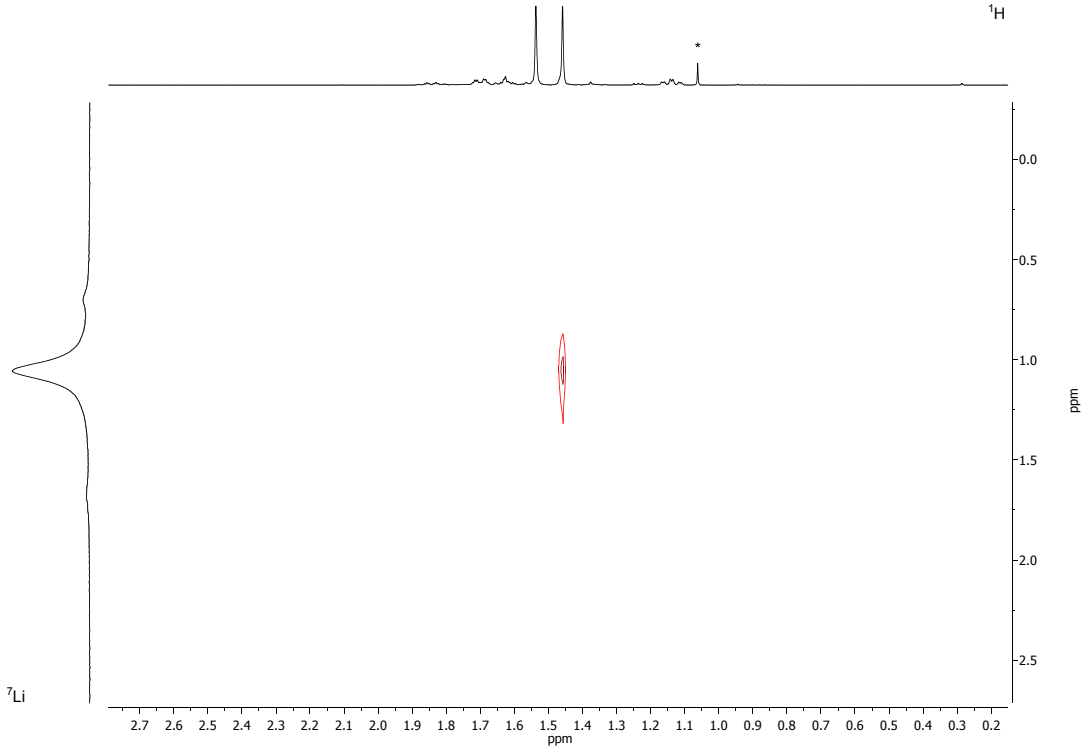

Figure 8.4: ^{1}H-^{7}Li HOESY spectrum of **19** in C_6D_6. * = TMPH.

suggests that *in situ* conversion of **21** to **19** is minimal. ^{1}H NMR spectroscopy revealed several broad features, which indicates either conformational lability or rapid equilibrium processes. ^{13}C NMR spectroscopy mirrored these features, with a doublet (due to coupling with $^{107/109}$Ag, $^{2}J_{\text{Ag-C}} = 3$ Hz) being observed for the TMP-2,6 environment only. In line with $(\text{TMP})_2\text{Cu(CN)Li}_2\text{(THF)}$,[167] but in contrast to **19**, the TMP-3,5 resonance exhibited significant broadening, and no $^{3}J_{\text{Ag-C}}$ coupling could be detected (*cf.* **19** above). In the same way that CN^- could be located by ^{13}C NMR spectroscopy in $(\text{TMP})_2\text{Cu(CN)Li}_2\text{(THF)}$,[104] its presence in **21** was confirmed by the observation of a resonance at δ 168.2 ppm.

The observation of Ag-C coupling in **19** and **21** raised the possibility that similar features might not have been observed in the original characterisation of TMPAg **20**[118] due to resolution limits of instrumentation at the time. Synthesis of **20** was therefore undertaken by modification of the literature procedure (Scheme 8.2). Gratifyingly, NMR spectroscopy now revealed 1:2:1 triplets for the ^{13}C NMR resonances assigned to the TMP-2,6 and TMP-3,5 carbons (*viz.* doublets in **19**), with coupling constants $^{2}J_{\text{Ag-C}} = 2$ Hz and $^{3}J_{\text{Ag-C}} = 3$ Hz, respectively (Figure 8.5). A further point of contrast between **19** and **20** lies in the observation of two TMP-Me resonances in the former, but only one in the latter, in spite of their being isostructural in the solid state. For **19** this suggests retention of the solid state conformation, meanwhile for **20**, processes which scramble TMP-Me_{ax} and TMP-Me_{eq} environments must be operating – for example, ring inversion or dissociative equilibria.

8.3 Summary

The synthesis of bis(amido)argentates has been attempted as a means of introducing a spectroscopically active group 11 metal to 'ate complexes. Generally, AgX (X = Cl, Br, I) are decomposed by addition of TMPLi. However better results have been achieved using AgSCN and AgCN. This has permitted the isolation of $(\text{TMP})_2\text{AgLi}$ **19** and $(\text{TMP})_2\text{Ag(CN)Li}_2\text{(THF)}$ **21**. In the solid state, the structures of **19** and **21** adopt the structure-types known for Gilman[104] and Lipshutz[167] amidocuprates, notwithstanding small differences arising from the presence of a larger group 11 metal. In benzene solution, ^{13}C NMR spectroscopy reveals multiplets for certain TMP-carbon resonances (doublets in **19** and **21**, triplets in **20**)

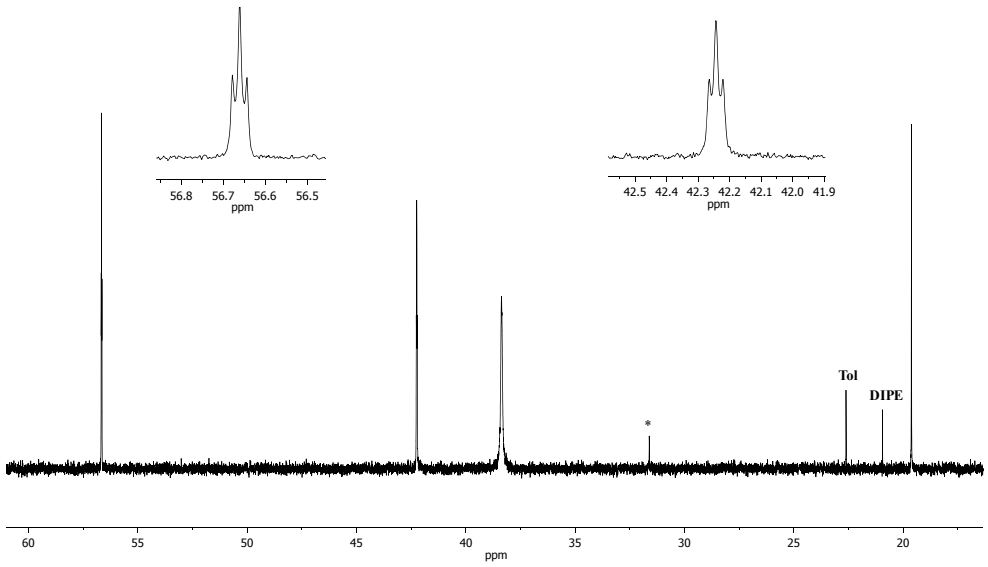

Figure 8.5: ^{13}C NMR spectrum of **20** in C_6D_6 with expansions (inset) of triplets due to coupling to Ag. Tol = toluene, DIPE = diisopropyl ether, * = TMPH.

which arise due to J-coupling with Ag. Taken together with the presence of a single TMP environment, this provides evidence that **19** and **20** remain aggregated in hydrocarbon media, and for **19**, suggests that the dimer observed in the solid state is retained.

Armed with the knowledge that Lipshutz and Lipshutz-type cuprates are active in DoCu,[167–169] **21** should be evaluated for its ability to effect DoAg on substrates such as *N*,*N*-diisopropylbenzamide. NMR spectroscopy on this system would be expected to reveal useful characteristics. In particular, direct metalation of the aromatic ring should give rise to large $^1J_{\text{Ag-C}}$ coupling (> 100 Hz).[75] The exact nature of these couplings could provide information on, for example, regioselectivity, which could then be monitored by *in situ* NMR spectroscopy.

Chapter 9

Studies of TMPLi-TMPCu Aggregates in Solution: Unexpected Reactivity with Aromatic Solvents

9.1 The structures of mixed TMPLi-TMPCu aggregates in solution

9.1.1 Introduction

The structures of unsolvated lithium amides in the solid state are understood to take the form of polymers ('ladders'[199]) or cyclic oligomers, with the latter structure-type being favoured by the presence of bulkier R-groups.[184,217] For copper(I) amides, cyclic oligomers dominate. Thus, in the solid state, **9a** has been crystallographically characterised as forming a trimer and a tetramer,[185] whilst the tetrameric form of **9e**[65] has been reported recently.[i] In solution, a similar picture is painted, with trimeric and tetrameric forms of **9a** having being identified in pentane.[185,218] For **9e**, the picture is less clear-cut, with DOSY measurements indicating a fast trimer-dimer equilibrium to be likely in benzene solution.[65]

Dynamic processes resulting in conformation changes to the TMP ligand have been

[i] $(TMP)_3Cu_3$ has been reported in unpublished work: J. Haywood, *PhD Thesis*, **2009**, University of Cambridge.

reported in the literature. For example, Collum reported that in lithium 2,2,4,6,6-pentamethylpiperidide, conformational locking is evident at ambient temperature in pentane, which allowed for the identification of conformational isomers. In contrast, for **9a** (which differs only in lacking the 4-Me substituent), decoalesence was only observed at −120 °C.[218] Importantly, even at 20 °C, no changes associated with either *intermolecular* or *intramolecular* exchange of Li in aggregates of **9a** have been reported (i.e. such processes are considered to occur slowy compared to NMR timescales).[218] Although no comparable experiments have been conducted for **9e**, the observation of a single broadened ^{13}C TMP-Me resonance suggests that similar conformational dynamic processes may be operating here (though this could also potentially be explained by dissociative equilibria).

In Chapter 7, the identification of *i*-**9c** – an isomeric variant of aggregated Gilman cuprate $\mathbf{9c}_2$ – highlights the structural complexity which can arise in TMP-based amidocuprate systems. This is due to the ability of monovalent Cu^+ and Li^+ to occupy the two-coordinate amide-bridging site, without significantly disrupting the bonding in the metallacyclic ring. The isostructural nature of the end member phases TMPLi **9a** and TMPCu **9e** leads to substitutional disorder in the solid state. However, in solution, this is manifest as a mixture of discreet aggregates with definite composition. Such mixed-metal aggregates would be best represented by the formula $TMP_{m+n}Cu_mLi_n$, where m and n are integer values. Solid-state work has highlighted the dominance of tri- and tetranuclear aggregates of the end member phases **9a**[185] and **9e**,[65] whilst, as noted above, Gilman cuprate $(TMP)_2CuLi$ **9c** is known to form a dimer.[104] On the basis of solid-state data, it is therefore expected that (m+n) could take a maximum value of 4; consequently, a finite number of mixed-metal amide species are expected in solution. Under most circumstances, identification of these would represent an intractable problem, since the chance of isolating any mixed-metal species in a pure state is very small (though they can occur fortuitously in *nearly* pure forms; one example of this type will be presented). To attempt the systematic formation of TMPLi-TMPCu aggregates, it was decided to pursue a different approach: to simply mix the end member phases in deuterated solvent and observe the evolution of mixed-metal species by NMR spectroscopy.

9.1.2 Results and discussion

The conformational behaviour of amidocuprate systems appears to differ significantly in comparison to **9a** and **9e**. For $(TMP)_2CuLi$ **9c**, TMP-Me_{ax} and TMP-Me_{eq} environments can be readily distinguished by ^1H and ^{13}C NMR spectroscopy at ambient temperatures (^1H-^7Li HOESY shows a single cross-peak, Figure 9.1). Moreover, complex coupling patterns can be distinguished for TMP-3,5 and TMP-4 protons, which are themselves chemically distinct (as confirmed by HSQC data, see Figure 9.2 and Figure 9.3). All of these evidences point towards conformational locking of the piperidide ring at ambient temperatures. In the absence of clear steric influences (N–Li and N–Cu bond lengths being comparable),[166] this suggests an electronic preference for the *endo*-TMP orientation (i.e. N→C4 and N→Cu vectors co-parallel). Such a preference could arise due to, for example, an electronic inequivalence of the lone pairs in the axial and equatorial positions of the TMP ligand.[219] As these inequivalent lone pairs would have different energies, there is likely to be one of the two possible pairs of interactions with Cu^+ and Li^+ which is most energetically favourable. Ring inversion would be disfavoured in this case, since this would simultaneously invert the N lone pairs and lead to the less favourable set of interactions.

Moving to mixed-metal aggregates, Cu-rich species have been isolated as by-products in the synthesis of TMP-cuprates, as $(TMP)_4M_4$ (M = Cu, Li) aggregates in the solid state (see **9** in Chapter 7). The ability of donor solvents (e.g. THF, Et_2O) to preferentially solvate Li-rich species can explain the dominance of Cu-rich species in the solid state. In such cases, crystallographic refinement can provide bulk composition in terms of metal type, but due to substitutional disorder, rarely provides any further insight into the identities of the aggregated species present. Nonetheless, in solution, one occasionally encounters samples which are clearly dominated by one type of aggregate.

One such example was obtained upon standing a sample of thiocyanatolithium cuprate **6** (see Chapter 6) at room temperature for several weeks, after which time plate-like crystals were obtained. ^7Li spectroscopy revealed a single resonance, at δ 0.95 ppm, whilst ^1H NMR spectroscopy showed four TMP-Me resonances in a 1:1:1:1 ratio (Figure 9.4). This suggests two TMP environments, each of which gives rise to distinct TMP-Me_{eq} and TMP-Me_{ax} resonances. Inspection of the ^{13}C

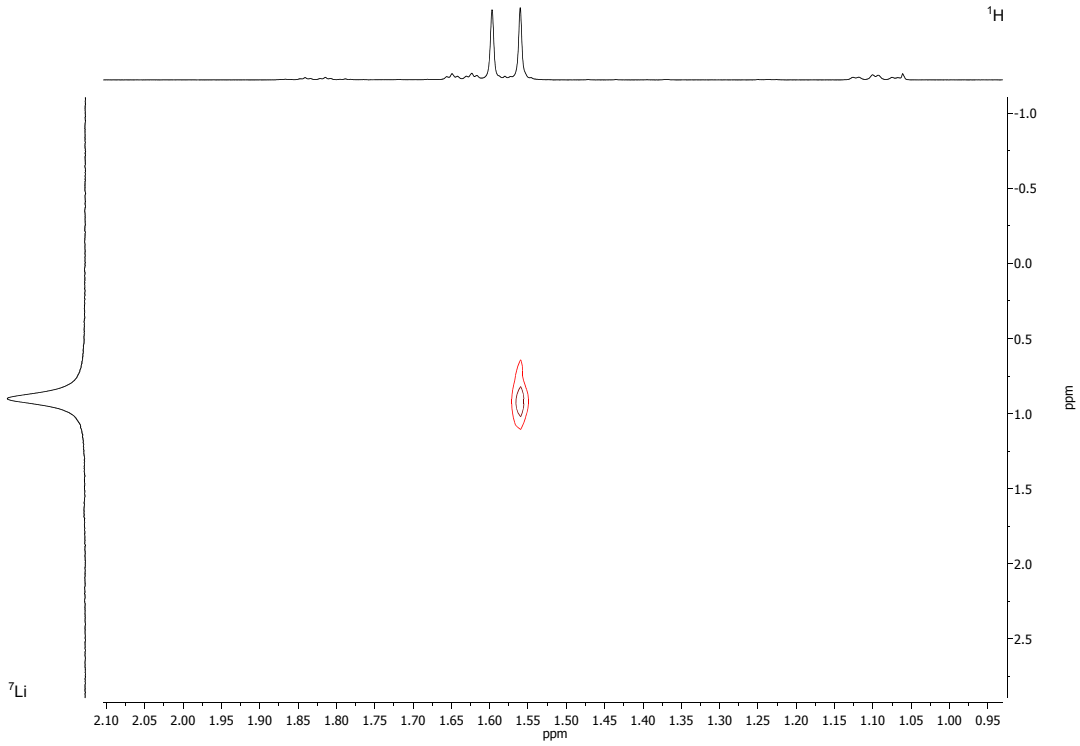

Figure 9.1: Inverse-detected ^{1}H-^{7}Li HOESY spectrum of **9c** in C_6D_6. Only one set of TMP-Me protons shows a cross-peak to Li.

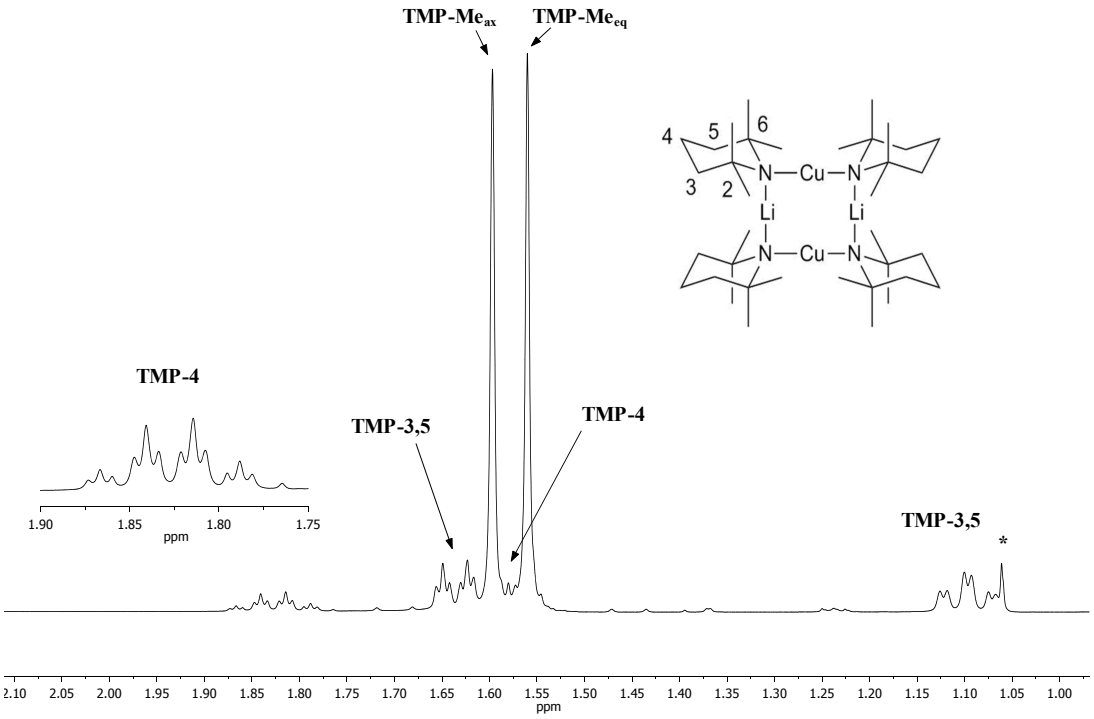

Figure 9.2: ^{1}H NMR spectrum of **9c** in C_6D_6, showing distinct TMP-Me environments and complex coupling patterns. Expansion of TMP-4 multiplet inset. * = TMPH.

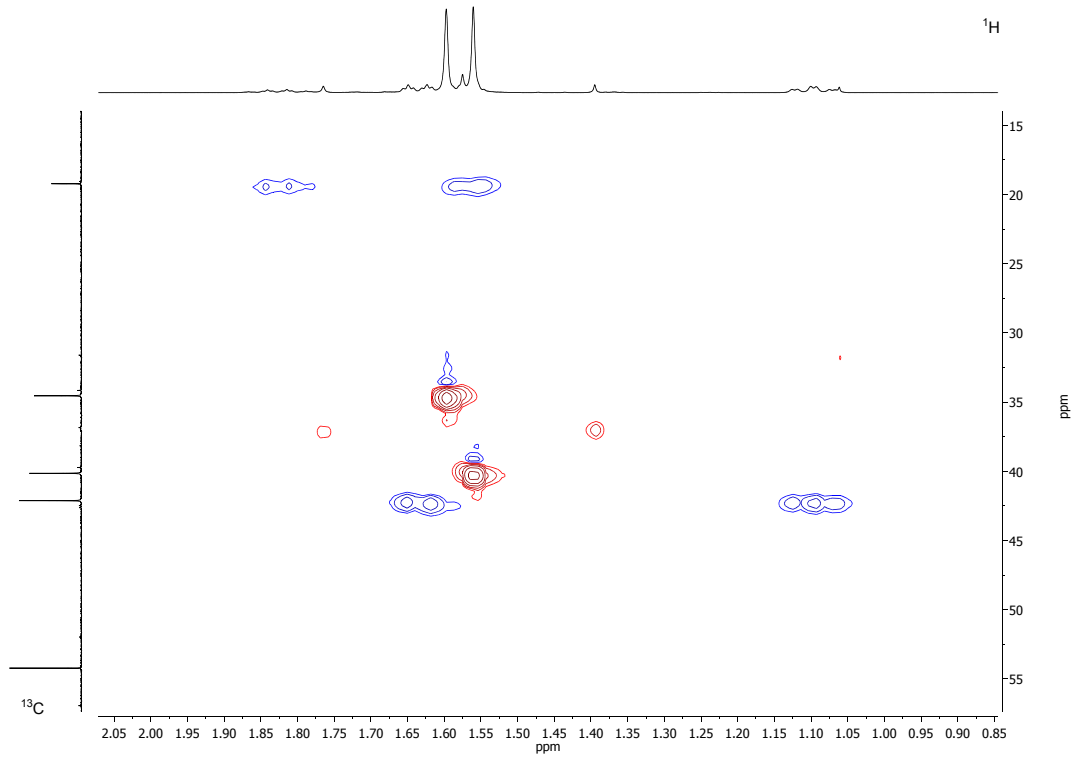

Figure 9.3: HSQC spectrum of **9c** in C_6D_6, showing well-resolved proton environments indicative of a fixed TMP ring conformation. Minor cross-peaks due to small quantities of *i*-**9c**.

NMR spectrum revealed two resonances in the TMP-2,6 region, at δ 56.92 and 54.24 ppm. These chemical shifts compare closely with those observed for TMP-2,6 carbons in TMPCu **9e** (δ 56.46 ppm) and and TMPLi **9c** (δ 54.22 ppm). However, comparison with authentic samples of **9e** and **9c** confirms that the present sample is not a mixture of **9e** and **9c**, but a new aggregate with TMP environments *approximating* those in **9e** and **9c** (i.e. one TMP bonded to two Cu centres, and the other bonded to one Cu and one Li centre). Overall, these data suggest the formula $(TMP)_4Cu_3Li$ **9d** (see Figure 9.5). It is clear that in this particular sample another minor species is present (^{1}H NMR δ 1.76 ppm, TMP-Me), which does not contain lithium and therefore corresponds to an aggregate of TMPCu.

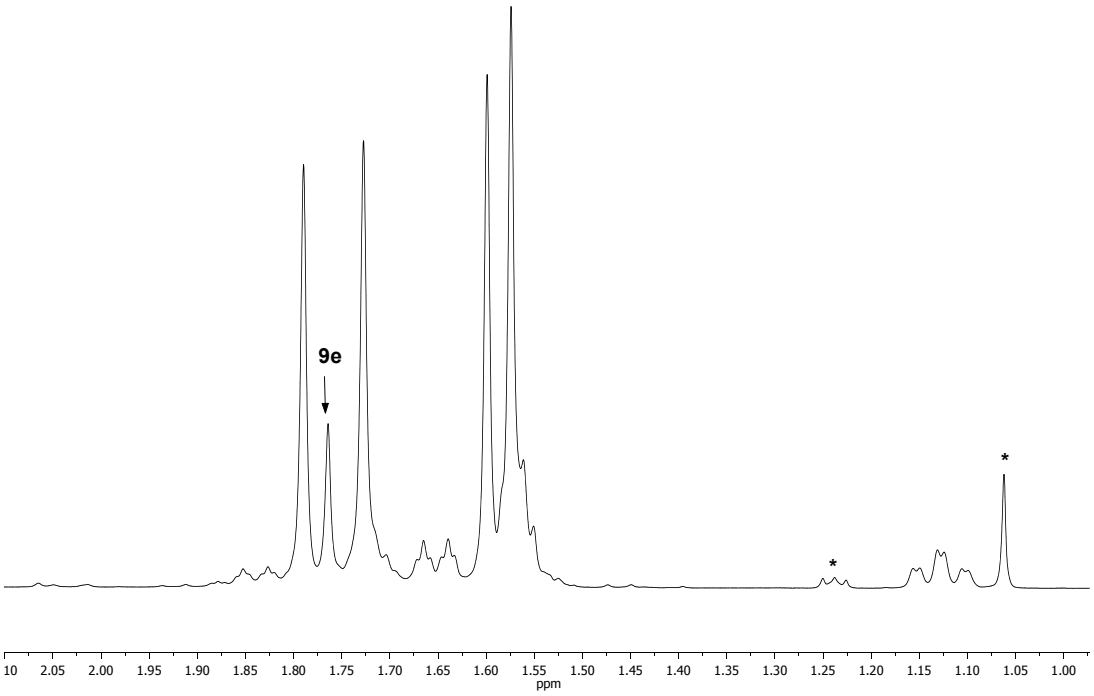

Figure 9.4: ^{1}H NMR spectrum of **9d** in C_6D_6. TMP-Me resonance of **9e** marked. * = TMPH.

A different approach was taken to fabricate the lithium rich TMPLi-TMPCu aggregates (e.g. $(TMP)_4CuLi_3$ **9b**). These have not generally been obtained fortuitously as by-products, suggesting their higher solubility in hydrocarbon and etherate solution. However, this same property made it feasible to attempt the synthesis of these compounds *in situ*, on a scale suitable for NMR spectroscopy.

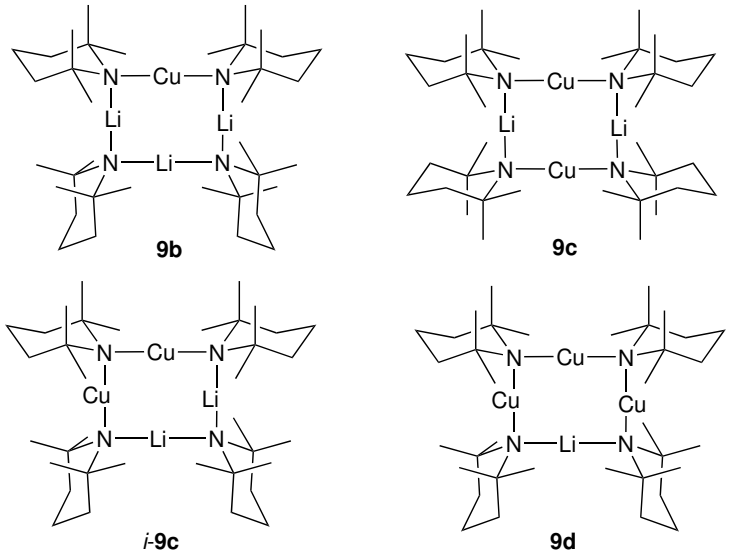

Figure 9.5: Proposed structures for mixed-metal amide aggregates **9b**–**9d**.

Previously, C_6D_6 has been the preferred choice of NMR solvent for amidocuprate compounds, due to its inertness to **9a**, **9e** and lithium cuprates of the type described in Chapters 5–7. However, to our surprise, C_6D_6 did not prove to be passive to *mixtures* of TMPLi and TMPCu. In fact, species of the type d_5-(μ-Ph)$(TMP)_3Cu_mLi_{4-m}$ (m = 1–3) could be identified, which arose from metalation of C_6D_6 *in situ* (see Section 9.2). Reasoning that a bulkier aromatic solvent might be more passive, mesitylene was used instead. This solvent was later removed and replaced with C_6D_6 immediately prior to spectroscopic measurement. Though species arising from reaction with mesitylene were clearly present – for example, (μ-$ArCH_2$)$(TMP)_2Cu_2Li$ (Ar = 3,5-dimethylphenyl) **23** could be identified (see Section 9.2.3) – these were typically minor products and did not complicate identification of TMPLi-TMPCu aggregates.

A sample containing TMPLi **9a** and TMPCu **9e** in a 3:1 molar ratio was heated to 50 °C in mesitylene for *ca.* 24h. Following replacement of the solvent by C_6D_6, ^{7}Li NMR spectroscopy revealed three resonances: unreacted **9a** (δ 2.21 ppm), **9c** (δ 0.90 ppm) and a dominant signal, at δ 1.65 ppm. Whilst the latter of these ^{7}Li resonances tallied with that reported for *i*-**9c**, ^{1}H and ^{13}C NMR spectroscopy painted a different picture. ^{1}H NMR spectroscopy revealed three TMP-Me resonances, at δ 1.59, 1.56 and 1.37 ppm, in a 1:1:2 integral ratio. After accounting for **9a** and **9c**, ^{13}C NMR spectroscopy revealed two resonances in the TMP-2,6

region corresponding to the unidentified species, at δ 54.17 and 52.00 ppm. These compare with the chemical shifts of those observed for TMP-2,6 carbon in **9c**, at δ 54.22 ppm and **9a**$^{\text{tetramer}}$, at δ 51.97 ppm. Once again, the use of authentic samples confirmed that these signals could not be accounted for by a mixture of **9c** and **9a**, but indicated a new aggregate with TMP environments closely approximating those in **9c** and **9a**. This suggests that there are two TMP environments in the dominant species, one TMP ligand bonded to two Li centres, and the other TMP ligand bonded to one Cu and one Li centre. These data point towards the formula $(TMP)_4CuLi_3$ **9b** (see Figure 9.5) and this is concordant with the overall Cu/Li content of the reaction mixture. Finally, ^{13}C NMR spectroscopy identified four distinct TMP-Me resonances, but HSQC indicated that the two of these associated with the 'TMPLi-like' portion of **9b** are overlapped in the ^1H NMR spectrum, at δ 1.37 ppm. This explains the 1:1:2 integral ratio of TMP-Me resonances (see Figure 9.7).

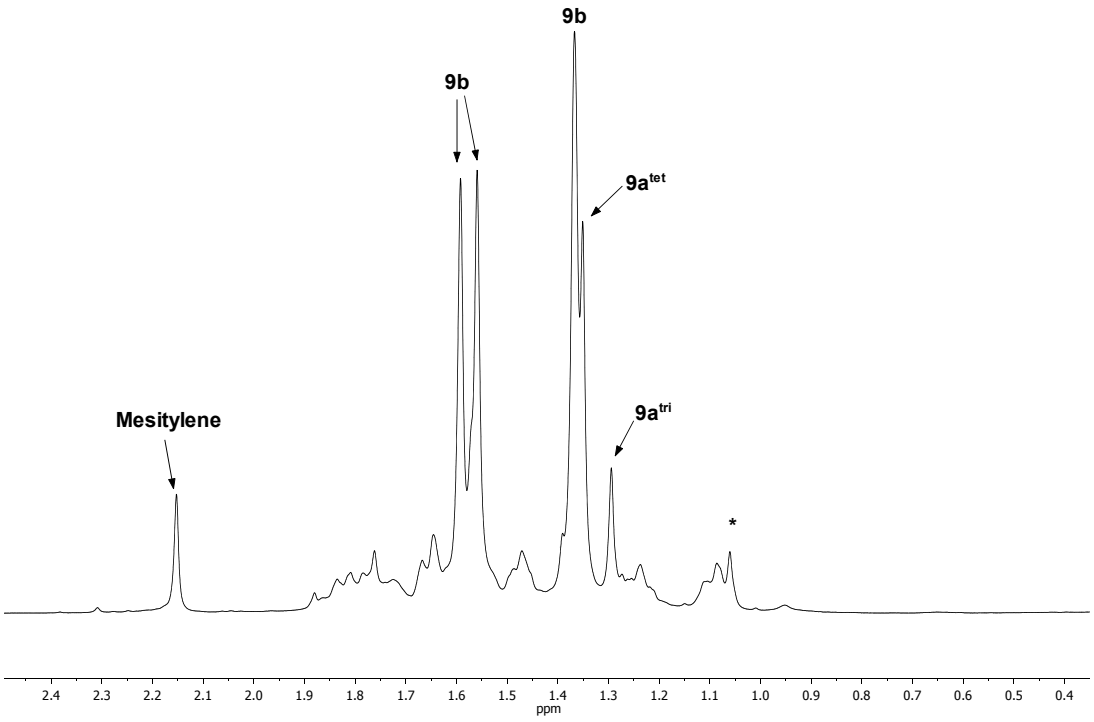

Figure 9.6: ^1H NMR spectrum, in C_6D_6, of the reaction mixture which contained TMPLi and TMPCu (3:1) in mesitylene and which was heated to 50 °C for *ca.* 24h. This mixture is dominated by **9b**. * = TMPH, tet = tetramer, tri = trimer.[185]

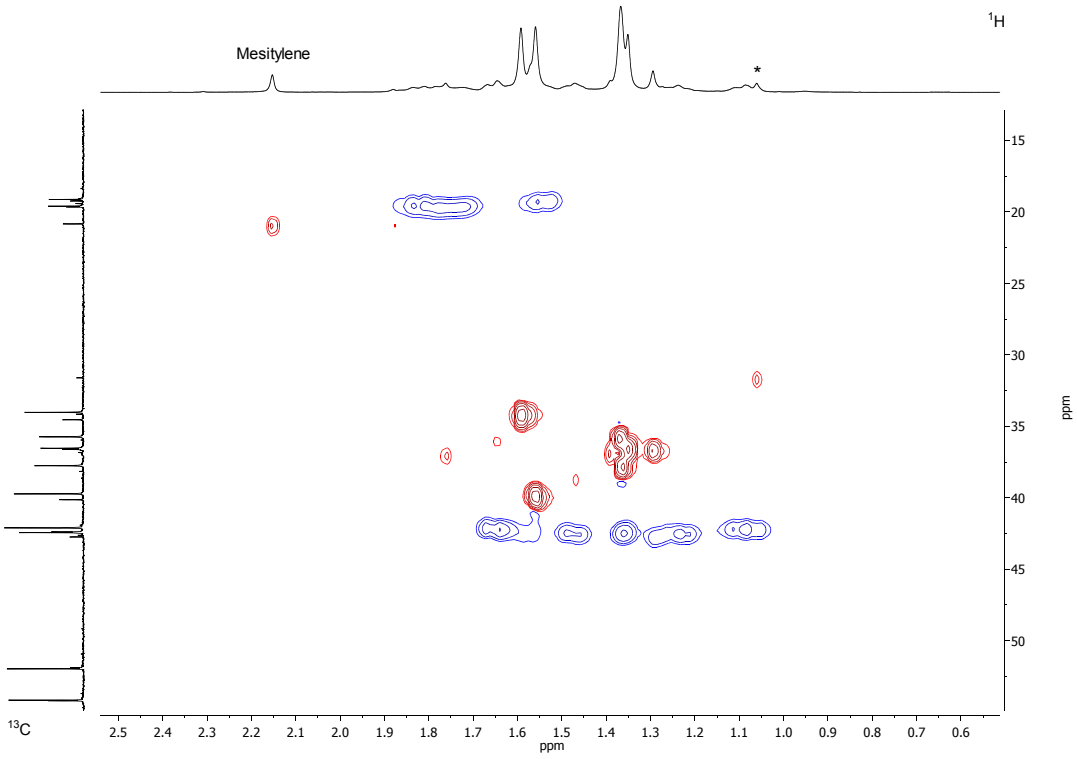

Figure 9.7: HSQC spectrum, in C_6D_6, of the reaction mixture which contained TMPLi and TMPCu (3:1) in mesitylene and which was heated to 50 °C for *ca.* 24h. This mixture is dominated by **9b**. The ^{1}H NMR resonance at δ 1.37 ppm shown two cross-peaks. * = TMPH

To investigate how the distribution of TMPLi-TMPCu aggregates varied with the Li/Cu composition of the reaction mixture, further reactions were conducted in mesitylene, using differing proportions of **9a** and **9e** in the starting mixture (3:1 to 1:3 molar ratio). Samples were heated to 50 °C for *ca.* 24h after which time the solvent was replaced with C_6D_6 for analysis (Figure 9.8). As expected, the final distribution of TMPLi-TMPCu aggregates reflected the composition of the starting mixture, with the dominance of **9a** and **9b** being established in Li-rich mixtures (see Table 9.1). In Cu-rich mixtures, **9c** became dominant, and the presence of *i*-**9c**, was established at intermediate compositions. Perhaps surprisingly, even with a molar ratio of 1:3 TMPLi : TMPCu, the system disfavoured the formation of Cu-rich **9d**, instead revealing unreacted TMPCu in the final mixture. Two factors may account for this: (1) the formation of **9d** may require the presence of a Lewis base (for example, see **9** in Chapter 7) and (2) the emergence of a Cu-rich, arene-containing species may act as a further sink for the excess Cu (see Section 9.2.3 for further details).

Table 9.1: Relative distribution of lithium between **9a**, **9b**, *i*-**9c** and **9c** as determined by ^{7}Li NMR spectroscopy. Relative molar ratios of TMPLi and TMPCu reported.

TMPLi : TMPCu	**9a**	**9b** + *i*-**9c**	**9c**
3 : 1	0.45	0.44	0.11
2 : 1	0.29	0.48	0.23
1 : 1	0.15	0.43	0.42
1 : 2	0.11	0.34	0.53
1 : 3	0.11	0.23	0.66

9.2 *In situ* metalation of aromatic solvents

9.2.1 Introduction

As introduced in the preceding section, attempts to use aromatic solvents for the *in situ* production of TMPLi-TMPCu aggregates led to unexpected reactivity. In particular, the metalation of C_6D_6 was indicated, giving rise to aryl(amido)cuprate aggregates d_5-(μ-Ph)$(TMP)_3Cu_mLi_{4-m}$ (m = 1–3) d_5-**22a**–**22c**. This is very un-

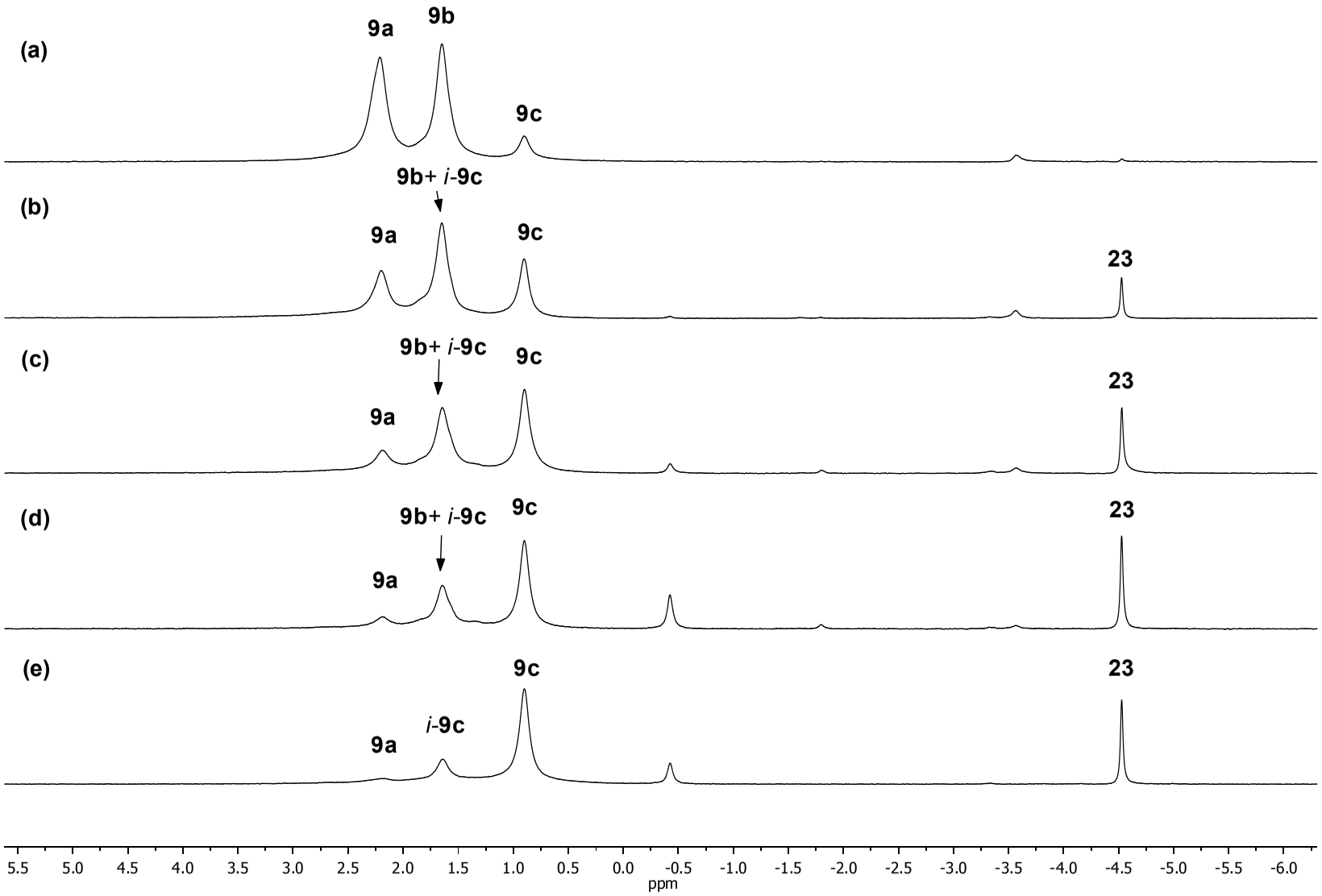

Figure 9.8: ^{7}Li NMR spectra, in C_6D_6, of the reaction mixture which contained TMPLi and TMPCu in molar ratios ratios (a)–(e), and which were heated in mesitylene for *ca.* 24h at 50 °C. TMPLi : TMPCu (a) 3:1 (b) 2:1 (c) 1:1 (d) 1:2 (e) 1:3. For further details on **23**, see Section 9.2.3

usual reactivity, and further introduction to the subject of the metalation of benzene is warranted.

Though Lewis acidic salts of certain metals, such as mercury, thallium[220] and lead[221] are assoicated with the autometalation of benzene, deprotonative metalation is more commonly achieved by using polar organometallics. For example, complexed alkyllithiums (e.g. 1:1 *n*BuLi-TMEDA) can achieve near quantitative metalation of benzene at room temperature over the course of a few hours.[36] In more recent years, the advent of superbases and development of alkali metal-mediated-metalation has proved somewhat of a renaissance for polar organometallic chemistry and several types of heterobimetallic base capable of deprotonating benzene have been reported. Examples include the mixed alkyllithium-potassium alkoxide base nBuLi$\cdot t$BuOK (LICKOR, 'Lochmann-Schlosser' superbase),[222] group I zincates,[147] magnesiates,[156,158] and manganates.[164] Magnesiate and manganate systems in particular are noteworthy for their ability to effect templated polymetalation of unactivated arenes. Furthermore, calculations have suggested that these bases, which often contain both alkyl and amido groups, act as kinetic amido bases.[223] It is notable that all examples of bimetallic bases which are capable of metalating benzene rely on the use of Na or K as the group I metal component. As the larger group 1 ions are less polarising than Li, it is thought that these act to impart stronger basicity to the amide ligand in these bimetallic complexes.[223] The use of heavier group I organometallics does not come without drawbacks: they are significantly less stable than are their lithium congeners, and often difficult to handle.[149,150] Consequently, any lithium 'ate complexes which are capable of metalating non-activated arenes (such as benzene) are of significant interest. During the course of preparing mixed TMPLi-TMPCu aggregates, it was discovered that this mixture could metalate aromatic substrates. The findings from these initial investigations, primarily concerning the metalation of benzene, are reported in the following section.

9.2.2 Results and discussion

Experiments were designed with the aim of monitoring the *in situ* production of lithium amidocuprate species by NMR spectroscopy. To do this, an NMR tube was charged with TMPLi, TMPCu and C_6D_6. The resulting mixture, which contained

some residual undissolved TMPCu, was heated to 50 °C for *ca.* 24h in order to dissolve the remaining TMPCu. Analysis indicated some degree of reaction with the NMR solvent (see below). Subsequently, these reactions were replicated using C_6H_6 as the solvent, using the arrangement described above (NMR tube, 50 °C, *ca.* 24h). The sample was then transferred to a new flask, whereupon the solvent was removed *in vacuo* and replaced with C_6D_6, for spectroscopic analysis. Experiments were conducted to rule out the possibility of monometallic basicity. It was found that the NMR spectra of neither TMPLi **9a** nor TMPCu **9e** showed any signifcant changes after heating in C_6D_6 for 24h at 50 °C. Next, **9a** and **9e** were mixed in the molar ratios from 3:1 to 1:3 in C_6D_6 and heated to 50 °C for *ca.* 24h. The solubility of TMPCu in benzene was found to be low, and it only partially dissolved in the reaction solvent. However, the residual solid TMPCu was found to dissolve over the course of the reaction. When the reaction mixtures were studied by ^{7}Li NMR spectroscopy, unusually high-field resonances were detected. Striking similarities between these spectroscopic features and those observed in the aryl(amido)cuprate system MesCu(TMP)Li, reported by Davies,[109] were noted. These high-field resonances suggested the shielding influence of diatropic ring current,[224] and therefore, the presence of arene$\cdots$Li π-interactions (see Figure 9.9).

Starting with Li-rich reaction mixtures, a 3:1 mixture of TMPLi and TMPCu was heated in C_6D_6 at 50 °C for *ca* 24h. ^{7}Li NMR spectroscopy indicated two Li resonances, which were not associated with TMPLi-TMPCu aggregates, at δ 2.09 and −4.33 ppm, in a 2:1 ratio (Figure 9.10a). The chemical shift of the former resonance was consistent with a Li centre interacting with a single aromatic ring.[109] The low-field resonance, on the other hand, was consistent with Li centres bridging amido ligands only.[109,185] Replicating this reaction in C_6H_6 allowed for the identification of Ph-protons by ^{1}H NMR spectroscopy (Figure 9.13a) and integration analysis, which pointed to there being three TMP ligands per Ph group (identified by six distinct TMP-Me resonances, three pairs of TMP-Me_{ax} and TMP-Me_{eq}, Figure 9.11a). Taken together, this evidence suggested the formula of the arene-containing species to be (d_5)-(μ-Ph)$(TMP)_3CuLi_3$ (d_5)-**22a**.

Next, starting with a 2:1 mixture of TMPLi and TMPCu, and employing the same reaction conditions, another species of the form (d_5)-(μ-Ph)$(TMP)_3M_4$ could be identified. In this case, two ^{7}Li NMR resonances, at δ 1.40 and −2.94 ppm, were

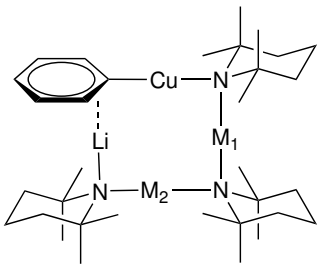

Figure 9.9: Proposed structures for **22a** (M_1 = M_2 = Li), **22b** (M_1 = Li, M_2 = Cu) and **22c** (M_1 = M_2 = Cu).

revealed in a 1:1 ratio (Figure 9.10b–d). The latter resonance indicated Li$\cdots$arene π-type interactions, but also suggested that the shielding effect of the Ph group was reduced relative to that in d_5-**22a**. This could potentially be explained by a reduction in hapticity.[109] The 3:1 ratio of TMP : Ph groups was confirmed by repeating the reaction in C_6H_6 and conducting NMR spectroscopy. This suggested the formula to be (d_5)-(μ-Ph)$(TMP)_3Cu_2Li_2$ (d_5)-**22b** (see Figure 9.11b and Figure 9.13b–d).

Starting from a 1:1 mixture of TMPLi and TMPCu, a third Ph-containing species emerged, associated with a single ^{7}Li resonance at δ −1.53 ppm (Figure 9.10c–e). Once again, replicating the reaction in C_6H_6, before replacement of the solvent by C_6D_6 for ^{1}H NMR spectroscopy, indicated the presence of a single Ph group per three TMP ligands (see Figure 9.11c and Figure 9.13c–e). Overall, these data suggested (d_5)-(μ-Ph)$(TMP)_3Cu_3Li$ (d_5)-**22c**, and this formula was consistent with the increasing Cu content of the reaction mixture.

Comparing the series of ^{7}Li spectra obtained for reactions conducted in C_6D_6 and C_6H_6, it is clear that there are differences in the distribution of products – for example, **22b** is more prominent in reactions performed in C_6H_6 that its d_5-analogue d_5-**22b** is in those reactions preformed C_6D_6. However, the same series of arene-containing species (notwithstanding deuteration) are readily identified in both series of reactions in C_6D_6 and C_6H_6. It is notable that for reactions conducted in C_6D_6, the deuteration of the the amine by-product can also be distinguished by ^{13}C NMR spectroscopy (TMPH-Me δ 31.61 ppm, TMPD-Me δ 31.56 ppm). Furthermore, ^{1}H NMR spectroscopy readily identifies the broad N−H resonance for TMPH, at δ 0.30 ppm, whereas this was absent in those reactions conducted in C_6D_6. The reasons for these differences are not clear at present, though it is

possible that the reaction kinetics are influenced by the presence/absence of deuterium. This point was highlighted by combining TMPLi and TMPCu in a 3:1 molar ratio in a 1:1 mixture of C_6H_6 and C_6D_6. This solvent mixture was later replaced by C_6D_6 immediately prior to data acquisition. Line fitting of the ^{7}Li NMR resonance δ −4.26 ppm (**22a**) together with the overlapping shoulder, at δ −4.34 ppm (d_5-**22a**), gave integral values of 1:0.15, indicating a near 7-fold selectivity for reaction with benzene. It is therefore compelling to suggest that isotope effects may be responsible for the differences in product distribution observed in C_6H_6 and C_6D_6 – perhaps due to differing rates of reaction. However, very little is known about the mechanisms of the underlying reactions, and the influence of heterogeneous effects cannot be discounted. For example, a heterogeneous process could be strongly influenced by the crystallinity and grain size of undissolved TMPCu.

One plausible reaction pathway that would explain these findings involves the generation of a reactive cuprate base *in situ*. The identification of three species differing only in their metal content suggests a common reaction pathway could be responsible for generating all three. Moreover, since each compound **22a**–**22c** formally contains the Li(μ-Ph)Cu(TMP) unit, it is reasonable to suggest that this monomer may be generated in solution by reaction of a cuprate base with the solvent, and trapped by whichever metal amide species are most abundant in that solution. In the case of TMPLi **9a** in excess, the capture of Li(μ-Ph)Cu(TMP) by a dimeric unit of **9a** leads to **22a**. Conversely, an excess of TMPCu leads to the capture of Li(μ-Ph)Cu(TMP) by a dimeric unit of **9e** to give **22c**. At intermediate ratios of metal amides, both species are present and are joined by **22b**, which logically forms by capture of Li(μ-Ph)Cu(TMP) by a monomeric unit of $(TMP)_2$CuLi **9c** (which is generated *in situ* from **9a** and **9e**) (Scheme 9.1). Implicit in this mechanism is that the Li(μ-Ph)Cu(TMP) unit, logically, should be generated from the putative monomeric base $(TMP)_2$CuLi **9c**.

The possibility that a reactive monomer of $(TMP)_2$CuLi may be implicated in the unusual reactivities of lithium-salt-free systems is of wider significance. DFT calculations have predicted that such a moiety is likely to be the active base in previously reported lithium amidocuprate systems. However, it has been demonstrated experimentally that pre-isolated Gilman cuprate, which is a dimer in the solid state, is inactive in DoCu and this has been attributed to the high disso-

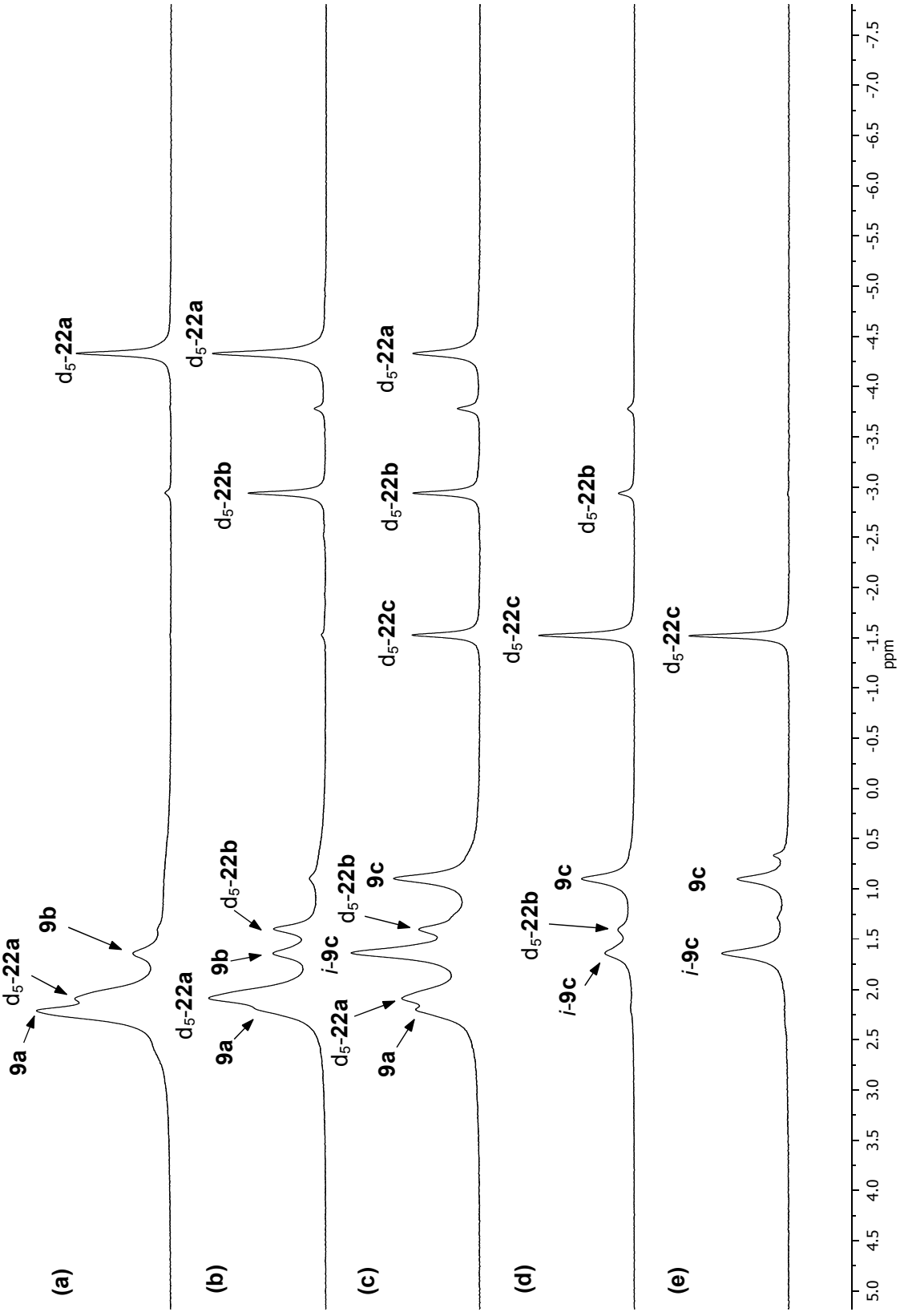

Figure 9.10: ^{7}Li NMR spectrum, in C_6D_6, of the reaction mixtures which contained TMPLi and TMPCu in ratios (a)–(e) in C_6D_6 and which were heated to 50 °C for *ca.* 24h. TMPLi : TMPCu (a) 3:1 (b) 2:1 (c) 1:1 (d) 1:2 (e) 1:3. In this series, **9a**–**e** correspond to $TMP_4Cu_mLi_{4-m}$. d_5-**22a**–**c** correspond to d_5-(μ-Ph)$(TMP)_3Cu_mLi_{4-m}$ (m = 1–3).

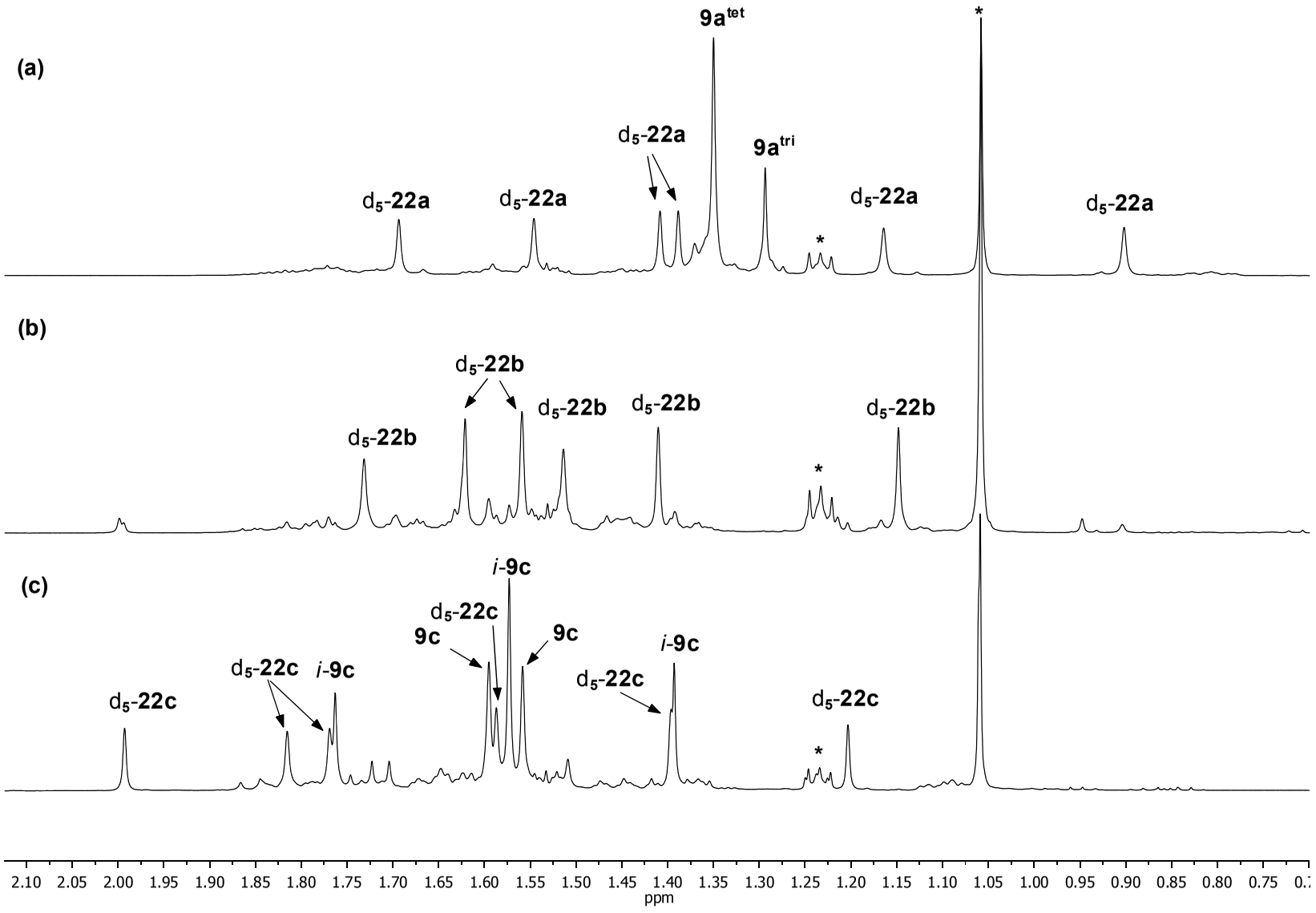

Figure 9.11: ^{1}H NMR spectra in C_6D_6 of reaction mixtures in which (a) d_5-**22a** (b) d_5-**9b** and (c) d_5-**22c** are dominant. In each case, six TMP-Me (three sets of TMP-Me_{ax} and TMP-Me_{eq}) are revealed.

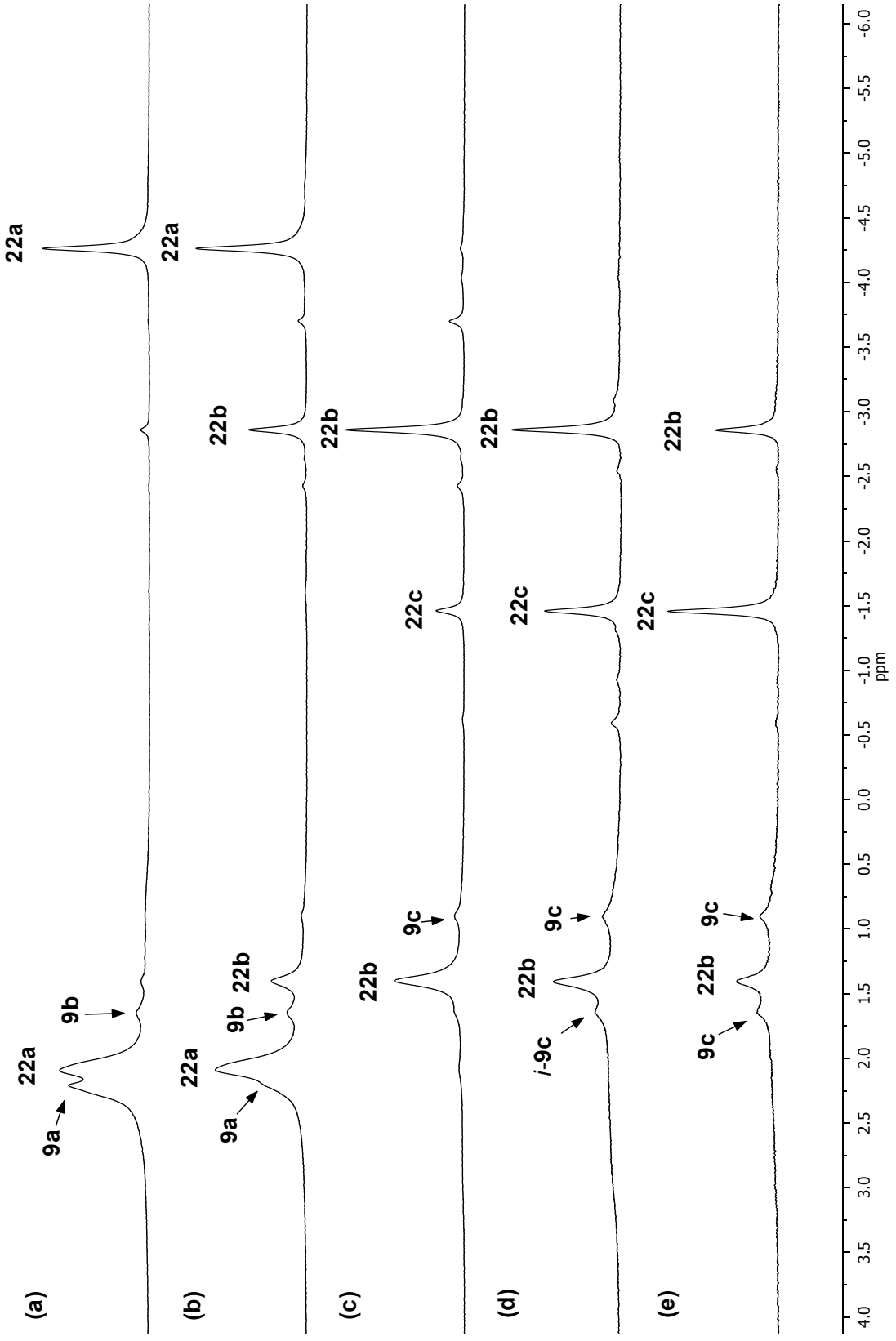

Figure 9.12: ^{7}Li NMR spectra, in C_6D_6, of the reaction mixtures which contained TMPLi and TMPCu in ratios (a)–(e) in C_6H_6 and which were heated to 50 °C for *ca.* 24h. TMPLi : TMPCu (a) 3:1 (b) 2:1 (c) 1:1 (d) 1:2 (e) 1:3. In this series, **9a**–**e** correspond to $TMP_4Cu_mLi_{4-m}$. **22a**–**c** correspond to (μ-Ph)$(TMP)_3Cu_mLi_{4-m}$ (m = 1–3).

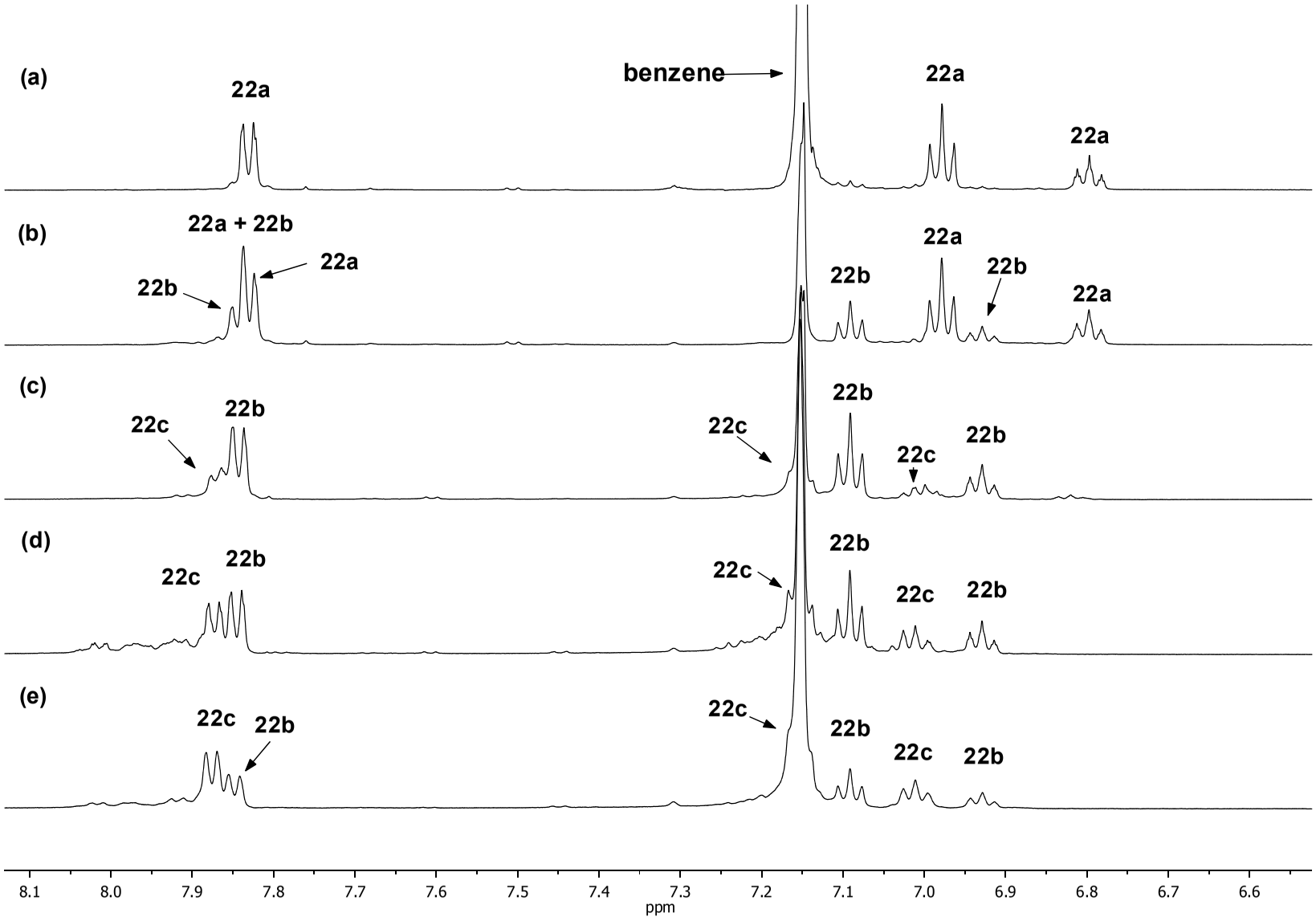

Figure 9.13: ^{1}H NMR spectrum, in C_6D_6, of the reaction mixtures which contained TMPLi and TMPCu in ratios (a)–(e) in C_6H_6 and which were heated to 50 °C for *ca.* 24h. TMPLi : TMPCu (a) 3:1 (b) 2:1 (c) 1:1 (d) 1:2 (e) 1:3.

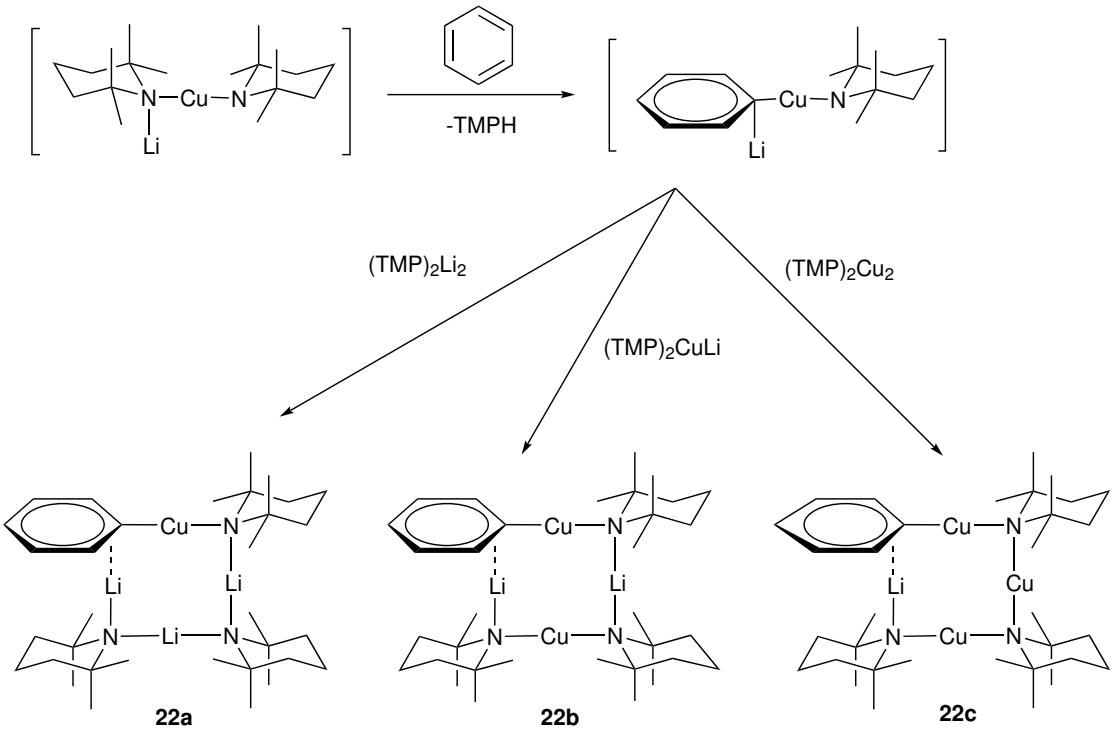

Scheme 9.1: Proposed mechanism for the generation of **22a**–**22c**, *via* reaction of Gilman monomer with benzene.

ciation energy of $\mathbf{9c}_2$.[104,166] To test this thesis in the current system, preformed crystalline $(TMP)_2CuLi$ was heated in C_6D_6 for 24h at 50 °C, after which time NMR spectroscopy revealed no significant changes compared to starting material. In summary, it can asserted that cooperative action of Li and Cu is essential for the metalation of benzene, and that this reactivity cannot be ascribed to previously *isolated* **9c**. It is suggested that an unsolvated monomer might be formed *in situ* from **9a** and **9e**, and that this transient monomeric species acts as the base in the deprotonation of benzene.

9.2.3 Reactions of TMPLi-TMPCu mixtures with mesitylene

As described in Section 9.1, TMPLi and TMPCu were combined in mesitylene, and heated in an NMR tube to 50 °C for *ca.* 24h. This was subsequently transferred to a new flask, the solvent was removed and replaced with C_6D_6 for NMR spectroscopy. The principal species identified in the reaction mixtures were those belonging to the series $TMP_4Cu_mLi_{4-m}$. However, it was evident from the high-field region of the ^{7}Li NMR spectra that several minor arene-containing species were being generated. These species – which did not tally with those previously reported for MesCu(TMP)Li[109] – could not be assigned due to their low abundance. However, growth of the ^{7}Li NMR resonance at δ −4.53 ppm in Cu-rich reaction mixtures prompted further investigation (see Figure 9.8b–d). A 1:1 ratio of TMPLi and TMPCu was chosen, since this resulted in the highest abundance of the species at δ −4.53 ppm, relative to other high-field species (see Figure 9.8c). This mixture was heated in mesitylene at 50 °C for an extended period of 72h. Over this time, a strong yellow colour developed. After replacing the solvent with C_6D_6, ^{7}Li NMR spectroscopy showed that the abundance of the species at δ −4.53 ppm had grown substantially (Figure 9.14).

With only two major Li-containing species present (one of which could be identified as **9c** by comparison with an authentic sample), assignment proved straightforward. As expected based on the results obtained in benzene, ^{1}H NMR spectroscopy pointed towards metalation of the aromatic solvent, by revealing signals at δ 6.66 and 5.88 ppm, in a 2:1 integral ratio. However, this also suggested the possibility of lateral metalation. This was confirmed by the observation of a

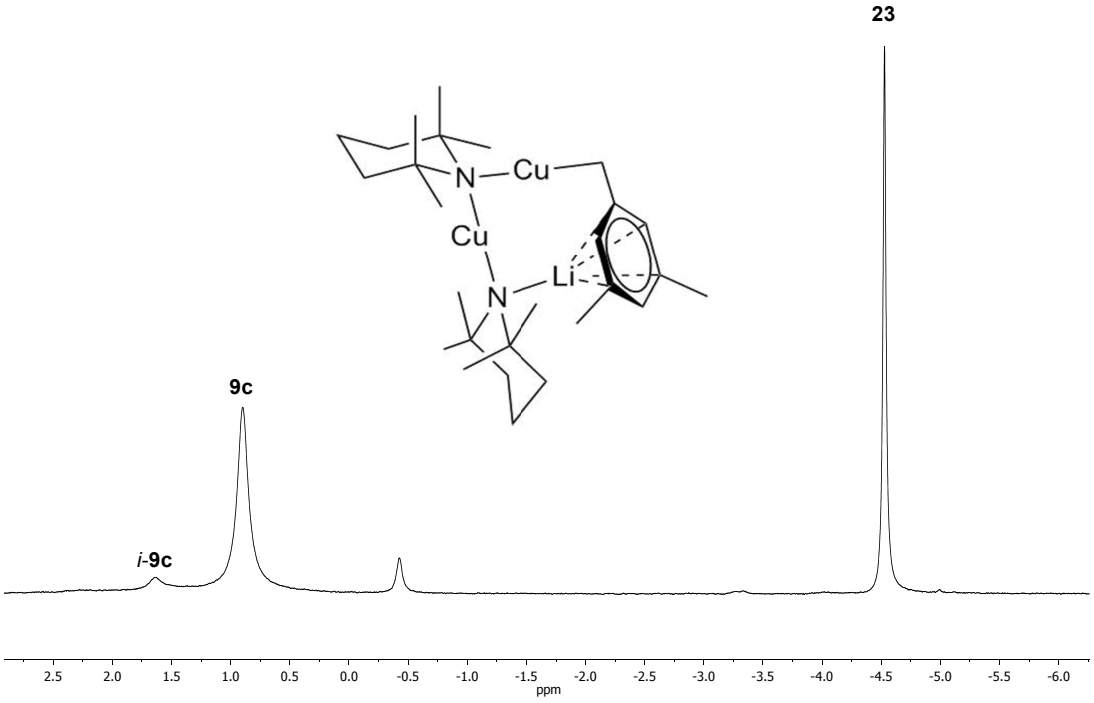

Figure 9.14: ^{7}Li NMR spectrum, in C_6D_6, of the reaction mixture which contained TMPLi and TMPCu in a 1:1 ratio in mesitylene and which was heated to 50 °C for 72h. Peak at δ −0.43 ppm unidentified. Proposed structure for (μ-ArCH_2)(TMP)$_2$Cu$_2$Li (Ar = 3,5-dimethylphenyl) **23** inset.

methylene resonance, at δ 2.38 ppm (see Figure 9.15 and Figure 9.16). ^{1}H NMR spectroscopy also revealed four TMP-Me resonances (each with an integral ratio relative to Ar-*o*-H of 6:2) corresponding two TMP ligands, each with chemically distinct TMP-Me_{ax} and TMP-Me_{eq} groups. Comparison of the ^{13}C NMR chemical shifts for the TMP-2,6 resonances, at δ 56.2 and 53.2 ppm, with samples of **9e** and **9c** suggested one TMP group bonded to two Cu centres and the other bonded to one Cu and one Li centre. Overall, these data suggested the formula (μ-$ArCH_2$)$(TMP)_2Cu_2Li$ (Ar = 3,5-dimethylphenyl) **23** (see inset of Figure 9.14).

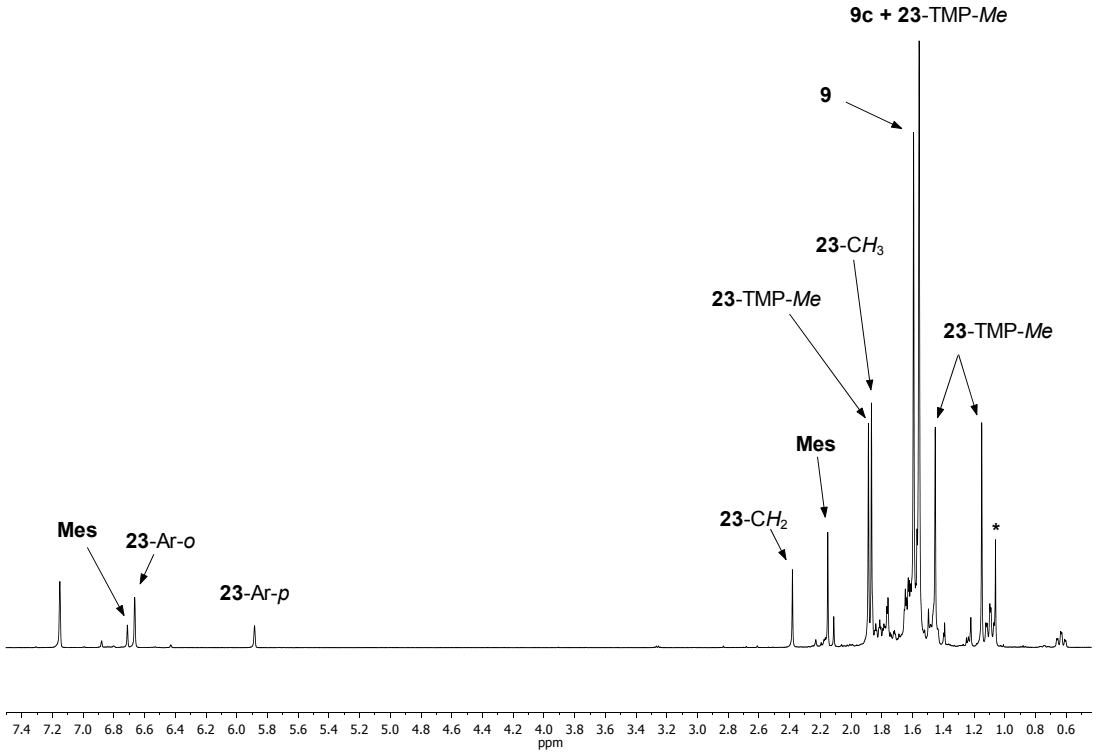

Figure 9.15: ^{1}H NMR spectrum in C_6D_6 of the reaction mixture, resulting from the combination of TMPLi and TMPCu (1:1 molar ratio) in mesitylene, after heating at 50 °C for *ca.* 72h. **23** is a major component of this mixture. Mes = mesitylene, * = TMPH.

It is proposed, tentatively, that the presence of the methylene spacer might facilitate cyclisation *via* Li$\cdots$arene interactions. Despite the formal localisation of the charge on the CH_2^- unit, significant delocalisation into the adjacent aromatic system is to be expected and this may enhance Li$\cdots$arene π-interactions. The proposed trinuclear structure would represent a rare mode of bonding in lithium 'ate complexes, with most crystallographically characterised examples exhibiting

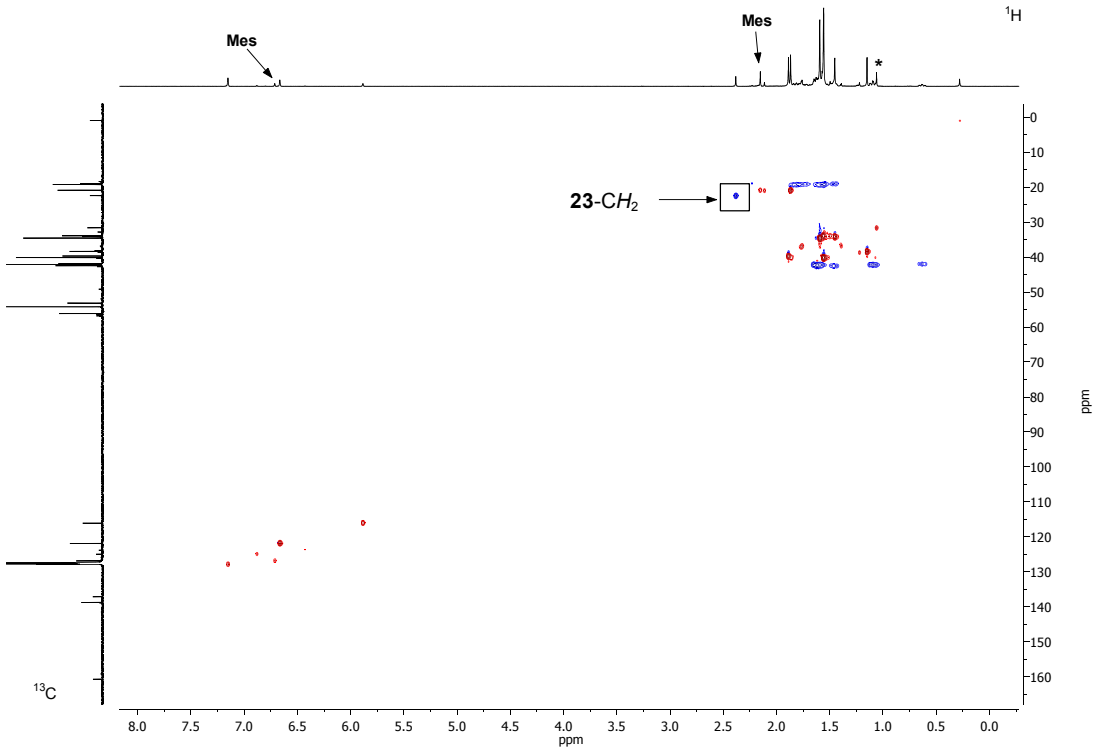

Figure 9.16: HSQC spectrum, in C_6D_6, of the reaction mixture which contained TMPLi and TMPCu (1:1) and which was heated to 50 °C for *ca.* 24h. **23** is a major component of this mixture. Methylene cross-peak highlighted. Mes = mesitylene, * = TMPH.

extensive solvation of the Li-centres by Lewis bases, such as THF.[225] It is likely that the proposed intramolecular Li$\cdots$arene interaction is only stable in the apolar conditions in which it is produced, with TMPH (a side product of the reaction) being a poor Lewis base on account of its steric bulk. The chemoselectivity exhibited here is noteworthy: lateral metalation is clearly preferred over aromatic metalation in spite of this being a facile process for benzene. Although this could potentially represent a steric effect, it is likely that the thermodyamic acidity plays a role (the benzylic carbons being more acidic[226]).

9.3 Summary

Aggregates of TMPLi **9a** and TMPCu **9e**, $(TMP)_{m+n}Cu_mLi_n$, have been studied by NMR spectroscopy in solution. For m + n = 4, the previously examined compounds, **9c** and *i*-**9c**, are added to by two species: $(TMP)_4CuLi_3$ **9b** and $(TMP)_4Cu_3Li$ **9d**. When mixtures of **9a** and **9e** are heated in an aromatic solvent at 50 °C for *ca.* 24h, some of these aggregates are formed and this is (more surprisingly) accompanied by that of species resulting from metalation of the solvent. In C_6H_6 (or C_6D_6), aggregates of the type (d_5)-$(\mu$-Ph$)(TMP)_3Cu_nLi_{4-n}$ (n = 1, (d_5)-**22a**; n = 2, (d_5)-**22b** and n = 3, (d_5)-**22c**) were identified. These results are interpreted as being consistent with the generation of a reactive form of cuprate (i.e. Gilman monomer) *in situ*, which reacts with benzene to give Li(μ-Ph)Cu(TMP). This is trapped by residual TMPCu-TMPLi aggregates to give **22a**–**22c**. This view is borne out by the fact that pure, pre-formed **9a**, **9e** and **9c** do not undergo any reaction with the aromatic solvent under the same conditions. It has been established that **9c** is a dimer in the solid state and that this is inert in DoCu.[104] Insofar as **9c** does not react with benzene, this lends weight to the view that pre-formed **9c** in an ineffective source of reactive Gilman monomers.

Lastly, mesitylene has been investigated as a solvent for the same TMPLi-TMPCu systems. Mesitylene is metalated much more slowly than benzene and this allows for the evolution of mixed-metal amide aggregates with fewer side products. However, when the length of the reaction time is increased, or the proportion of **9e** in the reaction mixture is increased, $(\mu$-Ar$CH_2)(TMP)_2Cu_2Li$ **23** is identifiable. In this compound, lateral metalation has occurred and this is rationalised by a combination of steric and thermodynamic factors.

Chapter 10

Conclusions

The work presented this thesis represents significant advances to our understanding of the structures of group 11 'ate complexes in the solid state and in solution. In this chapter, the findings presented in this thesis are summarised and some of the most interesting aspects are highlighted.

Several practical improvements to lithium bis(amido)cuprate systems have been sought. First, this focussed on improving the cost-to-benefit ratio of bis(amido)-cuprates through the formation of heteroleptic cuprates. Data are presented in Chapter 5. Through targeting heteroleptic cuprates, a number of inexpensive amide ligands were introduced, some of which are less sterically demanding than TMP. The racemic ligand 2-methylpiperidide was deployed to give a new homoleptic example of the rarely reported adduct[171] cuprate structure-type, $[(MP)_2CuLi(THF)_2]_2LiBr$ **1**. Meanwhile, a combination of MP and TMP furnished the first example of a heteroleptic bis(amido)cuprate, $MP(TMP)Cu(Br)Li_2(THF)_2$ **2**, which was found to adopt a Lipshutz-type structure in the solid state. This motif could be reproduced when MP was substituted for previously deployed (but also inexpensive) DMP, to give $DMP(TMP)Cu(Br)Li_2(THF)_2$ **3**. Lastly, combination of unsubstituted PIP with TMP allowed for the isolation of PIP(TMP)CuLi **4**, a heteroleptic Gilman cuprate which resisted THF-solvation. Several aspects of these cuprate systems are of significance. It is noteworthy that the formation of individually heteroleptic cuprates is preferred over a mixture of homoleptic cuprates. It is not clear whether this effect is kinetic or theromodynamic in nature, but it likely reflects the high steric repulsion associated with bis(TMP) cuprate

formation. In **2**–**4**, the tendency of the less sterically demanding amide ligand to adopt an *exo* orientation with respect to the N→Cu vector is highlighted by comparison with TMP, which sits in an *endo* fashion. In previously reported cuprate systems, this behaviour has been attributed to steric factors,[171] and these findings add weight to that argument.

Moving to solution-state studies, for **1**, structure retention was indicated in C_6D_6, notwithstanding complexities arising from the presence of multiple stereoisomers. However, for **2**, the presence of multiple species (evidenced by ^{7}Li NMR spectroscopy) suggested *in situ* generation of other complexes – for example, Gilman cuprates. This same behaviour was indicated for **3**, but to a much lesser degree. Meanwhile, for **4**, the use of inverse detected ^{1}H-^{7}Li HOESY suggested retention of the paddlewheel structure exposed in the solid state.

In Chapter 6, non-toxic and inexpensive CuSCN was investigated for its ability to participate in the formation of cuprate bases. Reactive Lipshutz-type thiocyanatocuprates were sought as less toxic alternatives to cyanide-based reagents. Focussing on structural aspects, the prevalence of flat structures in TMP-cyanocuprates in the solid state was established by extending the suite of cyanocuprates $(TMP)_2Cu(CN)Li_2(L)$ (L = Et_2O, THF) to include $(TMP)_2Cu(CN)Li_2(THP)$ **5**. This proved to be a point of significant contrast when Lipshutz-type thiocyanatocuprates $(TMP)_2Cu(SCN)Li_2(L)$ (L = Et_2O **6**, L = THF **7** and L = THP **8**) were synthesised, insofar as the geometries of these solid-state dimers were found to be influenced by the identity of the Lewis base. This arose from the ability of the central $Li_2(SCN)_2$ ring to adopt planar, chair- or boat-like conformations in $\mathbf{6}_2$, $\mathbf{7}_2$ and $\mathbf{8}_2$, respectively. Meanwhile, obviating Lewis base altogether provided Gilman cuprate $(TMP)_2CuLi$ **9c** in high purity.

NMR spectroscopic evidence was presented for the *in situ* conversion of Lipshutz-type **6**–**8** to Gilman cuprate **9c** in C_6D_6, accompanied by the deposition of LiSCN. The extent of *in situ* conversion was strongly influenced by the identity of the Lewis basic component of cuprates **6**–**8**, with near quantitative conversion to **9c** found for Et_2O-solvated **6**. In contrast, for THF-solvated **7**, retention of the Lipshutz-type species dominated. Meanwhile, for THP-solvated **8**, intermediate levels of conversion to **9c** were suggested.

Moving to the synthetic setting, **7** was successfully deployed in the metalation of

halopyridines **10** and **11** to give functionalised products **12a–d** and **13b–d**. Modest yields (46–71 %) were obtained, which were comparable with results obtained from the use of copper(I) chloride. Whilst these results may appear somewhat disappointing, it is not fair to dismiss thiocyanatocuprates on the basis of these results alone. In particular, for a fair comparison, pre-isolated Lipshutz-type **7** should be used. The combined solid-state and solution-state evidence suggests that it would be naive to assume that solutions of **7** prepared *in situ* in THF are wholly composed of Lipshutz-type cuprates. A more suitable comparison would be to deploy pre-isolated **7** with a strongly directing substrate, such as *N*,*N*-diisopropylbenzamide.

In Chapter 7, rarely utilised CuOCN was investigated for its suitability as a precursor to lithium cuprates. Unlike CuSCN, CuOCN did not react with TMPLi in a straightforward manner. Products which could be isolated and analysed by X-ray diffraction revealed substitutional disorder at the amide-bridging metal site. $(TMP)_2Cu_{0.1}Li_{0.9}(OCN)Li_2(THF)$ **14** was interpreted as a co-crystalline mixture, and despite containing only a small amount of Cu, adopted the Lipshutz-type motif well-known for amidocuprates. However, the behaviour of amide-briding Cu and Li clearly differed in that Cu remained two-coordinate (lower-order), whereas Li engaged in a weak transuannular interaction. These differences were emphasised when pure compounds $(TMP)_2Cu(OCN)Li_2(THF)$ **14a** and $(TMP)_2Li(OCN)Li_2(THF)_2$ **16** were synthesised. In particular, the three-coordinate nature of amide-bridging Li in **16**, which arises from transannulation, was highlighted. Insight into the fate of Cu in this system was gained through isolation of Cu-rich aggregate $TMP_4Cu_{2.70}Li_{1.30}$ **9**, in which substitutional disorder was sustained. The tendency for OCN^- to associate with Li^+ in these systems likely reflects the 'hard' nature of this anion, which favours interactions of an electrostatic nature. This behaviour could be replicated with a different ligand set: CuOCN reacted with DALi to give a novel lithium amide-lithium cuprate adduct $(DA)_4Cu(OCN)Li_4(TMEDA)_2$ **18**. Whilst metal disorder was absent from this complex, the bridging action of the cyanate ('side-on') contrasted with that in **14** and **16**, and in so doing, the number of electrostatic interactions of OCN^- with Li^+ was maximised. That Cu-Li substitution was not a feature unique to cyanate chemistry was exposed through attempts to fabricate monomeric Lipshutz-type cuprates. These could not be obtained in pure form; instead, $(DA)_2Cu_{0.1}Li_{0.9}(Br)Li_2(TMEDA)_2$ **17** was isolated. Just as in **14**, the two-

and three-coordinate nature of amide-bridging Cu and Li, respectively, was clear.

Advances to our understanding of cuprate systems in solution have been made with cyanate-based systems. Careful analysis of NMR spectroscopic data revealed that **14** formed part of a mixture of products, which also included **16**, **9c** and *i*-**9c**, a tetranuclear aggregate which is formally an isomer of $\mathbf{9c}_2$. Perhaps most importantly, the identification of multiple products in the reaction mixture has provided insight into the reactions generating these products and (in conjunction with the observations outlined above) shed light on why CuOCN behaves so uniquely. For **17**, NMR spectrosocopy has been used to identify Cu- and Li-only containing species in solution. These results have pointed toward the inclusion of higher levels of Cu in **17** than suggested by crystallography.

Several important conclusions can be drawn from the work presented in Chapter 7. First, the issue of Cu-Li substitution has been addressed. In particular, the isolation of a Cu-rich aggregate when cuprate synthesis is attempted in THF is of significance: these are common reaction conditions for synthetic protocols, yet clearly the reagents obtained under such conditions may be poorly defined. This is particularly important in light of recent work by Gschwind, which highlights the formation of low-polarity, Cu-rich cuprates as detrimental to the performance of cuprates in certain applications.[100] The second finding of major significance is that Lipshutz-type **14a** can be synthesised by combining Gilman cuprate **9c** and LiOCN in THF. This is the first time that this behaviour has been exposed in THF and it is important for two reasons: (1) THF is the most common solvent used for deprotocupration reactions[169,196] and (2) the ability to form Lipshutz-type cuprates, from which Gilman monomers can be accessed, is known to be necessary for high reactivity. If the Gilman-(Lipshutz-type) equilibrium is facile in THF, then it is not strictly necessary to employ LiOCN in a stoichiometric fashion. This opens up avenues of research which might lead to the transformation of deprotocupration to the catalytic regime with respect to the lithium salt additive. This would present an advantage over systems in which the stoichiometric formation of toxic by-products (e.g. LiCN) is implicated.

In Chapter 8, initial attempts at the fabrication of lithium bis(amido)argentates were presented. Ag(I) halides were decomposed by the addition of TMPLi. However, improved results were achieved by using AgCN, or better, AgSCN. Thus, by careful choice of solvents, $(TMP)_2AgLi$ **19** could be synthesised from AgSCN. In

the solid state, a dimer was revealed whose structure paralleled that previously reported for Gilman cuprate **9c**. Meanwhile, treatment of AgCN with TMPLi and then with THF gave $(TMP)_2Ag(CN)Li_2(THF)$ **21**, which also formed a dimer in the solid state, and adopted a Lipshutz motif that is well-known from lithium amidocuprate chemistry.[167] NMR spectroscopy revealed many similarities between cuprate **9c** and argentate **19** in benzene solution. Interestingly, $^2J_{C\text{-}Ag}$ and $^3J_{C\text{-}Ag}$ coupling could be observed clearly for **19** and $^2J_{C\text{-}Ag}$ coupling could be resolved for **21**, giving rise to doublets. Furthermore, re-characterisation of previously reported TMPAg **20** also revealed $^2J_{C\text{-}Ag}$ and $^3J_{C\text{-}Ag}$ coupling, giving rise to triplets. Hence, for **19** and **21**, it can be established that both TMP ligands remain coordinated to Ag in solution and that for **20**, the aggregation state must be *at least* a dimer.

Finally, in Chapter 9, advances to our understanding of the behaviour of TMP-cuprates in solution were made, by detailed analysis of NMR spectroscopic data. This allowed for the identification of mixed lithium amide-copper amide species belonging to the series $(TMP)_4Cu_nLi_{4-n}$ (n = 1–3; **9b**–**9d**). By attempting to systematically synthesise each of these aggregates by combination of TMPCu and TMPLi in aromatic solvents, highly unusual reactivity was discovered. When the respective homometallic amides were heated in benzene no reaction was observed, yet when mixtures of TMPLi and TMPCu were heated in the same solvent, analysis revealed three novel organo(amido)cuprate aggregates: (μ-Ph)$(TMP)_3CuLi_3$ **22a**, (μ-Ph)$(TMP)_3Cu_2Li_2$ **22b** and (μ-Ph)$(TMP)_3Cu_3Li$ **22c**. In contrast, pre-isolated Gilman cuprate **9c** proved completely unreactive under identical conditions. With mesitylene, thermodynamically preferred lateral metalation was observed, leading to the identification of novel metallacycle $(ArCH_2)(TMP)_2Cu_2Li$ (Ar = 3,5-dimethylphenyl) **23**. Reactions with both benzene and mesitylene demonstrate superbasic reactivity, which is unexpected, yet consistent with the growing body of evidence that bimetallic systems possessing organyl and amido ligands preferentially react as amide bases. The implications of these discoveries are significant. First, they lend support to theoretical work which implicates monomeric Gilman cuprate $(TMP)_2CuLi$ as the active base in DoCu. Second, it opens up further avenues of research which could eventually lead to new methods of functionalising otherwise inert hydrocarbons; this will be of great interest to the synthetic community.

Chapter 11

Further Work

The work discussed in this thesis has allowed for advances in several areas of group 11 'ate chemistry to be made. Both practical and more fundamental aspects of lithium bis(amido)cuprate chemistry have been explored. Additionally, preliminary investigations into lithium bis(amido)argentate chemistry have been presented. In this chapter, suggestions for further work, which draw on the findings from within this thesis, will be proposed.

11.1 Applications of heteroleptic cuprates to diastereoselective synthesis

In Chapter 5, the synthesis of heteroleptic bis(amido)cuprates was presented for a selection of amide ligands. Two examples of Lipshutz-type cuprates were exposed: MP(TMP)Cu(Br)Li_2(THF)$_2$ **2** and DMP(TMP)Cu(Br)Li_2(THF)$_2$ **3**. These complexes are expected to be active in DoCu. Assuming that these bases are reacted in a 1:1 ratio with a suitable aromatic substrate, an intriguing question is posed: which of the amido ligands will act as the base? Having similar donor properties, one might expect that the bulkier TMP ligand should take up this role. In addition to its greater basicity, loss of this ligand is expected to lead to the greatest relief of steric crowding in the cuprate complex. The less crowded amide could therefore function as a dummy ligand and this could be made chiral. The chiral aryl(amido)cuprate could then be deployed in asymmetric synthesis. Whilst the

Me group of MP is unlikely to induce much stereoselectivity, a ligand such as (*R*)- or (*S*)-*trans*-decahydroquinoline – which is still less crowded than TMP at the *nitrogen* centre – might be more effective (Scheme 11.1). Hence, further work on heteroleptic cuprates should focus on two topics in particular: (1) investigations into whether TMP-containing heteroleptic cuprates exhibit a preference for loss of TMPH and (2) the synthesis of enantiomerically pure cuprates. The first of these points could be addressed by performing an NMR-scale, *in situ* DoCu reaction using DMP(TMP)Cu(Br)Li_2(THF)$_2$ **3** and *N*,*N*-diisopropylbenzamide. The generation of the respective free amines, TMPH and DMPH, could then be monitored spectroscopically; this would indicate any preference for TMP- or DMP-basicity. The second point could be addressed by synthesising a cuprate from a mixture of achiral TMPH a second enatiomerically pure amine. This would involve the lithiation of a 1:1 mixture of these amines and subsequent reaction of this mixture with CuBr in the presence of THF. If these two points are satisfied, applications of these bases to stereoselective synthesis could be investigated. Rossiter has demonstrated the viability of stereoselective conjugate addition reactions employing organo(amido)cuprates.[227,228] However, the generality of such reactions has not been shown and they are known to be strongly influenced by factors such as solvent conditions and the choice of auxillary ligand.[229,230] Nonetheless, this is an area in which further investigation is warranted. Examples of potential applications include asymmetric 1,4-addition to α,β-unsaturated lactams[231] and asymmetric conjugate addition to chromones.[232]

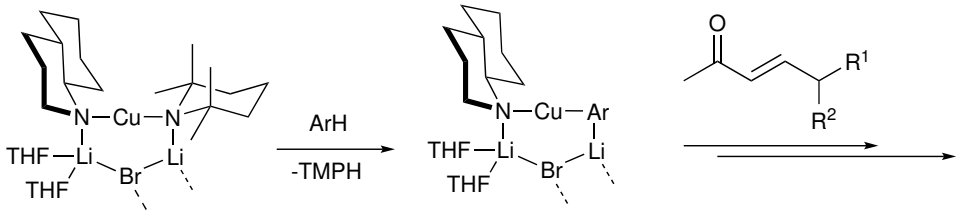

Scheme 11.1: Possible application of heteroleptic cuprates in stereoselective conjugate addition. $R^1 \neq R^2$.

11.2 Computational studies on structural aspects of lithium amidocuprates

The studies in heteroleptic cuprate formation presented in Chapter 5 lend weight to the argument that ligand sterics play a major role in determining cuprate structure type. However, other features are not so readily explained by ligand sterics. For example, why should the solid-state structures of the tetrameric aggregates of TMPLi **9a** and TMPCu **9e** exhibit *endo,exo* configurations of TMP ligands, whereas those in the dimer of $(TMP)_2CuLi$ **9c** exhibit *endo,endo* configurations (see Figure 11.1)? In the solid state, these features in **9c** could potentially be explained by crystal packing, yet evidence from NMR spectroscopy presented in Chapter 9 suggests that the TMP-ligand configuration is retained in solution. It has been documented previously that 2,6-diaxial substitution in piperidines can have a significant effect upon the energy of the lone pair, *via* hyperconjugative effects.[219] It is likely that such effects would be present in the anions also; however, as there are two lone pairs in the amide anions of the piperidines, these could conceivably become electronically inequivalent due to the effects of 2,6-diaxial substitution. Calculations should therefore be undertaken to determine if stereoelectronic effects can account for the structural features described above. These should focus specifically on the energy of the amide ligand lone pairs, and any preference for bonding to a particular metal-type which might emerge as a result of this.

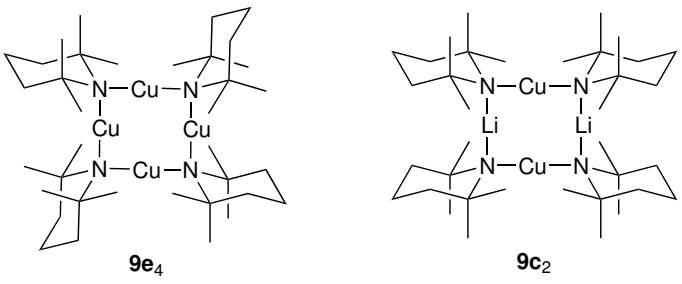

9e$_4$ **9c**$_2$

Figure 11.1: Comparison of the TMP ligand orientations in (a) **9e**$_4$, in which each Cu centre is flanked by TMP ligands in an *endo,exo* orientation and (b) **9c**$_2$, in which each Cu centre is flanked by TMP ligands in an *endo,endo* configuration.

11.3 Alternative amine precursors for cuprate synthesis

In the course of this work, several new amine precursors have been investigated for their ability to participate in the formation of lithium cuprates. Perhaps the most relevant of these is the utility amine *N*,*N*-diisopropylamine, which retails at a fraction of the cost of TMPH. Results have indicated low-level formation of Lipshutz-type cuprate $(DA)_2Cu(Br)Li_2(TMEDA)_2$ **17a**, as part of co-crystalline **17**. It is of considerable interest to develop a route which allows for the selective formation of **17a**, since this would allow for it to be screened for activity in DoCu. Potential routes to pure **17a** would include the synthesis of Gilman cuprate $(DA)_2CuLi$ and its subsequent combination with LiBr and TMEDA. Comparison with existing TMP-derived systems would be very important here, as previous studies have suggested that substituting DA for TMP in $MeCu(CN)(TMP)Li_2$ cuprates leads to inferior results in DoCu.[167] However, this study did not compare *bis(amido)*cuprates incorporating DA, so this restriction need not necessarily apply. Related to the previous point, the synthesis of a piperidine ligand which is even more crowded than TMPH at the nitrogen centre has been reported recently.[233] CPCH, synthesised in two steps from commercially available 1,2,2,6,6-pentamethyl-4-piperidone, can be lithiated and used to access CPC-zincates. These have demonstrated improved yields and regioselectivity in DoZn compared with those achievable by using established TMP-zincates.[141,143] It should prove a relatively straightforward task to access Lipshutz-type cuprates from this ligand (see Scheme 11.2), and it would be interesting to see if superior yields and regioselectivity could be achieved in substrates with weak directing groups, such as halopyridines.

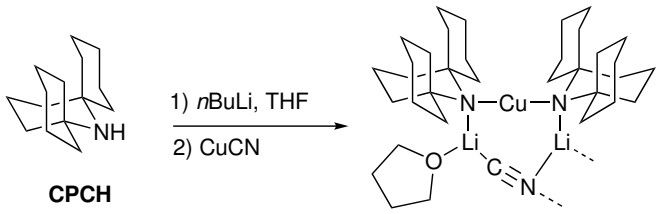

Scheme 11.2: Proposed synthesis of bis(CPC)cuprate.

11.4 Towards catalytic applications of lithium cuprates

Through the study of lithium cyanatocuprates, a new route to Lipshutz-type reagents has been developed. Combination of Gilman cuprate **9c** with LiOCN in THF, followed by recrystallisation from hexane gave $(TMP)_2Cu(OCN)Li_2(THF)$. The generality of this route should be explored thoroughly, as it has important implications for our understanding of how Lipshutz-type cuprates are formed and react. In particular, if thermodynamics dictate that LiX can be sequestered by Gilman cuprate to form a Lipshutz-type cuprate, then a reactive base (i.e. monomeric Gilman cuprate) ought to be accessible (Scheme 11.3). Perhaps the most attractive possibility offered by this method would be the addition of sub-stoichiometric or catalytic quantities of LiX additives to Gilman cuprate to promote activity. The use of smaller quantities of hazardous reagents (e.g. cyanides!) has obvious benefits with regards to safety.

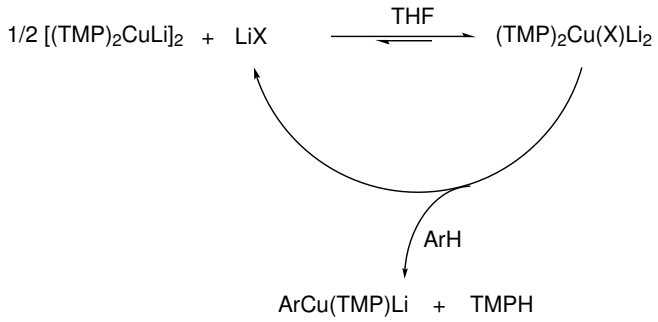

Scheme 11.3: Proposed pathway for DoCu that employs catalytic amounts of LiX (X = CN, OCN). THF-solvation omitted for simplicity.

Ultimately, the ability to employ either Cu or TMP in catalytic quantities would have the largest cost-saving impact. It has recently been reported that an amidocuprate (DALi-CuCN) can be successfully deployed in catalytic deconjugative α-alkylation of cyclic alkenenitriles.[234] In this system, DALi is consumed stoichiometrically, but addition of CuCN accelerates the reaction and minimises self condensation and other side-reactions. It could be investigated whether similar modifications are beneficial to DoLi reactions. For example, the addition of catalytic quantities of CuCN to TMPLi might have a beneficial influence upon regio- and chemoselectivity.

11.5 Further studies on heavier group 11 'ate complexes

In Chapter 8, initial investigations into the preparation of lithium bis(amido)argentate complexes were presented. Complex redox chemistry was encountered when procedures were adapted from analogous cuprate syntheses. Nonetheless, two argentates could be isolated: $(TMP)_2AgLi$ **19** and $(TMP)_2Ag(CN)Li_2(THF)$ **21**. These compounds were targeted for two reasons. First, to establish trends in structure and bonding amongst group 11 'ate complexes, and second, to identify any useful spectroscopic features which might arise from the presence of $^{107/109}Ag$ ($I = \frac{1}{2}$) nuclei. Valuable structural and spectroscopic information was gathered. However, it would be prudent to also investigate the reactivity of **21** with substrates such as *N*,*N*-diisopropylbenzamide, with a view to achieving DoAg (see Scheme 11.4). Comparisons could then be drawn with previosuly reported $(TMP)_2Cu(CN)Li_2(THF)$,[167] to establish whether this reaction is likely to be of interest to the synthetic community. Furthermore, from the perspective of inorganic chemistry, it would be satisfying to 'complete the set' of group 11 'ate complexes by targeting compounds such as $(TMP)_2AuLi$ or $(TMP)_2Au(CN)Li_2(THF)$. These could be synthesised by reaction of AuCN with TMPLi, to give $(TMP)_2AuLi$, and with subsequent treatment with THF giving $(TMP)_2Au(CN)Li_2(THF)$. There would be little synthetic interest in these aurates due to their cost. However, the high carbophilicity of Au[235] and the known stability of Au−C bonds[236] could be harnessed to assist in the isolation of *ortho* metalated intermediates for crystallographic elucidation. The information gathered from these complexes could be used to aid in the understanding of more applied systems (i.e. cuprates).

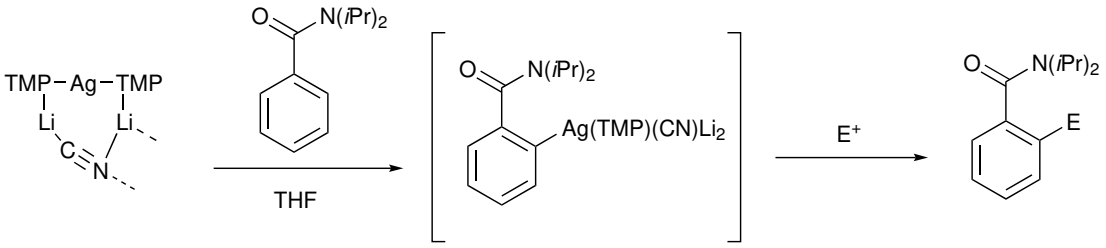

Scheme 11.4: Proposed reaction scheme for DoAg of *N*,*N*-diisopropylbenzamide. THF-solvation omitted for simplicity. E = general electrophile.

11.6 Further studies in the deprotonation of unactivated arenes

The exciting discovery, reported in Chapter 9, that TMPLi-TMPCu mixtures exhibit reactivity towards nominally unreactive hydrocarbons, such as benzene and mesitylene, warrants further research. Additional studies in this area should follow three paths. First, the explicit synthesis of the products identified by NMR spectroscopy should be attempted, for characterisation by X-ray crystallography. This could be achieved by combining TMPLi, TMPCu and PhLi (or PhCu) in the appropriate stoichiometries in hydrocarbon solution. Second, further studies into the mechanism of the deprotonation should be initiated. This would require further experimental work, primarily to distinguish between homogeneous (occurring in solution) and heterogeneous (for example, occurring at the surface of solid TMPCu) reactions. Computational work should also be undertaken. This would be with a view to assessing the energetics of the reaction, and in particular, explaining why these reactions have not been observed previously in solutions of Lipshutz-(type) cuprates. Third, the substrate scope should be surveyed. Anthracene and naphthalene are obvious choices, but heterocycles such as pyridine, quinoline and isoquinoline would also be of interest. Meanwhile, chemoselectivity (aromatic *vs.* lateral metalation) should be addressed by focussing on substrates such as toluene and xylenes. Establishment of the generality of the reactions could then allow for optimisation of stoichiometries and reaction conditions, after which the systems could be introduced to organic synthesis by combining the metalated aromatics with electrophiles. This is arguably the most pressing avenue of research to pursue, as it is likely to have the greatest impact on the wider scientific community.

Bibliography

(1) C. Elschenbroich, *Organometallics*, Wiley-VCH, 2006.

(2) P. R. Jenkins, *Organometallic Reagents in Synthesis*, Oxford University Press, 1992.

(3) S. Matar, M. J. Mirbach and H. A. Tayim, in *Catalysis in Petrochemical Processes*, Springer Netherlands, Dordrecht, 1989, ch. 2, pp. 19–34.

(4) W. Kaminsky and M. Arndt, in *Polymer Synthesis/Polymer Catalysis*, Springer, Berlin, Heidelberg, 1997, ch. 4, pp. 143–187.

(5) A. O. King and N. Yasuda, in *Organometallics in Process Chemistry*, Springer, Berlin, Heidelberg, 2004, vol. 6, pp. 205–245.

(6) J. Clayden, *Organolithiums: Selectivity for Synthesis*, Pergamon, 2002.

(7) M. Baumann and I. R. Baxendale, *Beilstein J. Org. Chem.*, 2013, **9**, 2265–2319.

(8) R. Akhtar, M. Yousaf, S. A. R. Naqvi, M. Irfan, A. F. Zahoor, A. I. Hussain and S. A. S. Chatha, *Synth. Commun.*, 2016, **46**, 1849–1879.

(9) J. D. Knight, S. J. Sauer and D. M. Coltart, *Org. Lett.*, 2011, **13**, 3118–3121.

(10) P. J. Harrington and E. Lodewijk, *Org. Process. Res. Dev.*, 1997, **1**, 72–76.

(11) C.-y. Chen and R. A. Reamer, *Org. Lett.*, 1999, **1**, 293–294.

(12) S. K. Nair, B. N. Rocke and S. Sutton, in *Synthetic Methods in Drug Discovery*, The Royal Society of Chemistry, 2016, vol. 2, ch. 11, pp. 1–74.

(13) C. Friedel and J. M. Crafts, *J. Chem. Soc.*, 1877, **32**, 725–726.

(14) E. J. Cho, V. Lee, B. R. Yoo and I. N. Jung, *J. Organomet. Chem.*, 1997, **548**, 237–245.

(15) G. A. Olah and M. W. Meyer, *J. Org. Chem.*, 1962, **27**, 3464–3469.

(16) H. Gilman, W. Langham and A. L. Jacoby, *J. Am. Chem. Soc.*, 1939, **61**, 106–109.

(17) G. Wittig and G. Fuhrmann, *Chem. Ber.*, 1940, **73**, 1197–1218.

(18) V. Snieckus, *Chem. Rev.*, 1990, **90**, 879–933.

(19) K. C. Nicolaou, P. G. Bulger and D. Sarlah, *Angew. Chem. Int. Ed.*, 2005, **44**, 4442–4489.

(20) M. Tsutomu, M. Kunio and O. Atsumu, *Bull. Chem. Soc. Jpn.*, 1971, **44**, 581–581.

(21) N. Miyaura and A. Suzuki, *Chem. Rev.*, 1995, **95**, 2457–2483.

(22) K. Sonogashira, *J. Organomet. Chem.*, 2002, **653**, 46–49.

(23) Z. Wang, in *Comprehensive Organic Name Reactions and Reagents*, John Wiley & Sons, Inc., 2010, ch. 126, pp. 575–581.

(24) K. Tamao, K. Sumitani and M. Kumada, *J. Am. Chem. Soc.*, 1972, **94**, 4374–4376.

(25) M. Rueping and B. J. Nachtsheim, *Beilstein J. Org. Chem.*, 2010, **6**, 6.

(26) R. E. Mulvey, *Acc. Chem. Res.*, 2009, **42**, 743–755.

(27) O. Kwon, F. Sevin and M. L. McKee, *J. Phys. Chem. A*, 2001, **105**, 913–922.

(28) A. Streitwieser, J. E. Williams, S. Alexandratos and J. M. McKelvey, *J. Am. Chem. Soc.*, 1976, **98**, 4778–4784.

(29) D. Barr, W. Clegg, R. E. Mulvey, R. Snaith and K. Wade, *J. Chem. Soc., Chem. Commun.*, 1986, 295–297.

(30) D. R. Armstrong, D. Barr, W. Clegg, R. E. Mulvey, D. Reed, R. Snaith and K. Wade, *J. Chem. Soc., Chem. Commun.*, 1986, 869–870.

(31) U. Schümann, J. Kopf and E. Weiss, *Angew. Chem. Int. Ed.*, 1985, **24**, 215–216.

(32) D. Slocum, D. Reed, F. Jackson and C. Friesen, *J. Organomet. Chem.*, 1996, **512**, 265–267.

(33) R. H. Shapiro and M. J. Heath, *J. Am. Chem. Soc.*, 1967, **89**, 5734–5735.

(34) G. Wittig and L. Löhmann, *Justus Liebigs Ann. Chem.*, 1942, **550**, 260–268.

(35) A. G. Brook, *Acc. Chem. Res.*, 1974, **7**, 77–84.

(36) M. Rausch and D. Ciappenelli, *J. Organomet. Chem.*, 1967, **10**, 127–136.

(37) H. Gilman, W. Langham and A. L. Jacoby, *J. Am. Chem. Soc.*, 1939, **61**, 106–109.

(38) J. D. Roberts and D. Y. Curtin, *J. Am. Chem. Soc.*, 1946, **68**, 1658–1660.

(39) W. Bauer and P. v. R. Schleyer, *J. Am. Chem. Soc.*, 1989, **111**, 7191–7198.

(40) J. Clayden and M. Julia, *J. Chem. Soc., Chem. Commun.*, 1993, 1682–1683.

(41) G. Klumpp and M. Sinnige, *Tetrahedron Lett.*, 1986, **27**, 2247–2250.

(42) N. J. R. van Eikema Hommes and P. v. R. Schleyer, *Angew. Chem. Int. Ed.*, 1992, **31**, 755–758.

(43) M. Stratakis, *J. Org. Chem.*, 1997, **62**, 3024–3025.

(44) D. Slocum, S. Dumbris, S. Brown, G. Jackson, R. LaMastus, E. Mullins, J. Ray, P. Shelton, A. Walstrom, J. M. Wilcox and R. Holman, *Tetrahedron*, 2003, **59**, 8275–8284.

(45) J. M. Saa, J. Morey, A. Frontera and P. M. Deya, *J. Am. Chem. Soc.*, 1995, **117**, 1105–1116.

(46) S. T. Chadwick, R. A. Rennels, J. L. Rutherford and D. B. Collum, *J. Am. Chem. Soc.*, 2000, **122**, 8640–8647.

(47) M. R. Reich, *C. R. Hebd. Seances Acad. Sci.*, 1923, **117**, 322.

(48) H. Gilman and J. M. Straley, *Recl. Trav. Chim. Pays-Bas*, 1936, **55**, 821–834.

(49) H. Gilman, R. G. Jones and L. A. Woods, *J. Org. Chem.*, 1952, **17**, 1630–1634.

(50) H. O. House, W. L. Respess and G. M. Whitesides, *J. Org. Chem.*, 1966, **31**, 3128–3141.

(51) E. J. Corey and G. H. Posner, *J. Am. Chem. Soc.*, 1967, **89**, 3911–3912.

(52) M. A. Willert-Porada, D. J. Burton and N. C. Baenziger, *J. Chem. Soc., Chem. Commun.*, 1989, 1633–1634.

(53) W. Harnischmacher and R. Hoppe, *Angew. Chem. Int. Ed.*, 1973, **12**, 582–583.

(54) M. Akira, Y. Takakazu and Y. Akio, *Bull. Chem. Soc. Jpn.*, 1977, **50**, 1109–1117.

(55) A. Camus and N. Marsich, *J. Organomet. Chem.*, 1968, **14**, 441–446.

(56) A. Cairncross and W. A. Sheppard, *J. Am. Chem. Soc.*, 1968, **90**, 2186–2187.

(57) A. Cairncross, H. Omura and W. A. Sheppard, *J. Am. Chem. Soc.*, 1971, **93**, 248–249.

(58) M. F. Lappert and R. Pearce, *J. Chem. Soc., Chem. Commun.*, 1973, 24–25.

(59) J. M. Guss, R. Mason, I. Søtofte, G. van Koten and J. G. Noltes, *J. Chem. Soc., Chem. Commun.*, 1972, 446–447.

(60) E. M. Meyer, S. Gambarotta, C. Floriani, A. Chiesi-Villa and C. Guastini, *Organometallics*, 1989, **8**, 1067–1079.

(61) T. Ikariya and A. Yamamoto, *J. Organomet. Chem.*, 1974, **72**, 145–151.

(62) P. Leoni, M. Pesquali and C. A. Ghilardi, *J. Chem. Soc., Chem. Commun.*, 1983, 240–241.

(63) M. Håkansson, H. Eriksson and S. Jagner, *Inorg. Chim. Acta*, 2006, **359**, 2519–2524.

(64) X. He, M. M. Olmstead and P. P. Power, *J. Am. Chem. Soc.*, 1992, **114**, 9668–9670.

(65) S. Sung, D. C. Braddock, A. Armstrong, C. Brennan, D. Sale, A. J. P. White and R. P. Davies, *Chem. Eur. J.*, 2015, **21**, 7179–7192.

(66) T. Greiser and E. Weiss, *Chem. Ber.*, 1976, **109**, 3142–3146.

(67) M. K. Davies, P. R. Raithby, M.-A. Rennie, A. Steiner and D. S. Wright, *J. Chem. Soc., Dalton Trans.*, 1995, 2707–2709.

(68) S. D. Bunge, J. A. Ocana, T. L. Cleland and J. L. Steele, *Inorg. Chem.*, 2009, **48**, 4619–4621.

(69) T. P. Robinson, R. D. Price, M. G. Davidson, M. A. Fox and A. L. Johnson, *Dalton Trans.*, 2015, **44**, 5611–5619.

(70) T. Tsuda, T. Hashimoto and T. Saegusa, *J. Am. Chem. Soc.*, 1972, **94**, 658–659.

(71) D. S. Surry and D. R. Spring, *Chem. Soc. Rev.*, 2006, **35**, 218–225.

(72) R. Bomparola, R. P. Davies, S. Hornauer and A. J. P. White, *Angew. Chem. Int. Ed.*, 2008, **47**, 5812–5815.

(73) R. G. Pearson and C. D. Gregory, *J. Am. Chem. Soc.*, 1976, **98**, 4098–4104.

(74) G. van Koten and J. G. Noltes, *J. Chem. Soc., Chem. Commun.*, 1972, 940–941.

(75) A. Leusink, G. van Koten, J. Marsman and J. Noltes, *J. Organomet. Chem.*, 1973, **55**, 419–425.

(76) G. van Koten and J. G. Noltes, *J. Organomet. Chem.*, 1974, **82**, C53–C55.

(77) G. van Koten, J. T. B. H. Jastrzebski, F. Muller and C. H. Stam, *J. Am. Chem. Soc.*, 1985, **107**, 697–698.

(78) G. van Koten and J. G. Noltes, *J. Am. Chem. Soc.*, 1979, **101**, 6593–6599.

(79) G. van Koten and J. T. Jastrzebski, *Tetrahedron*, 1989, **45**, 569–578.
(80) N. P. Lorenzen and E. Weiss, *Angew. Chem. Int. Ed.*, 1990, **29**, 300–302.
(81) H. Hope, M. M. Olmstead, P. P. Power, J. Sandell and X. Xu, *J. Am. Chem. Soc.*, 1985, **107**, 4337–4338.
(82) R. M. Gschwind, P. R. Rajamohanan, M. John and G. Boche, *Organometallics*, 2000, **19**, 2868–2873.
(83) P. G. Edwards, R. W. Gellert, M. W. Marks and R. Bau, *J. Am. Chem. Soc.*, 1982, **104**, 2072–2073.
(84) S. I. Khan, P. G. Edwards, H. S. H. Yuan and R. Bau, *J. Am. Chem. Soc.*, 1985, **107**, 1682–1684.
(85) H. Hope, D. Oram and P. P. Power, *J. Am. Chem. Soc.*, 1984, **106**, 1149–1150.
(86) J.-P. Gorlier, L. Hamon, J. Levisalles and J. Wagnon, *J. Chem. Soc., Chem. Commun.*, 1973, 88a.
(87) R. Nast and W. Pfab, *Chem. Ber.*, 1956, **89**, 415–421.
(88) B. H. Lipshutz, R. S. Wilhelm and D. M. Floyd, *J. Am. Chem. Soc.*, 1981, **103**, 7672–7674.
(89) S. H. Bertz, *J. Am. Chem. Soc.*, 1991, **113**, 5470–5471.
(90) G. Boche, F. Bosold, M. Marsch and K. Harms, *Angew. Chem. Int. Ed.*, 1998, **37**, 1684–1686.
(91) B. H. Lipshutz, E. L. Ellsworth and T. J. Siahaan, *J. Am. Chem. Soc.*, 1988, **110**, 4834–4835.
(92) J. P. Snyder, D. P. Spangler, J. R. Behling and B. E. Rossiter, *J. Org. Chem.*, 1994, **59**, 2665–2667.
(93) B. H. Lipshutz and B. James, *J. Org. Chem.*, 1994, **59**, 7585–7587.
(94) J. P. Snyder and S. H. Bertz, *J. Org. Chem.*, 1995, **60**, 4312–4313.
(95) S. H. Bertz, G. Miao and M. Eriksson, *Chem. Commun.*, 1996, 815–816.
(96) S. H. Bertz, *J. Am. Chem. Soc.*, 1990, **112**, 4031–4032.
(97) T. Stemmler, J. E. Penner-Hahn and P. Knochel, *J. Am. Chem. Soc.*, 1993, **115**, 348–350.
(98) C. M. P. Kronenburg, J. T. B. H. Jastrzebski, A. L. Spek and G. van Koten, *J. Am. Chem. Soc.*, 1998, **120**, 9688–9689.
(99) N. Krause, *Angew. Chem. Int. Ed.*, 1999, **38**, 79–81.
(100) M. Neumeier and R. M. Gschwind, *J. Am. Chem. Soc.*, 2014, **136**, 5765–5772.

(101) G. H. Posner, C. E. Whitten and J. J. Sterling, *J. Am. Chem. Soc.*, 1973, **95**, 7788–7800.

(102) S. H. Bertz, R. A. Hardin, T. J. Heavey, D. S. Jones, T. B. Monroe, M. D. Murphy, C. A. Ogle and T. N. Whaley, *Chem. Eur. J.*, 2013, **19**, 10138–10141.

(103) S. F. Martin, J. R. Fishpaugh, J. M. Power, D. M. Giolando, R. A. Jones, C. M. Nunn and A. H. Cowley, *J. Am. Chem. Soc.*, 1988, **110**, 7226–7228.

(104) J. Haywood, J. V. Morey, A. E. H. Wheatley, C.-Y. Liu, S. Yasuike, J. Kurita, M. Uchiyama and P. R. Raithby, *Organometallics*, 2009, **28**, 38–41.

(105) P. J. Harford, J. Haywood, M. R. Smith, B. N. Bhawal, P. R. Raithby, M. Uchiyama and A. E. H. Wheatley, *Dalton Trans.*, 2012, **41**, 6148–6154.

(106) A. H. Cowley, D. M. Giolando, R. A. Jones, C. M. Nunn and J. M. Power, *J. Chem. Soc., Chem. Commun.*, 1988, 208–209.

(107) R. P. Davies, S. Hornauer and P. B. Hitchcock, *Angew. Chem. Int. Ed.*, 2007, **46**, 5191–5194.

(108) R. P. Davies, S. Hornauer and A. J. P. White, *Chem. Commun.*, 2007, 304–306.

(109) R. Bomparola, R. P. Davies, S. Hornaeur and A. J. P. White, *Dalton Trans.*, 2014, **43**, 14359–14367.

(110) R. Bomparola, R. P. Davies, S. Hornauer and A. J. P. White, *Dalton Trans.*, 2009, 1104–1106.

(111) P. Reiß and D. Fenske, *Z. Anorg. Allg. Chem.*, 2000, **626**, 1317–1331.

(112) P. P. Power, K. Ruhlandt-Senge and S. C. Shoner, *Inorg. Chem.*, 1991, **30**, 5013–5015.

(113) R. Eujen, B. Hoge and D. J. Brauer, *Inorg. Chem.*, 1997, **36**, 1464–1475.

(114) G. Semerano and L. Riccoboni, *Chem. Ber.*, 1941, **74**, 1089–1099.

(115) J. Boersma, F. D. Tombe, F. Weijers and G. van der Kerk, *J. Organomet. Chem.*, 1977, **124**, 229–233.

(116) C. Beverwijk and G. van der Kerk, *J. Organomet. Chem.*, 1972, **43**, C7–C10.

(117) M. F. Ibad, A. Schulz and A. Villinger, *Organometallics*, 2015, **34**, 3893–3901.

(118) P. B. Hitchcock, M. F. Lappert and L. J.-M. Pierssens, *Chem. Commun.*, 1996, 1189–1190.

(119) C. M. P. Kronenburg, J. T. B. H. Jastrzebski, J. Boersma, M. Lutz, A. L. Spek and G. van Koten, *J. Am. Chem. Soc.*, 2002, **124**, 11675–11683.

(120) G. van Koten, J. T. B. H. Jastrzebski, C. H. Stam and N. C. Niemann, *J. Am. Chem. Soc.*, 1984, **106**, 1880–1881.

(121) C.-S. Hwang and P. P. Power, *J. Organomet. Chem.*, 1999, **589**, 234–238.

(122) Y. Y. Naoki Asao, Masaki Meguro, *Synlett*, 1994, **3**, 185–186.

(123) T. Murai, M. Yamamoto, S. Kondo and S. Kato, *J. Org. Chem.*, 1993, **58**, 7440–7445.

(124) S. Mori and E. Nakamura, *J. Mol. Struct. (Theochem)*, 1999, **461–462**, 167–175.

(125) S. Mori and E. Nakamura, *Tetrahedron Lett.*, 1999, **40**, 5319–5322.

(126) S. Mori, A. Hirai, M. Nakamura and E. Nakamura, *Tetrahedron*, 2000, **56**, 2805–2809.

(127) S. H. Bertz, S. Cope, M. Murphy, C. A. Ogle and B. J. Taylor, *J. Am. Chem. Soc.*, 2007, **129**, 7208–7209.

(128) H. Hu and J. P. Snyder, *J. Am. Chem. Soc.*, 2007, **129**, 7210–7211.

(129) T. Gärtner, W. Henze and R. M. Gschwind, *J. Am. Chem. Soc.*, 2007, **129**, 11362–11363.

(130) S. H. Bertz, S. Cope, D. Dorton, M. Murphy and C. A. Ogle, *Angew. Chem. Int. Ed.*, 2007, **46**, 7082–7085.

(131) D. Naumann, T. Roy, K.-F. Tebbe and W. Crump, *Angewandte Chemie International Edition in English*, 1993, **32**, 1482–1483.

(132) A. Casitas and X. Ribas, *Chem. Sci.*, 2013, **4**, 2301–2318.

(133) J. P. Snyder, *Angew. Chem. Int. Ed.*, 1995, **34**, 986–987.

(134) R. C. Walroth, J. T. Lukens, S. N. MacMillan, K. D. Finkelstein and K. M. Lancaster, *J. Am. Chem. Soc.*, 2016, **138**, 1922–1931.

(135) L. Lochmann and J. Trekoval, *J. Organomet. Chem.*, 1987, **326**, 1–7.

(136) I. Hiriyakkanavar, B. Oliver, W. A. J. and K. Paul, *Chem. Lett.*, 2006, **35**, 2–7.

(137) P. Benrath, M. Kaiser, T. Limbach, M. Mondeshki and J. Klett, *Angew. Chem. Int. Ed.*, 2016, **55**, 10886–10889.

(138) F. Blasberg, M. Bolte, M. Wagner and H.-W. Lerner, *Organometallics*, 2012, **31**, 1001–1005.

(139) M. Campbell, V. Snieckus and E. W. Baxter, in *Encyclopedia of Reagents for Organic Synthesis*, John Wiley & Sons, Ltd, 2001.

(140) D. R. Armstrong, A. R. Kennedy, R. E. Mulvey and S. D. Robertson, *Chem. Eur. J.*, 2011, **17**, 8820–8831.

(141) Y. Kondo, M. Shilai, M. Uchiyama and T. Sakamoto, *J. Am. Chem. Soc.*, 1999, **121**, 3539–3540.

(142) W. Clegg, S. H. Dale, E. Hevia, G. W. Honeyman and R. E. Mulvey, *Angew. Chem. Int. Ed.*, 2006, **45**, 2370–2374.

(143) Y. Kondo, J. V. Morey, J. C. Morgan, H. Naka, D. Nobuto, P. R. Raithby, M. Uchiyama and A. E. H. Wheatley, *J. Am. Chem. Soc.*, 2007, **129**, 12734–12738.

(144) W. Clegg, E. Lamb, S. T. Liddle, R. Snaith and A. E. H. Wheatley, *J. Organomet. Chem.*, 1999, **573**, 305–312.

(145) J. M. Cole, P. G. Waddell, A. E. H. Wheatley, G. J. McIntyre, A. J. Peel, C. W. Tate and D. J. Linton, *Organometallics*, 2014, **33**, 3919–3923.

(146) D. Braga, F. Grepioni, E. Tedesco, K. Biradha and G. R. Desiraju, *Organometallics*, 1997, **16**, 1846–1856.

(147) P. C. Andrikopoulos, D. R. Armstrong, H. R. L. Barley, W. Clegg, S. H. Dale, E. Hevia, G. W. Honeyman, A. R. Kennedy and R. E. Mulvey, *J. Am. Chem. Soc.*, 2005, **127**, 6184–6185.

(148) W. Clegg, S. H. Dale, A. M. Drummond, E. Hevia, G. W. Honeyman and R. E. Mulvey, *J. Am. Chem. Soc.*, 2006, **128**, 7434–7435.

(149) C. Schade, W. Bauer and P. v. R. Schleyer, *J. Organomet. Chem.*, 1985, **295**, c25–c28.

(150) R. Pi, W. Bauer, B. Brix, C. Schade and P. v. R. Schleyer, *J. Organomet. Chem.*, 1986, **306**, C1–C4.

(151) A. R. Kennedy, J. Klett, R. E. Mulvey and D. S. Wright, *Science*, 2009, **326**, 706–708.

(152) R. W. Hoffmann, *Chem. Soc. Rev.*, 2003, **32**, 225–230.

(153) S. R. Harutyunyan, T. den Hartog, K. Geurts, A. J. Minnaard and B. L. Feringa, *Chem. Rev.*, 2008, **108**, 2824–2852.

(154) H. Awad, F. Mongin, F. Trécourt, G. Quéguiner, F. Marsais, F. Blanco, B. Abarca and R. Ballesteros, *Tetrahedron Lett.*, 2004, **45**, 6697–6701.

(155) H. Awad, F. Mongin, F. Trécourt, G. Quéguiner and F. Marsais, *Tetrahedron Lett.*, 2004, **45**, 7873–7877.

(156) D. R. Armstrong, A. R. Kennedy, R. E. Mulvey and R. B. Rowlings, *Angew. Chem. Int. Ed.*, 1999, **38**, 131–133.

(157) E. Hevia, D. J. Gallagher, A. R. Kennedy, R. E. Mulvey, C. T. O'Hara and C. Talmard, *Chem. Commun.*, 2004, 2422–2423.

(158) P. C. Andrews, A. R. Kennedy, R. E. Mulvey, C. L. Raston, B. A. Roberts and R. B. Rowlings, *Angew. Chem. Int. Ed.*, 2000, **39**, 1960–1962.

(159) W. Clegg, B. Conway, P. García-Álvarez, A. R. Kennedy, R. E. Mulvey, L. Russo, J. Sassmannshausen and T. Tuttle, *Chem. Eur. J.*, 2009, **15**, 10702–10706.

(160) M. Uchiyama, H. Naka, Y. Matsumoto and T. Ohwada, *J. Am. Chem. Soc.*, 2004, **126**, 10526–10527.

(161) H. Naka, M. Uchiyama, Y. Matsumoto, A. E. H. Wheatley, M. McPartlin, J. V. Morey and Y. Kondo, *J. Am. Chem. Soc.*, 2007, **129**, 1921–1930.

(162) D. R. Armstrong, E. Crosbie, E. Hevia, R. E. Mulvey, D. L. Ramsay and S. D. Robertson, *Chem. Sci.*, 2014, **5**, 3031–3045.

(163) J. García-Álvarez, A. R. Kennedy, J. Klett and R. E. Mulvey, *Angew. Chem. Int. Ed.*, 2007, **46**, 1105–1108.

(164) L. M. Carrella, W. Clegg, D. V. Graham, L. M. Hogg, A. R. Kennedy, J. Klett, R. E. Mulvey, E. Rentschler and L. Russo, *Angew. Chem. Int. Ed.*, 2007, **46**, 4662–4666.

(165) R. E. Mulvey, V. L. Blair, W. Clegg, A. R. Kennedy, J. Klett and L. Russo, *Nat. Chem.*, 2010, **2**, 588–591.

(166) S. Komagawa, S. Usui, J. Haywood, P. J. Harford, A. E. H. Wheatley, Y. Matsumoto, K. Hirano, R. Takita and M. Uchiyama, *Angew. Chem. Int. Ed.*, 2012, **51**, 12081–12085.

(167) S. Usui, Y. Hashimoto, J. V. Morey, A. E. H. Wheatley and M. Uchiyama, *J. Am. Chem. Soc.*, 2007, **129**, 15102–15103.

(168) N. Marquise, P. J. Harford, F. Chevallier, T. Roisnel, V. Dorcet, A.-L. Gagez, S. Sablé, L. Picot, V. Thiéry, A. E. H. Wheatley, P. C. Gros and F. Mongin, *Tetrahedron*, 2013, **69**, 10123–10133.

(169) N. Marquise, P. J. Harford, F. Chevallier, T. Roisnel, A. E. H. Wheatley, P. C. Gros and F. Mongin, *Tetrahedron Lett.*, 2013, **54**, 3154–3157.

(170) R. Campbell, B. Conway, G. S. Fairweather, P. García-Álvarez, A. R. Kennedy, J. Klett, R. E. Mulvey, C. T. O'Hara and G. M. Robertson, *Dalton Trans.*, 2010, **39**, 511–519.

(171) P. J. Harford, A. J. Peel, J. P. Taylor, S. Komagawa, P. R. Raithby, T. P. Robinson, M. Uchiyama and A. E. H. Wheatley, *Chem. Eur. J.*, 2014, **20**, 3908–3912.

(172) R. H. Crabtree, *Organometallics*, 2011, **30**, 17–19.

(173) S. Tamba, K. Ide, K. Shono, A. Sugie and A. Mori, *Synlett*, 2013, **24**, 1133–1136.

(174) M. S. Hill, D. J. Liptrot and C. Weetman, *Chem. Soc. Rev.*, 2016, **45**, 972–988.

(175) R. A. Sheldon, *Chem. Commun.*, 2008, 3352–3365.

(176) N. Tezuka, K. Shimojo, K. Hirano, S. Komagawa, K. Yoshida, C. Wang, K. Miyamoto, T. Saito, R. Takita and M. Uchiyama, *J. Am. Chem. Soc.*, 2016, **138**, 9166–9171.

(177) S. H. Bertz, C. P. Gibson and G. Dabbagh, *Tetrahedron Lett.*, 1987, **28**, 4251–4254.

(178) R. K. Harris, E. D. Becker, S. M. Cabral de Menezez, P. Granger, R. E. Hoffman and K. W. Zilm, *Pure Appl. Chem.*, 2008, **80**, 59–84.

(179) G. M. Sheldrick, *Acta Cryst.*, 2015, **A71**, 3–8.

(180) G. M. Sheldrick, *Acta Cryst.*, 2015, **C71**, 3–8.

(181) A. J. Peel, M. Hedidi, G. Bentabed-Ababsa, T. Roisnel, F. Mongin and A. E. H. Wheatley, *Dalton Trans.*, 2016, **45**, 6094–6104.

(182) E. Söderbäck, *Acta Chim. Scand.*, 1957, 1622–1634.

(183) *APEX3*, Bruker AXS Inc., Madison, Wisconsin USA., 2016.

(184) M. F. Lappert, M. J. Slade, A. Singh, J. L. Atwood, R. D. Rogers and R. Shakir, *J. Am. Chem. Soc.*, 1983, **105**, 302–304.

(185) E. Hevia, A. R. Kennedy, R. E. Mulvey, D. L. Ramsay and S. D. Robertson, *Chem. Eur. J.*, 2013, **19**, 14069–14075.

(186) W. E. Rhine, G. Stucky and S. W. Peterson, *J. Am. Chem. Soc.*, 1975, **97**, 6401–6406.

(187) W. H. Ilsley, M. J. Albright, T. J. Anderson, M. D. Glick and J. P. Oliver, *Inorg. Chem.*, 1980, **19**, 3577–3585.

(188) W. Scherer, P. Sirsch, D. Shorokhov, G. S. McGrady, S. A. Mason and M. G. Gardiner, *Chem. Eur. J.*, 2002, **8**, 2324–2334.

(189) B. H. Lipshutz, J. A. Kozlowski and R. S. Wilhelm, *J. Org. Chem.*, 1983, **48**, 546–550.

(190) B. H. Lipshutz, *Synthesis*, 1987, **4**, 325–341.

(191) R. E. Mulvey and S. D. Robertson, *Angew. Chem. Int. Ed.*, 2013, **52**, 11470–11487.

(192) O. Reckeweg, A. Schulz, B. Blaschkowski et al., *Z. Naturforsch. B*, 2014, **69**, 17–24.

(193) K. Gregory, P. v. R. Schleyer and R. Snaith, 1991, **37**, 47–142.

(194) E. Marzi, A. Bigi and M. Schlosser, *Eur. J. Org. Chem.*, 2001, **2001**, 1371–1376.

(195) P. J. Harford, A. J. Peel, F. Chevallier, R. Takita, F. Mongin, M. Uchiyama and A. E. H. Wheatley, *Dalton Trans.*, 2014, **43**, 14181–14203.

(196) T. T. Nguyen, N. Marquise, F. Chevallier and F. Mongin, *Chem. Eur. J.*, 2011, **17**, 10405–10416.

(197) M. A. S. Goher and F. A. Mautner, *J. Chem. Soc., Dalton Trans.*, 1999, 1923–1924.

(198) V. Mdluli, P. J. Hubbard, D. R. Javier-Jimenez, A. Kuznicki, J. A. Golen, A. L. Rheingold and D. R. Manke, *Inorg. Chim. Acta*, 2017, **461**, 71–77.

(199) D. R. Armstrong, D. Barr, W. Clegg, S. M. Hodgson, R. E. Mulvey, D. Reed, R. Snaith and D. S. Wright, *J. Am. Chem. Soc.*, 1989, **111**, 4719–4727.

(200) F. S. Mair, W. Clegg and P. A. O'Neil, *J. Am. Chem. Soc.*, 1993, **115**, 3388–3389.

(201) A. J. Edwards, M. A. Paver, P. R. Raithby, C. A. Russell and D. S. Wright, *J. Chem. Soc., Dalton Trans.*, 1993, 3265–3266.

(202) H. Vitze, H.-W. Lerner and M. Bolte, *Acta Cryst.*, 2006, **E62**, 2853–2854.

(203) C. R. Groom, I. J. Bruno, M. P. Lightfoot and S. C. Ward, *Acta Cryst.*, 2016, **B72**, 171–179.

(204) B. S. Lim, A. Rahtu, J.-S. Park and R. G. Gordon, *Inorg. Chem.*, 2003, **42**, 7951–7958.

(205) H. Hope and P. P. Power, *Inorg. Chem.*, 1984, **23**, 936–937.

(206) J. García-Álvarez, D. V. Graham, E. Hevia, A. R. Kennedy and R. E. Mulvey, *Dalton Trans.*, 2008, 1481–1486.

(207) R. G. Pearson, *J. Chem. Educ.*, 1968, **45**, 581.

(208) P. de Frémont, N. M. Scott, E. D. Stevens, T. Ramnial, O. C. Lightbody, C. L. B. Macdonald, J. A. C. Clyburne, C. D. Abernethy and S. P. Nolan, *Organometallics*, 2005, **24**, 6301–6309.

(209) Y.-P. Xie and T. C. W. Mak, *J. Cluster Sci.*, 2014, **25**, 189–204.

(210) Y. Yamashita, X.-X. Guo, R. Takashita and S. Kobayashi, *J. Am. Chem. Soc.*, 2010, **132**, 3262–3263.

(211) Y. Yamashita, T. Imaizumi, X.-X. Guo and S. Kobayashi, *Chem. Asian J.*, 2011, **6**, 2550–2559.

(212) T. Kauffmann, C. Neiteler and S. Robbe, *Chem. Ber.*, 1992, **125**, 2409–2418.

(213) D. Barr, M. J. Doyle, S. R. Drake, P. R. Raithby, R. Snaith and D. S. Wright, *J. Chem. Soc., Chem. Commun.*, 1988, 1415–1417.

(214) D. Barr, M. J. Doyle, S. R. Drake, P. R. Raithby, R. Snaith and D. S. Wright, *Polyhedron*, 1989, **8**, 215–218.

(215) R. D. Shannon, *Acta Crystallogr.*, 1976, **A32**, 751–767.

(216) B. S. Fox, M. K. Beyer and V. E. Bondybey, *J. Am. Chem. Soc.*, 2002, **124**, 13613–13623.

(217) J. Jubb, P. Berno, S. Hao and S. Gambarotta, *Inorg. Chem.*, 1995, **34**, 3563–3566.

(218) B. L. Lucht and D. B. Collum, *J. Am. Chem. Soc.*, 1994, **116**, 7949–7950.

(219) M. D. Rozeboom and K. N. Houk, *J. Am. Chem. Soc.*, 1982, **104**, 1189–1191.

(220) G. A. Olah, I. Hashimoto and H. C. Lin, *Proc. Natl. Acad. Sci.*, 1977, **74**, 4121–4125.

(221) L. M. Stock and T. L. Wright, *J. Org. Chem.*, 1980, **45**, 4645–4648.

(222) C. Unkelbach, D. F. O'Shea and C. Strohmann, *Angew. Chem. Int. Ed.*, 2014, **53**, 553–556.

(223) D. Nobuto and M. Uchiyama, *J. Org. Chem.*, 2008, **73**, 1117–1120.

(224) J. A. N. F. Gomes and R. B. Mallion, *Chem. Rev.*, 2001, **101**, 1349–1384.

(225) A. J. Edwards, M. A. Paver, P. R. Raithby, M.-A. Rennie, C. A. Russell and D. S. Wright, *Organometallics*, 1994, **13**, 4967–4972.

(226) D. H. B. Ripin, in *Practical Synthetic Organic Chemistry*, John Wiley & Sons, Inc., 2011, ch. 18, pp. 771–803.

(227) B. E. Rossiter and M. Eguchi, *Tetrahedron Lett.*, 1990, **31**, 965–968.

(228) B. E. Rossiter, M. Eguchi, A. E. Herna´ndez, D. Vickers, J. Medich, J. Marr and D. Heinis, *Tetrahedron Lett.*, 1991, **32**, 3973–3976.

(229) B. E. Rossiter, G. Miao, N. M. Swingle, M. Eguchi, A. E. Hernández and R. Patterson, *Tetrahedron: Asymmetry*, 1992, **3**, 231–234.

(230) B. E. Rossiter, M. Eguchi, G. Miao, N. M. Swingle, A. E. Hernández, D. Vickers, E. Fluckiger, R. G. Patterson and K. V. Reddy, *Tetrahedron*, 1993, **49**, 965–986.

(231) M. Pineschi, F. Del Moro, F. Gini, A. J. Minnaard and B. L. Feringa, *Chem. Commun.*, 2004, 1244–1245.

(232) C. Vila, V. Hornillos, M. Fananas-Mastral and B. L. Feringa, *Chem. Commun.*, 2013, **49**, 5933–5935.

(233) S. Morisako, R. Shang and Y. Yamamoto, *Inorg. Chem.*, 2016, **55**, 10767–10773.

(234) X. Yang, D. Nath, J. Morse, C. Ogle, E. Yurtoglu, R. Altundas and F. Fleming, *J. Org. Chem.*, 2016, **81**, 4098–4102.

(235) A. Hoffmann-Röder and N. Krause, *Org. Biomol. Chem.*, 2005, **3**, 387–391.

(236) A. J. Markwell, *J. Organomet. Chem.*, 1985, **293**, 257–263.